Functionalized hydrogel for oral hard tissue regeneration

Lei Wang

VRIJE UNIVERSITEIT

Functionalized hydrogel for oral hard tissue regeneration

ACADEMISCH PROEFSCHRIFT

ter verkrijging van de graad Doctor of Philosophy aan
de Vrije Universiteit Amsterdam,
op gezag van de rector magnificus
prof.dr. J.J.G. Geurts,
in het openbaar te verdedigen
ten overstaan van de promotiecommissie
van de Faculteit der Tandheelkunde
op donderdag 29 september 2022 om 11.45 uur
in een bijeenkomst van de universiteit,
De Boelelaan 1105

door
Lei Wang
geboren te Zhejiang, China

This thesis is dedicated to

my parents, husband and daughter

致我的父亲母亲，先生和我的女儿王若瑜

TABLE OF CONTENTS

Chapter 1

General Introduction

ORAL HARD TISSUE

Oral hard tissue refers to the hard and mineralized tissues, such as enamel, dentin, and bone [1], which form an integral complex, playing a vital role in aesthetics and oral functions. According to the mineral density volume gradients, the mineral density range for normal enamel, dentin, and bone are 2820–3095, 1480–1590, and 570–1415 mg/cc, respectively. Enamel is the hardest substance in the human body and contains the highest percentage (about 96%) of mineral phase (hydroxyapatite crystals) with prisms and lattices structures [2]. Enamel functions to both provide a hard surface for food processing [3] and protect the underlying tissues, such as dentin and dental pulp [4]. Due to its acellular property, enamel cannot be regenerated or repaired physiologically in the human body [5]. Directly under the enamel, dentin is formed by odontoblasts and is comprised of a mineralized extracellular matrix with closely packed tubular structures [6, 7]. Dentin is composed of 70% inorganic hydroxyapatite crystals, 20% organic matter, and 10% fluids (by weight) [8]. Dentin provides protection to pulp against bacteria, bacterial products, and injury [9]. Due to the embryological, histological, and functional similarity, dentin and pulp are considered as a complex, which supports the enamel in dissipating masticatory forces and maintains the vitality and biological property of pulp and hence the teeth [6, 10]. Bone is a connective dynamic tissue composed of 65% mineral (primarily carbonate apatite [11]) and contains four types of bone cells, e. g. osteoprogenitor cells, osteoblasts, osteocytes, and osteoclasts [12], which delicately orchestrate bone homeostasis and regeneration. Apart from aesthetic role, oral bone tissues, such as maxillofacial bone and mandibular bone, are highly important to facilitate mandibular movement so as to enabling masticatory and speaking functions. The biological basis for this mandibular movement is bone tissue forms an anatomic and functional complex — osteochondral complex with articular cartilage, constituting temporomandibular joint (TMJ), the only joint in the maxillofacial region. Articular cartilage displays a complex multi-zonal organization consisting of surface, medial and deep zones and a subchondral junction with underlying bone tissue [13]. TMJ articular cartilage is the greatest growth center, contributing to growth of mandibular bone. Furthermore, the osteochondral complex of TMJ also functions to dissipate or transfer the masticatory force. In this thesis, we mainly focused on the regeneration of dentin, bone and osteochondral complex.

1. DENTIN DAMAGE AND REGENERATION

Dental pulp is a highly vascularized and innervated connective tissue that provides nutritive, protective, defensive and formative functions to teeth [14]. When exposed to pathogenic stimuli such as bacteria, bacterial products and injury from deep caries or trauma, dental pulp may rapidly transform into reversible and then irreversible pulpitis,

which leads to pulpal necrosis and periapical inflammation [15] as well as potential systemic complications, such as osteomyelitis [16] and bacteraemia [17]. To maintain the vitality of dental pulp tissue and induce reparative dentinogenesis, pulp-capping materials have been adopted in the clinic to cover nearly exposed, accidentally exposed or partially infected pulp [18]. Calcium hydroxide, mineral trioxide aggregate (MTA), have been used as pulp capping materials. However, the use of calcium hydroxide is associated with a series of clinical concerns, such as high solubility, poor mechanical properties and "tunnel defects" [19] while MTA with concerns such as discolouration [20], a long setting time [21] and handling difficulties [22]. Consequently, continuous efforts have been made in an attempt to develop alternative pulp-capping materials [23].

2. BUCCAL BONE RESORPTION DURING IMMEDIATE IMPLANTATION AND REGENERATION

Due to imperfect matching between implants and tooth extraction socket, a jumping gap or jumping distance may occur between the implant surface and surrounding bone during immediate implantation, resulting in unsupported bone plates. The bone plates, particularly the buccal ones, may undergo resorption due to the destruction of periodontal membrane-borne blood supply, which can cause soft tissue recession and thus aesthetic risk. A systematic review shows that the weighted mean buccal horizontal dimensional bone reduction and buccal vertical dimensional bone reduction was 1.07 mm and 0.78 mm, respectively [24], which may lead to a midfacial recession in the long term. More pronouncedly, the resorption may become to about 7.5 mm for the thin-wall bone phenotype [25]. In the clinic, particulate CaP-based bone grafts are used to fill the large (>2mm) jumping distance in order to prevent buccal bone resorption, which is, whereas, associated with a series of concerns, such as incomplete filling and easily being wrapped with connective tissues. Furthermore, most of the CaP-based bone grafts bear only certain osteoconductivity but no intrinsic osteoinductivity so that they cannot efficaciously prevent bone resorption. Therefore, a more suitable jumping distance-filling material with excellent filling adaptability and pro-osteogenic properties is highly needed to prevent bone resorption of the buccal bone plate, thereby minimizing aesthetic risks.

3. BONE DEFECTS AND GUIDED BONE REGENERATION

In the field of implant dentistry, guided bone regeneration (GBR) technique is widely used reconstructive procedure that adopts barrier membranes and particulate bone-defect-filling materials to direct the growth of new bone to restore bone volume and dimensions,

such as socket preservation, alveolar ridge augmentation, maxillary sinus elevation [26]. In the classic GBR technique, the barrier membrane mainly functions to prevent the invasion of surrounding connective tissues that bears proliferation advantage over osteoblasts so as to facilitate bone tissue regeneration [27]. Clinically available barrier membranes can be classified into non-resorbable and resorbable membrane. Non-resorbable membranes such as titanium mesh and polytetrafluoroethylene membranes are associated with a series of concerns, such as premature exposure, gingival irritation, infection and the need of second surgery for their removal [28]. Therefore, resorbable membranes with both naturally-derived (such as collagen and chitosan) and synthetic (such as polylactic acid) materials are widely used in clinic. However, these membranes have too mild stickiness to surrounding bone tissue to immobilize bone-defect-filling materials, the displacement or deformation of the graft is often found in clinical practice, which may lead to poor clinical outcomes such as delayed osteogenesis, even infection [29]. Consequently, continuous efforts have been attempted to develop more suitable membrane materials.

4. OSTEOCHONDRAL DAMAGE AND REGENERATION

Damage to the TMJ disc or condyle, which may from trauma, degeneration or arthritic conditions, can instigate lifetime pain, restrict the movement of jaw, severely impact the daily activities such as yawning, talking, eating, and cause facial asymmetry. The repair of osteochondral defects in TMJ is highly challenging due to its limited self-regenerative potential [30]. Most of current clinical therapies to treat osteochondral defect mainly by using various autografts, such as autologous chondrocytes implantation [31] and mosaicplasty [32, 33]. These treatments show beneficial effects in the healing of osteochondral defects by providing chondrocytes. However, their usage is highly limited due to the limited availability of autografts and donor-site pain and morbidity [34]. Therefore, developing a viable treatment option to repair the osteochondral defects in TMJ is highly challenging, and continuous efforts have been attempted to repair osteochondral defects.

APPLICATION OF HYDROGELS IN ORAL HARD TISSUE REGENERATION

Hydrogel is one major type of biomaterials for tissue engineering. Hydrogels bear three-dimensional interconnected porous networks for cell ingrowth, proliferation and differentiation. Their high-water contents enable the efficient exchange of cell nutrients, oxygen and metabolites to support cell activities. Furthermore, their sol-gel transition allows hydrogels to both flexibly fit into irregular-shaped defects and completely cover

intended areas. The hydrogels with naturally-derived compositions, such as gelatin and hyaluronic acid, are also capable of provide biomimetic microenvironment to support cell activities [35].

Methacrylated gelatin (Gel-MA), a photocrosslinkable hydrogel, is one of the most widely hydrogels in the field of bone tissue engineering. Gel-MA exhibits excellent biocompatibility, processability, tunability, and low immunogenicity [36]. Gelatin contains many adhesive ligands, such as arginine-glycine-aspartic acid sequences, which promote cell adhesion and migration. Gel-MA bears a good capacity to bond to mineralized tissue through non-covalent bonding mechanisms [37], such as molecular interactions [38]. The sufficient fluidity of Gel-MA precursor enables its flexible fit into irregular defects or full coverage on intended area. Moreover, the sol-gel transition of Gel-MA can be very quick after UV exposure, which is completely under control of clinicians. These properties make Gel-MA very suitable for the filling of fully exposed defects [39]. In this thesis, we adopted Gel-MA in exposed dental pulp and osteochondral defects in TMJ.

On the other hand, the usage of Gel-MA may not be very suitable for the partially exposed defects, such as, jumping gap in immediate implantation since the long and narrow geometry of, and the bleeding in jumping gap may largely hinder the gelation process and lead to insufficient gelation. To approach this situation, we resorted to another type of hydrogel — injectable self-healing hydrogels with dynamic crosslinking, which can be gelled without the needs of additional chemical/physical initiations. Self-healing hydrogels bear a unique reversible network structure through dynamic chemical bonding (for example, Schiff base reactions [40], Diels–Alder reactions [41], disulfide bonds [42], acylhydrazone bonds [43], phenylboronate esters [44]), that can automatically restore its network integrity and original mechanical property after damage. In addition, self-healing hydrogels may also repair the potential deformations at the gingival margin caused by the mechanical force during oral movements, so as to prevent the potential microgap and thus infection. To confirm the successful crosslinking of Schiff base reaction, we adopted gelatin and oxidized alginate (OSA) to construct an injectable self-healing hydrogel. We characterized the cell viability, *in-situ* gelation and *in-vivo* biocompatibility of the hydrogel. We also functionalized the self-healing hydrogel with bioactive agent, using sericin (SS) and OSA to orchestrate the self-healing hydrogel (SS/OSA) with pro-osteogenic property.

Barrier membrane is an indispensable element in GBR technique to prevent the invasion of surrounding connective tissues that bears proliferation advantage over osteoblasts so as to facilitate bone tissue regeneration. Resorbable collagen membranes are widely used in clinic, while they have nearly no stickiness to prevent the displacement or deformation of the particulate bone grafts, potentially damaging osteogenesis [29]. Gel-MA hydrogel may be a potential alternative membrane material since it bears certain stickiness to

mineralized tissue and UV crosslinking is also feasible in this application. However, the mechanical property of Gel-MA should still be improved to be used as a GBR membrane. One viable approach to modify the physicochemical and biofunctional properties of a hydrogel is to introduce a hybrid crosslinking mechanism, for example, thermal-photo-crosslinking [45] and ionically–covalently crosslinking [46]. With the inspiration of hybrid crosslinking, we wished to further enhance the mechanical property of Gel-MA by introducing an additional dynamic bond. For this purpose, we added a modified hyaluronic acid (HA) to Gel-MA. We first oxidized HA with sodium periodate to confer aldehyde groups to HA. Thereafter, the mixture of OHA and Gel-MA in different ratios was subjected to reaction condition with UV light at 37 °C for 2 min so as to achieve a hybrid-crosslinked (dynamic bond and photo-crosslinking) OHA/Gel-MA hydrogel membrane.

BIO-FUNCTIONALIZATION OF HYDROGELS

In the field of tissue engineering, hydrogels mainly function to provide a biocompatible and biodegradable interconnected porous scaffold for bone ingrowth. For oral hard tissue regeneration, hydrogels should still be improved in their osteogenic/dentinogenic capacities and physicochemical properties, particularly mechanical property, so as to meet the clinical demand for promoting healing efficacy. One viable approach is to functionalize hydrogels with bioactive agents, such as proteinous growth factors, peptides and small molecules. One of the most used proteinous growth factors for oral hard tissue regeneration is bone morphogenetic protein-2 (BMP2), a well-established osteoinductive growth factor under the TGF-β superfamily [47]. The classical role for BMP2 was considered to be the induction of (ectopic) cartilage and bone formation [48, 49]. In the USA, the product containing recombinant human (rh)BMP2 in absorbable collagen has already been approved for clinical application in nonunion bone fractures and spinal fusions [50]. And it is also adopted to promote the formation of reparative dentin [51]. However, the use of BMP2 in oral hard tissue regeneration is associated with a series of concerns. Firstly, pharmaceutical BMP2 is produced using a gene-recombinant technology, which is rather costly for its wide spreading [52]. Secondly, for the repair of osteochondral defects, BMP2 induces chondrocyte hypertrophy followed by cartilage calcification [53], which compromises the regeneration of cartilage layer. Thirdly, one major concern of BMP2 is the induction of postoperative inflammation [54], which may potentially exacerbate the inflammation in irritated dental pulp, leading to irreversible inflammation and dental pulp necrosis. Furthermore, in most situations, BMP2 can hardly improve physicochemical properties [55]. In contrast, most peptides and small-molecules are much cheaper and also exhibit various biofunctions, representing promising alternatives to functionalize hydrogels for oral hard tissue regeneration.

We adopted notoginsenoside R1 (NGR1) to improve the dentinogenic capacity and mechanical property of Gel-MA so as to develop a novel pulp-capping material for inducing reparative dentin formation. NGR1 is a bioactive monomer isolated from panax notoginseng [56]. It has been widely used for the clinical treatment of cardiovascular diseases [57] and osteoporosis [58]. NGR1 can protect cells from inflammation and apoptosis by reducing NADPH (nicotinamide adenine dinucleotide phosphate) oxidase and mitochondrion-derived superoxide via oestrogen receptor-dependent activation of Akt/Nrf2 (nuclear factor-erythroid 2 p45-related factor 2) pathways [59]. In addition, NGR1 can dramatically promote the expression of osteocalcin (OCN) (a late dentinogenic differentiation marker) and extracellular matrix mineralization [60]. These properties of NGR1 are important to protect the dental pulp from pulpal necrosis and periapical inflammation.

In this thesis, we used histatin1 (Hst1) to improve the chondrogenic capacity of Gel-MA so as to provide a viable treatment option for the repair of osteochondral defects in TMJ. Hst1 belongs to a cationic and histidine-rich peptide family originally found in the saliva of higher primates [61]. Hst1 bears a potent capacity to stimulate the adhesion and migration of epithelial cells [62-65], fibroblasts [66] and osteoblasts [67, 68]. Meanwhile, it can promote cell metabolic activity [65], maintain cell viability in various conditions [67, 68]. Furthermore, Hst1 shows a very strong angiogenetic property [69]. The abovementioned Hst1's cell-activating effects seem to be independent on cell types, thus bearing broad applicability. These properties are of paramount importance particularly for the application in repairing osteochondral defects, which needs the promotion of the functions of both osteoblasts and chondrocytes [50, 70].

We employed salvianolic acid B (SAB) to promote the pro-osteogenic property of the SS/OSA hydrogel so as to provide an ideal jumping gap distance-filling material for immediate implantation. SAB, a traditional water-soluble Chinese herbal medicine, is a potential bioactive molecular, which has been widely used in clinical practice for the treatment of cardiovascular disease [71] through its anti-oxidized function [72]. Previous studies show that SAB promotes the osteogenic differentiation of mesenchymal stem cells [73] by dose-dependently up-regulating the alkaline phosphatase (ALP) activity and osteogenesis-related markers, such as osteopontin (OPN), runt-related transcription factor 2 (RunX2), osterix (Osx), osteocalcin (OCN), and bone sialoprotein (BSP) [74, 75]. This promotion of SAB was achieved by activating the extracellular-signal-regulated kinases (ERK) signaling pathway [75]. These properties show a promising potency of SAB in promoting osteogenesis.

Another method for bio-functionalization is to introduce additional materials to dramatically change the physicochemical and biological functions. HA is an important component of the extracellular matrix (ECM) consisting of D-N-acetylglucosamine and D-glucuronic acid repeating units. With excellent biocompatible, biodegradable, and nonimmunogenic property [76], HA is commonly used as a scaffold component and a pro-osteogenic agent in the field of bone tissue engineering [77, 78]. In **chapter 6**, we first oxidized HA to produce aldehyde groups to realize dynamic bonds, and followed by hybrid-crosslinking with Gel-MA to enhance the osteogenic and mechanical properties of the hydrogel with an aim to develop a novel GBR membrane.

AIM AND OUTLINE OF THIS THESIS

The main aim of this thesis was to develop biofunctionalized hydrogels to repair and promote oral hard tissue regeneration. This thesis is subdivided into five chapters.

1. In **chapter 2,** we aimed to develop a novel pulp capping material. We prepared a Gel-MA/NGR1 hydrogel and studied the physicochemical properties and the efficacy of inducing *in-vitro* dentinogenesis and *in-vivo* reparative dentin formation.

2. In **chapter 3,** we aimed to provide a viable treatment option for repair of osteochondral defects in the temporomandibular joint (TMJ). We fabricated a Gel-MA/Histatin 1 hydrogel and investigated its repair capability in a critical-size TMJ defects model in a rabbit.

3. In **chapter 4,** we aimed to design and construct a novel hydrogel with injectable and self-healing property. We adopted gelatin and alginate to prepare GE/OSA/ADH hydrogels and investigated the *in-vivo* gel forming and self-healing properties and the porous structure stability.

4. In **chapter 5**, we aimed to design an injectable, self-healing, and pro-osteogenic hydrogel. We used alginate, sericin, and SAB to prepare a functionalized SS/OSA-SAB hydrogel and evaluated the rheological properties, physicochemical properties and *in-vitro* pro-osteogenesis of the hydrogel.

5. In **chapter 6**, we aimed to develop a hybrid crosslinking hydrogel with enhanced mechanical and pro-osteogenic properties for guided bone regeneration. We adopted oxidized hyaluronic acid (OHA) and Gel-MA to prepare an OHA/Gel-MA hydrogel and studied the physicochemical properties and the *in-vitro* extracellular mineralization capacity of the hydrogel.

REFERENCES

[1] L.K. McCauley, M.J. Somerman, Mineralized tissues in oral and craniofacial science: biological principles and clinical correlates, John Wiley & Sons2012.

[2] Broadhead GD, Maruyama GM, Bruininks RH. Examining differentiation in motor proficiency through exploratory and confirmatory factor analysis. Vol 1. Princeton, NJ: Princeton Books; 1985.

[3] R.S. Lacruz, S. Habelitz, J.T. Wright, M.L. Paine, Dental enamel formation and implications for oral health and disease, Physiological reviews 97(3) (2017) 939-993.

[4] H. Maeda, Aging and senescence of dental pulp and hard tissues of the tooth, Frontiers in Cell and Developmental Biology (2020) 1417.

[5] A. Angelova Volponi, L.K. Zaugg, V. Neves, Y. Liu, P.T. Sharpe, Tooth repair and regeneration, Current oral health reports 5(4) (2018) 295-303.

[6] J. Moradian-Oldak, A. George, Biomineralization of Enamel and Dentin Mediated by Matrix Proteins, Journal of dental research 100(10) (2021) 1020-1029.

[7] F. Farci, A. Soni, Histology, Tooth, StatPearls [Internet] (2021).

[8] M. Deng, X. Dong, X. Zhou, L. Wang, H. Li, X. Xu, Characterization of dentin matrix biomodified by Galla chinensis extract, Journal of endodontics 39(4) (2013) 542-7.

[9] G. Bergenholtz, Pathogenic mechanisms in pulpal disease, Journal of endodontics 16(2) (1990) 98-101.

[10] M. Goldberg, A.B. Kulkarni, M. Young, A. Boskey, Dentin: Structure, Composition and Mineralization: The role of dentin ECM in dentin formation and mineralization, Frontiers in bioscience (Elite edition) 3 (2011) 711.

[11] S. Djomehri, S. Candell, T. Case, A. Browning, G. Marshall, W. Yun, S. Lau, S. Webb, S. Ho, Mineral density volume gradients in normal and diseased human tissues, PloS one 10(4) (2015) e0121611.

[12] J. Buckwalter, R. Cooper, Bone structure and function, Instructional course lectures 36 (1987) 27-48.

[13] R.S. Decker, E. Koyama, M. Pacifici, Articular cartilage: structural and developmental intricacies and questions, Current osteoporosis reports 13(6) (2015) 407-414.

[14] C.C. Huang, R. Narayanan, N. Warshawsky, S. Ravindran, Dual ECM Biomimetic Scaffolds for Dental Pulp Regenerative Applications, Frontiers in Physiology 9(495) (2018).

[15] K.J. Heyeraas, E. Berggreen, Interstitial fluid pressure in normal and inflamed pulp, Crit Rev Oral Biol Med 10(3) (1999) 328-36.

[16] M. Pesis, E. Bar-Droma, A. Ilgiyaev, N. Givol, Deep Neck Infections, Life Threatening Infections of Dental Origin: Presentation and Management of Selected Cases, Israel Medical Association Journal 21(12) (2019) 806-811.

[17] L.C. Reis, I.N. Rocas, J.F. Siqueira, M. de Uzeda, V.S. Lacerda, R. Domingues, S.R. Moraes, R.M. Saraiva, Bacteremia after Endodontic Procedures in Patients with Heart Disease: Culture and Molecular Analyses, Journal of Endodontics 42(8) (2016) 1181-1185.

[18] L. Bjorndal, S. Simon, P.L. Tomson, H.F. Duncan, Management of deep caries and the exposed pulp, International Endodontic Journal 52(7) (2019) 949-973.

[19] W.L.O. da Rosa, A.R. Cocco, T.M.D. Silva, L.C. Mesquita, A.D. Galarca, A.F.D. Silva, E. Piva, Current trends and future perspectives of dental pulp capping materials: A systematic review, J Biomed Mater Res B Appl Biomater 106(3) (2018) 1358-1368.

[20] G. Bogen, J.S. Kim, L.K. Bakland, Direct pulp capping with mineral trioxide aggregate: an observational study, J Am Dent Assoc 139(3) (2008) 305-15; quiz 305-15.

[21] M. Torabinejad, C.U. Hong, F. McDonald, T.R. Pitt Ford, Physical and chemical properties of a new root-end filling material, J Endod 21(7) (1995) 349-53.

[22] A.D. Santos, J.C. Moraes, E.B. Araujo, K. Yukimitu, W.V. Valerio Filho, Physico-chemical properties of MTA and a novel experimental cement, Int Endod J 38(7) (2005) 443-7.

[23] A. Paula, M. Laranjo, C.M. Marto, A.M. Abrantes, J. Casalta-Lopes, A.C. Goncalves, A.B. Sarmento-Ribeiro, M.M. Ferreira, M.F. Botelho, E. Carrilho, Biodentine Boosts, WhiteProRoot((R))MTA Increases and Life((R)) Suppresses Odontoblast Activity, Materials 12(7) (2019).

[24] C.T. Lee, T.S. Chiu, S.K. Chuang, D. Tarnow, J. Stoupel, Alterations of the bone dimension following immediate implant placement into extraction socket: systematic review and meta-analysis, Journal of clinical periodontology 41(9) (2014) 914-926.

[25] V. Chappuis, O. Engel, M. Reyes, K. Shahim, L. Nolte, D. Buser, Ridge alterations post-extraction in the esthetic zone: a 3D analysis with CBCT, Journal of dental research 92 (2013) 195S-201S.

[26] M.A. Saghiri, A. Asatourian, F. Garcia-Godoy, N. Sheibani, The role of angiogenesis in implant dentistry part II: The effect of bone-grafting and barrier membrane materials on angiogenesis, Medicina Oral Patologia Oral Y Cirugia Bucal 21(4) (2016) E526-E537.

[27] T. Spinell, J. Saliter, B. Hackl, K. Unger, R. Hickel, M. Folwaczny, In-vitro cytocompatibility and growth factor content of GBR/GTR membranes, Dental Materials 35(7) (2019) 963-969.

[28] M. Trobos, A. Juhlin, F.A. Shah, M. Hoffman, H. Sahlin, C. Dahlin, In vitro evaluation of barrier function against oral bacteria of dense and expanded polytetrafluoroethylene (PTFE) membranes for guided bone regeneration, Clinical Implant Dentistry and Related Research 20(5) (2018) 738-748.

[29] J. Mir-Mari, H. Wui, R. Jung, C. Hämmerle, G. Benic, Influence of blinded wound closure on the volume stability of different GBR materials: an in vitro cone-beam computed tomographic examination, Clinical oral implants research 27(2) (2016) 258-65.

[30] S. Kuroda, K. Tanimoto, T. Izawa, S. Fujihara, J.H. Koolstra, E. Tanaka, Biomechanical and biochemical characteristics of the mandibular condylar cartilage, Osteoarthritis Cartilage 17(11) (2009) 1408-15.

[31] J.D. Harris, R.A. Siston, X. Pan, D.C. Flanigan, Autologous chondrocyte implantation: a systematic review, J Bone Joint Surg Am 92(12) (2010) 2220-33.

[32] K.H. Bridwell, P.A. Anderson, S.D. Boden, A.R. Vaccaro, J.C. Wang, What's New in Spine Surgery, J Bone Joint Surg Am 94(12) (2012) 1140-6.

[33] P. Abdel-Sayed, D.P. Pioletti, Strategies for improving the repair of focal cartilage defects, Nanomedicine (Lond) 10(18) (2015) 2893-905.

[34] G.C. Gracitelli, V.Y. Moraes, C.E. Franciozi, M.V. Luzo, J.C. Belloti, Surgical interventions (microfracture, drilling, mosaicplasty, and allograft transplantation) for treating isolated cartilage defects of the knee in adults, Cochrane Database Syst Rev 9 (2016) CD010675.

[35] J. Fang, P. Li, X. Lu, L. Fang, X. Lü, F. Ren, A strong, tough, and osteoconductive hydroxyapatite mineralized polyacrylamide/dextran hydrogel for bone tissue regeneration, Acta biomaterialia 88 (2019) 503-513.

[36] X. Fang, J. Xie, L. Zhong, J. Li, D. Rong, X. Li, J. Ouyang, Biomimetic gelatin methacrylamide hydrogel scaffolds for bone tissue engineering, Journal of materials chemistry. B 4(6) (2016) 1070-1080.

[37] X.J. Cai, J. Cai, K.N. Ma, P. Huang, L.L. Gong, D. Huang, T. Jiang, Y.N. Wang, Fabrication and characterization of Mg-doped chitosan-gelatin nanocompound coatings for titanium surface functionalization, Journal of Biomaterials Science-Polymer Edition 27(10) (2016) 954-971.

[38] C.K. Chiu, D.J. Lee, H. Chen, L.C. Chow, C.C. Ko, In-situ hybridization of calcium silicate and hydroxyapatite-gelatin nanocomposites enhances physical property and in vitro osteogenesis, Journal of Materials Science-Materials in Medicine 26(2) (2015).

[39] X.X. Fang, J. Xie, L.X. Zhong, J.R. Li, D.M. Rong, X.S. Li, J. Ouyang, Biomimetic gelatin methacrylamide hydrogel scaffolds for bone tissue engineering, Journal of Materials Chemistry B 4(6) (2016) 1070-1080.

[40] J. Xu, Y. Liu, S. Hsu, Hydrogels Based on Schiff Base Linkages for Biomedical Applications, Molecules (Basel, Switzerland) 24(16) (2019).

[41] D.Q. Li, S.Y. Wang, Y.J. Meng, Z.W. Guo, M.M. Cheng, J. Li, Fabrication of self-healing pectin/chitosan hybrid hydrogel via Diels-Alder reactions for drug delivery with high swelling property, pH-responsiveness, and cytocompatibility, Carbohydrate Polymers (2021) 118244.

[42] M.T.I. Mredha, J.Y. Na, J.-K. Seon, J. Cui, I. Jeon, Multifunctional poly (disulfide) hydrogels with extremely fast self-healing ability and degradability, Chemical Engineering Journal 394 (2020) 124941.

[43] M. Zhu, H. Jin, T. Shao, Y. Li, J. Liu, L. Gan, M. Long, Polysaccharide-based fast self-healing ion gel based on acylhydrazone and metal coordination bonds, Materials & Design 192 (2020) 108723.

[44] X. Pei, L. Fang, W. Chen, X. Wen, L. Bai, X. Ba, Facile Fabrication of Multiresponsive Self-Healing Hydrogels with Logic-Gate Responses, Macromolecular Chemistry and Physics 222(2) (2021) 2000339.

[45] J.W. Seo, S.R. Shin, M.-Y. Lee, J.M. Cha, K.H. Min, S.C. Lee, S.Y. Shin, H. Bae, Injectable hydrogel derived from chitosan with tunable mechanical properties via hybrid-crosslinking system, Carbohydrate Polymers 251 (2021) 117036.

[46] Y. Yang, X. Wang, F. Yang, L. Wang, D. Wu, Highly elastic and ultratough hybrid ionic–covalent hydrogels with tunable structures and mechanics, Advanced Materials 30(18) (2018) 1707071.

[47] M. Lykissas, I. Gkiatas, Use of recombinant human bone morphogenetic protein-2 in spine surgery, World journal of orthopedics 8(7) (2017) 531.

[48] M.R. Urist, Bone formation by autoinduction, Science 150(3698) (1965) 893-9.

[49] E.A. Wang, V. Rosen, P. Cordes, R.M. Hewick, M.J. Kriz, D.P. Luxenberg, B.S. Sibley, J.M. Wozney, Purification and characterization of other distinct bone-inducing factors, Proc Natl Acad Sci U S A 85(24) (1988) 9484-8.

[50] P.C. Bessa, M. Casal, R.L. Reis, Bone morphogenetic proteins in tissue engineering: the road from laboratory to clinic, part II (BMP delivery), J Tissue Eng Regen Med 2(2-3) (2008) 81-96.

[51] W.H. Ren, L.J. Yang, S.Z. Dong, Induction of reparative dentin formation in dogs with combined recombinant human bone morphogenetic protein 2 and fibrin sealant, Chin J Dent Res 2(3-4) (1999) 21-4.

[52] E.A. Olmsted-Davis, Z. Gugala, F.H. Gannon, P. Yotnda, R.E. McAlhany, R.W. Lindsey, A.R. Davis, Use of a chimeric adenovirus vector enhances BMP2 production and bone formation, Human gene therapy 13(11) (2002) 1337-1347.

[53] R. Aquino-Martínez, A. Angelo, F. Pujol, Calcium-containing scaffolds induce bone regeneration by regulating mesenchymal stem cell differentiation and migration, Stem cell research & therapy 8(1) (2017) 265.

[54] J. Shen, A.W. James, J.N. Zara, G. Asatrian, K. Khadarian, J.B. Zhang, S. Ho, H.J. Kim, K. Ting, C. Soo, BMP2-induced inflammation can be suppressed by the osteoinductive growth factor NELL-1, Tissue engineering. Part A 19(21-22) (2013) 2390-2401.

[55] S. Trujillo, C. Gonzalez-Garcia, P. Rico, A. Reid, J. Windmill, M.J. Dalby, M. Salmeron-Sanchez, Engineered 3D hydrogels with full-length fibronectin that sequester and present growth factors, Biomaterials 252 (2020) 120104.

[56] H.H. Fang, S.L. Yang, Y.Y. Luo, C. Zhang, Y. Rao, R.J. Liu, Y.L. Feng, J. Yu, Notoginsenoside R1 inhibits vascular smooth muscle cell proliferation, migration and neointimal hyperplasia through PI3K/Akt signaling, Scientific Reports 8 (2018).

[57] Y.L. Yu, G.B. Sun, Y. Luo, M. Wang, R.C. Chen, J.Y. Zhang, Q.D. Ai, N. Xing, X.B. Sun, Cardioprotective effects of Notoginsenoside R1 against ischemia/reperfusion injuries by regulating oxidative stress- and endoplasmic reticulum stress-related signaling pathways, Scientific Reports 6 (2016).

[58] T. Wang, D.Q. Wan, L. Shao, J.Z. Dai, C.Y. Jiang, Notoginsenoside R1 stimulates osteogenic function in primary osteoblasts via estrogen receptor signaling, Biochemical and Biophysical Research Communications 466(2) (2015) 232-239.

[59] B. Zhang, J.Y. Zhang, C.Y. Zhang, X.L. Zhang, J.X. Ye, S.H. Kuang, G.B. Sun, X.B. Sun, Notoginsenoside R1 Protects Against Diabetic Cardiomyopathy Through Activating Estrogen Receptor alpha and Its Downstream Signaling, Frontiers in Pharmacology 9 (2018).

[60] Y. Liu, Z. Lin, J. Guo, G. Xu, Y. Li, T. Xu, H. Lv, J. Chen, G. Wu, Notoginsenoside R1 significantly promotes in vitro osteoblastogenesis, Int J Mol Med 38(2) (2016) 537-44.

[61] P. Torres, M. Castro, M. Reyes, V.A. Torres, Histatins, wound healing, and cell migration, Oral Diseases 24(7) (2018) 1150-1160.

[62] M.J. Oudhoff, J.G. Bolscher, K. Nazmi, H. Kalay, W. van 't Hof, A.V. Amerongen, E.C. Veerman, Histatins are the major wound-closure stimulating factors in human saliva as identified in a cell culture assay, FASEB J 22(11) (2008) 3805-12.

[63] I.A. van Dijk, K. Nazmi, J.G. Bolscher, E.C. Veerman, J. Stap, Histatin-1, a histidine-rich peptide in human saliva, promotes cell-substrate and cell-cell adhesion, FASEB J 29(8) (2015) 3124-32.

[64] I.A. van Dijk, A.F. Beker, W. Jellema, K. Nazmi, G. Wu, D. Wismeijer, P.M. Krawczyk, J.G. Bolscher, E.C. Veerman, J. Stap, Histatin 1 Enhances Cell Adhesion to Titanium in an Implant Integration Model, J Dent Res 96(4) (2017) 430-436.

[65] D. Shah, M. Ali, D. Shukla, S. Jain, V.K. Aakalu, Effects of histatin-1 peptide on human corneal epithelial cells, PLoS One 12(5) (2017) e0178030.

[66] M.J. Oudhoff, P.A. van den Keijbus, K.L. Kroeze, K. Nazmi, S. Gibbs, J.G. Bolscher, E.C. Veerman, Histatins enhance wound closure with oral and non-oral cells, J Dent Res 88(9) (2009) 846-50.

[67] M. Castro, P. Torres, L. Solano, L.A. Cordova, V.A. Torres, Histatin-1 counteracts the cytotoxic and antimigratory effects of zoledronic acid in endothelial and osteoblast-like cells, J Periodontol 90(7) (2019) 766-774.

[68] G.Q. Huang, G.G. Yi, L.W. Wu, S.F. Feng, W. Wu, L. Peng, R.W. Yi, W. Ma, X. Lu, Protective effect of histatin 1 against ultraviolet-induced damage to human corneal epithelial cells, Exp Ther Med 15(1) (2018) 679-684.

[69] P. Torres, J. Diaz, M. Arce, P. Silva, P. Mendoza, P. Lois, A. Molina-Berrios, G.I. Owen, V. Palma, V.A. Torres, The salivary peptide histatin-1 promotes endothelial cell adhesion, migration, and angiogenesis, FASEB J 31(11) (2017) 4946-4958.

[70] P.M. van der Kraan, E.N. Blaney Davidson, W.B. van den Berg, Bone morphogenetic proteins and articular cartilage: To serve and protect or a wolf in sheep clothing's?, Osteoarthritis Cartilage 18(6) (2010) 735-41.

[71] R. Zhao, X. Liu, L. Zhang, H. Yang, Q. Zhang, Current Progress of Research on Neurodegenerative Diseases of Salvianolic Acid B, Oxidative medicine and cellular longevity 2019 (2019) 3281260.

[72] Y. Wu, S. Xu, X.Y. Tian, The effect of salvianolic acid on vascular protection and possible mechanisms, Oxidative Medicine and Cellular Longevity 2020 (2020).

[73] X. Zhang, L. Zou, J. Li, B. Xu, T. Wu, H. Fan, W. Xu, W. Yao, Y. Yang, Y. Liu, L. Cui, Salvianolic acid B and danshensu induce osteogenic differentiation of rat bone marrow stromal stem cells by upregulating the nitric oxide pathway, Experimental and therapeutic medicine 14(4) (2017) 2779-2788.

[74] Y. Bian, J. Xiang, Salvianolic acid B promotes the osteogenic differentiation of human periodontal ligament cells through Wnt/β-catenin signaling pathway, Archives of oral biology 113 (2020) 104693.

[75] D. Xu, L. Xu, C. Zhou, W. Lee, T. Wu, L. Cui, G. Li, Salvianolic acid B promotes osteogenesis of human mesenchymal stem cells through activating ERK signaling pathway, The international journal of biochemistry & cell biology 51 (2014) 1-9.

[76] J.B. Leach, K.A. Bivens, C.N. Collins, C.E. Schmidt, Development of photocrosslinkable hyaluronic acid-polyethylene glycol-peptide composite hydrogels for soft tissue engineering, Journal of Biomedical Materials Research Part A 70A(1) (2004) 74-82.

[77] P. Zhai, X. Peng, B. Li, Y. Liu, H. Sun, X. Li, The application of hyaluronic acid in bone regeneration, International journal of biological macromolecules 151 (2020) 1224-1239.

[78] A. Baldini, D. Zaffe, G. Nicolini, Bone-defects healing by high-molecular hyaluronic acid: preliminary results, Annali di stomatologia 1(1) (2010) 2.

Chapter 2

Notoginsenoside R1 functionalized gelatin hydrogels to promote reparative dentinogenesis

Lei Wang[#], Hui Fu[#], Wenwen Wang[#], Yi Liu, Xumin Li, Jijing Yang, Lingli Li[*], Gang Wu[*,&], Yihuai Pan[*,&]

* : Corresponding authors
# : These authors contributed equally to this work.
& : These authors shared last authorship.

ABSTRACT

Pulp-capping materials are commonly adopted in the clinic to form reparative dentin and thus protect dental pulp tissues from cases of deep caries, accidentally exposed pulps or partial pulpotomy. Some traditional pulp capping materials used in the clinic include calcium hydroxide and mineral trioxide aggregates. However, there are limitations to thin restorative dentin, and a long period of time is needed to cause degenerative changes in dental pulp. In this paper, injectable colloidal gels were developed to induce the formation of reparative dentin through a simple UV method from methacrylic acid functionalized gelatin loaded with notoginsenoside R1 (Gel-MA/NGR1). The results of the physicochemical property examinations showed that the prepared Gel-MA/NGR1 hydrogel possessed an appropriate interconnected porous microarchitecture with a pore size of 10.5 micrometres and suitable mechanical properties with a modulus of 50-60 kPa, enabling cell adhesion and proliferation. The hydrogel remained hydrophilic with sustained drug release performance. In addition, Gel-MA/NGR1 significantly enhanced the odontogenetic differentiation of mouse dental papilla cells by elevating the expression levels of the dentinogenic markers ALP and OCN and extracellular matrix mineralization. *In-vivo* stimulation was carried out by injecting the precursors into the predrilled alveolar cavity of Sprague-Dawley rats followed by immediate *in-situ* UV crosslinking. The results showed that Gel-MA/NGR1 has a strong capacity to promote reparative dentin formation. Haematoxylin & eosin, Masson, and immunohistochemical staining (DMP-1, DSPP, OCN and RunX2) and micro-CT were employed to illustrate the effectiveness of dentinogenesis, and the relative volumes of calcification were found to have increased ~175-fold. All of the results showed that the Gel-MA/NGR1 hydrogel promoted reparative dentin formation, which suggests that this hydrogel provides great potential as a pulp-capping material to induce dentin formation.

Keywords: Pulp-capping material; Methacrylated gelatin; Reparative dentin; Dentinogenesis; Notoginsenoside R1

GRAPHICAL ABSTRACT
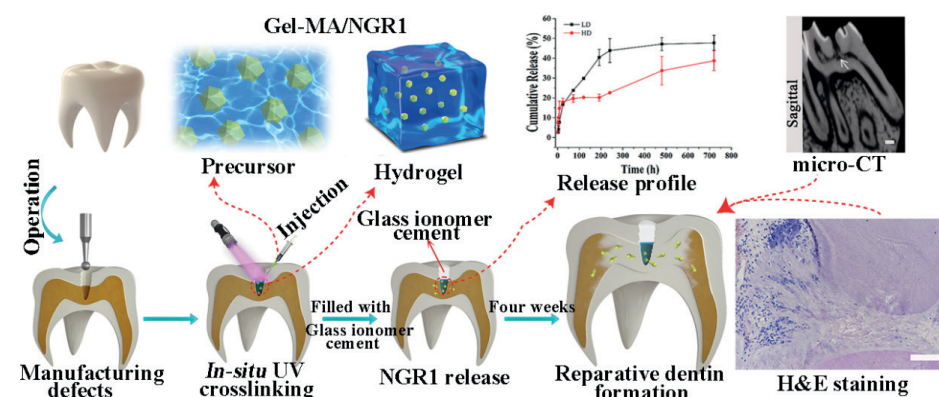
1. INTRODUCTION

Dental pulp is a highly vascularized and innervated connective tissue that provides nutritive, protective, defensive and formative functions to teeth [1]. Dental pulp is also highly sensitive and vulnerable to pathogenic stimuli such as bacteria, bacterial products and injury. When exposed to these stimuli from deep caries or trauma, dental pulp may rapidly develop into reversible and then irreversible pulpitis, which leads to pulpal necrosis and periapical inflammation [2] as well as potential systemic complications, such as osteomyelitis [3] and bacteraemia [4].

To maintain the vitality of dental pulp tissue, pulp-capping materials have been adopted in the clinic to cover nearly exposed, accidentally exposed or partially infected pulp [5]. A pulp-capping material should meet a series of basic requirements, such as a short setting time, adhesion to the tooth substrate, non-carcinogenicity and biocompatibility. Furthermore, an ideal pulp-capping material should be bioactive to pacify the inflammation of the dental pulp and stimulate the formation of reparative dentin, which enables the complete isolation of dental pulp from pathogens, thereby keeping the dental pulp vital. Calcium hydroxide has long been used as a pulp-capping material and was previously used as one of the gold standard therapies [6]. Additionally, it is frequently used as a positive control to test new materials [7]. However, the use of calcium hydroxide is associated with a series of clinical concerns, such as high solubility, poor mechanical properties and "tunnel defects" [7]. As an alternative, mineral trioxide aggregate (MTA) has shown more favourable results than calcium hydroxide in the clinic and is currently considered a gold-standard treatment option [6, 8, 9]. However, the use of MTA is also

associated with concerns, such as discolouration [10], a long setting time [11] and handling difficulties [12]. Consequently, continuous efforts have been made in an attempt to develop alternative pulp-capping materials [6].

Among these attempted alternative materials, photo-crosslinkable hydrogels show promising properties, such as realistic handling and good biocompatibility [13]. One major advantage of hydrogels over calcium phosphate-based materials is that hydrogels may act as a controlled drug delivery system for various bioactive agents, thereby conferring hydrogels with various potent functions [13]. Methacrylated gelatin (Gel-MA) is a hydrolyzed form of collagen, and has the same chemical composition as collagen, a major component in the extracellular matrix of dental pulp, which bears good biocompatibility without the risk of pathogen transmission that is found with collagen [14]. Gelatin contains many adhesive ligands, such as arginine-glycine-aspartic acid sequences, which promote cell adhesion and migration [15]. The good cytocompatibility of Gel-MA can also be suggested by its capacity to support human dental pulp stem cells and human umbilical vascular endothelial cells for dental pulp tissue regeneration [16]. Gel-MA bears a good capacity to bond to mineralized tissue through non-covalent bonding mechanisms [17], such as molecular interactions [18]. Its bonding strength may also be further enhanced by amino lysis [19], which can be facilitated by the weak acidic environment of irritated dental pulp. The fluidity of Gel-MA enables the complete coverage of exposed dental pulp. Immediately after a short photo-crosslinking time, Gel-MA can transform from a liquid to a hydrogel and reach a stiffness of 50-60 kPa, which is favourable for extracellular matrix mineralization and hard tissue formation [20]. To meet the other requirements of a pulp-capping material, the physicochemical properties of Gel-MA can be easily modulated through corresponding modifications, such as filling with inorganic nanoparticles to increase mechanical properties [21] and radiopacity [22]. However, Gel-MA still lacks the intrinsic capacity to pacify inflammation and induce dentinogenesis. This problem may be tackled by carrying bioactive agents to functionalize Gel-MA.

One promising bioactive agent is notoginsenoside R1 (NGR1), a bioactive monomer isolated from *Panax notoginseng* [23]. NGR1 has been widely used for the clinical treatment of cardiovascular diseases [24] and osteoporosis [25]. NGR1 can protect cells from inflammation and apoptosis by reducing NADPH (nicotinamide adenine dinucleotide phosphate) oxidase and mitochondrion-derived superoxide via oestrogen receptor-dependent activation of Akt/Nrf2 (nuclear factor-erythroid 2 p45-related factor 2) pathways [26]. On the other hand, our previous finding showed that NGR1 can dramatically promote the expression of osteocalcin (OCN) (a late dentinogenic differentiation marker) and extracellular matrix mineralization [27]. Our preliminary studies showed that NGR1 could also potently induce extracellular matrix mineralization

(a final dentinogenic differentiation marker) in odontoblast-like cells and human primary dental pulp stem cells. This finding suggested the promising application potential of NGR1 in pulp-capping therapy [8].

In the current study, we developed a photo-crosslinkable Gel-MA/NGR1 composite hydrogel as an alternative pulp-capping material with the potent abilities to pacify inflammation and induce reparative dentinogenesis. We investigated the physicochemical properties of Gel-MA/NGR1 and its efficacy to induce *in-vitro* dentinogenesis and *in-vivo* reparative dentin formation.

2. MATERIALS AND METHODS

2.1 Materials
Gelatin (from porcine skin, type A, ~300 g Bloom) was purchased from Sigma-Aldrich (USA). Methacrylic anhydride (MAA) and the photoinitiator Irgacure 2959 (I2959) were purchased from Sigma Chemical Co. (St. Louis, MO, USA). NGR1 ($C_{47}H_{80}O_{18}$, molecular weight = 933.13, purity ≥ 98%) was purchased from Nanjing Zelang Biological Technology Co., Ltd. (Nanjing, Jiangsu, China).

2.2 Hydrogel preparation
First, Gel-MA was synthesized according to our previous report [28]. The modification details can be found in the Supplementary Materials (Materials and Methods 1.1). Second, the as-prepared Gel-MA was dissolved in phosphate-buffered saline (PBS) to obtain 10%, 15% and 20% (w/v) precursor solutions. Predefined amounts of Gel-MA and 0.5 wt% photoinitiator I2959 (50 mg/mL in 75% ethanol solution) were mixed by vortexing for 30 seconds followed by full exposure to UV light (ZF-7A, Shanghai Jihui Scientific Analyze Instrument Co., Ltd., China). The NGR1-loaded hydrogels (HD: high drug loading, LD: low drug loading, ND: no drug loading) were prepared by adding NGR1 (1000 mg/mL in dimethyl sulfoxide) to the precursor solution (Table S1).

2.3 Characterization
1H-NMR spectra of gelatin and Gel-MA were recorded on a Bruker AVANCE III HD 600 spectrometer (Bruker, Germany) at 600 MHz. Attenuated total reflection Fourier transform infrared spectroscopy (ATR-FTIR) was recorded on a Bruker Tensor II (Bruker, Germany) over the range of 400-4000 cm^{-1} with 2 cm^{-1} resolution. Scanning electron microscopy (SEM) images of the hydrogels were observed using a scanning electron microscope (Nova NanoSEM200, FEI, USA). The prepared hydrogels (Φ 8 mm, distilled water was used as solvent when fabricating the SEM samples) were lyophilized for 48 hours and sputter-coated with gold for 60 seconds before observation. The surface

chemical elements of NGR1-loaded Gel-MA hydrogels (ND, LD, and HD) were analysed by X-ray photoelectron spectroscopy (XPS) (AXIS ULTRA DLD, Shimadzu, Japan) with a standard magnesium X-ray source (1253.6 eV).

2.4 *In-vitro* biocompatibility

The biocompatibility of the hydrogels was evaluated by directly embedding mouse dental papilla cells (mDPC6T) onto the hydrogels. In brief, the hydrogels (Gel-MA was sterilized by ethylene oxide and dissolved in sterilized PBS) were UV crosslinked *in situ* in 96-well plates, followed by seeding mDPC6T cells at a density of 1000 cells per well without cytokines. At pre-determined time points (days 1, 4, and 7), samples were rinsed with PBS and incubated with Cell Counting Kit-8 reagent (CCK-8, Beyotime Biotechnology, Shanghai, China) for 3 hours at 37 °C in the dark. OD values were measured using an ELISA plate reader (Varioskan LUX, Thermo Fisher, USA).

Furthermore, a Live/Dead assay (Life Technologies, USA) was applied to estimate the viability of the cells on the hydrogels. Briefly, mDPC6T cells were seeded onto the preformed hydrogels at a density of 1000 cells per well in 96-well TCPs. At specific time points, cells were stained with a Live/Dead Viability Cytotoxicity Kit, which the reagent is cleaved by metabolically active cells to yield green fluorescence, while dead cells produce red fluorescence. Samples treated with 75% ethanol for 10 minutes were used as positive controls and normal medium (90% DMEM + 10% FBS +1% penicillin-streptomycin) in TCPs were the negative controls. All samples were incubated in Live/Dead dye solution (0.25 μL of calcein-AM dye and 1.0 μL of ethidium homodimer-1 dye in 0.5 mL of PBS) for 30 minutes. After incubation, the samples were washed with PBS 3 times and observed under a DMi8 microscope (LEICA, Germany). All experiments were performed in triplicate.

2.5 Rheological study and other physical and chemical property studies

The rheological measurements were performed using a Discovery HR-2 rheometer (TA Instruments, USA) with a flat plate of 8 mm diameter and a gap of 1 mm. Detailed measurements can be found in the Supplementary Materials. Equilibrium water content (EWC), *in-vitro* biodegradation, water wettability, and *in-vitro* NGR1 release studies were performed, and the procedures are shown in the Supplementary Materials.

2.6 *In-vitro* dentinogenic differentiation assays

The precursors were UV-crosslinked in 48-well plates, and 3×10^4 mDPC6T cells were cultured onto the hydrogels. After 17 days of culture, we evaluated dentinogenic markers, such as the expression levels of alkaline phosphatase (ALP, an early dentinogenic differentiation marker) and osteocalcin (OCN, a late dentinogenic differentiation marker). The cells were fixed in 4% paraformaldehyde followed by a reaction with ALP

staining solution (Yeasen, Shanghai, China) for 20 minutes. The ALP-positive cells were stained blue and visualized by microscopy. The supernatant was collected and assessed with an OCN ELISA kit (NJJCBIO Co., Ltd, Nanjing, China). The extracellular matrix mineralization nodules—the final dentinogenic differentiation marker—were stained using an Alizarin red staining (ARS) kit (Cyagen, Guangzhou, China). Briefly, after 17 days of incubation, the hydrogel constructs were rinsed 3 times with PBS, fixed with 95% ethanol for 15 minutes, washed with distilled water 3 times and finally stained using Alizarin red staining solution for 1 hour at 37 °C. Stained samples were washed with distilled water 3 times, with each wash lasting one minute. Pictures of the top surface were taken using an optical microscope (Nikon, Japan). The calcified areas were photographed and then quantified using Image-Pro Plus 6.0 software (Media cybernetics, USA). For these experiments, dentinogenic induction medium (DM) without the presence of NGR1 or Gel-MA (Cyagen, Guangzhou, China) was used as control.

2.7 Evaluation of mRNA expression using real-time PCR

Odontoblast markers were detected by RT-qPCR. mDPC6T cells were seeded at 3×10^4 cells/well in 48-well plates. The mRNA expression levels of the dentinogenic genes alkaline phosphatase (ALP) and osteocalcin (OCN) were assessed by RT-qPCR (Bio-Rad CFX96, Bio-Rad Laboratories, Inc., USA). RNA was extracted from the samples and control groups using TRIzol reagent (Invitrogen, Thermo Fisher Scientific, Inc.). Complementary (c) DNAs were synthesized with 1 μg of total RNA and an oligo-dT primer using a Superscript II kit (Invitrogen, Molecular Probes, Eugene, OR). DNA was digested with gDNA Eraser (Takara, Otsu, Japan). RT-qPCR was performed with the SYBR Premix Ex Taq TM II kit (Takara Bio, Inc., Otsu, Japan). Briefly, the total reaction volume was 25 μL, and RT-qPCR was performed using 40 cycles with 10 minutes of denaturation at 95 °C, 15 seconds of annealing at 95 °C and 1 minute of extension at 60 °C. The relative expression level of each gene was normalized to ACTIN, and relative quantification of gene expression was performed using the $2^{-\Delta\Delta Cq}$ method.

2.8 *In-vivo* modified pulp-capping model in rats

To further verify the *in-vivo* ability to induce dentinogenesis and test the biocompatibility of the hydrogels, 4-week-old Sprague-Dawley rats weighing 200-300 g were used to create a modified pulp-capping model. In the current modified model, we extended the location of implantation to the bottom of the dental pulp chamber to enlarge the contact area, thus making the subsequent evaluations much easier. The maxillary first and second molars were chosen for surgery with $n = 6$ animals per group. Power analysis was performed to confirm the sufficiency of the sample size according to our data. The protocol of the study was approved by the ethics committee of the Animal Research Center of Wenzhou Medical University (wydw2017-0503). The animal model was chosen in accordance with the protocol for pulp capping for new material evaluation [29]. The rats were sedated

thirty minutes prior to the experimental surgery with trichloroacetaldehyde hydrate (10%, 3 mL/kg) (Solarbio, Beijing, China). The surgical procedure was as follows: 1) the central fossae of the first and second maxillary molars were drilled with a 1/4 rounded carbide bur (0.5 mm diameter, SS White Burs Inc., USA) to form a bowl-shaped cavity with a depth of approximately 1 mm followed by cooling with physiological saline. 2) An occlusal cavity was obtained by a dental reamer (20#, Maillefer Dentsply, Switzerland), and the cameral pulp parenchyma was removed with a rotary instrument. The cavity was first irrigated with 2% sodium hypochlorite (Longly biotechnology, Wuhan, China) followed by 2% chlorhexidine (Lircon, Dezhou, China), and haemostasis was performed with a sterilized cotton ball. Simultaneously, 100 mg/mL Gel-MA@NGR1 hydrogel (ND, LD, and HD) precursors were prepared as mentioned in section 2.2. 3) The precursors were aspirated in 1 mL syringes, and 100 µL was injected into each selected tooth with a 26-gauge syringe needle and immediately exposed to UV light (365 nm, 90 mW/cm² — a non-harmful radiation dosage [30, 31]) for crosslinking for 3 minutes. The above procedures were performed in dark. Dycal (Dentsply, Germany) was used as a control. The occlusal cavities in all groups were sealed with glass ionomer cement (GC, Fuji II, Japan), a calcium silicate-based restorative cement [32]. We retrieved the samples four weeks after transplantation. Four weeks is one of the most commonly used time points to evaluate the inducing effects of pulp-capping materials [32-35]. At this time point, the newly formed reparative dentin will be easily detected since dentinogenesis starts as early as 3 days after pulp-capping therapy [36]. Consequently, in our study, this time point was selected to illustrate the dentinogenic efficacy of Gel-MA/NGR1 in comparison with other materials. The rats were sacrificed under general anaesthesia by transcardial perfusion with 4% paraformaldehyde, and tooth samples were extracted and fixed in 4% paraformaldehyde for further analysis. To sufficiently fix the tissues, the restorative materials were removed to ensure complete penetration of the fixing solution into the dental pulp [37].

2.9 Micro-computed tomography imaging and analysis

All harvested teeth were scanned *ex vivo* 28 days after surgery with an X-ray micro-computed tomography (micro-CT) device (SkyScan 1176; Bruker, Germany). The micro-CT parameters were as follows: 20 × 10 mm field of view, 9 µm voxel size, Al 1 mm, 65 kV, 381 µA, and 46 minutes of exposure time. All data sets were 3-dimensionally reconstructed with NRecon software (Version 1.6.10.4) and exported in BMP format. Newly formed hard tissue (dentin bridge) was extracted from the surrounding tissue (tooth structure) with VGStudio Max (Version 1.2.1) software, in which a magic bar was used to automatically trace the edge of irregular mineralization in the pulp chamber followed by further margin correction by two experienced physicians. The above calculation was repeated three times. The quantitative morphometric characterization and the density of the hard tissue were analysed with CT Analyser software (version 1.15.4). These measurements were repeated five times.

2.10 Histological and immunohistochemical staining

After micro-CT scanning, samples were decalcified in 10% ethylenediaminetetraacetic acid (EDTA), which was changed twice per week for 3 weeks followed by dehydration in a series of graded concentrations of ethanol from 70% to 100%. Paraffin embedding was subsequently performed with the long axis parallel to the base plane. Longitudinal serial sections, 4 mm thick, were cut and mounted onto polylysine-coated microscope slides and then subjected to haematoxylin eosin (HE) staining, Masson staining and immunohistochemistry (IHC) staining to detect the morphology and levels of dentinogenic gene (dentin sialophosphoprotein (DSPP), 1:200 dilution, sc-73632; dentin matrix protein 1 (DMP-1), 1:200 dilution, sc-73633; osteocalcin (OCN), 1:200 dilution, sc-390877; and Runt-related transcription factor 2 (RunX2), 1:200 dilution, sc-101145, Santa Cruz Biotechnology) expression. Staining was performed according to the manufacturer's protocols. Finally, examination under microscopic light by using an Olympus DP71 microscope was performed (Olympus Co., Japan). The mean option density of IHC staining was calculated by ImageJ software (version 1.51j8, National Institute of Health, USA).

STATISTICAL ANALYSIS

The results are presented as the mean ± standard deviation (SD). Comparisons were made using analysis of variance (ANOVA) for multiple comparisons with Tukey's post hoc analysis for parametric data. Nonparametric tests were carried out using Kruskal–Wallis ANOVA with Dunn's post hoc analysis. Statistical significance was accepted for $p < 0.05$.

3. RESULTS

3.1 Gel-MA hydrogel preparation and chemical structure analysis

The two new peaks at 5.34 ppm and 5.60 ppm in the ^{1}H-NMR spectrum of Gel-MA represented the acrylic double bonds (Figure 1a, b), which showed the methacrylation of gelatin [28]. The calculation of the integral area ratio of a characteristic peak to a specified peak [38] showed that the degree of methacrylation was 25.10%. In the FTIR spectra (Figure 1c), the incisive absorption peaks at 1650 cm^{-1} and 1552 cm^{-1} corresponded to the C = O and C-N-H stretching vibrations, respectively, which indicated the presence of double bonds in Gel-MA [39]. In addition, the absorption peak from the hydroxyl group near 3400 cm^{-1} became acute in the spectrum of Gel-MA, which represented a reduced number of hydrogen bonds due to the consumption of amino groups in gelatin after the reaction with methylacrylate acid. The gelatinization process is shown in Figure 1d. The injectable Gel-MA solution was crosslinked with the aid of I2959 and uninjurious UV irradiation. No significant shrinkage occurred during the photopolymerization (Figure 1e).
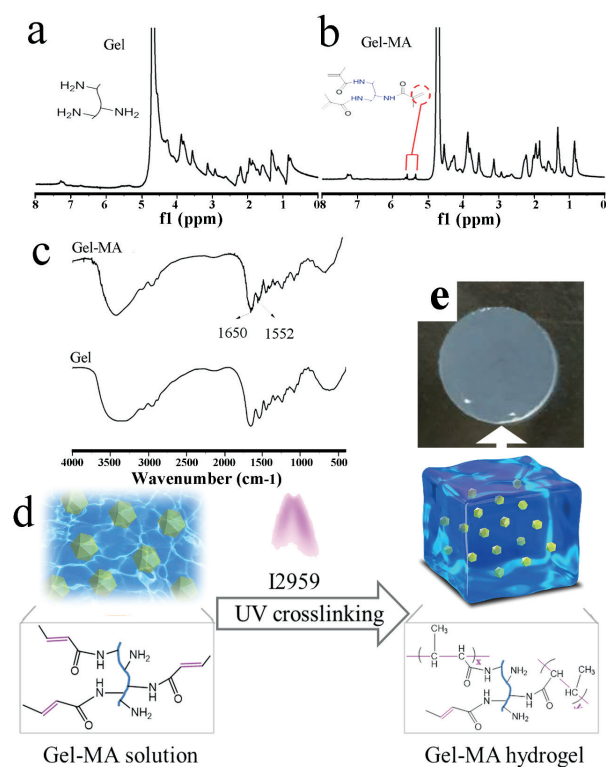

Figure 1. a-b) Modification of gelatin confirmed by ^{1}H-NMR. c) FTIR spectra of Gel-MA and Gel. d) Diagram of the UV crosslinking process. e) Photograph of the crosslinked Gel-MA hydrogel.

3.2 NGR1 could induce extracellular matrix mineralization in mDPC6T odontoblast-like cells

Seven days after treatment, 50 and 500 µg/mL NGR1 were associated with a significantly greater number of extracellular matrix mineralization nodules (3.6- and 2.8-fold, respectively) than the control group (Figure 2a, b). Furthermore, NGR1 at 50 µg/mL showed significantly higher efficacy than NGR1 at 500 µg/mL.
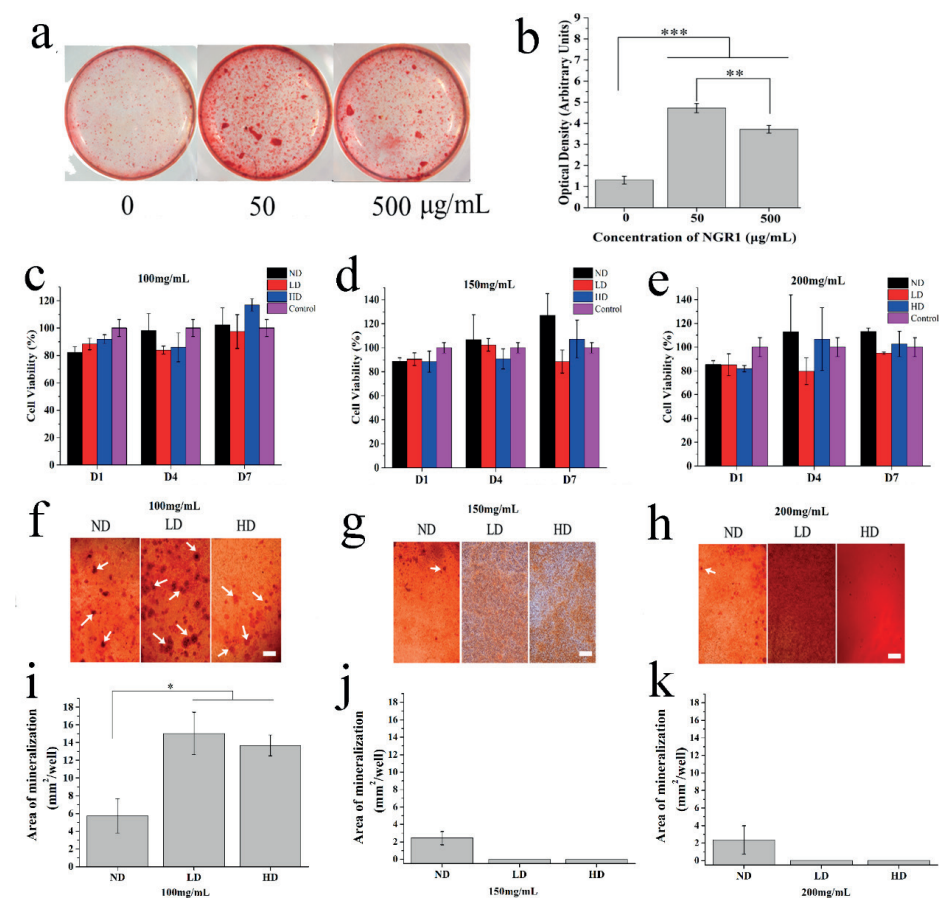

Figure 2. a) Alizarin red staining of the *in-vitro* dentinogenic differentiation of pure NGR1 on mDPC6T cells after 7 days of mineralization. b) Statistical analysis of extracellular matrix mineralization nodules stained by Alizarin red. c-e) *In-vitro* cell viability of the Gel-MA/NGR1 hydrogels over 7 days (CCK-8 assay, mean ± SD). f-h) Alizarin red staining of the *in-vitro* dentinogenic differentiation of mDPC6T cells on the Gel-MA/NGR1 scaffolds after 17 days of mineralization induction cultured on 100 mg/mL, 150 mg/mL and 200 mg/mL hydrogels (bar = 200 µm). i-k) Statistical analysis of extracellular matrix mineralization nodules stained by Alizarin red.

3.3 *In-vitro* biocompatibility of the NGR1-loaded hydrogels

The cell viabilities of the hydrogels in the ND groups with solid contents of 100 mg/mL, 150 mg/mL and 200 mg/mL were all higher than 80% that of the control (cells cultured on well plates) (Figure 2c, d). Thereafter, we further inspected the *in-vitro* biocompatibility of Gel-MA incorporating different amounts of NGR1 (Table S1). The viabilities of mDPC6T odontoblast-like cells in both the LD and HD groups were also higher than 80% of those in the control group (cells cultured on well plates) at 1, 4 and 7 days after treatment (Figure 2c-e).

3.4 Screening for the optimal combination of Gel-MA and NGR1

To screen the optimal combination of NGR1 (ND, LD and HD) and Gel-MA (with solid contents of 100, 150 and 200 mg/mL) to induce *in-vitro* dentinogenesis, we assessed the extracellular matrix mineralization of mDPC6T odontoblast-like cells on various Gel-MA/NGR1 hydrogels both qualitatively (Figure 2f-h) and quantitatively (Figure 2i-k). Our results showed that without NGR1, Gel-MA at different solid contents showed no significant differences in the number of extracellular matrix mineralization nodules (Figure 2i-k). For Gel-MA with a solid content of 100 mg/mL, the presence of NGR1 (both LD and HD) significantly promoted the extracellular matrix mineralization of mDPC6T cells in comparison with ND (Figure 2i). In contrast, NGR1 failed to promote mineralization for the Gel-MA hydrogels with solid contents of 150 and 200 mg/mL (Figure 2j, k, *p* >0.05). Therefore, we chose 100 mg/mL Gel-MA with LD and HD NGR1 in the following experiments.

3.5 Chemical structure and physical performance of the NGR1-loaded hydrogels

We further explored the potential influence of NGR1 on the physicochemical properties of Gel-MA. Figure 3a shows the frequency sweeps for the ND, LD and HD hydrogels. The storage modulus (G') was parallel to and higher than the corresponding loss modulus (G") for each hydrogel. Furthermore, the storage modulus (G') was also independent of the frequency for all hydrogels. The addition of NGR1 significantly increased the storage modulus (G') by an order of magnitude from 811 ± 21 Pa for ND to 52 ± 2 KPa for LD and 56 ± 2 KPa for HD (Figure 3b). Moreover, the water uptake, *in-vitro* biodegradation, morphology, pore size, WCA, crosslinking intensity and NGR1 release properties (Figures S1-S3) are shown and described in the Supplementary Materials.
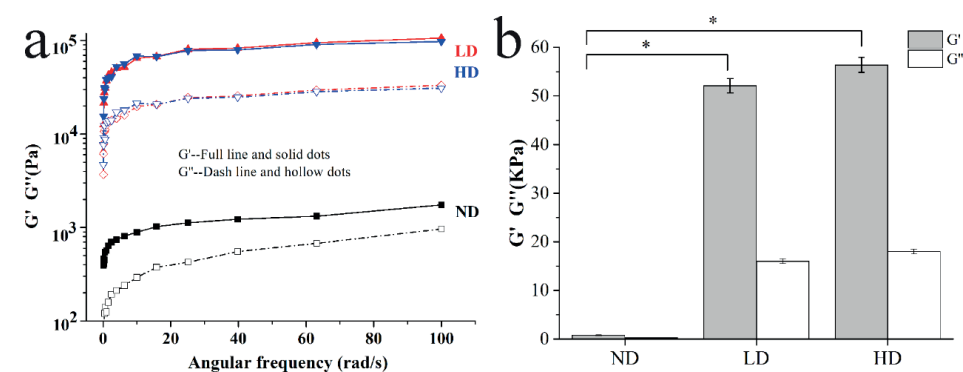

Figure 3. Rheological performance. a) G' and G" as a function of angular frequency at 37 °C. b) Statistical results of the modulus.

3.6 *In-vitro* dentinogenesis on Gel-MA/NGR1

A CCK-8 assay was performed to ascertain the biocompatibility of Gel-MA/NGR1 (Figure 4a). The OD value increased significantly with increasing culture time for all groups (p<0.01), from 0.14 ± 0.00 to 0.53 ± 0.02. In addition, the Live/Dead assay showed that mDPC6T cells attached well onto or into the hydrogels, presenting a wide-spreading morphology after a 48-hour culture and the cell density increased noticeably after a 5-day culture compared to the control group. Only very little red fluorescence was observed in the hydrogel groups, which indicated that there was not a significant number of dead cells in the ND, LD or HD groups (Figure 4b).

Irrespective of NGR1 dose, ALP gene expression in all the Gel-MA groups (ND, LD and HD) was significantly higher than that in the DM group (Figure 4c). The LD group showed an ALP mRNA expression level similar to that of the ND group, while the HD group displayed a significantly lower mRNA expression level of ALP than the LD and ND groups. A similar pattern was also found for ALP staining (Figure 4d). The mRNA expression levels of OCN in the LD and HD groups were 3.3 ± 0.3-fold and 2.5 ± 1.2-fold higher than that in the DM group, respectively (Figure 4e). Consistently, the OCN protein expression level in the LD group was similar to that in the HD group and was significantly higher than those in the ND and DM groups (Figure 4f).
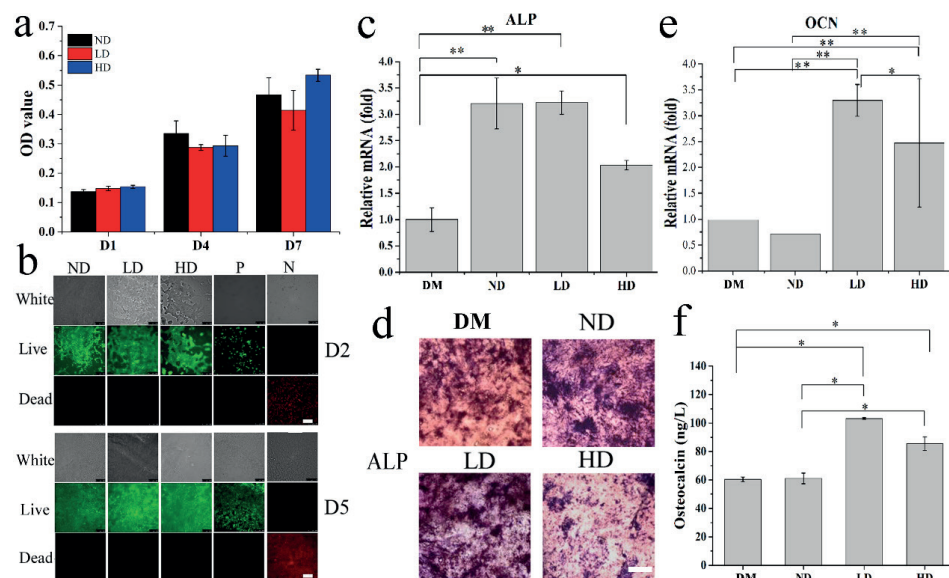
Figure 4. a) Cell proliferation of mDPC6T cells cultivated on the hydrogels after 1, 4 and 7 days by CCK-8 quantitative analysis, *p<0.05. b) Representative Live/Dead fluorescence images of mDPC6T cells encapsulated in the hydrogels after 2 and 5 days of culture (live cells: green; dead cells: red; bar = 250 μm). c) Relative mRNA expression of ALP in mDPC6T cells encapsulated in 100 mg/mL Gel-MA/NGR1 hydrogels after 7 days of mineralization induction culture (**$P<0.01$, *$P<0.05$). d) ALP staining after 17 days of mineralization induction culture on the LD, ND, HD hydrogels (bar = 200 μm). e) Relative mRNA expression of OCN in mDPC6T cells encapsulated in 100 mg/mL Gel-MA/NGR1 hydrogels after 7 days of mineralization induction culture (**$P<0.01$, *$P<0.05$). f) Osteocalcin concentration in the supernatants of the mDPC6T-encapsulated 100mg/mL Gel-MA/NGR1 hydrogels tested by ELISA.

3.7 Micro-CT analysis

The micro-CT results (Figure 5a) showed almost no newly formed mineralization area in the blank control group (BC, without any pulp capping material). In contrast, calcified shadows (white arrows) were detected surrounding the location of the injected materials in the other groups, e.g., Dycal control (DC) (positive control), ND, LD and HD groups. The relative volume of calcification in the ND group was 25 ± 6-fold that of the BC group (Figure 5b). The relative volumes of calcification in the LD group (155 ± 7-fold) and HD group (175 ± 22-fold) were significantly higher than those in the DC group (90 ± 8-fold), as presented in Figure 5b.
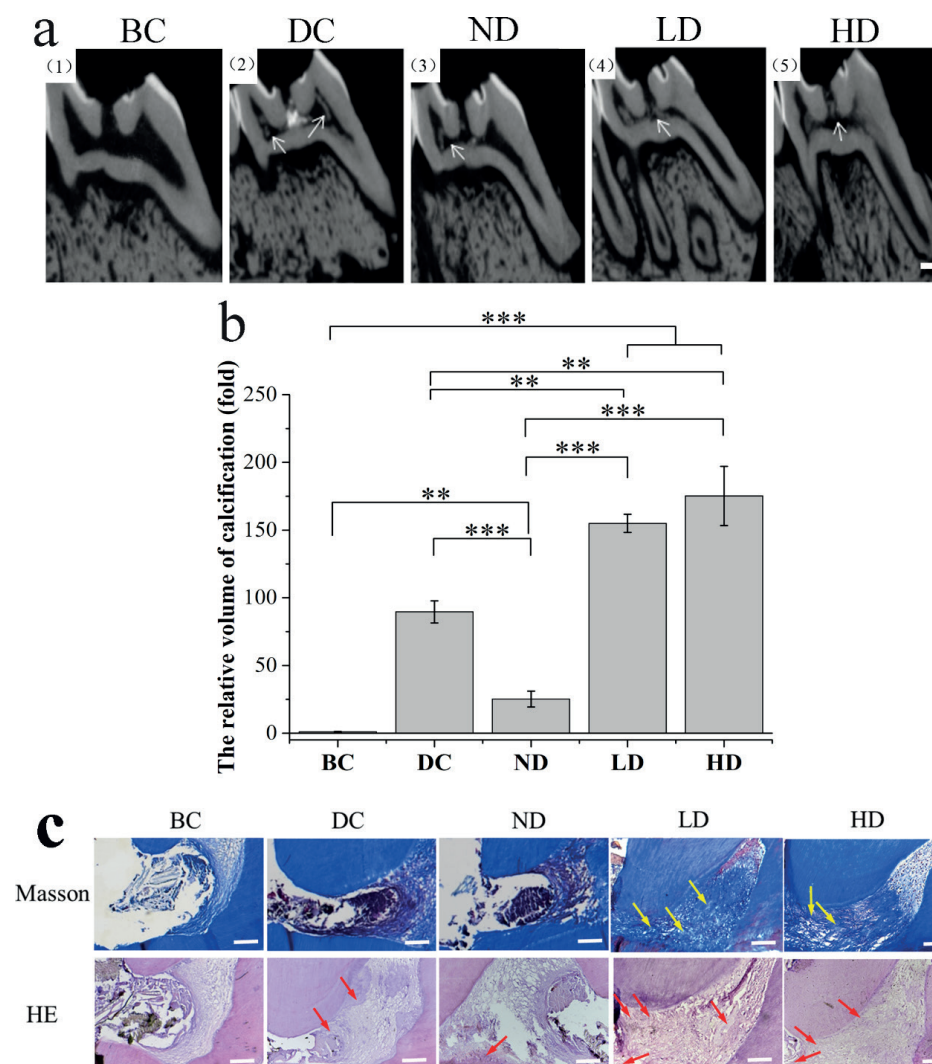
Figure 5. a) Micro-CT images of the surgical site of different samples via sagittal view on day 28 after surgery (BC: blank control, DC: Dycal control, ND: pure hydrogel, LD: hydrogel with low drug loading, HD: hydrogel with high drug loading; the white arrows represent the newly formed mineralized tissue; bar = 200 μm). b) Statistical relative volume of calcification based on the micro-CT results and analysed with CT Analyzer software (version 1.15.4) (*$P<0.05$, **$P<0.01$, ***$P<0.001$). c) Representative images from HE and Masson staining slices (at 28 days) of the control and Gel-MA/NGR1 groups (BC: blank control, DC: Dycal control, ND: pure hydrogel, LD: hydrogel with low drug loading, HD: hydrogel with high drug loading; red arrows represent the reparatively formed dentin; bar = 100 μm).

3.8 HE and IHC analyses

Figure 5c shows the HE and Masson staining results. Immediately after surgery (Figure S4a-d), histological processing was performed to identify the distribution of the hydrogels within the teeth (Figure S4g) with uninjured teeth (Figure S4e) and unfiled teeth (Figure S4f) as controls. The porous hydrogel reached the bottom of the pulp chamber and formed a broad interface with the dental pulp on the lateral sides (Figure S4g). The results showed that the precursors were loaded into the drilled sites and crosslinked, verifying the successful establishment of the *in-vivo* animal model. All animals were healthy after surgery and did not suffer from tooth necrosis. Masson staining showed a much less dense gelatinous network structure in the LD and HD groups, which might have resulted from the biodegradation of the implanted hydrogel (Figure 5c). In the three non-NGR1-containing groups (BC, DC and ND), the border of the dental pulp tissue surrounding the implantation sites moved towards the lateral sides, which may be caused by necrosis of the dental pulp tissues. In contrast, such a phenomenon was not detected in the LD and HD groups. Instead, bright blue staining (yellow arrows) was detected in the dental pulp tissues in the vicinity of the implanted hydrogels, which indicated the formation of mineralized tissue (Figure 5c). HE staining showed much more newly formed reparative dentin-like tissue (red arrows) in the DC, LD and HD groups than in the BC and ND groups. Immunohistochemical staining of DMP-1, OCN, DSPP and RunX2 and their quantitative analyses are shown in Figure 6. Light micrographs showed that much larger areas with deeper staining were detected in the dental pulp tissues surrounding the implanted sites in the DC, LD and HD groups than in the BC and ND groups. The mean option densities of the four markers in the LD and HD groups were higher than that in the DC group, while few proteins were expressed in the BC and ND groups, as displayed in Figure 6. LD was associated with the highest mean optical densities for all dentinogenic markers among all the selected groups.
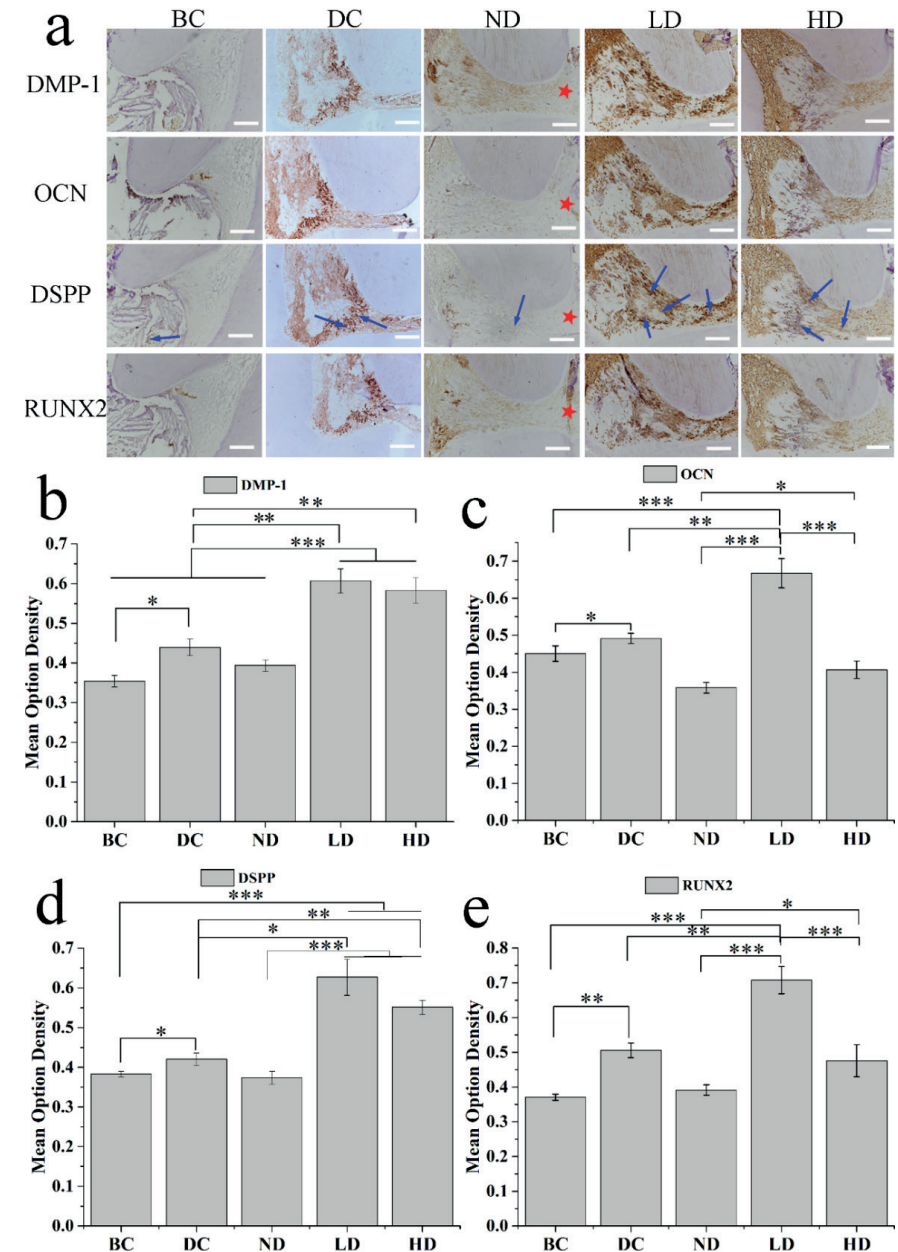
Figure 6. a) Representative histological images of DMP-1, OCN, DSPP, and RunX2 (at 28 days) in the control and Gel-MA/NGR1 groups (BC: blank control, DC: Dycal control, ND: pure hydrogel, LD: hydrogel with low drug loading, HD: hydrogel with high drug loading; red asterisk represents the injury site, blue arrow represents the reparatively formed dentin; Scalebar = 100 μm). b-e) Statistical mean option density of DMP-1, OCN, DSPP, and RunX2 (*$P<0.05$, **$P<0.01$, ***$P<0.001$).

4. DISCUSSION

As a promising pulp capping material, the Gel-MA hydrogel bears a series of advantageous properties, such as easy spreading, short and controllable setting time [7], tooth substrate adhesion [40], no carcinogenicity, biodegradability, biocompatibility [41], and, more importantly, providing a good carrier to accommodate various bioactive agents for functionalization [42]. In this study, we adopted NGR1 to functionalize Gel-MA with the aim of developing a potent anti-inflammatory and dentinogenic pulp-capping material. Our results showed that the optimized Gel-MA/NGR1 could strongly induce dentinogenic differentiation *in vitro* and newly formed mineralized tissue in dental pulp *in vivo*. These findings suggest the promising application potential of Gel-MA/NGR1 in pulp-capping techniques.

In this study, we, for the first time, showed that NGR1 could induce extracellular matrix mineralization of odontoblast-like cells — an important biological marker for dentinogenesis [43, 44]. The inducing effects of NGR1 at 50 μg/mL were significantly higher than that at 500 μg/mL. This result may be explained by the typical bell-shaped curve of growth factors [45]. This finding was inconsistent with our previous finding that NGR1 dose-dependently enhanced the extracellular matrix mineralization of the mouse MC3T3-E1 pre-osteoblast cell line at concentrations less than or equal to 1000 μg/mL [27]. In fact, we also found that NGR1 at higher concentrations (>100 μg/mL) inhibited the proliferation and ALP activity of pre-osteoblasts while significantly enhancing OCN expression [27]. Therefore, such consistency might be due to the greater sensitivity of odontoblast-like cells to the inhibitory effects of NGR1 on proliferation and ALP activity at 500 μg/mL than pre-osteoblasts. On the other hand, compromised *in-vitro* dentinogenesis may also be caused by overdose with DMSO (0.05%, 6.4 mM), the solvent of NGR1. NGR1 has low solubility in water (1 mg/mL) and therefore needs to be dissolved in an organic solvent such as DMSO to reach its pharmacological dosage. DMSO (0.05%) was previously shown to significantly compromise the total protein production of odontoblast-like cells [46], which may directly prevent the increase in ALP and further ECM mineralization [47]. Consequently, optimization of the NGR1 dose is highly important to induce the most efficacious dentinogenesis.

Thereafter, we assessed the best combination of Gel-MA and NGR1 for optimal efficacy in inducing dentinogenesis. Regardless of the solid contents (100, 150 and 200 mg/mL) and NGR1 dose (ND, LD and HD), all Gel-MA/NGR1 hydrogels showed sufficient cytocompatibility to support the viability and proliferation of mDPC6T odontoblast-like cells. Furthermore, the Live/Dead assay showed that the addition of NGR1 to Gel-MA did not cause cytotoxicity to mDPC6T odontoblast-like cells. These findings suggested good cytocompatibility of all selected combinations of Gel-MA and NGR1.

In the subsequent extracellular matrix mineralization assay, Gel-MA without NGR1 showed similar mineralization irrespective of the solid contents. This finding suggested that dentinogenesis was not significantly influenced by the different physicochemical properties of Gel-MA with different solid contents. Interestingly, the presence of NGR1 was associated with significantly enhanced *in-vitro* dentinogenesis on Gel-MA with a solid content of 100 mg/mL, while on Gel-MA with solid contents of 150 or 200 mg/mL, the addition of NGR1 resulted in compromised dentinogenesis. These findings suggested a complicated interaction between Gel-MA and NGR1. However, there is still a lack of research to identify the interaction between Gel-MA and NGR1, and further studies should be performed to elucidate the potential mechanisms. According to these results, we selected 100 mg/mL Gel-MA for the following experiments.

We further characterized the physicochemical properties of Gel-MA/NGR1 (Figures 3 and S1-S3). Regardless of whether or not NGR1 was present, the hydrogels did not show significant shrinkage during the crosslinking process, which is of great significance for a pulp-capping material to ensure complete coverage of the dental pulp tissue and to prevent any potential mechanical disturbance due to contraction. Irrespective of the dose, NGR1 did not significantly change the characteristic FTIR spectral peaks of Gel-MA [48], which suggested that there was no significant influence from NGR1 on the chemical structure of Gel-MA. XPS analysis confirmed the loading of NGR1 into the hydrogel. NGR1 did not significantly influence the water uptake (Figure S2a) or the interconnected porous structure (Figure S2c) of Gel-MA, which ensured high permeability for nutrients and metabolites to support cell adhesion, migration, proliferation and differentiation [49, 50]. On the other hand, the pore size slightly decreased, which could be attributed to the more compact network than Gel-MA alone due to the non-covalent interactions between NGR1 and Gel-MA [51, 52]_ENREF_39. The addition of NGR1 significantly decreased the WCA (Figure S2e), which brought even better hydrophilicity, a prerequisite to facilitate the immediate interaction between dental pulp cells and pulp capping material [53]. In the presence of collagenase (in the form of MMP-8 in dentin [54, 55]), the complete degradation time of Gel-MA/NGR1 _ENREF_27was approximately 20 days, which is sufficient to support reparative dentin formation [56, 57]. A slow-release profile (Figure S3) facilitates the continuous and stable delivery of bioactive agents to tissues to stimulate the dentinogenic differentiation of dental pulp cells. One major advantage of Gel-MA/NGR1 over other calcium phosphate-based pulp capping materials lies in its capacity to slowly release bioactive agents. It was noted that NGR1 was released via the diffusion and swelling mechanism (n > 0.5) [58] with varying release rates in the first 24 hours when the swelling effect was clearly greater than that of the erosion, degradation and dissolution effects.

G' slightly increased at higher frequencies on account of the failure movement and rearrangement of polymer chains in less time, which led to the properties of stiffness and solid-like behaviour [59]. The results indicated that the hydrogel formed in an ideal type [60, 61]. Gel-MA/NGR1 was associated with significantly enhanced mechanical properties (from 811 ± 21 Pa for ND to 52 ± 2 KPa for LD and 56 ± 2 KPa for HD) compared with Gel-MA alone. Such a phenomenon might be attributed to the non-covalent adsorption of NGR1 into the Gel-MA network, leading to a more compact structure, as shown by the SEM results (Figure S2c). Such a change in mechanical properties is highly meaningful for a pulp capping material to provide sufficient resistant force to protect the underlying dental pulp and support further restoration. From a biological point of view, hydrogels with an elastic modulus of 50-60 kPa have been shown to be favourable for supporting cell migration and proliferation [62].

We further evaluated the capacity of Gel-MA/NGR1 to induce other dentinogenic differentiation markers. Our results showed that Gel-MA could significantly promote ALP mRNA expression and ALP staining, which was consistent with previous findings [63]. On the other hand, the presence of NGR1 in the LD and HD groups did not further increase the ALP activity. This finding was consistent with our previous finding that NGR1 does not significantly promote ALP activity during osteoblastogenesis [27]. In contrast, ND did not influence the expression of OCN (a late dentinogenic marker [64]), while LD and HD were associated with significantly higher OCN levels than ND or DM (Figure 4e, f). This finding was also consistent with our previous finding that NGR1 significantly promoted OCN expression [27]. All of these findings lead us to conclude that the complementary capacities of Gel-MA and NGR1 in inducing ALP and OCN truly made the Gel-MA/NGR1 hydrogel an optimal combination to induce dentinogenesis.

To investigate whether the Gel-MA/NGR1 hydrogel could induce reparative dentin formation *in vivo*, a modified direct pulp capping model was adopted (Figure S4). In the conventional direct pulp capping rat model, implanted materials lie on the border between the dentin and dental pulp to mimic the clinical situation of direct pulp capping [65]. However, due to the much smaller volume of rat teeth than human teeth, the contact area between biomaterials and dental pulp is rather limited, which makes subsequent micro-CT and histological evaluation much more difficult. In the current modified model, we extended the location of implantation to the bottom of the dental pulp chamber to enlarge the contact area, thus making the subsequent evaluations much easier. On the other hand, the enlarged contact area also resulted in slightly more spreading area of the newly formed mineralized tissue in the dental chamber in some cases, which may raise concerns for clinicians due to the potential blocking of the root canals. In fact, HE staining showed that the newly formed reparative dentin did not actually enter the root canal. We

assumed that these concerns could be relieved in the clinic due to the limited contact area and much larger dental pulp chamber in real clinical situations. In our future study, we will perform large animal studies to determine whether this is a problem.

Four weeks post-surgery [32-35], micro-CT images showed that the newly formed mineralized tissue was mainly in the vicinity of the implanted Gel-MA/NGR1 hydrogel (white arrows), which was also confirmed by HE and Masson staining analyses. Quantitative micro-CT analysis showed that Gel-MA/NGR1 was associated with a significantly larger amount of newly formed mineralized tissue than the DC and ND groups, which indicated that NGR1 bore a potent capacity to induce *in-vivo* reparative dentin. As there was almost no dislocation of the material/dental pulp border in the LD and HD groups, this suggested that there was a potent cytoprotective effect and non-cytotoxic properties of the Gel-MA/NGR1 hydrogels.

The use of DMP-1, OCN, DSPP and RunX2 as markers allowed us to intuitively observe the differences in the dentinogenic capacities of different materials [35] since they are expressed during the dentinogenic differentiation process. DMP-1 and DSPP are positive regulators of reparative dentin formation, acting as nucleators of apatite crystal formation [66] (DSPP induces collagen mineralization; DMP-1 induces the deposition of mineral particles along the collagen fibril axis). Moreover, DSPP, one of the key non-collagenous proteins, is essential for dentin mineralization [35], which is proteolytically cleaved into dentin sialoprotein (DSP) and dentin phosphoprotein (DPP). The expression of RunX2 and OCN are markers of the dentinogenic differentiation process, indicating that the introduction of hydroxyapatite promotes the expression of cell adhesion proteins [67]. In our study, the LD group showed the highest mean optical densities of all the selected parameters, which was consistent with the data obtained from the *in-vitro* extracellular matrix mineralization assay. All of these findings indicated the promising application potential of LD in pulp-capping therapy.

Hitherto, the molecular mechanisms for the inducing effects of NGR1 on dentinogenesis remain unclear. NGR1 is a phytoestrogen, and estrogen receptor (ER) has been shown to mediate the dentinogenic effects of NGR1 [31]. In another study, NGR1 was shown to significantly increase the phosphorylation of MAPK (mitogen-activated protein kinase), JAK1 (Janus kinase 1), and STAT3 (signal transducer and activator of transcription 3) [68]. Furthermore, NGR1 also upregulates miR-23a expression, which positively modulates RunX2 and Osx expression as well as ALP activity. An miR-23a inhibitor has been shown to reduce the phosphorylation of MAPK, JAK1 and STAT3 induced by NGR1 [68]. Further studies are needed to illustrate the potential roles of ER, MAPK, JAK1, STAT3 and miR23 in the dentinogenic effects of NGR1.

One limitation of this study is the adoption of an odontoblast-like cell line. Further experiments using human primary dental pulp stem cells should be performed to corroborate the current findings. For its application as a pulp-capping material, Gel-MA/NGR1 may be further optimized with respect to its mechanical strength [21], dentinogenic capacity [63] and radiopacity, possibly by adding calcium-containing micro/nanoparticles. After such optimization, further studies should also be performed to compare the performance of Gel-MA/NGR1 with several clinical gold-standard products, such as MTA [36], to corroborate its clinical application potential.

5. CONCLUSION

In this study, we developed an injectable Gel-MA/NGR1 composite hydrogel as a promising pulp-capping material with a potent capacity to induce *in-vitro* dentinogenesis and *in-vivo* reparative dentin formation. The Gel-MA/NGR1 hydrogels retained their porous inner structures and hydrophilicity with sustained drug release performance. The mechanical properties were enhanced by drug loading. The Gel-MA/NGR1 composite hydrogel showed no cytotoxicity and supported dentinogenic cell proliferation. Gel-MA/NGR1 LD could significantly promote *in-vitro* dentinogenic markers ALP and OCN and extracellular matrix mineralization. Finally, the hydrogels were proven to promote reparative dentin-like tissue after implantation *in vivo* in a Sprague-Dawley rat model followed by *in-situ* UV crosslinking. All of the results suggest that the Gel-MA/NGR1 composite is a highly promising pulp-capping material candidate to induce reparative dentin formation.

ACKNOWLEDGEMENTS

SUPPLEMENTARY MATERIALS

The detailed rheological, physical and chemical studies (the water uptake, *in-vitro* biodegradation, morphology, pore size, WCA, crosslinking intensity and NGR1 release properties) can be found in the Supplementary Materials.

REFERENCES

[1]   C.C. Huang, R. Narayanan, N. Warshawsky, S. Ravindran, Dual ECM Biomimetic Scaffolds for Dental Pulp Regenerative Applications, Frontiers in Physiology 9(495) (2018).

[2]   K.J. Heyeraas, E. Berggreen, Interstitial fluid pressure in normal and inflamed pulp, Crit Rev Oral Biol Med 10(3) (1999) 328-36.

[3]   M. Pesis, E. Bar-Droma, A. Ilgiyaev, N. Givol, Deep Neck Infections, Life Threatening Infections of Dental Origin: Presentation and Management of Selected Cases, Israel Medical Association Journal 21(12) (2019) 806-811.

[4]   L.C. Reis, I.N. Rocas, J.F. Siqueira, M. de Uzeda, V.S. Lacerda, R. Domingues, S.R. Moraes, R.M. Saraiva, Bacteremia after Endodontic Procedures in Patients with Heart Disease: Culture and Molecular Analyses, Journal of Endodontics 42(8) (2016) 1181-1185.

[5]   L. Bjorndal, S. Simon, P.L. Tomson, H.F. Duncan, Management of deep caries and the exposed pulp, International Endodontic Journal 52(7) (2019) 949-973.

[6]   A. Paula, M. Laranjo, C.M. Marto, A.M. Abrantes, J. Casalta-Lopes, A.C. Goncalves, A.B. Sarmento-Ribeiro, M.M. Ferreira, M.F. Botelho, E. Carrilho, Biodentine Boosts, WhiteProRoot((R))MTA Increases and Life((R)) Suppresses Odontoblast Activity, Materials 12(7) (2019).

[7]   W.L.O. da Rosa, A.R. Cocco, T.M.D. Silva, L.C. Mesquita, A.D. Galarca, A.F.D. Silva, E. Piva, Current trends and future perspectives of dental pulp capping materials: A systematic review, J Biomed Mater Res B Appl Biomater 106(3) (2018) 1358-1368.

[8]   A.B. Paula, M. Laranjo, C.M. Marto, S. Paulo, A.M. Abrantes, J. Casalta-Lopes, M. Marques-Ferreira, M.F. Botelho, E. Carrilho, Direct pulp capping: what is the most effective therapy?-Systematic review and meta-analysis, Journal of Evidence-Based Dental Practice 18(4) (2018) 298-314.

[9]   A. Paula, E. Carrilho, M. Laranjo, A.M. Abrantes, J. Casalta-Lopes, M.F. Botelho, C.M. Marto, M.M. Ferreira, Direct Pulp Capping: Which is the Most Effective Biomaterial? A Retrospective Clinical Study, Materials 12(20) (2019).

[10]   G. Bogen, J.S. Kim, L.K. Bakland, Direct pulp capping with mineral trioxide aggregate: an observational study, J Am Dent Assoc 139(3) (2008) 305-15; quiz 305-15.

[11]   M. Torabinejad, C.U. Hong, F. McDonald, T.R. Pitt Ford, Physical and chemical properties of a new root-end filling material, J Endod 21(7) (1995) 349-53.

[12]   A.D. Santos, J.C. Moraes, E.B. Araujo, K. Yukimitu, W.V. Valerio Filho, Physico-chemical properties of MTA and a novel experimental cement, Int Endod J 38(7) (2005) 443-7.

[13]   T. Komabayashi, A. Wadajkar, S. Santimano, C. Ahn, Q. Zhu, L.A. Opperman, L.L. Bellinger, J. Yang, K.T. Nguyen, Preliminary study of light-cured hydrogel for endodontic drug delivery vehicle, Journal of Investigative and Clinical Dentistry 7(1) (2016) 87-92.

[14]   Y.B. Wang, H.X. Li, Y.H.Z. Feng, P.L. Jiang, J.S. Su, C. Huang, Dual micelles-loaded gelatin nanofibers and their application in lipopolysaccharide-induced periodontal disease, International Journal of Nanomedicine 14 (2019) 963-976.

[15] C. Puckert, E. Tomaskovic-Crook, S. Gambhir, G.G. Wallace, J.M. Crook, M.J. Higgins, Molecular interactions and forces of adhesion between single human neural stem cells and gelatin methacrylate hydrogels of varying stiffness, Acta Biomaterialia 106 (2020) 156-169.

[16] A. Khayat, N. Monteiro, E.E. Smith, S. Pagni, W. Zhang, A. Khademhosseini, P.C. Yelick, GelMA-Encapsulated hDPSCs and HUVECs for Dental Pulp Regeneration, Journal of Dental Research 96(2) (2017) 192-199.

[17] X.J. Cai, J. Cai, K.N. Ma, P. Huang, L.L. Gong, D. Huang, T. Jiang, Y.N. Wang, Fabrication and characterization of Mg-doped chitosan-gelatin nanocompound coatings for titanium surface functionalization, Journal of Biomaterials Science-Polymer Edition 27(10) (2016) 954-971.

[18] C.K. Chiu, D.J. Lee, H. Chen, L.C. Chow, C.C. Ko, In-situ hybridization of calcium silicate and hydroxyapatite-gelatin nanocomposites enhances physical property and *in vitro* osteogenesis, Journal of Materials Science-Materials in Medicine 26(2) (2015).

[19] A.E. Pazarceviren, Z. Evis, D. Keskin, A. Tezcaner, Resorbable PCEC/gelatin-bismuth doped bioglass-graphene oxide bilayer membranes for guided bone regeneration, Biomedical Materials 14(3) (2019).

[20] X.X. Fang, J. Xie, L.X. Zhong, J.R. Li, D.M. Rong, X.S. Li, J. Ouyang, Biomimetic gelatin methacrylamide hydrogel scaffolds for bone tissue engineering, Journal of Materials Chemistry B 4(6) (2016) 1070-1080.

[21] T.W. Xin, Y. Gu, R.Y. Cheng, J.C. Tang, Z.Y. Sun, W. Cui, L. Chen, Inorganic Strengthened Hydrogel Membrane as Regenerative Periosteum, Acs Applied Materials & Interfaces 9(47) (2017) 41168-41180.

[22] C.W. Wang, T.Y. Chiang, H.C. Chang, S.J. Ding, Physicochemical properties and osteogenic activity of radiopaque calcium silicate-gelatin cements, Journal of Materials Science-Materials in Medicine 25(9) (2014) 2193-2203.

[23] H.H. Fang, S.L. Yang, Y.Y. Luo, C. Zhang, Y. Rao, R.J. Liu, Y.L. Feng, J. Yu, Notoginsenoside R1 inhibits vascular smooth muscle cell proliferation, migration and neointimal hyperplasia through PI3K/Akt signaling, Scientific Reports 8 (2018).

[24] Y.L. Yu, G.B. Sun, Y. Luo, M. Wang, R.C. Chen, J.Y. Zhang, Q.D. Ai, N. Xing, X.B. Sun, Cardioprotective effects of Notoginsenoside R1 against ischemia/reperfusion injuries by regulating oxidative stress- and endoplasmic reticulum stress-related signaling pathways, Scientific Reports 6 (2016).

[25] T. Wang, D.Q. Wan, L. Shao, J.Z. Dai, C.Y. Jiang, Notoginsenoside R1 stimulates osteogenic function in primary osteoblasts via estrogen receptor signaling, Biochemical and Biophysical Research Communications 466(2) (2015) 232-239.

[26] B. Zhang, J.Y. Zhang, C.Y. Zhang, X.L. Zhang, J.X. Ye, S.H. Kuang, G.B. Sun, X.B. Sun, Notoginsenoside R1 Protects Against Diabetic Cardiomyopathy Through Activating Estrogen Receptor alpha and Its Downstream Signaling, Frontiers in Pharmacology 9 (2018).

[27] Y. Liu, Z. Lin, J. Guo, G. Xu, Y. Li, T. Xu, H. Lv, J. Chen, G. Wu, Notoginsenoside R1 significantly promotes *in vitro* osteoblastogenesis, Int J Mol Med 38(2) (2016) 537-44.

[28] L. Wang, C.L. Lu, H.H. Liu, S. Lin, K.H. Nan, H. Chen, L.L. Li, A double network strategy to improve epithelization of a poly(2-hydroxyethyl methacrylate) hydrogel for corneal repair application, Rsc Advances 6(2) (2016) 1194-1202.

[29] I. Vidovic, A. Banerjee, R. Fatahi, B.G. Matthews, N.A. Dyment, I. Kalajzic, M. Mina, alpha SMA-Expressing Perivascular Cells Represent Dental Pulp Progenitors In Vivo, Journal of Dental Research 96(3) (2017) 323-330.

[30] W. Zhu, H. Cui, B. Boualam, F. Masood, E. Flynn, R.D. Rao, Z.-Y. Zhang, L.G. Zhang, 3D bioprinting mesenchymal stem cell-laden construct with core-shell nanospheres for cartilage tissue engineering, Nanotechnology 29(18) (2018).

[31] B. Li, L. Wang, F. Xu, X. Gang, U. Demirci, D. Wei, Y. Li, Y. Feng, D. Jia, Y. Zhou, Hydrosoluble, UV-crosslinkable and injectable chitosan for patterned cell-laden microgel and rapid transdermal curing hydrogel in vivo, Acta Biomaterialia 22 (2015) 59-69.

[32] M. Okamoto, Y. Takahashi, S. Komichi, P.R. Cooper, M. Hayashi, Dentinogenic effects of extracted dentin matrix components digested with matrix metalloproteinases, Scientific Reports 8 (2018).

[33] W. Kiba, S. Imazato, Y. Takahashi, S. Yoshioka, S. Ebisu, T. Nakano, Efficacy of polyphasic calcium phosphates as a direct pulp capping material, Journal of Dentistry 38(10) (2010) 828-837.

[34] H.P. Lin, H.P. Tu, Y.P. Hsieh, B.S. Lee, Controlled release of lovastatin from poly(lactic-co-glycolic acid) nanoparticles for direct pulp capping in rat teeth, International Journal of Nanomedicine 12 (2017) 5473-5485.

[35] S.Y. Liu, S.N. Wang, Y.M. Dong, Evaluation of a Bioceramic as a Pulp Capping Agent *In Vitro* and In Vivo, Journal of Endodontics 41(5) (2015) 652-657.

[36] A.B. Paula, M. Laranjo, C.M. Marto, S. Paulo, A.M. Abrantes, B. Fernandes, J. Casalta-Lopes, M. Marques-Ferreira, M.F. Botelho, E. Carrilho, Evaluation of dentinogenesis inducer biomaterials: an in vivo study, Journal of Applied Oral Science 28 (2020).

[37] S. Mastrogiacomo, N. Guvener, W. Dou, H.S. Alghamdi, W.A. Camargo, J.G.O. Cremers, P.J.A. Borm, A. Heerschap, E. Oosterwijk, J.A. Jansen, X.F. Walboomers, A theranostic dental pulp capping agent with improved MRI and CT contrast and biological properties, Acta Biomaterialia 62 (2017) 340-351.

[38] B.F. Pierce, G. Tronci, M. Roessle, A.T. Neffe, F. Jung, A. Lendlein, Photocrosslinked Co-Networks from Glycidylmethacrylated Gelatin and Poly(ethylene glycol) Methacrylates, Macromolecular Bioscience 12(4) (2012) 484-493.

[39] M. Uyaniklar, G. Gunal, A. Tevlek, P. Hosseinian, H.M. Aydin, Hybrid Cornea: Cell Laden Hydrogel Incorporated Decellularized Matrix, Acs Biomaterials Science & Engineering 6(1) (2020) 122-133.

[40] J. Ribeiro, E. Bordini, J. Ferreira, L. Mei, N. Dubey, J. Fenno, E. Piva, R. Lund, A. Schwendeman, M.J.A.a.m. Bottino, interfaces, Injectable MMP-Responsive Nanotube-Modified Gelatin Hydrogel for Dental Infection Ablation, 12(14) (2020) 16006-16017.

[41] X.D. Sun, X. Zhao, L.L. Zhao, Q. Li, M. D'Ortenzio, B. Nguyen, X. Xu, Y. Wen, Development of a hybrid gelatin hydrogel platform for tissue engineering and protein delivery applications, Journal of Materials Chemistry B 3(30) (2015) 6368-6376.

[42] Q. Zhang, C.Y. Qian, W.S. Xiao, H.J. Zhu, J. Guo, Z.L. Ge, W.G. Cui, Development of a visible light, cross-linked GelMA hydrogel containing decellularized human amniotic particles as a soft tissue replacement for oral mucosa repair, Rsc Advances 9(32) (2019) 18344-18352.

[43] C. Beguekirn, A.J. Smith, J.V. Ruch, J.M. Wozney, A. Purchio, D. Hartmann, H. Lesot, Effects of dentin proteins, transforming growth-factor beta-1 (tgf-beta-1) and bone morphogenetic protein-2 (bmp2) on the differentiation of odontoblast invitro, International Journal of Developmental Biology 36(4) (1992) 491-503.

[44] D. Tziafas, K. Kodonas, Differentiation Potential of Dental Papilla, Dental Pulp, and Apical Papilla Progenitor Cells, Journal of Endodontics 36(5) (2010) 781-789.

[45] Y. Zheng, G. Wu, J. Zhao, L. Wang, P. Sun, Z.J.T.e.P.A. Gu, rhBMP2/7 heterodimer: an osteoblastogenesis inducer of not higher potency but lower effective concentration compared with rhBMP2 and rhBMP7 homodimers, 16(3) (2010) 879-87.

[46] J. Hebling, L. Bianchi, F.G. Basso, D.L. Scheffel, D.G. Soares, M.R. Carrilho, D.H. Pashley, L. Tjaderhane, C.A. de Souza Costa, Cytotoxicity of dimethyl sulfoxide (DMSO) in direct contact with odontoblast-like cells, Dent Mater 31(4) (2015) 399-405.

[47] S. Mechiche Alami, S.C. Gangloff, D. Laurent-Maquin, Y. Wang, H. Kerdjoudj, Concise Review: *In Vitro* Formation of Bone-Like Nodules Sheds Light on the Application of Stem Cells for Bone Regeneration, Stem Cells Transl Med 5(11) (2016) 1587-1593.

[48] W. Xiao, J. Li, X. Qu, L. Wang, Y. Tan, K. Li, H. Li, X. Yue, B. Li, X.J.M.s. Liao, M.f.b.a. engineering. C, Cell-laden interpenetrating network hydrogels formed from methacrylated gelatin and silk fibroin via a combination of sonication and photocrosslinking approaches, 99 (2019) 57-67.

[49] D. Gupta, A.K. Singh, A. Dravid, J. Bellare, Multiscale Porosity in Compressible Cryogenically 3D Printed Gels for Bone Tissue Engineering, ACS applied materials & interfaces (2019).

[50] C.M. Hwang, S. Sant, M. Masaeli, N.N. Kachouie, B. Zamanian, S.-H. Lee, A. Khademhosseini, Fabrication of three-dimensional porous cell-laden hydrogel for tissue engineering, Biofabrication 2(3) (2010).

[51] A.A. Nada, E.A. Ali, A.A.F. Soliman, Biocompatible chitosan-based hydrogel with tunable mechanical and physical properties formed at body temperature, International journal of biological macromolecules 131 (2019) 624-632.

[52] S. Khorshidi, A. Karkhaneh, A self-crosslinking tri-component hydrogel based on functionalized polysaccharides and gelatin for tissue engineering applications, Materials Letters 164 (2016) 468-471.

[53] T.T. Yu, F.Z. Cui, Q.Y. Meng, J. Wang, D.C. Wu, J. Zhang, X.X. Kou, R.L. Yang, Y. Liu, Y.S. Zhang, F. Yang, Y.H. Zhou, Influence of Surface Chemistry on Adhesion and Osteo/Odontogenic Differentiation of Dental Pulp Stem Cells, Acs Biomaterials Science & Engineering 3(6) (2017) 1119-1128.

[54] M. Sulkala, T. Tervahartiala, T. Sorsa, M. Larmas, T. Salo, L. Tjaderhane, Matrix metalloproteinase-8 (MMP-8) is the major collagenase in human dentin, Archives of Oral Biology 52(2) (2007) 121-127.

[55] A.K.B. Bedran-Russo, C.S. Castellan, M.S. Shinohara, L. Hassan, A. Antunes, Characterization of biomodified dentin matrices for potential preventive and reparative therapies, Acta Biomaterialia 7(4) (2011) 1735-1741.

[56] A. Guentsch, K. Seidler, S. Nietzsche, A.F. Hefti, P.M. Preshaw, D.C. Watts, K.D. Jandt, B.W. Sigusch, Biomimetic mineralization: Long-term observations in patients with dentin sensitivity, Dental Materials 28(4) (2012) 457-464.

[57] F. MW, Cariology And Endodontics, People's Medical Publishing House, Beijing, 2012.

[58] C. Maderuelo, A. Zarzuelo, J.M. Lanao, Critical factors in the release of drugs from sustained release hydrophilic matrices, Journal of Controlled Release 154(1) (2011) 2-19.

[59] M.J. Moura, M.M. Figueiredo, M.H. Gil, Rheological study of genipin cross-linked chitosan hydrogels, Biomacromolecules 8(12) (2007) 3823-3829.

[60] L. Koivusalo, J. Karvinen, E. Sorsa, I. Jonkkari, J. Valiaho, P. Kallio, T. Ilmarinen, S. Miettinen, H. Skottman, M. Kellomaki, Hydrazone crosslinked hyaluronan-based hydrogels for therapeutic delivery of adipose stem cells to treat corneal defects, Materials Science & Engineering C-Materials for Biological Applications 85 (2018) 68-78.

[61] J. Karvinen, J.T. Koivisto, I. Jonkkari, M. Kellomaki, The production of injectable hydrazone crosslinked gellan gum-hyaluronan-hydrogels with tunable mechanical and physical properties, Journal of the Mechanical Behavior of Biomedical Materials 71 (2017) 383-391.

[62] N. Huebsch, E. Lippens, K. Lee, M. Mehta, S.T. Koshy, M.C. Darnell, R.M. Desai, C.M. Madl, X. Xu, X.H. Zhao, O. Chaudhuri, C. Verbeke, W.S. Kim, K. Alim, A. Mammoto, D.E. Ingber, G.N. Duda, D.J. Mooney, Matrix elasticity of void-forming hydrogels controls transplanted-stem-cell-mediated bone formation, Nature Materials 14(12) (2015) 1269-1277.

[63] J. Ramis, M. Blasco-Ferrer, J. Calvo, O. Villa, M. Cladera, C. Corbillo, A. Gayà, M.J.J.o.t.e. Monjo, r. medicine, Improved physical and osteoinductive properties of demineralized bone matrix by gelatin methacryloyl formulation, 14(3) (2020) 475-485.

[64] F. Asghari, R. Salehi, M. Agazadeh, E. Alizadeh, K. Adibkia, M. Samiei, A. Akbarzadeh, N.A. Aval, S. Davaran, The odontogenic differentiation of human dental pulp stem cells on hydroxyapatite-coated biodegradable nanofibrous scaffolds, International Journal of Polymeric Materials and Polymeric Biomaterials 65(14) (2016) 720-728.

[65] H. Qian, X.J.J.o.c. Guan, m. medicine, Follicle-stimulating hormone impairs dental pulp stem cells odontogenic differentiation, (2020).

[66] J. Martín-González, A. Pérez-Pérez, D. Cabanillas-Balsera, T. Vilariño-García, V. Sánchez-Margalet, J.J.A.o.o.b. Segura-Egea, Leptin stimulates DMP-1 and DSPP expression in human dental pulp via MAPK 1/3 and PI3K signaling pathways, 98 (2019) 126-131.

[67] J. Xu, H. Aoki, S. Kasugai, M.J.M.s. Otsuka, M.f.b.a. engineering. C, Enhancement of mineralization on porous titanium surface by filling with nano-hydroxyapatite particles fabricated with a vacuum spray method, 111 (2020) 110772.

[68] C. Wang, H. Sun, Y.J.A.c. Zhong, nanomedicine,, biotechnology, Notoginsenoside R1 promotes MC3T3-E1 differentiation by up-regulating miR-23a via MAPK and JAK1/STAT3 pathways, 47(1) (2019) 603-609.

SUPPLEMENTARY MATERIALS

Notoginsenoside R[1] functionalized gelatin hydrogels to promote reparative dentinogenesis

Lei Wang#, Hui Fu#, Wenwen Wang#, Yi Liu, Xumin Li, Jijing Yang, Lingli Li *, Gang Wu*,&, Yihuai Pan*,&

* : Corresponding authors

# : These authors contributed equally to this work.

& : These authors shared last authorship.

1. MATERIALS AND METHODS

1.1 Modification of gelatin with Methylacrylic anhydride (Gel-MA)

Gel-MA was synthesized according to our previous report [1]. Briefly, gelatin was dissolved in phosphate buffered saline (PBS) at 50 °C to form a 10% (w/v) solution. MAA was added to the gelatin solution at a rate of 0.5 mL min^{-1} under rigorous stirring (800 rpm) until the final concentration of MAA was 1% (v/v). Then, 5M NaOH was used to adjust the pH value of the reacting mixture to a value of 7.4–8 and the mixture was allowed to react for 3 h at 50 °C. The samples were dialyzed against deionized water for 5 days at 50 °C using 3.5 kDa cut-off dialysis tubes to remove unreacted MAA and additional by-products. The dialyzed samples were frozen at -80 °C, freeze-dried for 48 h and stored at room temperature in the dark.

1.2 Preparation of the Gel-MA/NGR1 hydrogels

The NGR1 loaded hydrogel (HD: high drug loading, LD: low drug loading, ND: no drug loading) was prepared ditto by adding NGR1 (1000 mg/mL in dimethylsulfoxide) in the precursor solution (Table S1).

Table S1. Hydrogel preparation

Sample Name	Concentration of Gel-MA (mg/mL)	Gel-MA (µL)	NGR1 concentration	I2959 (µL)
200mg/mL-HD		100	2 wt%-0.4 µL	2.0
200mg/mL-LD	200	100	1 wt%-0.2 µL	2.0
200mg/mL-ND		100	0 wt%-0 µL	2.0
150mg/mL-HD		100	2 wt%-0.4 µL	1.5
150mg/mL-LD	150	100	1 wt%-0.2 µL	1.5
150mg/mL-ND		100	0 wt%-0 µL	1.5
100mg/mL-HD		100	2 wt%-0.4 µL	1.0
100mg/mL-LD	100	100	1 wt%-0.2 µL	1.0
100mg/mL-ND		100	0 wt%-0 µL	1.0

1.3 Rheological study

The rheological measurements were performed using a Discovery HR-2 rheometer (TA Instruments, USA) with a flat plate of 8 mm diameter and a gap of 1 mm. An oscillatory sweep experiment was carried out to determine the mechanical properties of the

hydrogels. The G' and G" as a function of frequency at 37 °C were recorded. The frequency sweep experiment was conducted under a fixed strain of 0.4%, and the angular frequency was swept from 0.01 to 100 rad s^{-1}.

1.4 Equilibrium water content (EWC)

Since the swelling ratio of pure hydrogels reaches the equilibrium point after 24 h immersing into PBS solution, the equilibrium water content of drug-loaded hydrogels was calculated according to mass addition at the point of 24 h. The dried hydrogel was weighed (m_o) and immersed in PBS (pH 7.4) for 24 h at 37 °C for fully swelling to equilibrium. Then, the excess PBS on the surface was removed and the hydrogel with equilibrium swelling state was weighed (m_e). The equilibrium water content of hydrogels was calculated as equation (1):

$$EWC = (m_e - m_o) / m_e \times 100\% \qquad (1)$$

Where m_e was the weight of the fully swelled hydrogel, m_o was the dried weight. Each sample was repeated three times.

1.5 *In-vitro* biodegradation

The degradation profile of hydrogels was followed *in vitro* by measuring the weight loss in PBS with 10 IU collagenase (type II, MP Biomedicals, USA) at 37 °C over time. After wiping away excess water on the surfaces, the weight of the hydrogel samples was measured immediately at specified time points. The degradation rate was calculated using equation (2), where W_t is the weight of the hydrogel after degradation and W_o, the weight of hydrogel after incubating for 24 h, was chosen to be the initial weight of degradation because of its swelling behavior:

$$Remaining\ Weight\ (\%) = W_t/W_o \times 100\% \qquad (2)$$

1.6 Water wettability of the hydrogels

A water wettability test was performed following a method described previously [2] by a water contact angle (WCA) analyzer (Theta, Biolinscientific, Sweden) using the static sessile drop manner. In brief, a drop of 2 μL deionized water was applied on the surface of the scaffolds and then immediately photographed for contact angle calculation. All the scaffolds were tested in triplicate.

1.7 *In-vitro* NGR1 release profile

The *in-vitro* release behavior of NGR1 from the hydrogel was studied by using a dialysis method. Briefly, 200 μg or 400 μg NGR1 loaded hydrogels were enclosed into a dialysis bag (molecular weight cut-off: 3500 Da). Then the dialysis bags were transferred into a 50-ml BD tube and 20 ml phosphate-buffered saline solution (PBS, pH 7.4) was added as the release medium. The system was placed in an air shaker at 37 °C with gentle stirring (100 rpm) for periodical study. At predetermined time points (1, 2, 4, 8, 24, 72, 120, 192, 240, 480 and 720 h), 1 ml of release medium was withdrawn and quantified by high-performance liquid chromatography (HPLC; Waters Alliance 2695; Milford, MA, USA) and all release medium was replaced with pre-warmed fresh PBS. HPLC analysis was performed on a reverse-phase C18 column (4.6 X 150 mm, 5 mm, Sunfire Analysis column; Milford, MA, USA) at room temperature. The mobile phase was acetonitrile, which was filtered through a 0.22-mm Millipore filter and degassed before use. The flow-rate was 0.8 ml/min and the eluent was detected by Waters PDA detector at 203 nm. All measurements were performed in triplicate and the results were expressed as a mean value ± S.D.

2 RESULTS

2.1 ATR-FTIR and XPS

The ATR-FTIR of Gel-MA and Gel-MA/NGR1 hydrogel with solid content at 100 mg/mL was shown in Figure S1a. In ATR-FTIR spectra, the peak at 2350 cm^{-1} corresponded to the C-N bond of gelatin. The peaks at 1635 cm^{-1} and 1535 cm^{-1} corresponded to the C = O stretching vibration and NH$_2$, respectively [3]. Instead, the peak of 1635 cm^{-1} blue shifted to 1654 cm^{-1} and 1688 cm^{-1} in the spectra of LD and HD, respectively due to the steric hindrance of NGR1 to the hydrogel [4], indicating the effective loading of NGR1. The XPS survey spectra of ND, LD and HD with binding energy ranging from 1200 to 0 eV were present in Figure S1b. All XPS spectra showed the presence of O1s (534 eV), N1s (401 eV) and C1s (287 eV) due to the same constitution of Gel-MA and Gel-MA/NGR1. The N1s peak (6.35%) was less intense in the XPS spectrum of HD than that of ND (16.05%), which revealed the conjunction of the NGR1 to the hydrogel since there was no nitrogen in NGR1 (Figure S1c). The surface elemental compositions determined by XPS are listed in Table S2. The mass ratio of oxygen to nitrogen in LD (44.51%) and HD (48.20%) was higher than ND (36.87%) because pure NGR1 (m_o/m_C = 51.1%) contained a large number of oxygen-containing groups, such as hydroxyl and ester bond in comparison with Gel-MA.

2.2 Water uptake and *in-vitro* biodegradation

The water uptake ability of Gel-MA/NGR1 was evaluated by measuring the equilibrium water content (EWC). The EWCs ranged from 85.3 ± 3.9% to 90.3 ± 3.0% for Gel-MA hydrogel (Figure S2a). The *in-vitro* biodegradation pattern of all the hydrogels appeared to be similar to each other, as shown in Figure S2b. In the first 48 h, the hydrogel degraded quickly with 36.6% degradation. Thereafter, a plateau period lasted about 10 days with an average degradation rate of 3.56% per day. 12 days post incubation, a second rapid degradation

stage occurred with an average degradation rate of 2.71% till complete degradation at 20 days when samples broke into pieces with visible debris in media and were not possible to weigh. The biodegradation profile of Gel-MA/NGR1 composite hydrogel was similar to Gel-MA hydrogel.

2.3 SEM and WCA

SEM results (Figure S2c) showed that all the crosslinked hydrogels displayed interconnected and porous network structures and the pore size remained within micrometer ranges from 6.4 to 10.5 micrometers (Figure S2d). Compared with the ND groups, the pore size of LD and HD hydrogels decreased as presented in Figure S2d. As shown in Figure S2e, all the groups of the Gel-MA hydrogels exhibited excellent hydrophilicity with WCAs below 15 degrees. The addition of NGR1 into Gel-MA resulted in a significant decrease in WCA with the lowest value occurred at LD.

2.4 The NGR1 release profile

The release profiles of NGR1 from LD and HD Gel-MA hydrogels were shown in Figure S3. At the first 8 h, $14.7 \pm 1.9\%$ NGR1 and $7.6 \pm 0.6\%$ were released from HD and LD respectively, which should be ascribed to the initial burst release drugs from superficial matrix of hydrogels in the early stage. After 24h, the release percentage of LD hydrogels remained higher than that of HD, reaching $47.8 \pm 3.8\%$ for LD and $38.7 \pm 5.0\%$ for HD at 30 days post incubation.

There are four probable mechanisms for drug release: 1) Fickian diffusion, 2) polymer swelling, 3) polymer swelling and dissolution of the polymer and drug and 4) the erosion and degradation of the polymer [5]. To explore the drug release kinetics and for further applied to subsequent *in-vivo* experiments, the release curves were fitted by a power Korsmeyer–Peppas model [6]:

$$Mt/ M_\infty = \varkappa t^n \quad (3)$$

$$Log\ M_t/M_\infty = nlogt + log\varkappa \quad (4)$$

where M_t/M_∞ is defined as the fraction of drug released at time t, $\varkappa$ is release constants (depends on the polymer characteristics), n represents the release exponents (defines the mechanism of drug release: diffusion-controlled or diffusion, swelling, degradation and erosion controlled). The value of n was determined from the slope of the plot of the logarithm of release rate and the logarithm of time (t) (Equation 4, Figure S3). Table S3 showed the values of the kinetic exponent (n) and regression coefficient (R^2) for all the groups before 24 h while the values of n were all below 0.5 after 24 h release (data not shown, non-covalent interaction affect mechanism attribution, which cannot be explained by simple mechanism model).
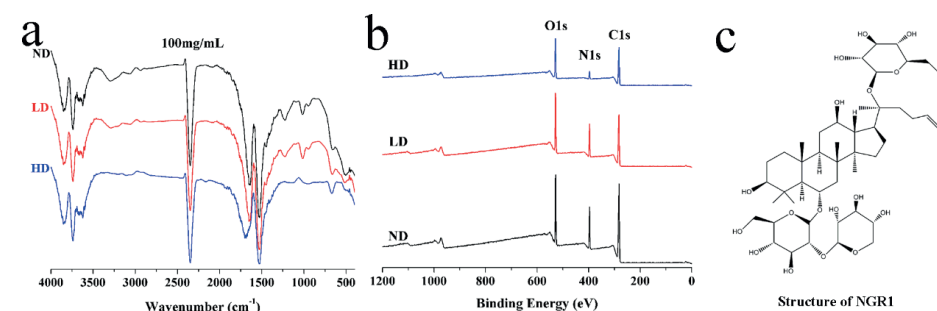
Figure S1. a) ATR-FTIR of Gel-MA and Gel-MA/NGR1 hydrogels. b) XPS wide spectra of the ND, LD, and HD. c) Molecular structure of NGR1.
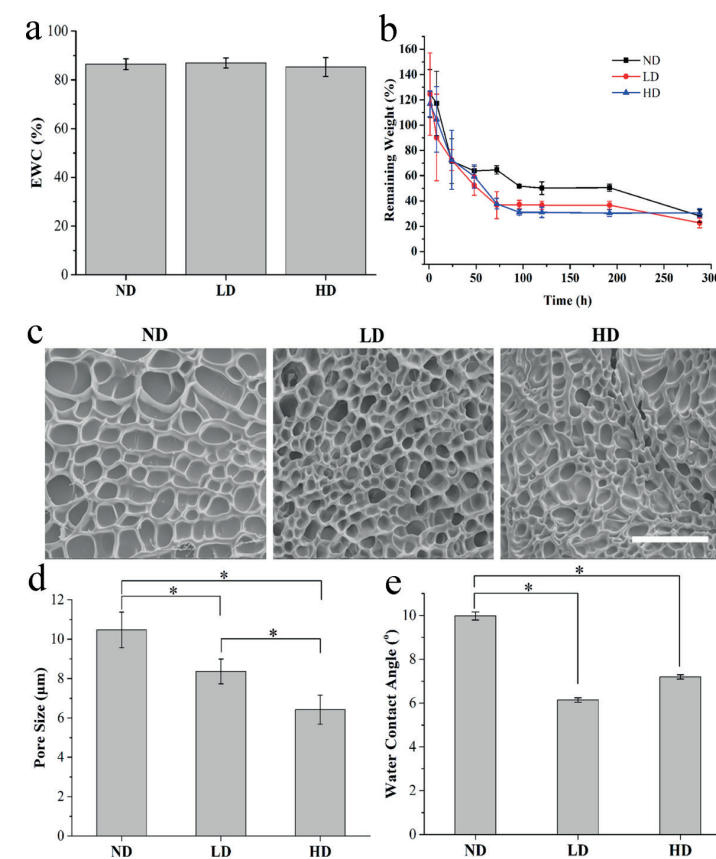

Figure S2. Physical performance of the NGR1-loaded hydrogel. a) Equilibrium water content. b) *In-vitro* degradation. c) SEM. d) Pore size. e) Water contact angle properties of the hydrogels. Scale bar = 50 μm
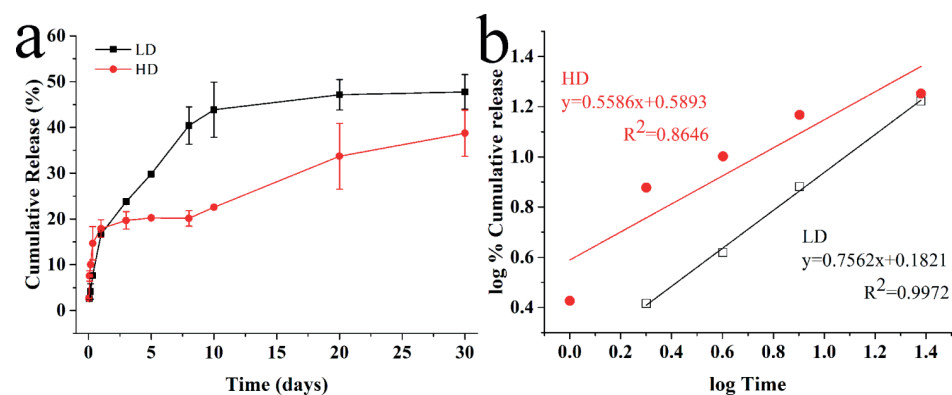
Figure S3. a) Cumulative release of NGR1. b) The plot of log % cumulative release versus log time, according to the Korsmeyer–Peppas model for LD and HD groups.
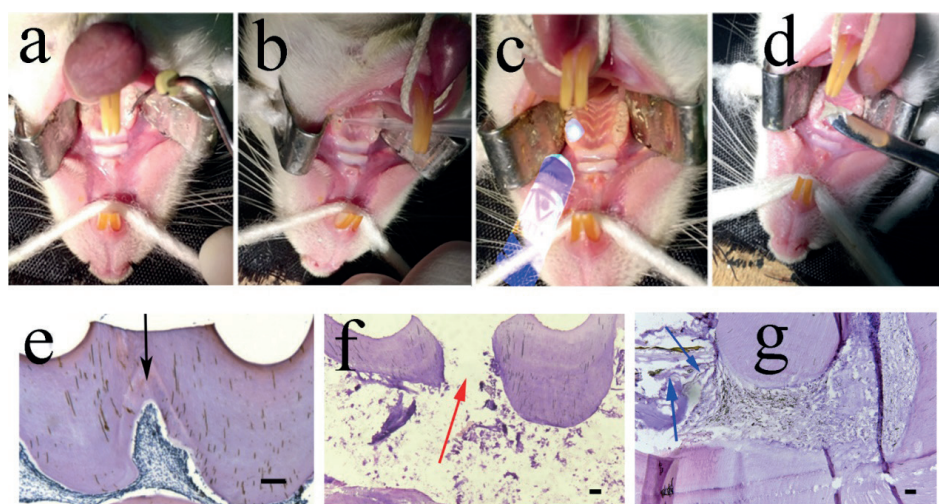

Figure S4. a-d) Digital photographs showing the surgical procedure for implantation of hydrogels injected into dentin of rat (a: alveolar bone defect in SD rat. b: injection of Gel-MA/NGR1 hydrogel. c: *in-situ* UV crosslinking. d: filled with glass ionomer cement. e-g): Representative histological images of different process (e: normal group. black arrow represented surgical site. f: after being drilled. red arrow represented the drilled hole. g: filled with Gel-MA/NGR1. blue arrow represented the gelled hydrogel). Scale bar = 100 μm

TABLES

Table S1. Hydrogel preparation

Sample Name	Solid content of Gel-MA (mg/mL)	Gel-MA (μL)	NGR1 concentration	I2959 (μL)
200mg/mL-HD		100	2 wt%-0.4 μL	2.0
200mg/mL-LD	200	100	1 wt%-0.2 μL	2.0
200mg/mL-ND		100	0 wt%-0 μL	2.0
150mg/mL-HD		100	2 wt%-0.4 μL	1.5
150mg/mL-LD	150	100	1 wt%-0.2 μL	1.5
150mg/mL-ND		100	0 wt%-0 μL	1.5
100mg/mL-HD		100	2 wt%-0.4 μL	1.0
100mg/mL-LD	100	100	1 wt%-0.2 μL	1.0
100mg/mL-ND		100	0 wt%-0 μL	1.0

Table S2. The Elemental Composition of ND, LD, and HD.

Groups	Atomic concentration (%)			Mass concentration (%)			m_o/m_c (%)
	O 1s	N 1s	C 1s	O 1s	N 1s	C 1s	
ND	18.45	14.94	66.61	22.62	16.05	61.33	36.87
LD	21.35	14.73	63.92	25.97	15.68	58.35	44.51
HD	24.99	5.95	69.06	30.46	6.35	63.19	48.20

Table S3. Release kinetics of NGR1 from the prepared hydrogels; expression of diffusional exponent (n) and regression value (R^2) with the probable release pattern.

Groups	Diffusion exponent value (n)	Regression coefficient (R^2)	Release mechanism
LD	0.7652	0.9972	Diffusion and swelling
HD	0.5586	0.8646	Diffusion and swelling

REFERENCES

[1]   L. Wang, C.L. Lu, H.H. Liu, S. Lin, K.H. Nan, H. Chen, L.L. Li, A double network strategy to improve epithelization of a poly(2-hydroxyethyl methacrylate) hydrogel for corneal repair application, Rsc Advances 6(2) (2016) 1194-1202.

[2]   M. Koosha, M. Raoufi, H. Moravvej, One-pot reactive electrospinning of chitosan/PVA hydrogel nanofibers reinforced by halloysite nanotubes with enhanced fibroblast cell attachment for skin tissue regeneration, Colloids and surfaces. B, Biointerfaces 179 (2019) 270-279.

[3]   M. Uyaniklar, G. Gunal, A. Tevlek, P. Hosseinian, H.M. Aydin, Hybrid Cornea: Cell Laden Hydrogel Incorporated Decellularized Matrix, Acs Biomaterials Science & Engineering 6(1) (2020) 122-133.

[4]   M.C. Chang, C.C. Ko, W.H. Douglas, Preparation of hydroxyapatite-gelatin nanocomposite, Biomaterials 24(17) (2003) 2853-2862.

[5]   C. Maderuelo, A. Zarzuelo, J.M. Lanao, Critical factors in the release of drugs from sustained release hydrophilic matrices, Journal of Controlled Release 154(1) (2011) 2-19.

[6]   C. Ferrero, A. Munoz-Ruiz, M.R. Jimenez-Castellanos, Fronts movement as a useful tool for hydrophilic matrix release mechanism elucidation, International Journal of Pharmaceutics 202(1-2) (2000) 21-28.

Chapter 3

Human salivary histatin-1-functionalized Gelatin Methacrylate Hydrogels promotes the regeneration of cartilage and subchondral bone in temporomandibular joint

Changjing Shi [#], Yu Yao [#], Lei Wang [#], Ping Sun, Jianying Feng [*] and Gang Wu [*]

* : Corresponding authors
# : These authors contributed equally to this work.

ABSTRACT

The avascular structure and lack of regenerative cells make the repair of osteochondral defects in the temporomandibular joint (TMJ) highly challenging in clinic. To provide a viable treatment option, we developed a gelatin-Methacryloyl (Gel-MA) hydrogel functionalized with human salivary histatin-1 (Hst1). Gel-MA is highly biocompatible, biodegradable, and cost-effective. Hst1 is capable of activating a series of cell activities, such as adhesion, migration, differentiation, and angiogenesis. To evaluate the efficacy of Hst1/Gel-MA, critical-size osteochondral defects (3mm in diameter and 3 mm in depth) of TMJ in New Zealand White rabbits were surgically created and randomly assigned to the three treatment groups: 1) control (no filling material); 2) Gel-MA hydrogel; 3) Hst1/ Gel-MA hydrogel. Samples were retrieved 1, 2, and 4 weeks post-surgery and subjected to gross examination and a series of histomorphometric and immunological analyses. In comparison with the control and Gel-MA alone groups, Hst1/Gel-MA hydrogel was associated with significantly higher International Cartilage Repair Society score, Modified O 'Driscoll Score, area percentages of newly formed bone, cartilage, collagen fiber and glycosaminoglycan, and expressions of collagen II and aggrecan expression. In conclusion, Hst1/Gel-MA hydrogels significantly enhance bone and cartilage regeneration, thus bearing promising application potential in repairing osteochondral defects.

Keywords: Histatin-1; Gel-MA hydrogels; Cartilage repair; Tissue engineering; Temporomandibular joint

1. INTRODUCTION

Osteochondral defects in temporomandibular joint (TMJ) can be resulted from acute injury, overloading or abnormal immune response [1, 2]. Patients suffering from osteochondral defects may lead to a lifetime of pain and restricted jaw motion even in daily activities such as talking, eating, and yawning [3].

The repair of osteochondral defects in TMJ is highly challenging due to its limited self-regenerative potential [1]. Firstly, the avascular property of condyle cartilage tissue leads to the lacking of classic healing cascade, such as coagulation, inflammation, blood invasion, and accumulation of pluripotent mesenchymal stem cells (MSCs) [4]. Secondly, the chondrocytes in the surrounding cartilage tissue show poor migration and proliferation [4, 5]. All these properties result in nearly no healing occurring to TMJ cartilage. Thirdly, when defects further enlarge to affect subchondral bone tissues, the blood supplies from bone tissues may, to some extent, trigger classic healing pattern and enhance MSCs' migration [6]. However, such a blood supply and migration of MSCs are too limited to facilitate the complete repair of osteochondral defects [7]. Meanwhile, the reduced TMJ area will result in mechanical overloading on the rest TMJ tissues, which may cause secondary mechanical damage to TMJ [1]. In clinic, osteochondral defects are managed mainly using various autografts, such as autologous chondrocytes implantation [8] and mosaicplasty [9, 10]. These treatments show beneficial effects in the healing of osteochondral defects by providing chondrocytes. However, their usage is highly limited due to the limited availability of autografts and donor-site pain and morbidity [11]. Consequently, continuous efforts have been attempted to repair osteochondral defects.

Cartilage tissue engineering (TE) is a promising technique that elaborately involves various combinations of biomaterial scaffolds, bioactive agents and stem cells to facilitate tissue reconstruction [12]. Scaffolds are the essential part of TE, for they provide a scaffolding matrix for cell migration and neo-tissue generation in the repair site. One of the most commonly used TE scaffolds is methacrylated gelatin (Gel-MA) that is a hydrolyzed form of, and has the same chemical composition as collagen, thus bearing good biocompatibility without the risk of pathogen transmission as collagen [13]. Gelatin contains lots of adhesive ligands, such as arginine-glycine-aspartic acid sequences so as to promote cell adhesion and migration [14]. Its excellent fluidity before crosslinking makes Gel-MA flexibly fit into the complicated form of defects [15]. Right after a short photo-crosslinking time, Gel-MA can transit from liquid to hydrogel and reach 50-60 KPa stiffness, which is favorable for cartilage and bone tissue formation [16]. Albeit so, Gel-MA still lacks intrinsic capacities of inducing angiogenesis and MSCs homing, thus being unable to facilitate sufficient repair of osteochondral defects [17]. This limitation of Gel-MA may be approached by encapsulating MSCs [18] or bioactive agents [19]. In contrast to

MSCs-based TE, bioactive agents-based TE technique bears a series of advantages, such as low cost, wide sources, and low regulatory barriers in clinical translation [20, 21]. An ideal bioactive agent should be able to induce both angiogenesis and MSCs migration from bone defect area to cartilage lesion site so as to facilitate the repair of osteochondral defects.

One of such bioactive agents is Histatin-1 (Hst1) that belongs to a cationic and histidine-rich peptide family originally found in the saliva of higher primates [22]. Hst1 bears a potent capacity to stimulate the adhesion and migration of epithelial cells [23-26], fibroblasts [27] and osteoblasts [28, 29]. Meanwhile, it can promote cell metabolic activity [26] and maintain cell viability in various conditions [28, 29]. Furthermore, Hst1 shows a very strong angiogenetic property [30]. Recently, in an ectopic bone induction model, we show that Hst1 significantly promotes bone morphogenetic protein 2 (BMP2)-induced angiogenesis and osteogenesis [31]. However, the effect of Hst1 on the repair of osteochondral defects remains unexplored. In this study, we hypothesized that Hst1-functionalized Gel-MA hydrogels could sufficiently promote the repair of critical-size osteochondral defects in TMJ.

2. RESULTS

2.1 Postoperative course

All the animals recovered well postoperatively and had adequate food intake to maintain baseline body weight. There were no significant postoperative complications within the 4-week monitoring span.

2.2 Selection of Hst1's dosage

To determine the optimal dosage of Hst1 to promote osteochondral repair, preliminary study was carried out to explore the repair effects of Gel-MA with 3 different dosages of Hst1: 50, 500 and 1000 (µg) per defect. At 2 weeks, only mild new bone formation but not cartilage formation was detected in the defects with 50 µg Hst1/Gel-MA (Figure. 1 A-A1, D-D1). In contrast, much more new bone formation and several islands of newborn cartilage could be observed in the defects treated with 500 µg Hst1/Gel-MA (Figure. 1 B-B1, E-E1). Interestingly, the defects treated with 1000 µg Hst1/Gel-MA were almost fulfilled with tremendous new bone tissue (Figure. 1 C-C1, F-F1), while newly formed cartilage tissue was rarely detected. Thus, we chose 500 µg Hst1 per defect in the following experiments.
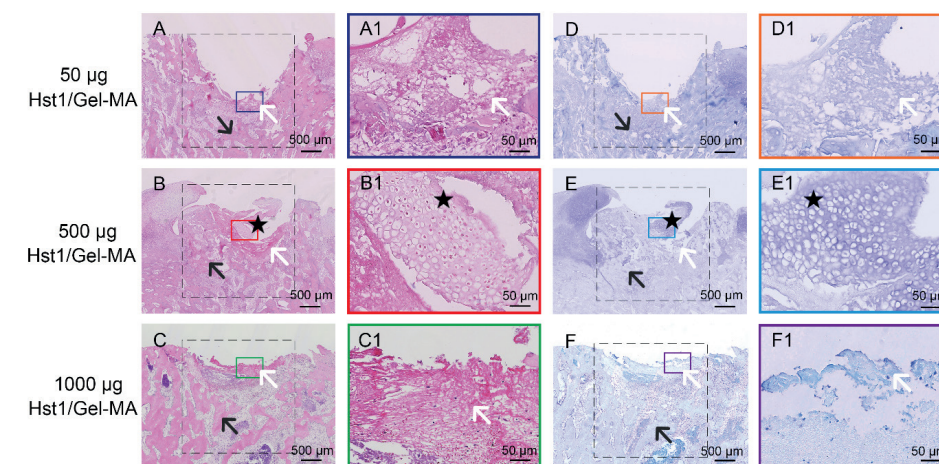

Figure 1. Light micrographs of H&E-stained (A-C) and toluidine blue stained (D-F) tissue sections of rabbit condyles with critical-size (3 mm in diameter and 3 mm in depth) osteochondral defects that were treated using Gel-MA with 3 different dosages of Hst1 (A, D) 50, (B, E) 500 and (C, F) 1000 (µg) per defect. The tissues were retrieved at 2 weeks post-operation and then subjected to histologic processing and sectioning. The dotted square area indicated the original defect area. Black star: immature cartilage cells; Black arrow: newly formed subchondral bone; White arrow: Hst1/Gel-MA materials. Scale bar = 500 µm in **A**-**F;** Scale bar = 50 µm in **A1**-**F1**.

2.3 Macroscopic evaluation

At 1 week, the defects were still hollow and showed distinct edges from the surrounding cartilage in the control group (Figure. 2 A). In Gel-MA group, the defects were filled with white rough tissue with a clear border. The surface of the defects remained concave (Figure. 2 B). Moreover, the defects of Hst1/Gel-MA group were filled with pale pinkish tissue. There was little depression in the defects and the margin with normal cartilage was indistinct (Figure. 2 C). The International Cartilage Repair Society (ICRS) macroscopic scores of Hst1/Gel-MA group were significantly higher than the scores of Gel-MA group and control group ($P < 0.05$) (Figure. 2 J).

At 2 weeks, the tissues in the vicinity of the original defect further collapsed, resulting in a pronounced extension of the defect order and the enlargement of the defect area (Figure. 2 D). The defect surfaces of Gel-MA group showed a red, irregular, depressed morphology without visible collapse of the surrounding tissues (Figure. 2 E). The defect border was still sharply defined. In comparison, cartilage defects were filled with pale red tissue with obscure demarcation from surrounding cartilage in Hst1/Gel-MA group (Figure. 2 F). The ICRS macroscopic scores of Hst1/Gel-MA group were significantly higher than those of Gel-MA group and control group. Statistically significant differences could be found between each two groups at this time point ($P < 0.05$) (Figure. 2 K).

At 4 weeks, further enlargement of the defect border could be observed in the control group. Irregular fibrous-like tissue formation was found in the defects (Figure. 2 G). In comparison, the defects of Gel-MA group were filled with reddish tissue, and the surface remained depressed (Figure. 2 H). In contrast, in Hst1/Gel-MA group, there was firm, smooth, cartilage-like tissue filled in the defects. Additionally, the color and morphology of the newly regenerated tissue were similar to the adjacent normal cartilage (Figure. 2 I). The ICRS macroscopic scores of Hst1/Gel-MA group were significantly higher than those of Gel-MA group ($P < 0.05$) and control group ($P < 0.001$). Notably, the mean score of Hst1/Gel-MA group was three times that of control group (Figure. 2 L).
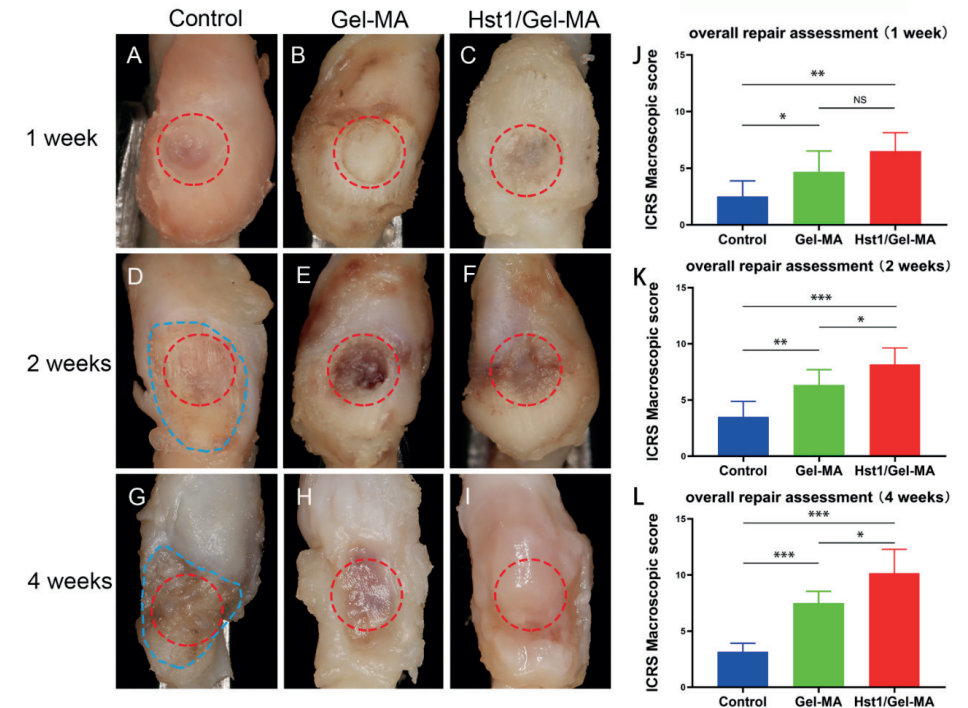

Figure 2. Photographs and macroscopic evaluation of rabbit condyle osteochondral defects of TMJ, which were treated as control group (A, D, G), Gel-MA group (B, E, H) and Hst1/Gel-MA group (C, F, I). The tissues were retrieved at 1, 2 and 4 weeks post operation and then photographed and scored using ICRS macroscopic scores (J-L). The red circle area represents the original defect area, and the blue irregular area represents the enlarged absorption area. (n = 6, $^*P < 0.05$; $^{**}P < 0.01$; $^{***}P < 0.001$ and NS = not significant).

2.4 Histologic observation and histomorphometric analysis on HE-stained tissue sections

At 1 week, in control group, nearly no newly regenerated tissue could be detected in the defects of the control group with the bone surface uncovered. There were still a large amount of porous Gel-MA materials in both Gel-MA group and Hst1/Gel-MA group. However, only in the Hst1/Gel-MA group, some immature chondrocytes and other cells infiltrated into the porous structures of Gel-MA. The area percentages of the newly formed subchondral bone tissue and cartilage in the Hst1/Gel-MA group were significantly higher than Gel-MA group ($P < 0.05$) and control group ($P < 0.01$). However, there were no significant difference between Gel-MA group and control group (Figure. 4 A-B). Meanwhile, the Modified O'Driscoll Score (MODS) in the groups of Hst1/Gel-MA

and Gel-MA were significantly higher than that MODS in the control group. Whereas no significant difference in MODS could be detected between Hst1/Gel-MA group and Gel-MA group (Figure. 4 C).

At 2 weeks, the defects in control group still showed the absence of tissue repair with the subchondral bone surface still exposed. In Gel-MA group, few cells infiltrated into the porous Gel-MA materials. In comparison, new cartilage and bone tissue formed and replaced the Gel-MA materials gradually in Hst1/Gel-MA group. The area percentages of the newly formed cartilage in Hst1/Gel-MA group and Gel-MA group were significantly higher than control group ($P < 0.01$) (Figure. 4 A). Whereas no significant difference in the area percentages of the newly formed cartilage could be detected between Hst1/Gel-MA group and Gel-MA group (Figure. 4 A). Meanwhile, the area percentages of the newly formed subchondral bone tissue in Hst1/Gel-MA group were significantly higher than Gel-MA group ($P < 0.01$) and control group ($P < 0.001$) (Figure. 4 B). Whereas, there were no significant difference between Gel-MA group and control group (Figure. 4 B). In addition, Hst1/Gel-MA group and Gel-MA group had significantly higher MODS than control group ($P < 0.01$) (Figure. 4 D). However, no significant difference in MODS could be detected between Hst1/Gel-MA group and Gel-MA group (Figure. 4 D).

At 4 weeks, the defect area in control group was significantly enlarged and remained hollow with a layer of fibrous tissue on its surface (Figure. 3 A-A1). In Gel-MA group, only a few cells could be detected within the remained Gel-MA materials. There was mainly fibrous tissue along with Gel-MA materials in the defects (Figure. 3 B-B1). Meanwhile, the new subchondral bone formation could be detected (Figure. 3 B-B2). In comparison, large areas of newly formed cartilage were detected in Hst1/Gel-MA group (Figure. 3 C). Notably, chondrocytes exhibited a typical lacunae structure with columnar alignment (Figure. 3 C1). Besides, right above the newly formed chondrocyte layer, there appeared to be a fibrous layer – similar to that found in the native mandibular condylar cartilage (Figure. 3 C1). At the bottom of the defect, improved subchondral bone remodeling with a large number of osteoblasts and osteoclasts infiltrated was observed (Figure. 3 C2). Evidence of neovascularization was detected in the junction between subchondral bone and hydrogel (Figure. 3 C2). Additionally, the mean area percentage of newly formed cartilage in Hst1/Gel-MA group was almost two times that of the Gel-MA group ($P < 0.01$), and they were both significantly higher than control group ($P < 0.001$) (Figure. 4 A). The area percentages of the newly formed subchondral bone tissue in Hst1/Gel-MA group were significantly higher than Gel-MA group ($P < 0.05$) and control group ($p < 0.001$) (Figure. 4 B). Meanwhile, Hst1/Gel-MA group had significantly higher MODS compared to Gel-MA group ($P < 0.01$) and control group ($P < 0.001$). Gel-MA group had significantly higher MODS than control group ($P < 0.01$) (Figure. 4 E).
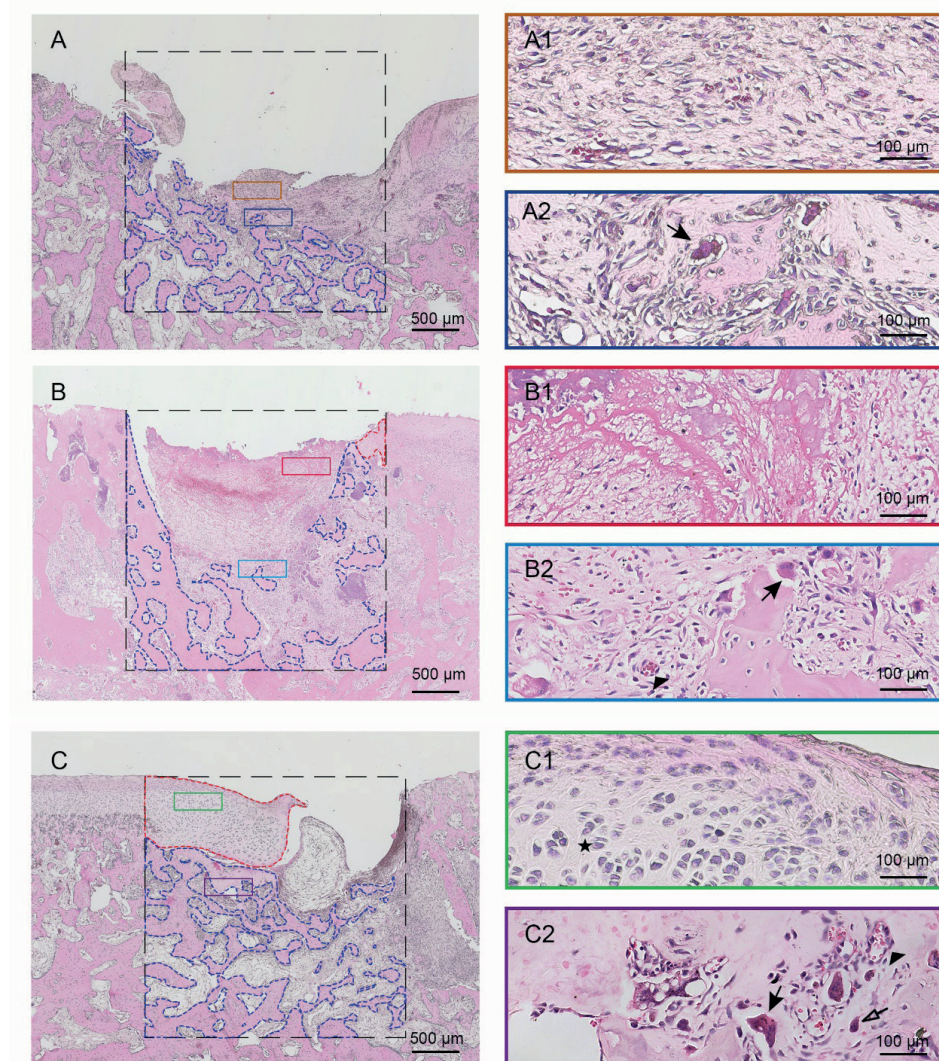
Figure 3. Light micrographs of H&E-stained tissue sections of rabbit condyles with critical-size (3 mm in diameter and 3 mm in depth) osteochondral defects that were treated as control group (A, A1-A2), Gel-MA group (B, B1-B2) and Hst1/Gel-MA group (C, C1 -C2). The tissues were retrieved at 4 weeks and then subjected to histologic processing and sectioning. The dotted square area is the original defect area (3mm*3mm). The newly formed cartilage is delineated by the red dotted line, and the new subchondral bone is delineated by the blue dotted line. Solid arrow: osteoclasts; Hollow arrow: osteoblasts; Black star: immature cartilage cells; Triangle: neovascularization. Scale bar = 500 µm in A-C; Scale bar = 50 µm in A1-C2.
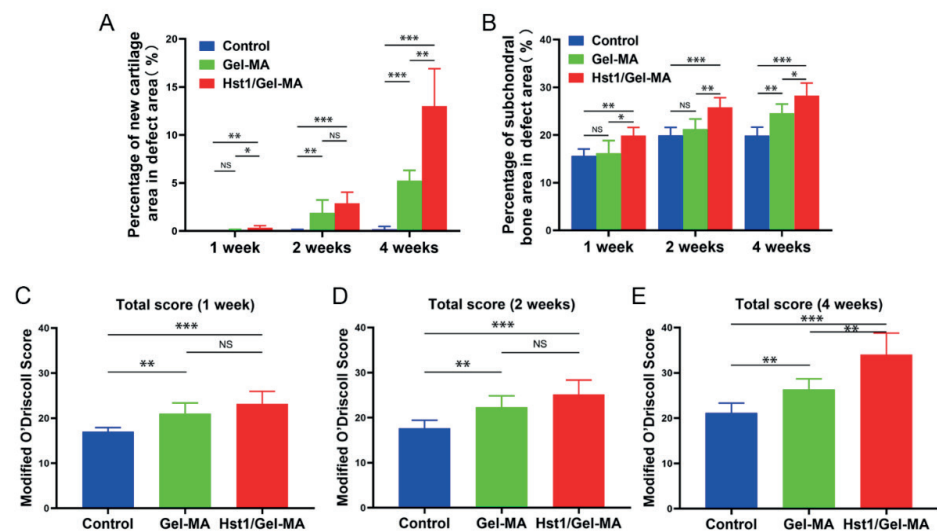
Figure 4. Quantitative analysis of newly formed cartilage (A) and subchondral bone area (B), and the MODS evaluation for repaired osteochondral defects at 1, 2, and 4 weeks post-implantation (C-E). (n = 6, *P < 0.05, **P < 0.01, ***P < 0.001 and NS = not significant).

2.5 Histologic observation and histomorphometric analysis on sections with alcian blue staining or Masson's trichrome staining

At 2 weeks, the Masson's trichrome staining exhibited very little blue staining in the Gel-MA materials, which revealed that nearly no collagen fibers especially collagen type II formation (Figure. 5 A-A1). Alcian blue staining also showed little to no glycosaminoglycan (GAG) production with staining was almost absent in the defects (Figure. 5 C-C1). In comparison, the existence of collagen fibers especially collagen type II in the newly formed cartilage was proved by Masson's trichrome staining in Hst1/Gel-MA group (Figure. 5 B-B1). The alcian blue staining also revealed the content of GAG of the extracellular matrix (ECM) in the cartilage islands in the defects (Figure. 5 D-D1). Histomorphometric analysis displayed Hst1/Gel-MA group had significantly higher GAG and collagen fibers content than Gel-MA group and control group (P < 0.001) (Figure. 6 A, C, E).

At 4 weeks, in Gel-MA group, little collagen deposition, which was stained blue by Masson's trichrome staining, was found in the Gel-MA materials (Figure. 5 E-E1). Alcian blue staining exhibited rare GAG formation in the defects (Figure. 5 G-G1). In Hst1/Gel-MA group, Masson's trichrome staining showed strongly blue staining in the newly formed cartilage, indicating collagen fibers were produced in the ECM in the repair tissues (Figure. 5 F-F1). Meanwhile, alcian blue staining confirmed the presence of GAG

in the ECM in the newly formed cartilage (Figure. 5 H-H1). Histomorphometric analysis showed Hst1/Gel-MA group had significantly higher GAG and collagen fibers content than Gel-MA group and control group (P < 0.001) (Figure. 6 B, D, F).
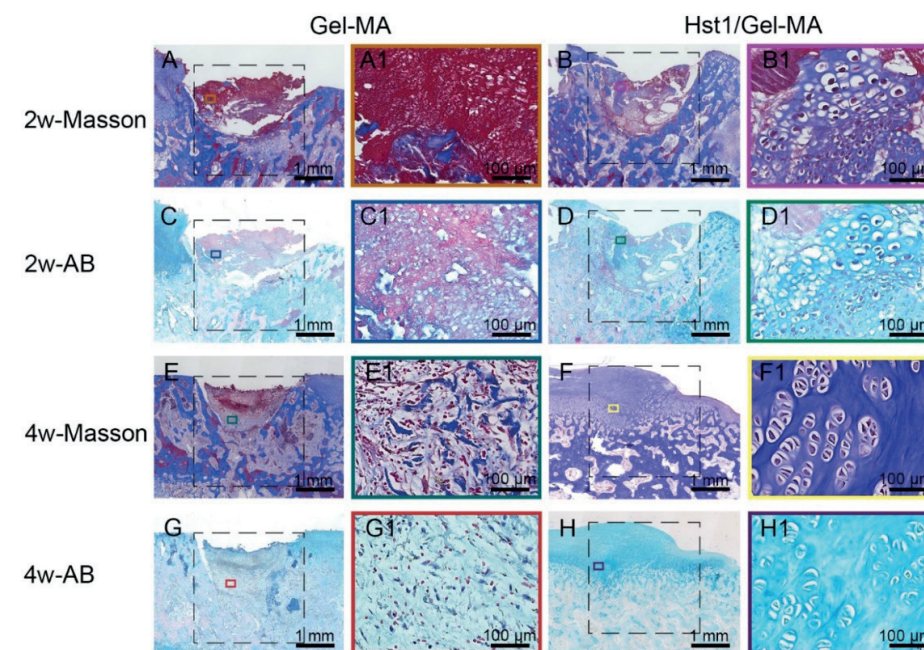

Figure 5. Light micrographs of alcian blue stained and Masson's trichrome stained tissue sections of repaired osteochondral defects in Gel-MA group and Hst1/Gel-MA group. Masson's trichrome staining at 2 weeks (A, B) and 4 weeks (E, F); alcian blue staining at 2 weeks (C, D) and 4 weeks (G, H). The dotted square area indicated the original defect area (3mm*3mm). Scale bar = 1 mm in A-H; Scale bar = 100 μm in A1-H1.
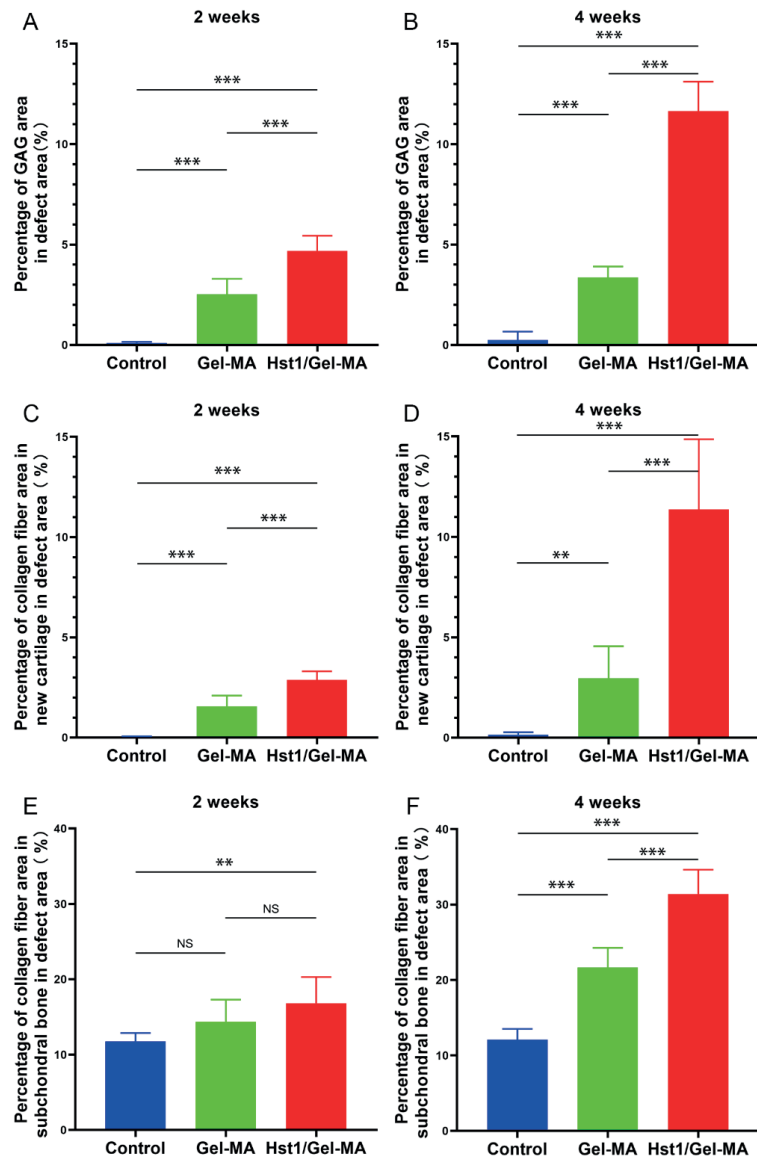
Figure 6. Quantitative analysis of the formation of GAG, collagen fiber in new cartilage and subchondral bone in defect area at 2 and 4 weeks. Percentage of GAG area in defect area at 2 (A) and 4 weeks (B). Percentage of collagen fiber area in new cartilage in defect area at 2 (C) and 4 weeks (D). Percentage of collagen fiber area in subchondral bone in defect area at 2 (E) and 4 weeks (F). (n = 6, **P < 0.01, ***P < 0.001 and NS = not significant).

2.6 Immunohistochemical Evaluation

In Hst1/Gel-MA group, the expression of collagen II and aggrecan increased gradually over time, approaching that of normal cartilage by 4 weeks after implantation (Figure. 7 C-D). However, in Gel-MA group, there was almost no presentation of collagen II and aggrecan in the repaired tissue at 1 and 2 weeks. While slight staining of collagen II and aggrecan is visible in Gel-MA group at 4 weeks (Figure. 7 A-B). No positive immunostaining for collagen II and aggrecan was observed in control group at all time points. The Hst1/Gel-MA group has statistically higher collagen II and aggrecan expression compared to Gel-MA group and control group at 4 weeks (P < 0.001) (Figure. 7 E-F).
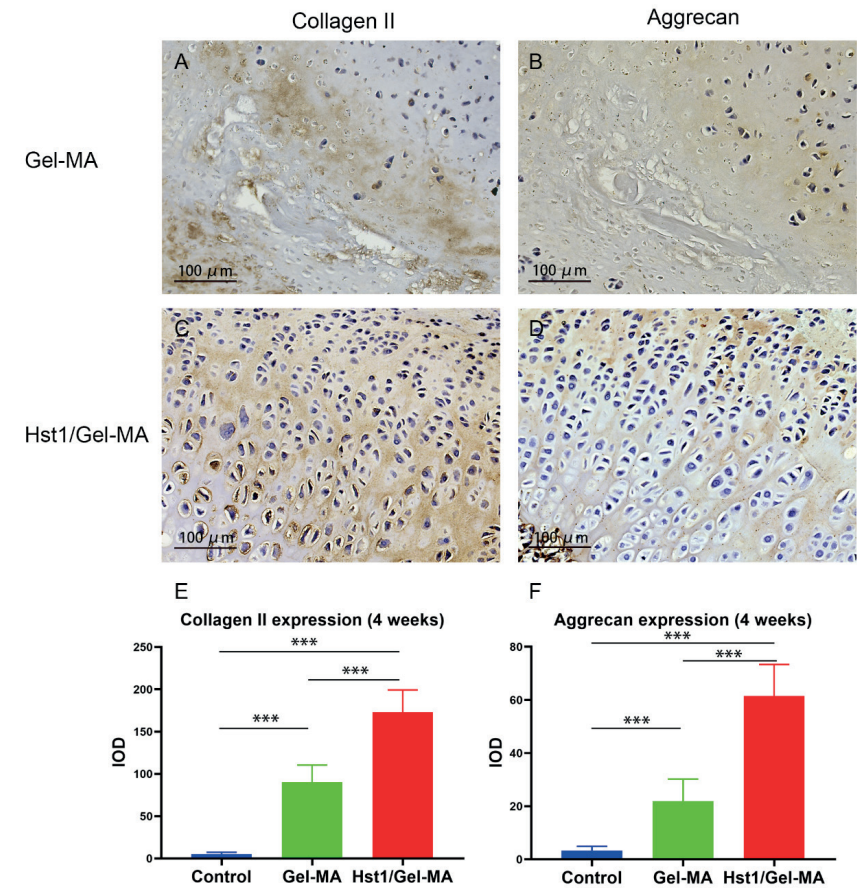

Figure 7. Light micrographs of immunohistochemical-stained tissue sections of collagen II (A, C) and aggrecan (B, D) in Gel-MA group (A, B) and Hst1/Gel-MA group (C, D). The tissues were retrieved at 4 weeks post-operation and then subjected to immunohistochemical processing and sectioning. Quantitative analysis of collagen II (E) and aggrecan (F) expression at 4 weeks. Scale bar = 100 μm in A-D. (n = 6, ***P < 0.001).

3. DISCUSSION

The major difficulty in the repair of critical-size osteochondral defects in TMJ mainly lies in insufficient self-regenerative cells in lesion areas [32]. Most of current clinical therapies try to approach this problem by auto-transplanting chondrocytes or cartilage, which is, whereas, restricted by its very limited availability and donor site morbidity [11]. In this study, to provide a viable treatment option, we developed a Hst1-functionalized Gel-MA hydrogel to combine the chondroconductive property of Gel-MA and the potent angiogenetic and cell-activating capacity of Hst1. To our best knowledge, this was the first study to show the effects of Hst1 on the repair of osteochondral defects in TMJ. Our data showed that Hst1/Gel-MA hydrogel group possessed a significant higher ICRS score and MODS in comparison with the Gel-MA group and control group. Furthermore, histomorphometric analysis showed significantly higher expression of collagen II, aggrecan, collagen fiber, GAG, and more newly formed subchondral bone and cartilage in Hst1/Gel-MA hydrogel group than the Gel-MA group and control group. Our data suggested a promising application potential of Hst1/Gel-MA hydrogels in promoting the repair of critical-size osteochondral defects in TMJ.

The spontaneous healing efficacy of osteochondral defects in TMJ is highly dependent on the size, shape and depth of the lesions. For example, nearly no spontaneous tissue repair can be detected in a 2-mm-diameter and 2-mm-deep defect in rabbit TMJ 3 weeks postoperatively since the lesions are largely restricted in cartilage or on bone-cartilage interface that bears limited resources of blood supply and regenerative cells [33]. When defects are deeper and affect the subchondral bone area, the blood supply from subchondral bone area will trigger classical healing cascade and bring self-regenerative MSCs [6]. In this situation, the healing efficacy shows a diameter-dependent pattern. In a deep (3-mm in-depth) and non-critical-size (1-mm in diameter) defect, the healing efficacy varied with some defects filled with disorganized fibrocartilage and others filled with a nearly continuous layer of cartilage at 6 weeks post-operation [3]. Most *in-vivo* studies reported that when the defects with a diameter of less than 3 mm, may partially heal [34, 35]. Therefore, the osteochondral defects with a 3-mm depth and 3-mm diameter in rabbit TMJ can be considered as critical-size defects. In our current study, we surgically created critical-size osteochondral defects (3 mm in depth and 3 mm in diameter) in the TMJ of rabbits to investigate the healing efficacy of Hst1/Gel-MA hydrogel. We found that only some bone formation but nearly no newly formed cartilage in the untreated defects. This finding suggested that blooding and blood-borne MSCs from subchondral bone were insufficient to trigger chondrogenesis. Instead, the defects further collapsed and caused the breakdown of the surrounding tissues. This phenomenon might be attributed to the secondary mechanical damages and further breakdown surrounding the lesions [1] since the loading of TMJ may be redistributed to a much less surface area of TMJ condyle.

As alternative to the auto-transplantations in clinic, a large variety of TE techniques have been developed to repair osteochondral defects. Scaffold material is an indispensable element for TE to facilitate cell migration, proliferation and differentiation as well as the slow release of bioactive agents [36]. In recent TE techniques, there is a trend in the design of material scaffolds to contain three parts with different physicochemical and biological properties in order to facilitate the regeneration of bone, cartilage, and the osteochondral interface, separately [37]. However, such complicated designs are less favorable for their industrial fabrication and clinical application. To develop a filling material with more promise for clinical application, we adopted Gel-MA hydrogels as the scaffold material. Gel-MA hydrogels possess a series of advantages, such as biocompatible, biodegradable, nonimmunogenic, physicochemical modifiable, and cost-effective [38]. They are highly similar to the natural ECM both to provide a free entrance for nutrients and to support cellular growth [39]. Furthermore, Gel-MA can also support its encapsulated chondrocytes to produce the ECM such as, proteoglycan and type II collagen deposition as well as chondrogenesis-related gene expression [40]. In our study, compared with the absence of tissue repair in the defects and even further breakdown of the surrounding tissues in control group, in Gel-MA group, cell infiltration in the non-degraded scaffold could be detected with subchondral bone deposition at 4 weeks. In addition, Masson's trichrome staining and alcian blue staining confirmed that there were little collagen fibers and GAG formation in the defects, which indicated that Gel-MA supported the cartilage ECM formation. Meanwhile, the score of ICRS and MODS of Gel-MA group were significantly higher than the control group ($P<0.05$). However, Gel-MA hydrogel alone is not sufficient to heal the critical-size osteochondral defects in TMJ.

To further promote the healing efficacy, scaffold materials need to be functionalized by bioactive agents, particularly proteinous growth factors, such as BMP2 and transforming growth factor-β (TGF-β). Osteochondral regeneration is delicately regulated by several macromolecular protein growth factors, such as bone morphogenetic proteins (BMPs). BMP2 belongs to BMP family, a group of proteinaceous growth factors under the TGF-β superfamily [41]. The classical role for BMP2 was considered to be the induction of (ectopic) cartilage and bone formation [42, 43]. In the USA, the product containing recombinant human (rh)BMP2 in absorbable collagen has already been approved for clinical application in nonunion bone fractures and spinal fusions [44]. However, the use of BMP2 is associated with the concern that BMP2 induces chondrocyte hypertrophy followed by cartilage calcification [45], which compromises the regeneration of cartilage layer. In the field of TE, there is a trend to combine growth factors to specifically induce and maintain the zonal phenotypes of cartilage. For example, cultivation of MSCs with TGF-β1 (3 ng/mL) and BMP7 (300 ng/mL) induced the synthesis of superficial zone protein, a marker for chondrocytes in the superficial zone [46], whereas insulin-like growth factor-1 (IGF-1) did not [47, 48]. Cultivation of chondrocytes isolated from the middle zone

with TGF-β1 (30 ng/mL) and IGF-1 (100 ng/mL) significantly increased collagen synthesis [49, 50]. TGF-β1 also contributes to the maintenance of calcified cartilage zone as deletion of TGF-β1 receptor gene from chondrocytes delayed endochondral ossification [51] and cultivation of bovine hypertrophic chondrocytes with a combination of TGF-β1 (30 ng/mL) and 3% (w/v) hydroxyapatite (HA) increased matrix deposition and mineralization [51, 52]. However, such complex of zonal arrange of growth factors is less feasible for biomedical application. In addition, proteinous growth factors bear low production yield, thus high cost, which further limits their clinical application. As promising alternatives to the macromolecular protein growth factors, peptides can be chemically and standardly synthesized, thus bearing better reproducibility and yielding efficiency [53].

In this study, we adopted Hst1 — a salary bioactive peptide that can promote a series of cell activities, such as cell adhesion [23, 24, 27, 30, 54], spreading [23, 24], migration [22], cell-cell adhesion [24, 55], angiogenesis [30] and metabolic activity [26, 28, 29, 56]. Furthermore, Hst1's cell-activating effects seem to be independent on cell types, thus bearing broad applicability. Such a property is of paramount importance particularly for the application in repairing osteochondral defects, which needs the promotion of the functions of both osteoblast and chondrocytes [44, 45]. To identify the optimal concentration of Hst1, we first performed a preliminary study to investigate the dose-dependent effects of Hst1 on the repair of critical-size osteochondral defects. We found that 50 μg Hst1/Gel-MA was associated with insufficient new bone and cartilage formation, while 1000 μg Hst1/Gel-MA resulted in overstimulation of bone regeneration with compromised cartilage formation. It seems that over-dosed Hst1 will be more beneficial for bone regeneration and detrimental for cartilage formation. This may be due to the angiogenetic effect of Hst1. As for other cell types, Hst1 can promote the adhesion, spreading, and migration of endothelial cells [30]. Furthermore, Hst1 can also promote vascular morphogenesis and angiogenesis through activating Rac1 via a "RIN2/Rab5/Rac1 signaling pathway axis [30]. And it is well established that overstimulated angiogenesis can cause cartilage resorption and bone deposition [57]. Consequently, overdosed Hst1 may harm cartilage regeneration through overstimulated angiogenesis.

On the other hand, angiogenesis is an indispensable biological event to deliver nutrients, oxygen and hematopoietic stem cells to cartilage defect, thereby facilitating cartilage regeneration. Consequently, elaborate modulation of Hst1 dosage is critical for balanced bone and cartilage formation. In this study, we showed that 500 μg Hst1/Gel-MA hydrogels significantly promoted the deposition of ECM compositions (collagen II and aggrecan) and the formation of zonally-structured cartilage in the defects in comparison with Gel-MA hydrogels and the control (P<0.05). The score of ICRS and MODS in Hst1/Gel-MA group were also significantly higher than Gel-MA group. In addition, numerous chondroblasts in the newly formed cartilage layer, osteoblasts and

osteoclasts in the subchondral bone could be observed in our study, indicating a high level of metabolism and remodeling. Consequently, 500 μg Hst1/Gel-MA hydrogel proves to be the most efficacious in repairing osteochondral defects in TMJ. In comparison with the complicated designed osteochondral constructs, the 500 μg Hst1/Gel-MA hydrogel is much more feasible and simpler, thus bearing more promising potential in biomedical application.

However, hitherto, there is no report about the effect on how Hst1 facilitate chondrogenesis. One mechanism can be its well-established promoting effect on the adhesion, spreading and migration of hematopoietic stem cells from subchondral bone and/or the chondrocytes from adjacent cartilage. The latter may be possible since that newly formed cartilage islands first occurred in the vicinity of the remaining cartilage. However, it is also well known that mature chondrocytes hardly migrate to repair cartilage defect [4]. Therefore, it may also be explained that Hst1 induced the secretion of growth factors and cytokines from mature chondrocytes so as to stimulate the chondrogenic differentiation of hematopoietic stem cells. It is recently established that Hst1 promoted osteogenic differentiation [58, 59]. Furthermore, our recent study shows that Hst1 significantly promotes BMP2-induced angiogenesis and osteogenesis [31]. Therefore, the interaction of exogenous Hst1 and endogenous BMP2 may be also responsible for the promotion of cartilage formation in the current study. Previous studies suggested that Hst's effect is associated with several signaling pathways, such as RAC1 [30], ERK [23], p38 [58], NF-κB [59], etc. However, there has been no report on the effect of Hst1 on chondrocytes.

4. MATERIALS AND METHODS

4.1 The preparation of hydrogel prepolymer solution and Hst1
The freeze-dried Gel-MA was purchased from Wenzhou institute (Wenzhou institute, Wenzhou, China). 200 mg of freeze-dried Gel-MA macromer was dissolved in 1 ml of PBS containing 0.5% (w/v) 2-hydroxy-1-(4-(hydroxyethoxy)phenyl)-2-methyl-1-propanone (Irgacure2959, CIBA Chemicals, Basel, Switzerland) at 80 °C and then filtered with a bacteria filter. The prepolymer solution was stored at 40 °C in a constant temperature water bath. It was prepared freshly before surgery and stored in bacteria-free bottles.

The lyophilized linear Hst1 peptide was obtained from the University of Amsterdam (Amsterdam, Holland) and stored at -20 °C. 500 μg Hst1 peptide was dissolving in 21.1 μL (defect volume) prepolymer solution to prepare as the implantation.

4.2 Group set-up

In order to screen the optimal dosage of Hst1, we first performed a preliminary experiment, where we selected three dosages of Hst1: 50, 500, and 1000 μg per defect according to the findings in our recent publication [31]. In that study, we evaluated the promoting effect of Hst1 at 50, 200, 500 μg/sample on BMP2-induced osteogenesis and angiogenesis. Micro-CT analysis showed that Hst1 dose-dependently increased the total volume of BMP2-induced newly formed bone. Furthermore, 50 μg of Hst1 per sample could already significantly enhance trabecular number of, and decrease trabecular separation of new bone. Immunostaining analysis showed that 500 μg of Hst1 per sample significantly enhanced the BMP2-induced osteogenic markers (RunX2, Collagen) and angiogenic markers (FGF-2, CD105 and CD31). According to these results, in the preliminary experiment of the current study, we chose 50 and 500 μg, and also added 1000 μg to see whether we could get more beneficial effects with the higher dosage. Two weeks post-surgery, animals were sacrificed and subjected to histological process. According to the histological staining result, 500 μg Hst1/Gel-MA was associated with a sufficient and balanced bone and cartilage formation in comparison with 50 μg Hst1/Gel-MA and 1000 μg Hst1/Gel-MA (see details in the section 2.2). Consequently, we chose 500 μg Hst1 per defect in the following experiments.

In the formal experiments, we set up 3 groups: Control group (the defects receiving no filling material); Gel-MA alone group (the defects filled with Gel-MA hydrogels without Hst1); and 500 μg Hst1/Gel-MA group (the defects filled with 500 μg Hst1-functionalized Gel-MA hydrogels). Fifty-four adult male New Zealand white rabbits (Zhejiang Chinese Medical University, China) were randomly divided into the 3 groups with 18 animals in each group. Six animals per group per time point were euthanized at 1, 2, and 4 weeks post-surgery.

4.3 Animal surgery

The animal study was reviewed and approved by the Institutional Animal Care and Use Committee of Zhejiang Chinese Medical University (no. IACUC-20180625-04). With the animals under general anesthesia, a pre-auricular skin incision was per-formed over the right TMJ. Then the condyle was exposed, and an osteochondral defect, 3 mm in diameter and 3 mm in depth, was created in the condyle with a 3 mm diameter drill. Surgery was performed on the right condyle of TMJ in all 54 animals, and the left remained intact. In Control group, the defects were created but not treated. Gel-MA group was given Gel-MA hydrogels. Hst1-functionalized Gel-MA hydrogels were injected into the defect sites in Hst1/Gel-MA group. The Gel-MA prepolymer solution was photopolymerized by Ultraviolet rays (365 nm, 90 s) in Gel-MA group and Hst1/Gel-MA group (Figure. 8). The articular capsule and skin were closed independently with nylon sutures. After

all procedures were finished, animals were returned to the animal facility. Penicillin (1 : 100000) was intraperitoneally administered every 24 hours in the first three days after surgery.
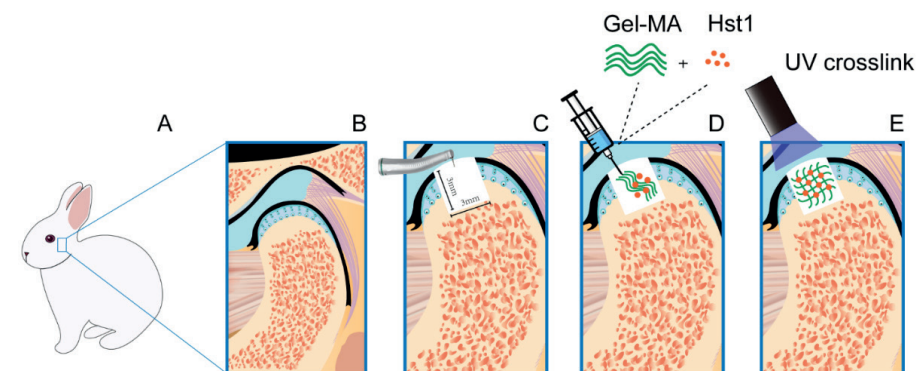

Figure 8. The schematic diagram of the rabbit mandibular joint condyle critical-size (3 mm in diameter and 3 mm in depth) osteochondral defects model (3 mm*3 mm) established procedure.

4.4 Macroscopic score evaluation

The right TMJ and surrounding tissues were retrieved for macroscopic score evaluation. The gross appearance of the defect sites was photographed and blindly scored by 3 independent observers using ICRS macroscopic scoring system which contains four categories: the degree of repair, integration to border zone, macroscopic appearance, and overall repair assessment [60].

4.5 Histological examination

The specimens for histological analysis were fixed in 10% neutral formalin (Sigma-Aldrich, USA) after macroscopic evaluation for 24 h at 4 °C, and then decalcified with 10% ethylenediaminetetraacetate (EDTA) - buffered saline solution (Sigma-Aldrich, USA) for 28 days. The specimens were cut into 4 μm thickness after embedded in paraffin (Sigma-Aldrich, USA). The sagittal sections were stained with Hematoxylin Eosin, Masson's trichrome, and Alcian blue (Sigma-Aldrich, USA). At the same time, the sections were immunohistochemistry for type II collagen (COL II) and Aggrecan content, which were performed following the manufacturer's protocol. Under a light microscope (CX51; Olympus), all slices were examined, and a digital charge-coupled device camera (TrueChrome Metrics; Tucson Photonics) was used for recording. The sections were blindly scored by 3 different experienced pathologists using MODS [61].

4.6 Histomorphometry analysis

The original defect area is bounded by a 3*3 mm square in all slices of the samples. The top of the square is aligned with the cartilage surface on both sides. Percentage of newly formed subchondral bone area, new cartilage area, collagen fiber area and GAG area in defect area was detected and calculated by Image Analysis Software (image pro plus 6.0). The areas of newly formed subchondral bone and new cartilage were selected through a manual delineation by researchers (as indicated by the blue (for bone tissue) and red (for cartilage tissue) dotted lines in Figure 3) but not the grey value-based automatic selection by software. The content of collagen II and aggrecan was expressed by integrated optical density (IOD) measured using image pro plus 6.0.

4.7 Statistical analysis

Statistical analysis between all groups was performed using One-way ANOVA and Tukey's HSD post hoc test using the SPSS 18.0 statistical analytical software (SPSS Inc, USA). All the data were presented as mean ± standard deviation (SD). In all cases, P-values < 0.05 were considered to indicate a statistically significant difference, and P-values < 0.01 and 0.001 were considered highly significant differences.

5. CONCLUSION

In this study, we, for the first time, demonstrated that Hst1-functionalized Gel-MA hydrogel was a simple, feasible and efficacious construct to facilitate the repair of osteochondral defects of TMJ in rabbits. In contrast to the current therapies, such as auto-transplantation of chondrocytes or cartilages, Hst1/Gel-MA bears unlimited availability and no donor-site morbidity. All these properties conferred Hst1/Gel-MA a promising potential in biomedical application. Further studies should be performed to investigate the effects and molecular mechanisms of Hst1 on chondrogenesis.

REFERENCES

[1] S. Kuroda, K. Tanimoto, T. Izawa, S. Fujihara, J.H. Koolstra, E. Tanaka, Biomechanical and biochemical characteristics of the mandibular condylar cartilage, Osteoarthritis Cartilage 17(11) (2009) 1408-15.

[2] L. LeResche, Epidemiology of temporomandibular disorders: implications for the investigation of etiologic factors, Crit Rev Oral Biol Med 8(3) (1997) 291-305.

[3] N.H. Dormer, K. Busaidy, C.J. Berkland, M.S. Detamore, Osteochondral interface regeneration of rabbit mandibular condyle with bioactive signal gradients, J Oral Maxillofac Surg 69(6) (2011) e50-7.

[4] A.P. Newman, Articular Cartilage Repair, Am J Sports Med 26(2) (1998) 309-24.

[5] A.C.A. Marijnissen, F.P.J.G. Lafeber, Re: E. B. Hunziker. Articular cartilage repair: basic science and clinical progress. A review of the current status and prospects. Osteoarthritis and Cartilage 2002; 10:432–63, Osteoarthritis and Cartilage 11(4) (2003) 300-301.

[6] J. Buckwalter, Mechanical Injuries of Articular Cartilage, Iowa Orthopaedic Journal 12(50) (1992).

[7] K. Mithoefer, T. McAdams, R.J. Williams, P.C. Kreuz, B.R. Mandelbaum, Clinical Efficacy of the Microfracture Technique for Articular Cartilage Repair in the Knee, The American Journal of Sports Medicine 37(10) (2009) 2053-2063.

[8] J.D. Harris, R.A. Siston, X. Pan, D.C. Flanigan, Autologous chondrocyte implantation: a systematic review, J Bone Joint Surg Am 92(12) (2010) 2220-33.

[9] K.H. Bridwell, P.A. Anderson, S.D. Boden, A.R. Vaccaro, J.C. Wang, What's New in Spine Surgery, J Bone Joint Surg Am 94(12) (2012) 1140-6.

[10] P. Abdel-Sayed, D.P. Pioletti, Strategies for improving the repair of focal cartilage defects, Nanomedicine (Lond) 10(18) (2015) 2893-905.

[11] G.C. Gracitelli, V.Y. Moraes, C.E. Franciozi, M.V. Luzo, J.C. Belloti, Surgical interventions (microfracture, drilling, mosaicplasty, and allograft transplantation) for treating isolated cartilage defects of the knee in adults, Cochrane Database Syst Rev 9 (2016) CD010675.

[12] W. Bao, M. Li, Y. Yang, Y. Wan, X. Wang, N. Bi, C. Li, Advancements and Frontiers in the High Performance of Natural Hydrogels for Cartilage Tissue Engineering, Front Chem 8 (2020) 53.

[13] Y. Wang, H. Li, Y. Feng, P. Jiang, J. Su, C. Huang, Dual micelles-loaded gelatin nanofibers and their application in lipopolysaccharide-induced periodontal disease, Int J Nanomedicine 14 (2019) 963-976.

[14] C. Puckert, E. Tomaskovic-Crook, S. Gambhir, G.G. Wallace, J.M. Crook, M.J. Higgins, Molecular interactions and forces of adhesion between single human neural stem cells and gelatin methacrylate hydrogels of varying stiffness, Acta Biomater 106 (2020) 156-169.

[15] Jane Ru Choi et al. , Recent advances in photo-crosslinkable hydrogels for biomedical applications 2019.66(1):40-53.

[16] X. Fang, J. Xie, L. Zhong, J. Li, D. Rong, X. Li, J. Ouyang, Biomimetic gelatin methacrylamide hydrogel scaffolds for bone tissue engineering, J Mater Chem B 4(6) (2016) 1070-1080.

[17] M.-E. Han, B.J. Kang, S.-H. Kim, H.D. Kim, N.S. Hwang, Gelatin-based extracellular matrix cryogels for cartilage tissue engineering, Journal of Industrial and Engineering Chemistry 45 (2017) 421-429.

[18] W. Zhu, H. Cui, B. Boualam, F. Masood, E. Flynn, R.D. Rao, Z.Y. Zhang, L.G. Zhang, 3D bioprinting mesenchymal stem cell-laden construct with core-shell nanospheres for cartilage tissue engineering, Nanotechnology 29(18) (2018) 185101.

[19] G. Irmak, M. Gümüşderelioğlu, Photo-activated platelet-rich plasma (PRP)-based patient-specific bio-ink for cartilage tissue engineering, Biomedical Materials 15(6) (2020).

[20] H. Madry, M. Alini, M.J. Stoddart, C. Evans, T. Miclau, S. Steiner, Barriers and strategies for the clinical translation of advanced orthopaedic tissue engineering protocols, European Cells and Materials 27s (2014) 17-21.

[21] Y.R. Lee, Y.H. Lee, K.H. Kim, S.A. Im, C.K. Lee, Induction of Potent Antigen-specific Cytotoxic T Cell Response by PLGA-nanoparticles Containing Antigen and TLR Agonist, Immune Netw 13(1) (2013) 30-3.

[22] P. Torres, M. Castro, M. Reyes, V.A. Torres, Histatins, wound healing, and cell migration, Oral Diseases 24(7) (2018) 1150-1160.

[23] M.J. Oudhoff, J.G. Bolscher, K. Nazmi, H. Kalay, W. van 't Hof, A.V. Amerongen, E.C. Veerman, Histatins are the major wound-closure stimulating factors in human saliva as identified in a cell culture assay, FASEB J 22(11) (2008) 3805-12.

[24] I.A. van Dijk, K. Nazmi, J.G. Bolscher, E.C. Veerman, J. Stap, Histatin-1, a histidine-rich peptide in human saliva, promotes cell-substrate and cell-cell adhesion, FASEB J 29(8) (2015) 3124-32.

[25] I.A. van Dijk, A.F. Beker, W. Jellema, K. Nazmi, G. Wu, D. Wismeijer, P.M. Krawczyk, J.G. Bolscher, E.C. Veerman, J. Stap, Histatin 1 Enhances Cell Adhesion to Titanium in an Implant Integration Model, J Dent Res 96(4) (2017) 430-436.

[26] D. Shah, D. Ali, D. Shukla, S. Jain, V.K. Aakalu, Effects of histatin-1 peptide on human corneal epithelial cells, PLoS One 12(5) (2017) e0178030.

[27] M.J. Oudhoff, P.A. van den Keijbus, K.L. Kroeze, K. Nazmi, S. Gibbs, J.G. Bolscher, E.C. Veerman, Histatins enhance wound closure with oral and non-oral cells, J Dent Res 88(9) (2009) 846-50.

[28] M. Castro, P. Torres, L. Solano, L.A. Cordova, V.A. Torres, Histatin-1 counteracts the cytotoxic and antimigratory effects of zoledronic acid in endothelial and osteoblast-like cells, J Periodontol 90(7) (2019) 766-774.

[29] G.Q. Huang, G.G. Yi, L.W. Wu, S.F. Feng, W. Wu, L. Peng, R.W. Yi, W. Ma, X. Lu, Protective effect of histatin 1 against ultraviolet-induced damage to human corneal epithelial cells, Exp Ther Med 15(1) (2018) 679-684.

[30] P. Torres, J. Diaz, M. Arce, P. Silva, P. Mendoza, P. Lois, A. Molina-Berrios, G.I. Owen, V. Palma, V.A. Torres, The salivary peptide histatin-1 promotes endothelial cell adhesion, migration, and angiogenesis, FASEB J 31(11) (2017) 4946-4958.

[31] P. Sun, A. Shi, C. Shen, Y. Liu, G. Wu, J. Feng, Human salivary histatin-1 (Hst1) promotes bone morphogenetic protein 2 (BMP2)-induced osteogenesis and angiogenesis, FEBS Open Bio 10(8) (2020) 1503-1515.

[32] S. Zhou, Z. Cui, J.P. Urban, Factors influencing the oxygen concentration gradient from the synovial surface of articular cartilage to the cartilage-bone interface: a modeling study, Arthritis Rheum 50(12) (2004) 3915-24.

[33] T. Suzuki, K. Bessho, K. Fujimura, Y. Okubo, N. Segami, T. Iizuka, Regeneration of defects in the articular cartilage in rabbit temporomandibular joints by bone morphogenetic protein-2, Br J Oral Maxillofac Surg 40(3) (2002) 201-6.

[34] A.M. Haleem, C.R. Chu, Advances in Tissue Engineering Techniques for Articular Cartilage Repair, Oper Tech Orthop 20(2) (2010) 76-89.

[35] C.R. Chu, M. Szczodry, S. Bruno, Animal models for cartilage regeneration and repair, Tissue Eng Part B Rev 16(1) (2010) 105.

[36] J.R. Choi, K.W. Yong, J.Y. Choi, A.C. Cowie, Recent advances in photo-crosslinkable hydrogels for biomedical applications, Biotechniques 66(1) (2019) 40-53.

[37] M.T. Frassica, M.A. Grunlan, Perspectives on Synthetic Materials to Guide Tissue Regeneration for Osteochondral Defect Repair, ACS Biomater Sci Eng 6(8) (2020) 4324-4336.

[38] S. Xiao, T. Zhao, J. Wang, C. Wang, J. Du, L. Ying, J. Lin, C. Zhang, W. Hu, L. Wang, K. Xu, Gelatin Methacrylate (GelMA)-Based Hydrogels for Cell Transplantation: an Effective Strategy for Tissue Engineering, Stem Cell Rev Rep 15(5) (2019) 664-679.

[39] M. Sun, X. Sun, Z. Wang, S. Guo, G. Yu, H. Yang, Synthesis and Properties of Gelatin Methacryloyl (GelMA) Hydrogels and Their Recent Applications in Load-Bearing Tissue, Polymers (Basel) 10(11) (2018).

[40] T. Lam, T. Dehne, J.P. Kruger, S. Hondke, M. Endres, A. Thomas, R. Lauster, M. Sittinger, L. Kloke, Photopolymerizable gelatin and hyaluronic acid for stereolithographic 3D bioprinting of tissue-engineered cartilage, J Biomed Mater Res B Appl Biomater 107(8) (2019) 2649-2657.

[41] P. Ducy, G. Karsenty, The family of bone morphogenetic proteins, Kidney Int 57(6) (2000) 2207-14.

[42] M.R. Urist, Bone formation by autoinduction, Science 150(3698) (1965) 893-9.

[43] E.A. Wang, V. Rosen, P. Cordes, R.M. Hewick, M.J. Kriz, D.P. Luxenberg, B.S. Sibley, J.M. Wozney, Purification and characterization of other distinct bone-inducing factors, Proc Natl Acad Sci U S A 85(24) (1988) 9484-8.

[44] P.C. Bessa, M. Casal, R.L. Reis, Bone morphogenetic proteins in tissue engineering: the road from laboratory to clinic, part II (BMP delivery), J Tissue Eng Regen Med 2(2-3) (2008) 81-96.

[45] P.M. van der Kraan, E.N. Blaney Davidson, W.B. van den Berg, Bone morphogenetic proteins and articular cartilage: To serve and protect or a wolf in sheep clothing's?, Osteoarthritis Cartilage 18(6) (2010) 735-41.

[46] J.A. Andrades, S.C. Motaung, P. Jimenez-Palomo, S. Claros, J.M. Lopez-Puerta, J. Becerra, T.M. Schmid, A.H. Reddi, Induction of superficial zone protein (SZP)/lubricin/PRG 4 in muscle-derived mesenchymal stem/progenitor cells by transforming growth factor-beta1 and bone morphogenetic protein-7, Arthritis Res Ther 14(2) (2012) R72.

[47] E.M. Darling, K.A. Athanasiou, Growth factor impact on articular cartilage subpopulations, Cell Tissue Res 322(3) (2005) 463-73.

[48] S.V. Eleswarapu, N.D. Leipzig, K.A. Athanasiou, Gene expression of single articular chondrocytes, Cell Tissue Res 327(1) (2007) 43-54.

[49] E. Coates, J.P. Fisher, Gene expression of alginate-embedded chondrocyte subpopulations and their response to exogenous IGF-1 delivery, J Tissue Eng Regen Med 6(3) (2012) 179-92.

[50] Z. Lin, C. Willers, J. Xu, M.-H. Zheng, The chondrocyte: biology and clinical application, Tissue Eng 12(7) (2006) 1971-84.

[51] T. Sueyoshi, K. Yamamoto, H. Akiyama, Conditional deletion of Tgfbr2 in hypertrophic chondrocytes delays terminal chondrocyte differentiation, Matrix Biol 31(6) (2012) 352-9.

[52] T. Niikura, A.H. Reddi, Differential regulation of lubricin/superficial zone protein by transforming growth factor beta/bone morphogenetic protein superfamily members in articular chondrocytes and synoviocytes, Arthritis Rheum 56(7) (2007) 2312-21.

[53] A. Mousavizadeh, A. Jabbari, M. Akrami, H. Bardania, Cell targeting peptides as smart ligands for targeting of therapeutic or diagnostic agents: a systematic review, Colloids Surf B Biointerfaces 158 (2017) 507-517.

[54] M.J. Oudhoff, K.L. Kroeze, K. Nazmi, P.A. van den Keijbus, W. van 't Hof, M. Fernandez-Borja, P.L. Hordijk, S. Gibbs, J.G. Bolscher, E.C. Veerman, Structure-activity analysis of histatin, a potent wound healing peptide from human saliva: cyclization of histatin potentiates molar activity 1,000-fold, FASEB J 23(11) (2009) 3928-35.

[55] I.A. van Dijk, M.L. Ferrando, A.E. van der Wijk, R.A. Hoebe, K. Nazmi, W.J. de Jonge, P.M. Krawczyk, J.G.M. Bolscher, E.C.I. Veerman, J. Stap, Human salivary peptide histatin-1 stimulates epithelial and endothelial cell adhesion and barrier function, FASEB J 31(9) (2017) 3922-3933.

[56] D. Ma, W. Sun, K. Nazmi, E.C.I. Veerman, F.J. Bikker, R.T. Jaspers, J.G.M. Bolscher, G. Wu, Salivary Histatin 1 and 2 Are Targeted to Mitochondria and Endoplasmic Reticulum in Human Cells, Cells 9(4) (2020).

[57] J. Harper, M. Klagsbrun, Cartilage to bone--angiogenesis leads the way, Nat Med 5(6) (1999) 617-8.

[58] W. Sun, D. Ma, J.G.M. Bolscher, K. Nazmi, E.C.I. Veerman, F.J. Bikker, P. Sun, H. Lin, G. Wu, Human Salivary Histatin-1 Promotes Osteogenic Cell Spreading on Both Bio-Inert Substrates and Titanium SLA Surfaces, Front Bioeng Biotechnol 8 (2020) 584410.

[59] P. Torres, N. Hernandez, C. Mateluna, P. Silva, M. Reyes, L. Solano, S. Venegas, A. Criollo, K. Nazmi, F.J. Bikker, J.G.M. Bolscher, M. Garrido, M. Caceres, V.A. Torres, Histatin-1 is a novel osteogenic factor that promotes bone cell adhesion, migration, and differentiation, Journal of Tissue Engineering and Regenerative Medicine (2021).

[60] M.P. van den Borne, N.J. Raijmakers, J. Vanlauwe, J. Victor, S.N. de Jong, J. Bellemans, D.B. Saris, S. International Cartilage Repair, International Cartilage Repair Society (ICRS) and Oswestry macroscopic cartilage evaluation scores validated for use in Autologous Chondrocyte Implantation (ACI) and microfracture, Osteoarthritis Cartilage 15(12) (2007) 1397-402.

[61] D.E. Bonasia, A. Marmotti, A.D. Massa, A. Ferro, D. Blonna, F. Castoldi, R. Rossi, Intra- and inter-observer reliability of ten major histological scoring systems used for the evaluation of in vivo cartilage repair, Knee Surg Sports Traumatol Arthrosc 23(9) (2015) 2484-93.

SUPPORTING INFORMATION

Human salivary histatin-1-functionalized Gelatin Methacrylate Hydrogels promotes the regeneration of cartilage and subchondral bone in temporomandibular joint

Changjing Shi #, Yu Yao #, Lei Wang #, Ping Sun, Jianying Feng * and Gang Wu *

* : Corresponding authors
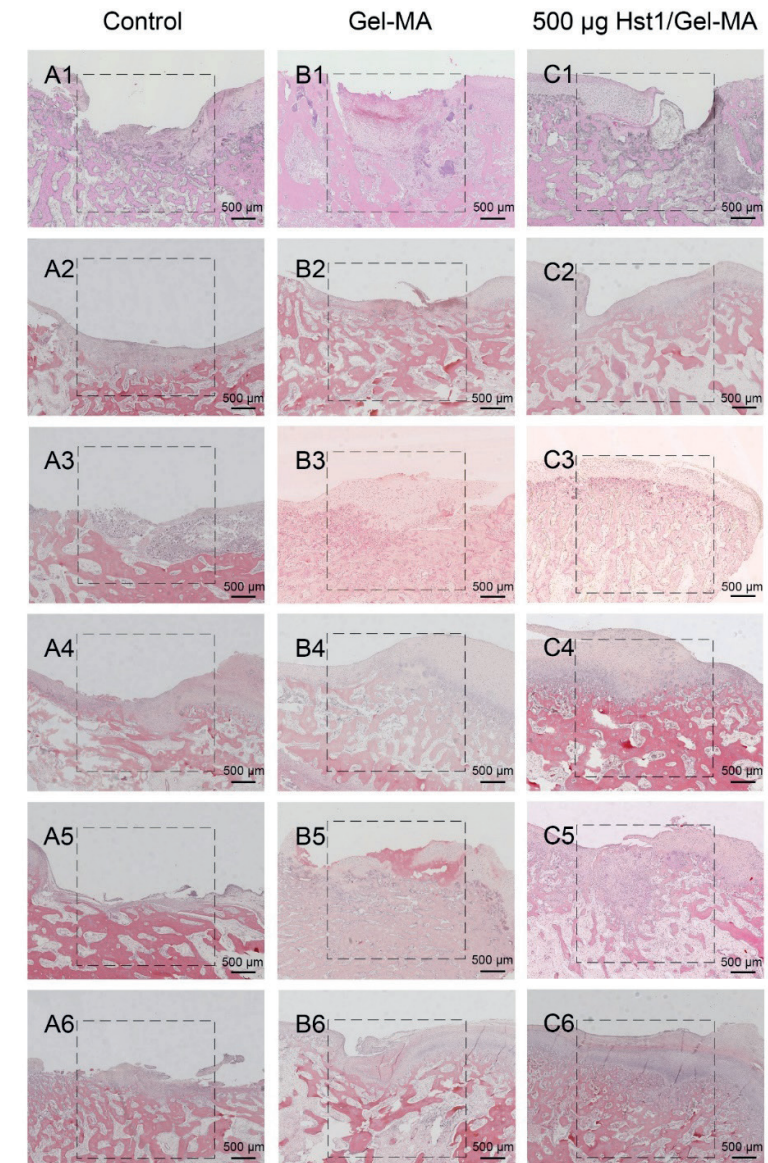
# : These authors contributed equally to this work.

Figure S1. Light micrographs of H&E-stained tissue sections of rabbit condyles with critical-size (3 mm in diameter and 3 mm in depth) osteochondral defects that were treated as control group (A1–A6), Gel-MA group (B1–B6) and Hst1/Gel-MA group (C1–C6). N = 6 animals per group. The tissues were retrieved at 4 weeks post operation and then subjected to histologic processing and sectioning. The dotted square area is the original defect area (3 mm*3 mm). Scale bar = 500 μm.

Chapter 4

Construction of injectable self-healing macroporous hydrogels via a template-free method for tissue engineering and drug delivery

Lei Wang, Fen Deng, Wenwen Wang, Afeng Li, Conglie Lu, Hao Chen, Gang Wu, Kaihui Nan*, Lingling Li*

* Corresponding author

ABSTRACT

Because of their ease of handling and excellent biocompatibility, injectable macroporous hydrogels have received a considerable interest in the fields of tissue engineering and drug delivery systems because of their unique application in minimally invasive surgical procedures. In this study, *in-situ* forming, injectable, macroporous, self-healing gelatin (GE)/oxidized alginate (OSA)/adipic acid dihydrazide (ADH) hydrogels were prepared using a high-speed shearing treatment and were stabilized by Schiff base reaction and acylhydrazone bonds. Their injectability, self-healing ability, rheology, microstructure, equilibrium water content, and *in-vitro* biodegradation were investigated. We found that the injectable GE/OSA/ADH precursors remained in a liquid form, flowed easily for several minutes, and gelled rapidly at body temperature. The gelation time could be regulated by varying the ratio of GE, OSA and ADH. The obtained hydrogels had an interconnected macroporous structure and self-healing ability. Human epidermal growth factor was loaded by *in-situ* mixing in GE/OSA/ADH hydrogels and was released with good bioactivity as evaluated by ELISA. Moreover, L929 cells proliferated on GE/OSA/ADH hydrogels, as verified by Cell Counting Kit-8 and Live/Dead assays. Furthermore, encapsulation of NIH 3T3 cells within GE/OSA/ADH hydrogels demonstrated that the hydrogel promoted cell survival, proliferation, and migration. *In-vivo* studies showed that the hydrogels had a good injectability, *in-situ* gelation, and tissue biocompatibility. Therefore, GE/OSA/ADH hydrogel represented a novel and safe injectable macroporous self-healing hydrogel for tissue engineering scaffold and drug delivery vehicle purposes.

Keywords: Macroporous hydrogel; Gelatin/oxidized alginate/adipic acid dihydrazide; Injectable; Self-healing; Drug release; Cell encapsulation; Tissue engineering

1. INTRODUCTION

In the past years, the development of minimally invasive surgical (MIS) techniques has undergone exponential growth, as evidenced by the increasing number of related reports [1]. MIS are performed through a small incision, and when compared to traditional surgical techniques, are characterized by a reduced tissue exposure to pathogens, reduced skin disturbance, and reduced operative site dead space [2]. Consequently, MIS have the advantages of a shorter hospitalization period, reduced discomfort, and reduced risks of postoperative infections [3]. The rapid development of MIS requires the establishment of different injectable biomaterials to meet its clinical needs. Ideally, injectable materials are administered as a flowable liquid that can travel through needles, fit to complicated tissue defects, achieve good contact with neighboring tissues, and solidify by chemical cross-linking or physical gelation *in situ* [4]. Furthermore, injectable biomaterials must be biocompatible, biologically stable, biodegradable, mechanically robust, and have beneficial therapeutic effects by promoting the regeneration of new tissue.

For such complex applications, an injectable hydrogel is ideal. However, the pores in injectable hydrogels are generally smaller than mammalian cells, which are typically around 20-30μm, therefore cellular infiltration is limited and the regeneration of new tissues is impaired. Thus, injectable hydrogels should be prepared containing macropores with a size of 50-300 μm, and a high degree of interconnectivity to facilitate transport of nutrients and oxygen, as well as cell migration and attachment [5, 6]. In the past, several approaches have been employed to generate injectable macroporous hydrogels, including cryogelation techniques [6, 7] and porogens co-encapsulations [8-10]. Cryogelation seemed promising in terms of preparation of injectable macroporous hydrogels because the formed hydrogels contained shape memory properties, and ice crystals are biocompatible porogens that would leach out during reaction [11]. However, this method required that prior to polymerization precursors are kept in a semi-frozen state, which severely affects their injectability. In addition, stable reaction kinetics cannot be ensured in all conditions [12]. Regarding porogens co-encapsulations, generation of a homogeneous mix of porogens and uniform dispersion are major challenges. Moreover, insufficient diffusion of fluids through the hydrogels may leave porogens undissolved, thereby posing threats to the structural integrity and biocompatibility of the hydrogels.

Inevitably, a macroporous structure would weaken the inherent strength of injectable hydrogels, making them susceptible to mechanical fracture. However, the mechanical strength of hydrogels can be modulated by several toughening techniques, such as the formation of a double-network hydrogel [13], sliding-ring hydrogels [14], hydrophobically-associated hydrogels [15], hydrogen-bonding enhanced hydrogels [16], and nano [17] or micro composite hydrogels [18]. Among them, double-network hydrogels have shown

great potential in the production of hydrogels with versatile mechanical properties [19, 20]. Instead of gelation by the formation of covalent bonds, such as photo [21, 22], redox initiated polymerization [22, 23] and additional cross-linking reactions [24, 25], double-network hydrogels are cross-linked by non-covalent bonds, (for example ionic crosslinking [26], hydrogen bonding [16]) or dynamic covalent bonds (for example Diels-Alder reactions [27], disulfide bonds [28], acylhydrazone bonds [29], phenylboronate esters [30]), which enable the hydrogels to autonomously repair cracks, thereby maintaining network integrity and stability of mechanical properties, and meeting the requirements of long-term use [25].

In this study, we designed a novel macroporous gelatin (GE)/oxidized alginate (OSA)/ adipic acid dihydrazide (ADH) hydrogel, which was prepared *in situ* by mixing of OSA, GE, and ADH solutions via one-pot synthesis. Alginate, a natural polysaccharide, is composed of two uronic acid units, such as β-(1,4), that are linked to D-mannuronic acid (M) and α-(1−4) linked L-guluronic acid (G), extracted from brown sea algae that have been widely used to fabricate hydrogels for tissue engineering purposes [31, 31]. Due to its excellent biocompatibility and biodegradation properties, gelatin, a partial derivative of collagen, has been extensively used in the field of tissue engineering and drug delivery [33, 34]. A macroporous structure was obtained by a high-speed shearing treatment, in which air is blended into the precursors' mixture to produce macro pores without using any porogens, templates, or other treatments. The self-healing ability of hydrogels was ascribed to two coexisting dynamic covalent bonds in the network, including an imine linkage formed by a Schiff base reaction between OSA and GE, as well as acyldrazone bonds between OSA and ADH. The self-healing ability of hydrogels not only better dissipates energy and helps them recover after fractures, but also strengthens their mechanical properties when macropores weaken the structural integrity of hydrogels. To the best of our knowledge, we were the first to realize injectable self-healing hydrogels with an *in situ*-forming macroporous structure, thereby taking advantage of our ingenuous high-speed shearing method. We hypothesize that our novel strategy and simple one-pot approach, along with the versatile gel system, may have great potential in the development of a novel generation of injectable self-healing hydrogels with a macroporous structure. These injectable macroporous self-healing hydrogels may be used in biomedical applications in the fields of tissue engineering, drug delivery, or regenerative medicine.

2. EXPERIMENTAL PROCEDURES

2.1 Materials

GE (Bloom 300), sodium alginate, ADH, sodium metaperiodate (NaIO$_4$) and human epidermal growth factor (hEGF) were purchased from Sigma-Aldrich (St. Louis, MO, USA). The human EGF ELISA kit was purchased from Thermo-Fisher (Waltham, MA, USA). Mouse fibroblast cell lines L929 and NIH 3T3 were obtained from the institute of Biochemistry and Cell Biology (Chinese Academy of Sciences, China). Dulbecco's modified Eagle Medium (DMEM), fetal bovine serum (FBS), penicillin-streptomycin solution; Live/Dead viability assay kit and Cell Counting Kit-8 (CCK-8) were purchased from Life Technology (Carlsbad, CA, USA). All aqueous solutions were prepared from analytical grade reagents (Sigma-Aldrich, St. Louis, MO, USA).

2.2 Oxidized Sodium Alginate Synthesis

OSA was synthesized as previously described.35 In brief, 5 g sodium alginate was dispersed in 25 mL ethanol. NaIO$_4$ (~4.32 g) was dissolved in 25 mL ultrapure water to prepare NaIO$_4$ solution, which was added dropwise to the sodium alginate dispersion and stirred at room temperature for 8 hours. The reaction was quenched by addition of equimolar ethylene glycol (1.124 mL) under continuous stirring for 30 min. The resultant suspension was dialyzed against ultrapure water (UPT-11-20T, Ulupure, China) using a dialysis membrane (MWCO: 3500 Da, Spectrum Lab, USA) for 7 days. Ultrapure water was changed several times until periodate was no longer detected. OSA was obtained by lyophilizing the dialysate.

The oxidation degree of sodium alginate was determined by quantifying the concentration of unconsumed periodates by iodometry as described previously [35]. In brief, 1 mL reaction mixture was mixed with a sufficient quantity of potassium iodide solution, and allowed to react for 10 min to consume all unreacted periodate ions. Next, liberated iodine was titrated with a standardized sodium thiosulphate solution using starch as the indicator. The titration volume of used sodium thiosulphate was monitored and indicated by disappearance of the color. Oxidation degree values were calculated as the average of three independent oxidation experiments.

Table 1. Formulations of GE/OSA/ADH hydrogels

Samples	GE:OSA (w/w)	GE (20%, µL)	OSA (10%, µL)	ADH (50%, µL)	ADH Concentration (%)
GE$_1$/OSA$_1$/ADH$_4$	1:1	100	200	26	
GE$_1$/OSA$_2$/ADH$_4$	1:2	50	200	21.7	
GE$_1$/OSA$_5$/ADH$_4$	1:5	30	300	28.7	4%
GE$_2$/OSA$_1$/ADH$_4$	2:1	200	200	34.8	
GE$_5$/OSA$_1$/ADH$_4$	5:1	150	60	18.3	
GE$_1$/OSA$_1$/ADH$_8$	1:1	100	200	57	
GE$_1$/OSA$_2$/ADH$_8$	1:2	50	200	47.6	
GE$_1$/OSA$_5$/ADH$_8$	1:5	30	300	62.9	8%
GE$_2$/OSA$_1$/ADH$_8$	2:1	200	200	76.2	
GE$_5$/OSA$_1$/ADH$_8$	5:1	150	60	40	

2.3 Fabrication of hydrogels

Desired amounts of precursors (GE, OSA, and ADH) were dissolved in phosphate buffered saline (PBS) to prepare 20%, 10%, and 50% (w/v) solutions, respectively. Then, pre-determined volumes of these solutions (Table 1) were pipetted into plastic tubes to obtain different formulations, which immediately underwent high-speed shearing treatment (IKA T10, Germany) for 60 s to produce the macroporous structure. Subsequently, macroporous formulations were placed in a water bath at 37 °C for 5 min to generate macroporous hydrogels. The gelation time was determined using the inverted tube test. To investigate the influence of formulation, shearing frequency and treatment time on the structure and morphology of hydrogels, different formulation, frequency and duration were adopted to prepare hydrogels. For each sample, the measurement was performed in triplicate.

2.4 Rheological characterization

Rheological characterization of hydrogels was performed using a rheometer (AR-2000, TA instrument, USA). The storage modulus (G') and loss modulus (G'') of the hydrogels were tested in the oscillatory mode using a parallel plate configuration (25 mm in diameter) at 37 °C. G' and G'' were quantified as a function of time at a constant angular frequency of 1 Hz and a constant strain of 1% from start to 10 min. Using a fixed strain level of 1%, the angular frequency was swept from 0.01 rad s^{-1} to 100 rad s^{-1}. Using a same frequency (1Hz), continuous step change of oscillatory strain between 1% and 1000% was used to assess the strain-induced damage and self-healing behavior of the hydrogel. To prevent water evaporation, a thin layer of silicon oil was used to seal the samples.

2.5 Injectability and self-healing properties of hydrogels

To verify the injectability of hydrogels prior to the gelation and self-healing process after crosslinking, each formulation was prepared and drawn into 26-gauge syringes. Hydrogel precursors were slowly injected into petri dishes and molds of different shapes. The self-healing characteristics of GE/OSA/ADH hydrogels were evaluated by keeping the surfaces at moist conditions for 5 min at room temperature without any external intervention. To monitor the injecting and self-healing process of the hydrogels, representative images were taken at specific time intervals.

2.6 Porosity and pore size

The pore volume was estimated by immersing the frozen dried samples of the hydrogels (volume of the hydrogel in swollen state was 1 mL) into the cyclohexane for 2h followed by measurement of the weight of the swollen samples. The porosity was calculated as follows:

$$\text{Porosity} = (m_{\text{swollen gel}} - m_{\text{dried gel}})/\, m_{\text{swollen gel}} \times 100\% \qquad (1)$$

All groups were done in triplicate and average value was shown.

The pore size of hydrogel scaffolds was characterized by using a field-emission scanning electron microscope (Nova NanoSEM200, FEI, USA). 6 images were taken for each sample. Average pore size of the hydrogel was calculated by Image J.

2.7 Scanning electron microscopy

Fractured lyophilized pieces of macroporous hydrogels were sputter-coated with gold for 60s. Both the surface and cross-sectional morphology were captured using a scanning electron microscope (Nova Nano SEM200, FEI, USA) at 15 kV.

2.8 Micro-computed tomography

Micro-computed tomography (micro-CT) Scanner (Y. Cheetah, YXLON International GmbH, Germany) was performed to create a three-dimensional image of the macroporous structure. The parameters for scanning were as follows: X-ray voltage = 55 kV, X-ray current = 90 µA, detector size = 1024×1024, and voxel resolution = 20 µm. The obtained images were reconstructed to create 3D geometry using VG Studio Max (Volume Graphics, Germany).

2.9 Equilibrium water content

To perform water content measurements, hydrogels were frozen dried to obtain a constant weight and immersed in PBS (pH 7.4) at 37 °C. At specific intervals, swollen hydrogels were removed from PBS and weighed until equilibrium was reached. The equilibrium water content of the hydrogels was calculated using the following equation:

$$EWC = (W_e - W_d) / W_d \times 100\% \qquad (2)$$

Where W_e and W_d represented the weights of the equilibrium-swollen and dry hydrogels, respectively. The equilibrium water content (EWC) was the mean ± standard deviation of three individual measurements.

2.10 In-vitro biodegradation

The degradation profile of hydrogels was followed *in vitro* by measuring the weight loss in PBS containing 10 IU/mL collagenase at 37 °C over time. After the removal of excess water on the surfaces, the weight of the hydrogel samples was immediately measured at indicated time points. The degradation rate was calculated using equation (3), in which W_t represented the weight of the hydrogel after degradation and W_o (the weight of hydrogel after incubating for 6 h) was chosen as the initial weight of degradation because of its swelling behavior:

$$Remaining\ weight\ (\%) = W_t/W_o \times 100\% \qquad (3)$$

2.11 Human epidermal growth factor release profile

HEGF was used as a model drug to investigate the *in-vitro* protein release ability of the hydrogels. To prepare hEGF-loaded hydrogels, hEGF was dissolved at different ratios in hydrogel precursor solution. In brief, similar volumes of the solutions (Table 1) and 10 μL of 20 μg/mL hEGF in PBS were mixed and pipetted into a micro centrifuge tube to obtain uniform solutions, which immediately underwent high-speed dispersion treatment (IKA T10) for 60 s, and were incubated at 37 °C for 5 min to form macroporous hydrogels. Hydrogels were transferred into dialysis membranes (MWCO: 10000 Da, Spectrum Lab, USA) and immersed into 20 mL PBS solution at 37 °C. One mL slow-released liquid was collected at 1 h, 2 h, 4 h, 8 h, 24 h, 48 h, 72 h, and 96 h and stored at −80 °C. The removed liquid was replaced with 1 mL fresh pre-warmed solution, and the level of released hEGF was determined by ELISA at designated time points (eBioscience, USA). Experiments were performed in triplicate.

2.12 In-vitro biocompatibility

L929 cells were used to test the *in-vitro* cytocompatibility of macroporous hydrogels, and were directly seeded onto hydrogel surfaces. OSA, GE, and ADH were sterilized by ethylene oxide and dissolved in sterilized PBS. L929 mouse fibroblasts (ATCC, USA) were cultured in medium (90% DMEM + 10% FBS + 1% penicillin–streptomycin) and seeded onto preformed hydrogels at a density of 1000 cells per well of 96-well tissue culture plate (TCPs). Cells that were cultured on TCP with same medium, in culture medium containing 10% DMSO and culture medium alone were set as negative control, positive control respectively. At indicated time points (1 day, 3 days, 5 days, and 7 days), samples were washed with PBS and incubated with CCK-8 for 3 h at 37 °C in the dark. OD values were measured using an ELISA plate reader (Varioskan LUX, Thermo-Fisher, USA) and cell viability (%) was calculated using the following equation:

$$Cell\ viability\ (\%) = OD_{test}/OD_{control} \times 100\%. \qquad (4)$$

In addition, a Live/Dead assay was carried out to evaluate the viability of cells on the hydrogels. Briefly, L929 cells were seeded onto preformed hydrogels at a density of 1000 cells per well of 96-well TCPs. At specific time intervals, cells were stained with "Live/Dead" solution, containing 2 mM calcein AM and 4 mM ethD-1 in PBS for 30 min at 37 °C. Cells treated with 75% ethanol for 10 min were set as positive controls. After 30 min of incubation, cells were rinsed 3 times with pre-warmed PBS and observed under a DMi8 microscope (LEICA, Germany). Experiments were performed in triplicate.

2.13 Encapsulation and proliferation of cells within hydrogels

To evaluate the proliferation of cells that were encapsulated within hydrogels, a lipophilic dye, CM-DiI (Molecular Probes/Invitrogen detection technologies, USA) was used to track CM-DiI-staineded NIH 3T3 cells. First, 10 μg/mL CM-DiI solution was prepared using the same medium as that of L929 cells and added to a 80% confluent cell monolayer. After incubation for 60 min at 37 °C, CM-DiI-containing medium was removed and cells were rinsed thoroughly with PBS. CM-DiI-stained cells were detached from the flask using trypsin and resuspended in fresh medium. Secondly, the CM-DiI stained cell suspension was added to the high-speed shearing treated $GE_1/OSA_1/ADH_4$ precursor solution under gentle vortexing to a final cell density of 2.5×10^5 cells/mL. The mixture was added to 24-well TCPs (200 μL/well) and after incubation for 5 min at 37 °C, cell-encapsulated hydrogels were formed. Next, 1 mL of fresh medium was added to each hydrogel and hydrogels were cultured for specific time intervals, during which the medium was changed every other day. At day 1, day 4, and day 8, cells inside the hydrogels were observed using a scanning laser confocal microscope (A1, Nikon, Japan), equipped with an argon laser. A series of images were collected throughout the z direction, and a three-dimensional composite image was created.

2.14 *In-vivo* biocompatibility

To further verify the *in-vivo* hydrogel formation ability and tissue biocompatibility of GE/OSA/ADH hydrogels, 500 μL of $GE_1/OSA_1/ADH_4$ hydrogels were subcutaneously injected into the dorsal area of Sprague Dawley rats using a 26-gauge syringe needle. The experimental procedures were performed in accordance with the international regulations for the care and use of laboratory animals as approved by the Chinese government (GB14925-2010). Sixteen male Sprague Dawley rats (age: 2 weeks; mean weight: 150±10 g) were randomly divided into two groups: a hydrogel group and a saline group. Rats were anesthetized by intravenous injection of chloral hydrate (10%, 30 mg/kg) (Leigen Biotechnology Company, Beijing, China), and hydrogels were subcutaneously injected into the dorsal area, which was shaved, marked, and sterilized prior to injection. At designated time points, two animals per group were sacrificed, and the hydrogel and its surrounding tissue were surgically removed and collected. The inflammatory responses were evaluated by hematoxylin & eosin (H&E) staining of tissue sections according to a standard protocol [36].

2.15 Statistical analysis

Data are expressed as the mean ± standard deviation (SD). To test the significance of differences between groups, one-way analysis of variance (ANOVA) was performed. $P < 0.05$ was considered statistically significant.

3. RESULTS AND DISCUSSION

3.1 Preparation of hydrogels

Periodate breaks vicinal glycols in sodium alginate to produce its dialdehyde derivatives (Figure 1a) [37]. The obtained OSA has an oxidation degree of 80.16% as confirmed by a titrimetric approach [35]. Macroporous GE/OSA/ADH hydrogels were prepared by homogeneously mixing solutions of OSA, GE, and ADH at 25°C with high-speed shearing. After high-speed shearing, the transparent solutions turned into milky precursors. When warmed to 37 °C, the precursors were solidified to be opaque hydrogels with the help of two dynamic bonds (imine bonds and acylhydrazone bonds), which were obtained via the reaction of aldehyde groups (from OSA) with amino groups (from GE) and hydrazides (from ADH) (Figure 1b). The gelation of GE/OSA/ADH hydrogels was confirmed by the tube inversion method.

To form ideal injectable hydrogels, an appropriate gelation rate is very important. A fast gelation process would lead to difficulties during injection, whereas a slow gelation rate may result in diffusion of the hydrogel precursors, encapsulated drug, or cells away from the desired site [38]. As determined by the tube inversion method, the gelation time of injectable hydrogels roughly increased from several seconds to 5 min, except for $GE_5/OSA_1/ADH_4$, which needed more than 10 min to cure (Figure 2a-e).
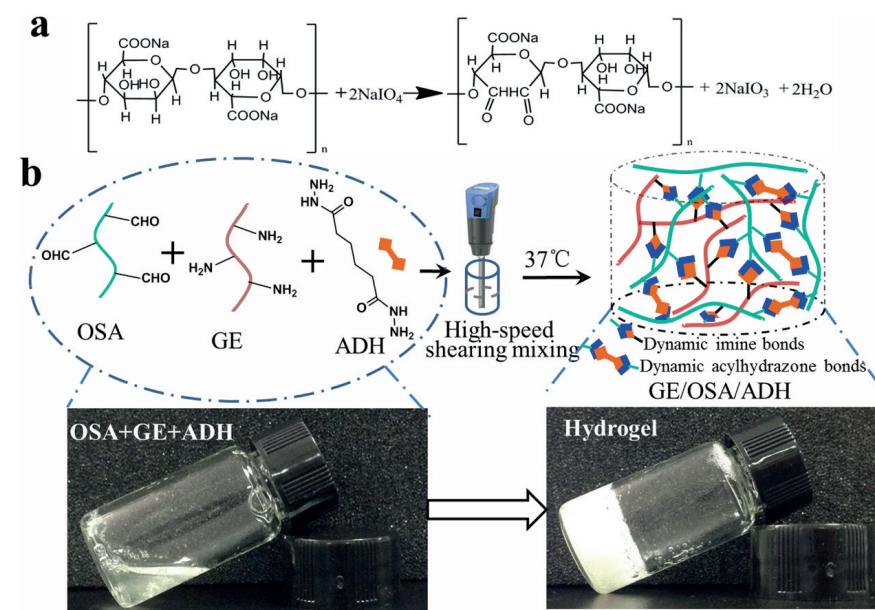

Figure 1. Synthesis of hydrogel : (a) the synthesis scheme of oxidized sodium alginate; (b) construction of macroporous GE/OSA/ADH hydrogels with high-speed shearing based on imine bonds and acylhydrazone bonds.

3.2 Rheology behavior

Rheometer was adopted to confirm the sol-to-gel transition of injectable macroporous hydrogels and their mechanical properties. The viscoelastic characteristics of injectable macroporous hydrogels were evaluated by monitoring the variations of G' and G" against time and frequency at 37 °C. As shown in Figure 2 (a-e), using a 4% ADH ratio, G' and G" increased with time; however, G' increased faster than G" and finally went beyond G". As expected, a faster gelation was observed for hydrogels with a higher OSA content. Precursors with a low modulus and rapid gelation characteristics made hydrogels injectable.
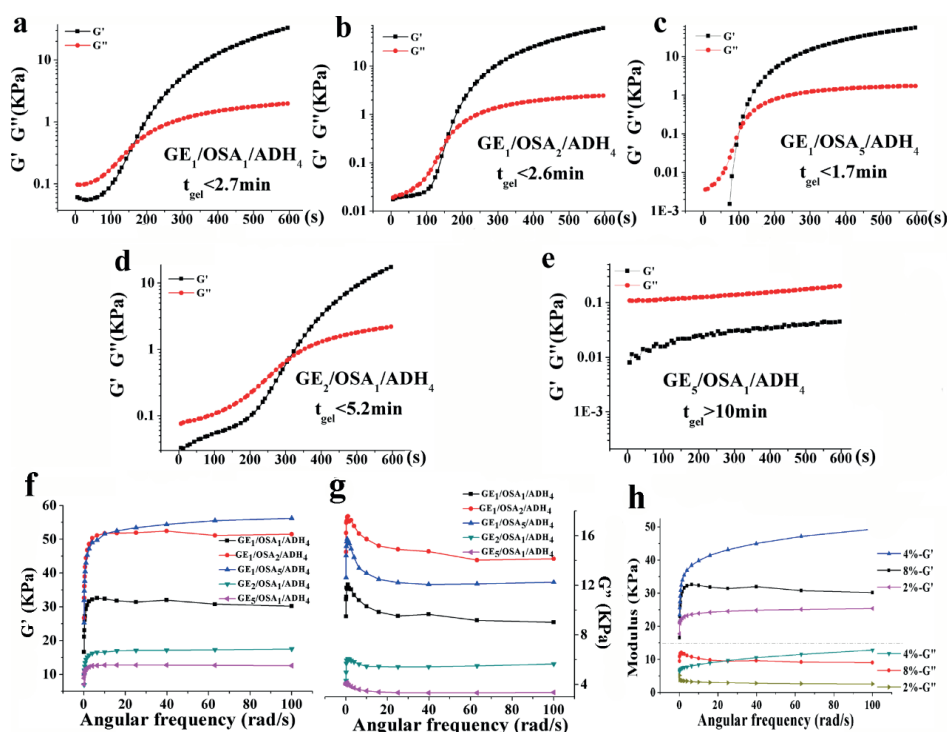

Figure 2. Rheological characterizations of the hydrogels. (a-e) GE/OSA/ADH$_4$ hydrogels formation was monitored by dynamic time sweep measurements using an oscillatory rehometer; (f,g) Storage modulus G' and loss modulus G" of as-prepared hydrogels (ADH 4%) as function of frequency. (h) Storage modulus G' and loss modulus G" of hydrogels with different ADH ratio as function of frequency.

The mechanical properties of different hydrogels were analyzed by measuring the mechanical response to deformation under an oscillatory strain when different OSA and GE ratios were used. The quantitative information of GE/OSA/ADH$_4$ hydrogels is presented in Figure 2f-g. In a frequency sweep test, crossover frequency (ω_c) referred to the frequency at which the elastic modulus was equivalent to the viscous modulus. The G' of the hydrogels was greater than G" and remained unchanged in the frequency range tested, indicating the gel-like character of the hydrogels. Moreover, the G' of all hydrogels increased with increasing ADH content, as a higher cross-linking density was obtained, demonstrating better mechanical properties (Figure 2h). Hydrogels with an ADH ratio of 8% were also tested and exhibited a similar rheological behavior in frequency sweep test (Figure S1). For time sweep test, the gelation of these hydrogels processed too soon to be recorded which make them inappropriate for clinical operation. All the partial formulations were tested as control. As shown in Figure S2, all of the partial formed hydrogels were mechanically weaker than GE/OSA/ADH hydrogels, thereby, posing certain limitation on their applications in injectable hydrogels.

3.3 Injectability and self-healing properties of hydrogels

It is critical that injectable hydrogels that are used in the bioengineering field can be injected into desired site via a small incision, so as to form a gel *in situ* allowing for damage recovery to maintain structural and functional integrity. By using a 26-gauge syringe, macroporous hydrogel precursors were injected into molds of different shapes, and after 5 min, hydrogels were formed at 37 °C without any external intervention (Figure 3a-d). Thus, the injectability characteristics of hydrogels make them highly suitable for MIS techniques.

The visual evidence of the self-healing properties is shown in Figure 3e-h, where a triangular hydrogel was cut into half and the two fragments immediately healed into one piece when brought together under moist conditions. All of the hydrogels exhibited self-healing behavior, and the self-healed hydrogels could be lifted vertically and horizontally without a problem. Rheology analyses were also conducted to confirm the self-healing properties of the hydrogel. Structure destruction was induced via application of 1000% strain for 2 min. Then, the strain was decreased to 1% for 2 min to allow the hydrogel to recover from damage. The step strain measurements of the hydrogel (GE$_1$/OSA$_1$/ADH$_4$Hydrogel) under low (1%) and high (1000%) strain were conducted as shown in figure 3i. Under 1% strain, G' is larger than G", suggesting a sol-to-gel transition and the formation of hydrogel network. Under a 1000% strain, G' and G" decreased quickly and inverted, indicating the hydrogel was converted to sol state. This self-healing behavior was ascribed to the storage of dynamic imine bonds and acylhydrazone existing in the

network as was reported previously [39]. Furthermore, because of the macroporous structure, the surface energy of the hydrogel increased and facilitated mutual molecular recognition on the surface of the hydrogels during the process of self-healing.

The integrity of injectable hydrogels can be damaged by stress from several environmentally and therapeutically-related instruments, surgeries, pharmaceuticals, and biological species. For injectable hydrogels that are used as cell delivery carriers or drug depots, the damage would induce random dispersion of therapeutic agents to neighboring tissues, thereby causing unexpected problems. Moreover, the damage could cause diffusion of the precursor or rapid degradation of implanted hydrogels. In our design, the self-healing ability of OSA/GE/ADH macroporous hydrogels allows for structural recovery upon damage, providing mechanical support or protection, and a suitable microenvironment for cell proliferation and drug release.

3.4 Porosity and morphology

It is believed that macroporous structure can facilitate cellular infiltration, nutrient diffusion and provide sufficient space for tissue in-growth [40]. For this purpose, macroporous structure were fabricated using high-speed shearing method. The effect of formulation, shearing frequency and treatment time on the macrostructure, porosity, pore size and morphology were studied respectively.

The morphology of the hydrogels was evaluated using scanning electron microscopy (SEM), and representative results are shown in Figure S3, S4. As expected, all hydrogels displayed a continuous and macroporous three-dimensional structure compared to non-treatment group. However, the average pores diameter increased with shearing frequency and treatment time for all hydrogels as shown in Figure S5a. After high-speed shearing treatment, the average pore diameters of hydrogels were enlarged from approximately 50μm to 300μm. However, as shown in Figure S5b, porosity of hydrogels didn't continue to grow with shearing frequency and treatment time with 30000 rpm/30 s showing a porosity of approx. 83%, and decrease slowly to approx. 60% for 30000 rpm/120 s. For compositions of precursors formulations, we observed that pore sizes were similar in size irrespective of the ratios of GE, OSA, and ADH, but porosities ranged from 60%-80% as displayed in Figure 4a, b. A representative image of the as-prepared hydrogels obtained by X-ray micro-computer tomography is shown in Figure 4c, d. The macroporous structure of the hydrogels was generated by blending air bubbles to the original composition via high-speed shearing. Compared to organic or inorganic porogens, the high-speed shearing approach as used in our study avoids freeze-drying or additional washing steps of the scaffold. Moreover, hydrogels can be gelled at body temperature by a Schiff-base

reaction and acylhydrazone bonds. Additional crosslinking is not required, therefore the number of steps required for scaffold preparation and the risks of toxic crosslinking is reduced [41].

Morphological analysis of the hydrogels showed well-interconnected pores with a diameter ranging between 100-300 μm, which may contribute to enhanced cell migration and penetration inside the hydrogels and drug release from the hydrogels. Cyclohexane uptake results indicated that most of the hydrogels exhibited proper porosities (60-80%) required by favoring tissue engineered scaffold, because as reported that porous scaffolds exhibiting a porosity greater than 80% cannot sustain *in-vivo* load-bearing mechanical strain [42]. Rheological characterization also proved that G' and G" did not vary significantly with compositions of formulations, shearing frequency and time (Figure S6). Therefore, 30000 rpm/60 s was chosen to prepare macroporous hydrogels for the following study.
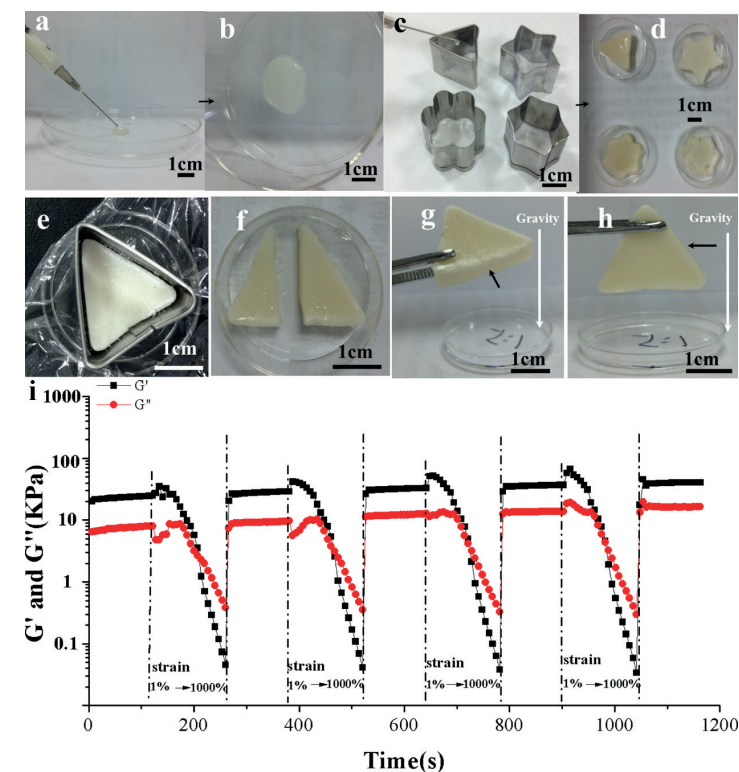

Figure 3. Injectable and self-healing properties of the hydrogels ($GE_1/OSA_1/AHD_4$ hydrogels are shown as examples). (a–d) photographs demonstrating the injectability of the hydrogel; (e-h) photograph of the self-healing process of the hydrogel; (i) the self-healing property of hydrogels demonstrated by the continuous step strain (1%→1000%→1%) measurements at 37 °C.
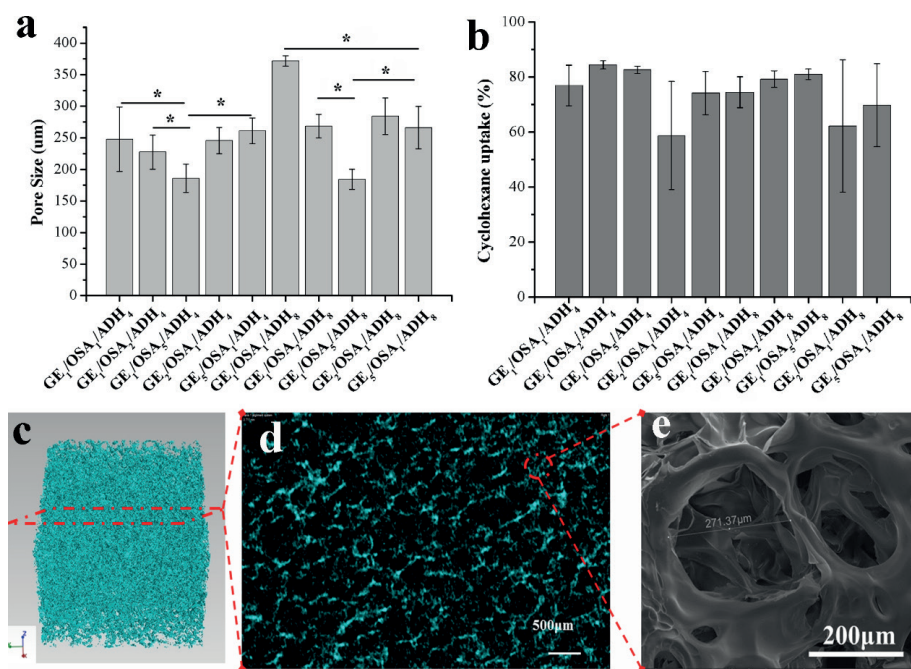
Figure 4. (a) Pore size of lyophilized hydrogels prepared with different formulations; (b) porosity of hydrogels with different formulations evaluated by cyclohexane uptake; (c,d) representative micro-CT photos of the hydrogel; (e) representative SEM image of the hydrogel. Value represents mean $\pm$ SD. An asterisk represents p<0.05.

3.5 Water content

Hydrogels are three-dimensional macromolecular networks, capable of maintaining a high amount of biological fluids at a relatively stable state. The water content of GE/OSA/ADH hydrogels at 37 °C was evaluated and was shown in Figure 5a. All hydrogels had a high water content, which was contributed by the many hydrophilic groups in the structures of OSA and GE that help the hydrogels to be fully hydrated. The great water content may facilitate maintaining a significant extent of fluid and nutrients for the tissue-engineered scaffold, make hydrogels suitable for encapsulation of cells, and provide proper structural cues to cells to proliferate and migrate.

In our study, the water content was affected by crosslinking density and network composition. In general, the water content of $GE/OSA/ADH_8$ was lower compared to that of $GE/OSA/ADH_4$, which could be ascribed to a higher ADH ratio in higher crosslinking density and reduced liquid uptake by hydrogels. However, in the $GE/OSA/ADH_4$ group, the water content in $GE_2/OSA_1/ADH_4$ and $GE_5/OSA_1/ADH_4$ hydrogels was higher compared to that of $GE_1/OSA_5/ADH_4$, $GE_1/OSA_2/ADH_4$, and $GE_1/OSA_1/ADH_4$ hydrogels. This indicated

that an excessive gelatin content was present in $GE_2/OSA_1/ADH_4$ and $GE_5/OSA_1/ADH_4$ hydrogels that had a greater capacity to hold water compared to OSA, and contributed to a greater water uptake.

3.6 *In-vitro* biodegradation

The *in-vitro* enzymatic degradation of hydrogels was evaluated by incubating the hydrogels in the presence of collagenase and monitoring the variation of the dry mass of the hydrogels as a function of time. In the presence of collagenase, gelatin will degrade [43], whereas alginate can be broken down by hydrolytic degradation [44]. Since all hydrogels contain different amounts of OSA, GE, and ADH, their *in-vitro* degradation appeared similar, as shown in Figure 5b and c. The GE to OSA ratio was the dominant factor of hydrogel degradation *in vitro*. In both $GE/OSA/ADH_4$ and $GE/OSA/ADH_8$ groups, when GE: OSA = 1:2 and 1:5, hydrogels degraded at a slower rate and exhibited a reduction in mass loss after 20 days; however, when GE: OSA = 2:1 and 5:1, hydrogels greatly reduced in weight at 24 hrs. Furthermore, after 20 days, $GE_1/OSA_2/ADH_4$ and $GE_1/OSA_2/ADH_8$ hydrogels exhibited a larger remaining weight compared to $GE_1/OSA_5/$ ADH_4, $GE_1/OSA_1/ADH_4$ and $GE_1/OSA_5/ADH_8$, which was ascribed to higher gelatin content and crosslinking density. Moreover, the *in-vitro* biodegradation profile at 20 days proved that the hydrogels provided enough time for new tissues to grow and therapeutic agents to be released [36].

3.7 *In-vitro* drug release kinetics

Injectable hydrogels are a unique tool in the field of regenerative medicine for the delivery of bioactive drugs and cells [45, 46]. The potential of GE/OSA/ADH hydrogels for tuning drug release was observed in PBS at 37 °C using hEGF as model drug *in vitro*. As shown in Figure 6, hEGF was slowly released and increased with time thereby avoiding the problem of local drug accumulation [47]. After pelleting the hydrogels in PBS, approximately 2% of hEGF from the gels was detected in 1 hour. After 96 h, the cumulative release percentage was 30% to 50% in the $GE/OSA/ADH_4$ group, and 40% to 60% in the $GE/OSA/ADH_8$ group, indicating efficient entrapment of hEGF in GE/OSA/ADH macroporous hydrogels. The release of hEGF from hydrogels was based on the diffusion and internal structure change of the hydrogels. Partial erosion of the crosslinked structure was gradually induced by hydrolysis and degradation when hydrogels were placed in a large amount of release medium for an indicated time interval. Consequently, hEGF was slowly released from the hydrogels and was accompanied by partial dissociation of the framework.
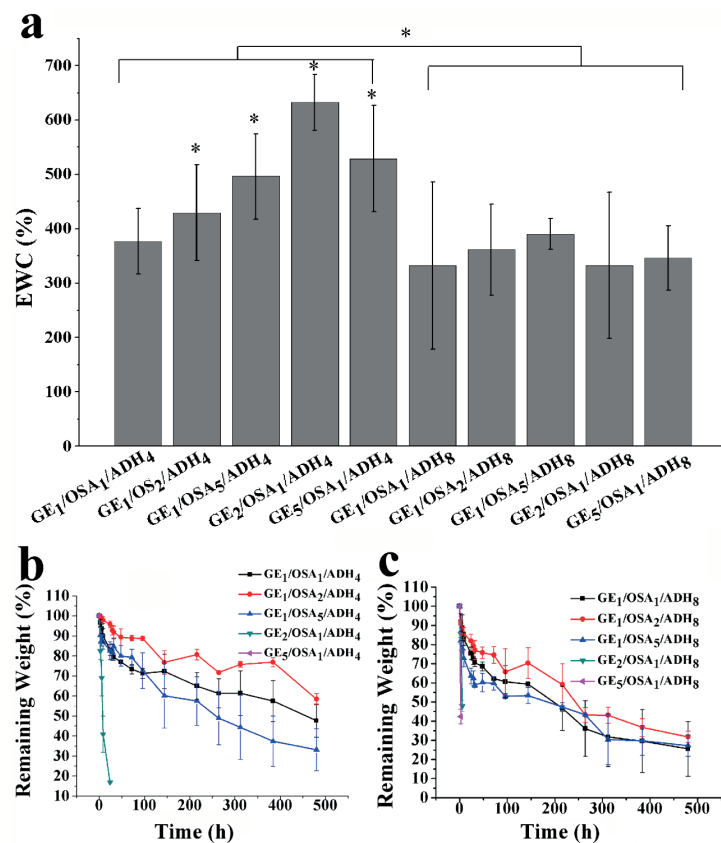
Figure 5. (a) hydrogels' EWC at physiological pH and 37 °C; (b, c) weight loss of GE/OSA/ADH$_4$ (b) and GE/OSA/ADH$_8$ (c) hydrogels as a function of time at 37 °C in PBS, respectively.
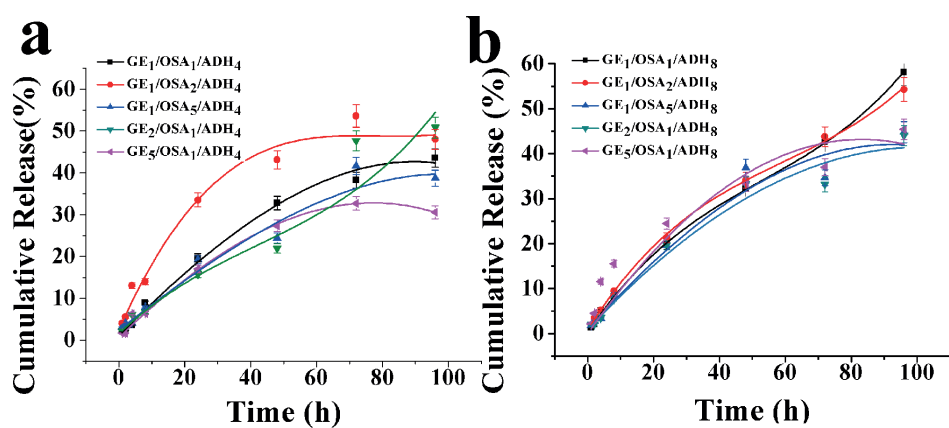

Figure 6. Drug release kinetics of GE/OSA/ADH hydrogels. HEGF Loaded hydrogels showed sustained HEGF release behavior in GE/OSA/ADH$_4$ (a) and GE/OSA/ADH$_8$ (b) hydrogels.
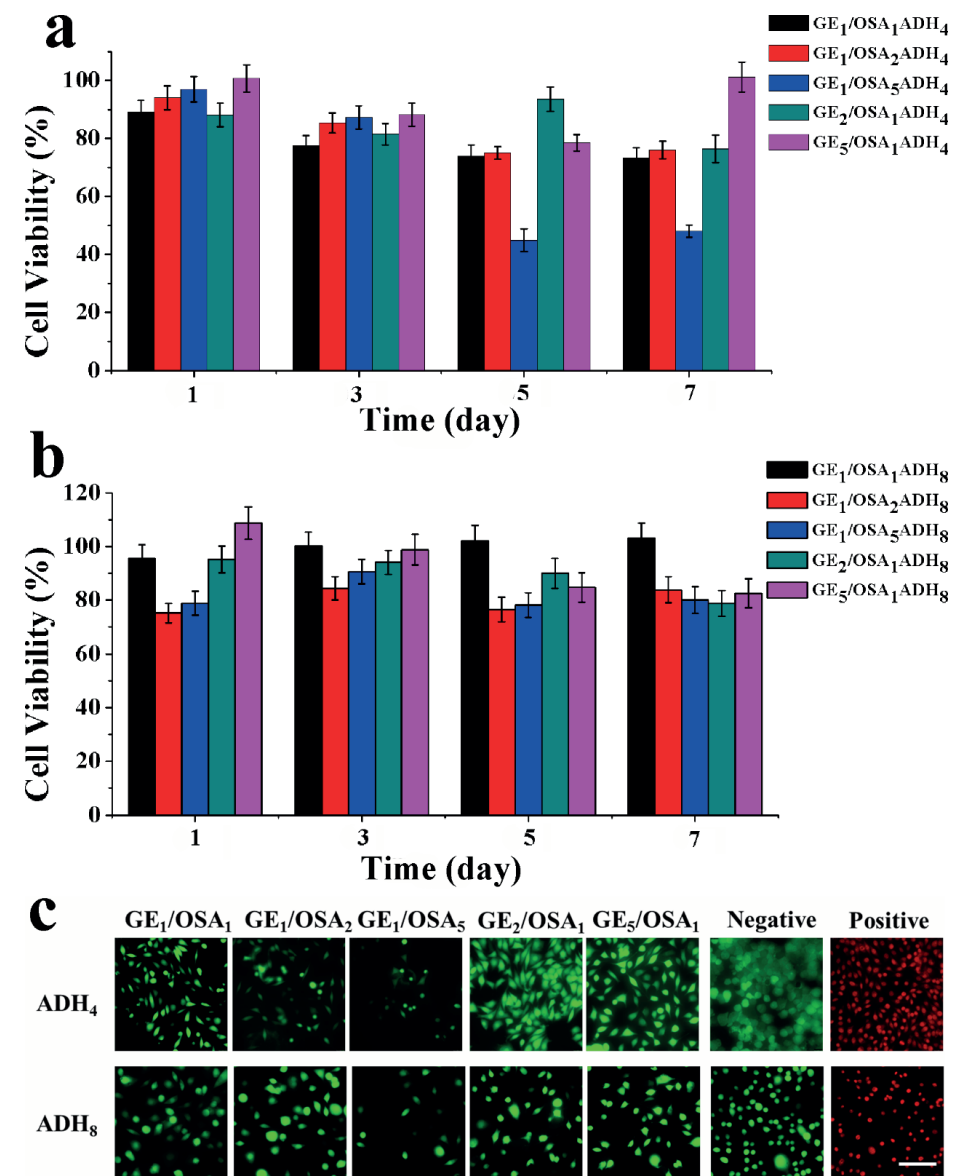

Figure 7. *In-vitro* cell cytotoxicity of GE/OSA/ADH$_4$ (a) and GE/OSA/ADH$_8$ (b) in 7 days (CCK-8 assay, mean ± SD. *$P < 0.05$); (c) microscopic images of cells on GE/OSA/ADH$_4$ and GE/OSA/ADH$_8$ hydrogels stained with Live/Dead assay (green/red, respectively) after 48 h culture. Scale bar = 100 μm.

3.8 In-vitro biocompatibility of hydrogels

To investigate the biocompatibility of GE/OSA/ADH hydrogels, the response of cells to the hydrogels was evaluated using L929 and NIH 3T3 cells. As shown in Figure 7a, b, cells cultured on hydrogels or TCPS showed continuous proliferation, except for those that proliferated on $GE_1/OSA_5/ADH_4$ hydrogels. This may be due to unreacted aldehyde groups in OSA, leading to an adverse condition for the proliferation of L929 cells [48]. Our findings revealed that GE/OSA/ADH hydrogels did not have an obvious deleterious effect on cellular growth. These data were further proven by a Live/Dead assay after 48 hrs, in which living cells were stained in green and dead cells were stained in red. In Figure 7c, it is shown that L929 cells were uniformly dispersed on or into the hydrogels and showed a typical spread morphology. Only viable cells were visible, and no cells on the hydrogels showed red fluorescence. The number of living cells increased with the ratio of GE to OSA, which may be due to its advantageous natural properties, e.g., bio-responsive behavior [49]. In addition, few dead cells were observed in almost every group. These results indicated that GE/OSA/ADH hydrogels did not have a significant adverse effect on proliferation, morphology and viability of L929 cells, and demonstrated that GE/OSA/ADH hydrogels may be promising biocompatible scaffolds for tissue engineering or potential carriers of therapeutic agents.

To confirm the possibility of using GE/OSA/ADH hydrogels as cell carriers, NIH 3T3 cells were encapsulated inside $GE_1/OSA_1/ADH_4$ and $GE_1/OSA_1/ADH_8$ hydrogels and viability, proliferation, and distribution were investigated (Figure 8). Cell-encapsulated hydrogels were easily fabricated by blending NIH 3T3 cell suspension with hydrogels precursors that were pre-dissolved in cell culture medium under physiological conditions. NIH 3T3 cells were uniformly distributed in macroporous hydrogels and exhibited good viability for 8 days. In addition, in the three-dimensional environment of the hydrogels, cell numbers significantly increased with time, indicating that hydrogels provided excellent pore connectivity and efficient nutrient/metabolic waste transportation for live cell to adhere, proliferate, and migrate within the network. The total number of cells in $GE_1/OSA_1/ADH_8$ hydrogels was less compared to that of $GE_1/OSA_1/ADH_4$ hydrogels at day 8, which may be due to the more compact network of $GE_1/OSA_1/ADH_8$ hydrogels, preventing cell migration and the transport of nutrients. Together, these results demonstrated that hydrogels did not have an obvious deleterious effect on entrapped cells and their proliferative ability, thereby suggesting that the hydrogels may be used as vehicles for delivery of therapeutic cells.
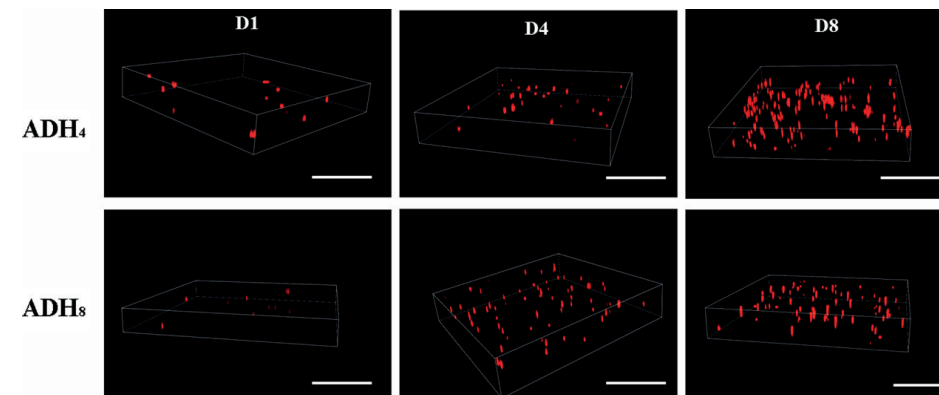

Figure 8. Representative images of the encapsulated NIH 3T3 cells in GE_1/OSA_1 hydrogels at 1, 4, and 8 days after cell seeding (scale bar = 500μm).

3.9 In-vivo hydrogel biocompatibility

The in-vivo biocompatibility of $GE_1/OSA_1/ADH_4$ hydrogels was evaluated by dorsal subcutaneous injection in Sprague Dawley rats. The formation of in-situ hydrogels was observed in the subcutaneous layer at 5 min post injection, indicating that $GE_1/OSA_1/ADH_4$ hydrogels could easily be delivered into the body, rapidly forming a hydrogel in vivo. Precursors were sterilized without the requirement of special equipment. All surgeries were performed without complications and no signs of local irritation were observed during the course of the study. During gross observation, no abnormal behavior, infections, or local inflammatory responses were found at the surgical site, and normal weight gain was observed in the experimental group when compared to saline control group. The hydrogels and surrounding tissues were collected and stained with H&E for qualitative histological examination. Figure 9 showed that the precursor formed a visible hydrogel mass in the subcutaneous space. At 1 week post injection, no clear differences were observed at the injected site between the hydrogel group and the saline group, however slight signs of inflammation were observed in the peri-implanted tissue. After 2 weeks, several parts of the hydrogel were infiltrated by immune cells, which were stained in a red color, such as macrophages and neutrophils, and indeed, an appreciable inflammatory response in the implanted tissue and peri-implanted tissue was observed. After 3-4 weeks, the hydrogels were gradually replaced by vascularized connective tissue, indicating clearance of cell-mediated components. In addition, at the injection site, no signs of inflammation, tissue damage, or chronic effects were observed, which was consistent with that of a typical foreign body reaction to an implanted biomaterial [50].
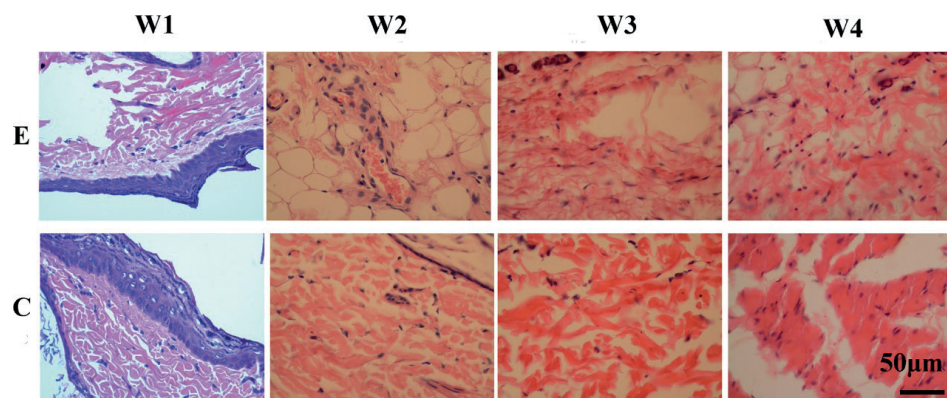
Figure 9. Post-injection histological examination of subcutaneous tissue by H&E staining at week 1, 2, 3 and 4. (E: hydrogel group, C: saline group)

4. CONCLUSION

In this study, we demonstrated a novel approach to prepare injectable, template-free, and self-healed macroporous hydrogels that promoted cell survival, proliferation, and migration and were able to hold a drug and slowly release it. The effect of the precursor's composition on the gelation, injectable and rheologic behavior was investigated. The water content and *in-vitro* biodegradation characteristics can be regulated by the ratio of GE, OSA, and ADH, and hydrogels were able to autonomously heal within several minutes. Cells were co-cultured with hydrogels by direct seeding and encapsulation and sufficient viability was achieved. HEGF could be loaded within the hydrogel and was slowly released with good bioactivity. Finally, hydrogels were proven to be *in-vivo* biodegradable and caused mild inflammatory and toxic responses when subcutaneously injected in a Sprague Dawley rat model. We hypothesized that our approach for fabricating self-healing hydrogels without molds under modest conditions has potential for applications in tissue engineering, including biological scaffolds, cell encapsulation, and drug delivery.
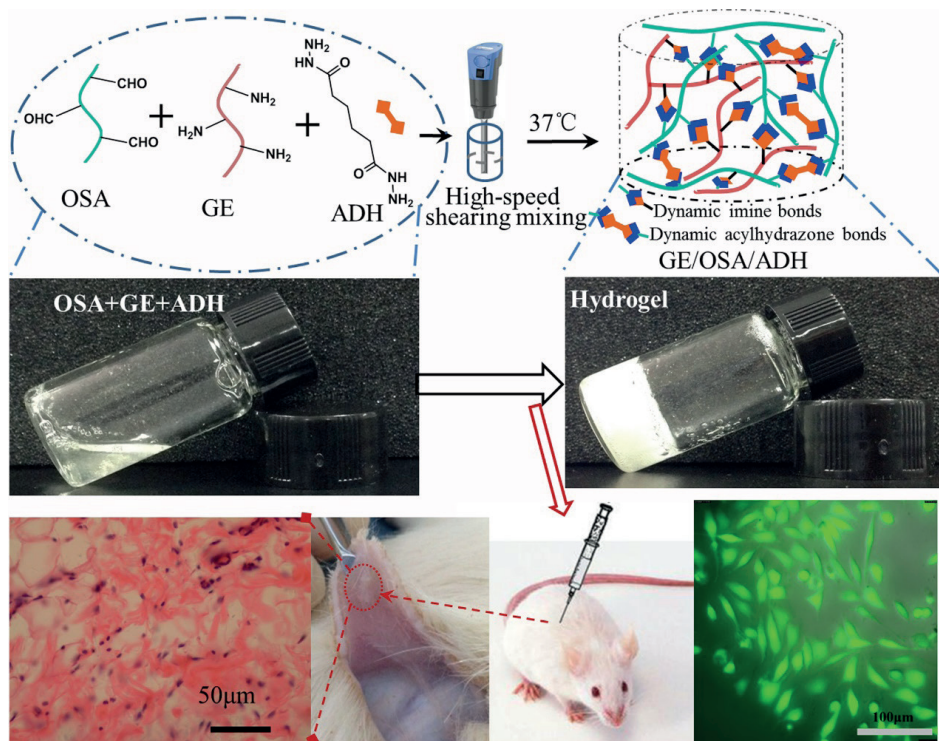
ACKNOWLEDGEMENTS

SUPPORTING INFORMATION

Storage modulus G' and loss modulus G" of as-prepared hydrogels (ADH 8%) as function of frequency; rheological characterizations of partial formulations as control; representative SEM images of $GE_1/OSA_1/ADH_4$ with different shearing speed and time; representative SEM images with different GE, OSA and ADH ratio at 30000 RPM/60 s; pore size and cyclohexane uptake of $GE_1/OSA_1/ADH_4$ with different shearing speed and time; storage modulus G' and loss modulus G" of hydrogels with different shearing speed and time.

REFERENCES

[1] Prieto, E. M.; Page; J. M.; Harmata, A. J.; Guelcher, S. A. Injectable foams for regenerative medicine. *Wires. Nanomed. Nanobi.* 2014, 6, 136-154.

[2] Otoole, J. E.; Eichholz, K. M.; Fessler, R. G. Surgical site infection rates after minimally invasive spinal surgery. J. Neurosurg. 2009, 11, 471-476.

[3] Hilborn, J. In vivo injectable gels for tissue repair. Wires. Nanomed. Nanobi. 2011, 3, 589-606.

[4] Young, D.; Christman, K. L. Injectable biomaterials for adipose tissue engineering. Biomed. Mater. 2012, 7, 024104.

[5] Hollister, S. J. Porous scaffold design for tissue engineering. Nat. Mater. 2005, 4, 518-524.

[6] Bencherif, S. A.; Sands, R.W.; Bhatta, D.; Arany, P. R.; Verbeke, C.; Edwards, D. A.; Mooney, D. J. Injectable preformed scaffolds with shape-memory properties. Proc. Natl. Acad. Sci. U. S. A. 2012, 109, 19590-19595.

[7] Hwang, Y.; Zhang, C.; Varghese, S. Poly(ethylene glycol) cryogels as potential cell scaffolds: effect of polymerization conditions on cryogel microstructure and properties. J. Mater. Chem. 2009, 20, 345-351.

[8] Murphy, W. L.; Dennis, R. G.; Kileny, J.L.; Mooney, D. J. Salt Fusion: An Approach to Improve Pore Interconnectivity within Tissue Engineering Scaffolds. Tissue Eng. 2002, 8, 43-52.

[9] Hwang, C. M.; Sant, S.; Masaeli, M.; Kachouie, N.N.; Zamanian, B.; Lee, S.; Khademhosseini, A. Fabrication of three-dimensional porous cell-laden hydrogel for tissue engineering. Biofabrication 2010, 2, 035003.

[10] Scott, E.A.; Nichols, M. D.; Kuntzwillits, R.; Elbert, D. L. Modular scaffolds assembled around living cells using poly(ethylene glycol) microspheres with macroporation via a non-cytotoxic porogen. Acta Biomater. 2010, 6, 29-38.

[11] Aimetti, A. A.; Tibbitt, M. W.; Anseth, K. S. Human neutrophil elastase responsive delivery from poly(ethylene glycol) hydrogels. Biomacromolecules 2009, 10, 1484-1489.

[12] Malmsjo, M.; Ingemansson, R.; Martin, R.; Huddleston, E. Negative-pressure wound therapy using gauze or open-cell polyurethane foam: Similar early effects on pressure transduction and tissue contraction in an experimental porcine wound model. Wound Repair Regen. 2009, 17, 200-205.

[13] Chen, Q.; Zhu, L.; Chen, H.; Yan, H.; Huang, L.; Yang, J.; Zheng, J. A Novel Design Strategy for Fully Physically Linked Double Network Hydrogels with Tough, Fatigue Resistant, and Self-Healing Properties. Adv. Funct. Mater. 2015, 25, 1598-1607.

[14] Okumura, Y.; Ito, K. The Polyrotaxane Gel: A Topological Gel by Figure-of-Eight Cross-links. Adv. Mater. 2001, 13, 485-487.

[15] Li, W.; An, H.; Tan, Y.; Lu, C.; Liu, C.; Li, P.; Xu, K.; Wang, P. Hydrophobically associated hydrogels based on acrylamide and anionic surface active monomer with high mechanical strength. Soft Matter. 2012, 8, 5078-5086.

[16] Tang, L.; Liu, W.; Liu, G. High-Strength Hydrogels with Integrated Functions of H-bonding and Thermoresponsive Surface-Mediated Reverse Transfection and Cell Detachment. Adv. Mater. 2010, 22, 2652-2656.

[17] Haraguchi, K.; Takehisa, T. Nanocomposite Hydrogels: A Unique Organic–Inorganic Network Structure with Extraordinary Mechanical, Optical, and Swelling/De-swelling Properties. Adv. Mater. 2002, 14, 1120-1124.

[18] Huang, T.; Xu, H.; Jiao, K.; Zhu, L.; Brown, H. R.; Wang, H. L. A Novel Hydrogel with High Mechanical Strength: A Macromolecular Microsphere Composite Hydrogel. Adv. Mater. 2007, 19, 1622-1626.

[19] Fan, C.; Liao, L.; Zhang, C.; Liu, L. A tough double network hydrogel for cartilage tissue engineering. J. Mater. Chem. B 2013, 1, 4251-4258.

[20] Waters, D. J.; Engberg, K.; Parkehouben, R.; Ta, C. N.; Jackson, A. J.; Toney, M. F.; Frank, C. W. Structure and Mechanism of Strength Enhancement in Interpenetrating Polymer Network Hydrogels. Macromolecules 2011, 44, 5776-5787.

[21] Nguyen, K. T.; West, J. L. Photopolymerizable hydrogels for tissue engineering applications. Biomaterials 2002, 23, 4307-4314.

[22] Ifkovits, J. L.; Tous, E.; Minakawa, M.; Morita, M.; Robb, J. D.; Koomalsingh, K. J.;Gorman, J. H; Gorman, R. C.; Burdick, J. A. Injectable hydrogel properties influence infarct expansion and extent of postinfarction left ventricular remodeling in an ovine model. Proc. Natl. Acad. Sci. U. S. A. 2010, 107, 11507-11512.

[23] Jin, R.; Moreira Teixeira, L. S.; Krouwels, A.; Dijkstra, P. J.; van Blitterswijk, C. A.; Karperien, M.; Feijen, J. Synthesis and characterization of hyaluronic acid-poly(ethylene glycol) hydrogels via Michael addition: An injectable biomaterial for cartilage repair. Acta Biomater. 2010, 6, 1968-1977.

[24] Lehn, J. M. Perspectives in Supramolecular Chemistry-From Molecular Recognition towards Molecular Information Processing and Self-Organization. Angew. Chet. Edit. 1990, 29, 1304–1319.

[25] Wei, Z.; Yang, J. H.; Liu, Z. Q.; Xu, F.; Zhou, J. X.; Zrínyi, M.; Osada, Y.; Chen, Y. M. Novel Biocompatible Polysaccharide-Based Self-Healing Hydrogel. Adv. Funct. Mater. 2015, 25, 1352-1359.

[26] Darnell, M. C.; Sun, J. Y.; Mehta, M.; Johnson, C.; Arany, P. R.; Suo, Z.; Mooney, D. J. Performance and biocompatibility of extremely tough alginate/polyacrylamide hydrogels. Biomaterials 2013, 34, 8042-8048.

[27] Wei, Z.; Yang, J. H.; Du, X. J.; Xu, F.; Zrinyi, M.; Osada, Y.; Li, F.; Chen, Y. M. Dextran-Based Self-Healing Hydrogels Formed by Reversible Diels–Alder Reaction under Physiological Conditions. Macromol. Rapid Comm. 2013, 34, 1464-1470.

[28] Pepels, M.; Filot, I.; Klumperman, B.; Goossens, H. Self-healing systems based on disulfide–thiol exchange reactions. Polym. Chem. 2013, 4, 4955-4965.

[29] Liu, F.; Deng, G.; Li, F.; Zhang, B.; Liu, C.; Chen, Y.; Zhang, B.; Zhang, J.; Liu, C. Rheological Images of Dynamic Covalent Polymer Networks and Mechanisms behind Mechanical and Self-Healing Properties. Macromolecules 2012, 45, 1636-1645.

[30] He, L.; Fullenkamp, D. E.; Rivera, J. G.; Messersmith, P. B. pH responsive self-healing hydrogels formed by boronate–catechol complexation. Chem.Commun. 2011, 47, 7497-7499.

[31] Dumitriu, S. *Polymeric Biomaterials*, Revised and Expanded; CRC Press; 2001.

[32] Abd El-Ghaffar, M. A.; Hashem, M. S.; El-Awady, M. K.; Rabie, A. M. pH-sensitive sodium alginate hydrogels for riboflavin controlled release. Carbohyd. Polym. 2012, 89, 667-675.

[33] Vandelli, M. A.; Rivasi, F.; Guerra, P.; Forni, F.; Arletti, R. Gelatin microspheres crosslinked with D, L-glyceraldehyde as a potential drug delivery system: preparation, characterisation, in vitro and in vivo studies. Int. J. Pharm. 2001, 215, 175-184.

[34] Oyen, M. L. Mechanical characterisation of hydrogel materials. Int. Mater. Rev. 2014, 59, 44-59.

[35] Balakrishnan, B.; Jayakrishnan, A. Self-cross-linking biopolymers as injectable in situ forming biodegradable scaffolds. Biomaterials 2005, 26, 3941-3951.

[36] Waters, R.; Pacelli, R.; Maloney, R.; Medhi, I.; Ahmed, P. R.; Paul, A. Stem cells secretome-rich nanoclay hydrogel: a dual action therapy for cardiovascular regeneration. Nanoscale 2016, 8(14), 7371-7376.

[37] Boucard, N.; Viton, C.; Agay, D.; Mari, E.; Roger, T.; Chancerelle, Y.; Domard, A. The use of physical hydrogels of chitosan for skin regeneration following third-degree burns. Biomaterials 2007, 28, 3478-3488.

[38] Lee, F.; Chun, J. E.; Kurisawa, M. An Injectable Hyaluronic Acid-Tyramine Hydrogel System for Protein Delivery. J.Control. Release 2009, 134, 186-193.

[39] Kakuta, T.; Takashima, Y.; Nakahata, M.; Otsubo, M.; Yamaguchi, H.; Harada, A. Preorganized Hydrogel: Self-Healing Properties of Supramolecular Hydrogels Formed by Polymerization of HostGuest-Monomers that Contain Cyclodextrins and Hydrophobic Guest Groups. Adv. Mater. 2013, 25, 2849-2853.

[40] Flegeau, K; Pace, R; Gautier, H; Rethore, G; Guicheux, J; Le Visage, C; Weiss, P. Toward the development of biomimetic injectable and macroporous biohydrogels for regenerative medicine. Advances in Colloid and Interface Science. 2017, 247, 589-609.

[41] Azami, M.; Moztarzadeh, F. Glutaraldehyde crosslinked gelatin/hydroxyapatite nanocomposite scaffold, engineered via compound techniques. Polym. Composite. 2010, 31, 2112-2120.

[42] Salerno, A; *Biomedical Foams for Tissue Engineering Applications*, Woodhead Publishing: UK, 2014.

[43] Nguyen, A.; Mckinney, J.; Miller, T.; Bongiorno, T.; McDevitt, T. C. Gelatin methacrylate microspheres for controlled growth factor release. Acta Biomater. 2014, 13, 101-110.

[44] Cha, C.; Kohmon, R.; Kong, H. Biodegradable polymer crosslinker: independent control of stiffness, toughness, and hydrogel degradation rate. Adv. Funct. Mater. 2009, 19, 3056-3062.

[45] Annabi, N.; Tamayol, A.; Uquillas, J. A.; Akbari, M.; Bertassoni, L. E.; Cha, C.; Camci-Unal, G.; Dolmeci, M. R.; Peppas, N. A.; Khademhosseini, A. 25th anniversary article: Rational design and applications of hydrogels in regenerative medicine. Adv. Mater. 2014, 26, 85-124.

[46] Pakulska, M. M.; Vulic, K.; Tam, R. Y.; Shoichet, M. S. Hybrid Crosslinked Methylcellulose Hydrogel: A Predictable and Tunable Platform for Local Drug Delivery. Adv. Mater. 2015, 27, 5002-5008.

[47] Lin, S.; Deng, F. F.; Huang, P.; Li, L. L.; Wang, L.; Li, Q.; Chen, L.; Chen, H.; Nan, K. H. A novel legumain protease-activated micelle cargo enhances anticancer activity and cellular internalization of doxorubicin. J. Mater. Chem. B 2015, 3, 6001-6012.

[48] Su, W. Y.; Chen, Y. C.; Lin, F. H. Injectable oxidized hyaluronic acid/adipic acid dihydrazide hydrogel for nucleus pulposus regeneration. Acta Biomater. 2010, 6, 3044-3055.

[49] Wang, L.; Lu, C. L.; Liu, H. H.; Lin, S.; Nan, K. H.; Chen, H.; Li, L. L. A double network strategy to improve epithelization of a poly(2-hydroxyethyl methacrylate) hydrogel for corneal repair application. Rsc Adv. 2016, 6, 1194-1202.

[50] Anderson, J. M.; Rodriguez, A.; Chang, D. T. Foreign Body Reaction to Biomaterials, Semin. Immunol. 2008, 22(2), 86-100.

GRAPHIC ABSTRACT

SUPPORTING INFORMATION

Construction of injectable self-healing macroporous hydrogels via a template-free method for tissue engineering and drug delivery

Lei Wang, Fen Deng, Wenwen Wang, Afeng Li, Conglie Lu, Hao Chen , Gang Wu, Kaihui Nan*, Lingling Li*
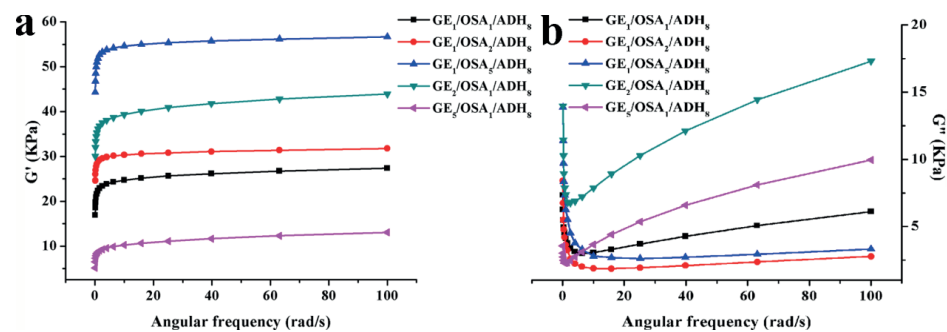
*: Corresponding authors

Figure S1. Storage modulus G' and loss modulus G" of as-prepared hydrogels (ADH 8%) as a function of frequency.
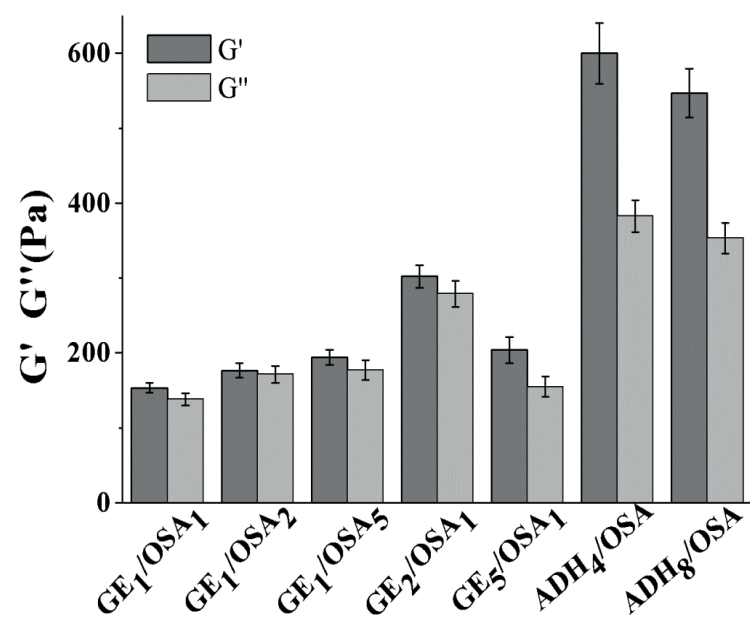

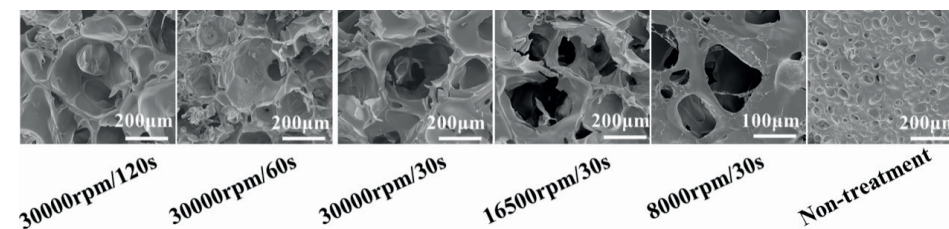**Figure S2.** Rheological characterizations of partial formulations as control.

Figure S3. Representative SEM images of GE$_1$/OSA$_1$/ADH$_4$ with different shearing speed and time.
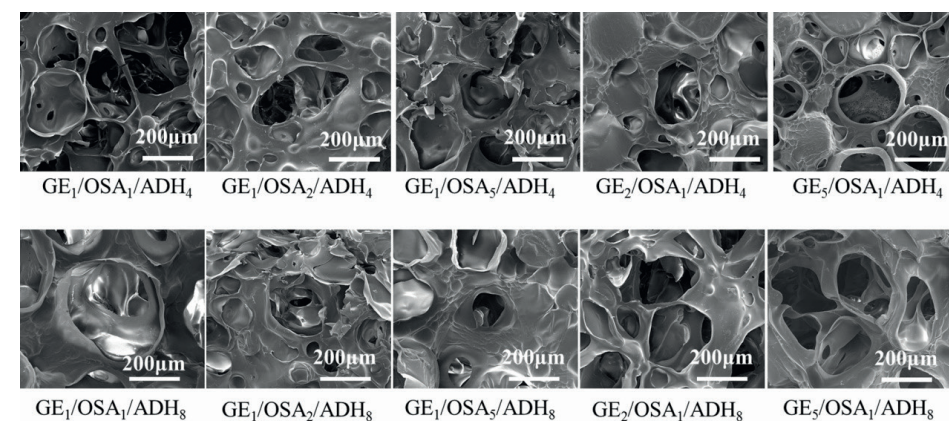
Figure S4. Representative SEM images with different GE, OSA and ADH ratio at 30000 rpm/60 s.
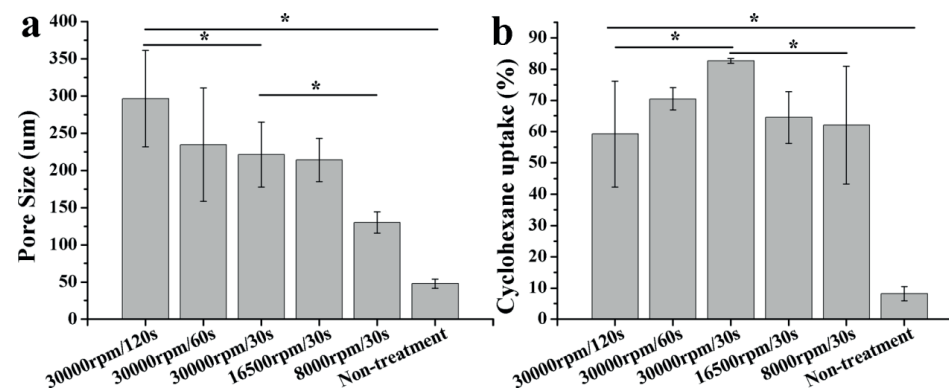

Figure S5. Pore size and cyclohexane uptake of GE$_1$/OSA$_1$/ADH$_4$ with different shearing speed and time.
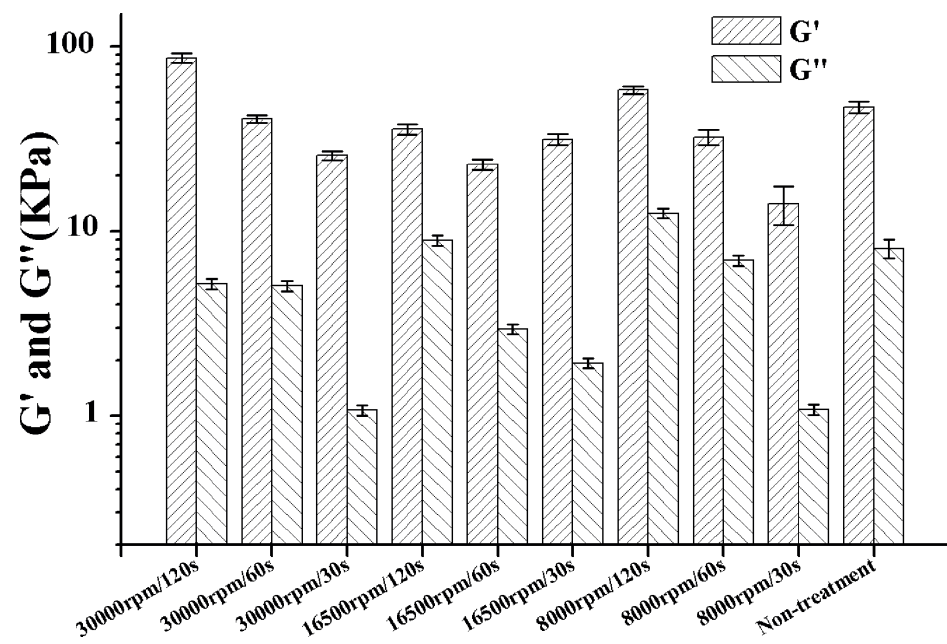
Figure S6. Storage modulus G' and loss modulus G" of hydrogels with different shearing speed and time.
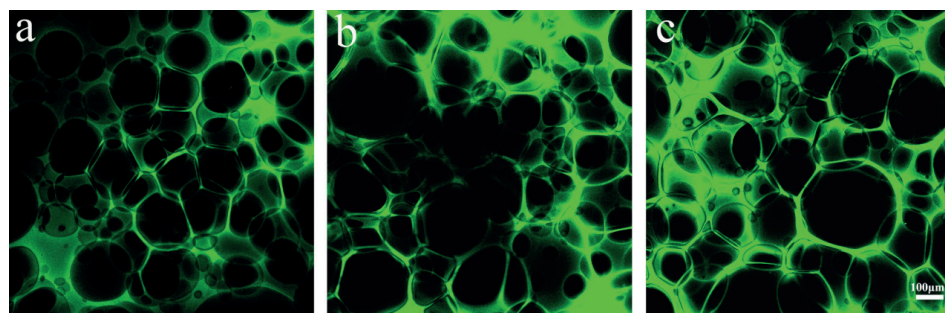
Figure S7. The porosity structure of the $GE_1/OSA_1/ADH_4$ hydrogel after being subcutaneous injection. (a-top, b-bottom, c-middle)

Chapter 5

A novel injectable self-healing sericin-alginate/salvianolic acid B hydrogel as jumping distance fillings

Lei Wang[#], Wenwen Wang[#], Chengwei Tu[#], Danni Wu, Yihuai Pan, Kaihui Nan, Tymour Forouzanfar, Lingli Li[*], Gang Wu[*]

* : Corresponding authors
# : These authors contributed equally to this work.

ABSTRACT

Due to the excellent biocompatibility and microporous property, naturally derived self-healing hydrogels become promising candidate scaffolds for guided bone regeneration. In this paper, an injectable, self-healing, pro-osteogenic hydrogel was developed using naturally-derived polymers (alginate and sericin) and bioactive agent (salvianolic acid B, SAB). The physicochemical property studies showed that the pore size and the mechanical moduli could be regulated by adjusting the formulations of the hydrogels. The pore size was ranged from 50 micrometers to 200 micrometers. The mechanical properties described in terms of storage modulus was 6.8 KPa to 22 KPa. The hydrogel enabled cell adhesion and proliferation. The hydrogel remained hydrophilic with sustained drug release performance of SAB. In addition, the drug-loaded hydrogel (SS/OSA-SAB) has a strong capacity to promote osteogenesis. It significantly enhanced the osteogenic differentiation of bone marrow mesenchymal stem cells by elevating the expression levels of osteogenic markers (ALP, OPN, RunX2, and OCN), and extracellular matrix mineralization. Furthermore, the enhancement of osteogenesis was dependent on the ratio of SS/OSA. In summary, the developed injectable self-healing SS/OSA hydrogel is provided with a step-release capacity of drug, good biocompatibility, and easy osteogenesis controllability, which may be a promising jumping gap filling material.

Keywords: Injectable, Self-healing hydrogel, Alginate, Sericin, Salvianolic acid B, Osteogenesis

1. INTRODUCTION

Immediate implantation is a clinical technique to install dental implants in fresh extraction sockets to minimize alveolar reports, aiming to both reduce visit times and achieve optimal aesthetics and functions. In these cases, due to imperfect matching between implants and tooth extraction socket, a space, called jumping gap or jumping distance, may occur between the implant surface and surrounding bone, resulting in unsupported bone plates. The bone plates, particularly the buccal ones, may undergo resorption due to the destruction of periodontal membrane-borne blood supply, which can cause soft tissue recession and thus aesthetic risk. Clinical data show that the height and width of the mean buccal plate reduce 1.07 mm and 0.78 mm respectively [1], which may lead to a midfacial recession in the long term. The resorption may become much pronounced to about 7.5 mm [2] for the thin-wall bone phenotype. In these cases, maintaining buccal bone height is critical to achieve desired aesthetics. In the clinic, particulate CaP-based bone grafts are used to fill the large (>2 mm) jumping distance in order to prevent buccal bone resorption, which is, whereas, associated with a series of concerns, such as incomplete filling and easily being wrapped with connective tissues. Furthermore, most of the CaP-based bone grafts bear only certain osteoconductivity but no intrinsic osteoinductivity so that they cannot efficaciously prevent bone resorption. Therefore, a more suitable jumping distance-filling material with excellent filling adaptability and pro-osteogenic properties is highly needed to prevent bone resorption of the buccal bone plate, thereby minimizing aesthetic risks.

Among several candidate materials, injectable and self-healing hydrogels may be highly promising for filling jumping distance. Self-healing hydrogels bear a unique reversible network structure through dynamic chemical bonding (for example, Schiff base reactions [3], Diels–Alder reactions [4], disulfide bonds [5], acylhydrazone bonds [6], phenylboronate esters [7]), that can automatically restore its network integrity and original mechanical property after damage. Firstly, hydrogels, particularly the ones containing naturally-derived components, bear excellent biocompatibility and tunable biodegradability. The high fluidity of hydrogel precursors can easily enable the adaptive fit into the irregular, deep and narrow defects in the jumping distance and can be gelled without the needs of additional chemical/physical initiations. In addition, the self-healing hydrogel may also repair the potential deformations at the gingival margin caused by the mechanical force during oral movements, so as to prevent the potential microgap and thus infection. Importantly, hydrogels may act as a controlled drug delivery system for various bioactive agents to acquire intended biological functions, thereby further promoting bone regeneration.

In this study, we wished to design a novel injectable, self-healing, and pro-osteogenic hydrogel with naturally-derived polymers (alginate and sericin) and bioactive agent in order to provide an ideal jumping distance-filling material. Alginate is a natural polysaccharide, composed of two kinds of uronic acid units, β-(1,4), linked to D-mannuronic acid (M) and α-(1-4)-linked L-gluronic acid (G). Alginate is biocompatible, biodegradable, and low immunogenic [8], thus has become one of the most widely used biomaterials in the field of bone tissue engineering. Moreover, the adjacent double hydroxyl groups are abundantly available in alginate and can be oxidized into aldehyde groups, one indispensable chemical group for the Schiff base reaction. We adopted sericin — a naturally-derived, biocompatible, and hydrophilic glycoprotein — to provide plenty of side amino groups for Schiff base reaction. In addition, sericin bears many bioactive motifs (serine-rich repetitive domains and fibrous structure of binding ligands to cell surface receptors) to favor cell attachment and growth [9, 10], which can compensate the lack of cell attachment sites in alginate [11]. Moreover, sericin is also shown to promote osteogenic differentiation of bone marrow mesenchymal stem cells (BMSCs) [12, 13] as evidenced by significantly enhanced osteogenic differentiation markers, such as bone sialoprotein, osteocalcin, and alkaline phosphatase [14]. In this study, we, for the first time, synthesized SS/OSA hydrogel and evaluated its physicochemical and biological properties to identify its potential as a jumping distance-filling material.

To further promote the pro-osteogenic property of the SS/OSA hydrogel, we incorporated salvianolic acid B (SAB), a traditional water-soluble Chinese herbal medicine into the SS/OSA hydrogel. SAB has been widely used in clinical practice for the treatment of cardiovascular disease [15] through its anti-oxidized function [16]. Previous studies show that SAB promotes the osteogenic differentiation of mesenchymal stem cells [17] by dose-dependently up-regulating the alkaline phosphatase (ALP) activity and osteogenesis-related markers, such as osteopontin (OPN), runt-related transcription factor 2 (RunX2), osterix (Osx), osteocalcin (OCN), and bone sialoprotein (BSP) [18, 19]. This promotion of SAB was achieved by activating the extracellular-signal-regulated kinases (ERK) signaling pathway [19].

In the current study, we wished to identify the feasibility and efficacy of SS/OSA-SAB hydrogel in order to illustrate the application potential in filling the large jumping distance area. We characterized the rheological properties, the surface morphology, the swelling and degradation performances, and the SAB release profile of the hydrogel. The cytocompatibility of the hydrogel was evaluated by culturing L929 cells and BMSCs onto the SS/OSA hydrogel. Live/Dead staining was further adopted to assess the cell adhesion behavior on the hydrogel. The osteogenic differentiation of BMSCs on the hydrogel was estimated using alizarin red staining. Real-time PCR was also employed to study the osteogenic differentiation mechanism using ALP, OPN, OCN, and RunX2 as biomarkers.

2. MATERIALS AND METHODS

2.1 Materials
Sericin was purchased from Silk energy Biology & Technology. Sodium alginate, adipic acid dihydrazide (ADH), sodium metaperiodate (NaIO$_4$), Alizarin red S mono sodium salt were purchased from Sigma-Aldrich (St. Louis, MO). Salvianolic acid B (SAB) was purchased from Yuanye (Shanghai yuanye Bio-Technology Co., Ltd, China). Bone marrow stromal cells (BMSCs) were obtained from Cyagen (Guangzhou Cyagen Biosciences Inc, China). Dulbecco's modified eagle medium (DMEM), Fetal Bovine Serum (FBS), Penicillin-Streptomycin, Live/Dead assay was purchased from Life Technology (Thermo Fisher Scientific Inc. USA), Cell Counting Kit 8 (CCK-8) was purchased from Beyotime (Shanghai Beyontime Biotechnology, China). ALP activity Kit and ALP staining kit were purchased from Jiancheng (NJJCBIO Co., Ltd, Nanjing, China).

2.2 Hydrogel Preparation
2.2.1 Modification of alginate
Alginate was oxidized according to the previous study [20]. Briefly, 5 g alginate was dispersed in 25 mL ethanol and 4.32 g NaIO$_4$ was dissolved in 25 mL ultrapure water to prepare oxidization solution. The NaIO$_4$ solution was added to the alginate dispersion and stirred at room temperature for 8 h. Equimolar ethylene glycol (1.124 mL) was added with continuous stirring of 30 minutes to quench the reaction. The resultant suspension was dialyzed against ultrapure water (UPT-11-20T, Ulupure, China) using a dialysis membrane with molecular 3500 Da (Spectru Lab, USA) for 7 days. Ultrapure water was changed several times until periodate was no longer detected. The oxidized sodium alginate (OSA) was obtained by lyophilizing the dialysate. The oxidation degree of alginate was determined by quantifying the concentration of unconsumed periodates by iodometry as described previously [21]. In brief, 1 mL of the reaction mixture was mixed with a sufficient quantity of potassium iodide solution and allowed to react for 10 min to consume all unreacted periodate ions. Next, liberated iodine was titrated with a standardized sodium thiosulfate solution using starch as the indicator. The titration volume of used sodium thiosulfate was monitored and indicated by the disappearance of the color. Oxidation degree values were calculated as the average of three independent oxidation experiments.

2.2.2 Preparation of SS/OSA hydrogels
The sericin (SS), OSA, ADH were dissolved in phosphate-buffered saline (PBS) to prepare 20%, 10%, 50% (w/v) solutions, respectively. Then three of the solutions was pipetted into plastic tubes according to our predesigned ratio (Table 1) to obtain serious formulations, which immediately underwent high-speed shearing treatment (IKA T10, Germany) for 10-30 seconds (based on our previous research [20]) to produce the microporous

structure. Subsequently, the tubes were placed in a water bath at 37 °C for 5 min to generate microporous hydrogels. The gelation time was determined using the inverted tube test. The drug-loaded hydrogel was prepared via the same procedure as described while adding SAB solution before high-speed shearing.

Table 1. Formulations of SS/OSA hydrogels

SS:OSA	SS	OSA	ADH
(w/w)	(20%, μL)	(10%, μL)	(50%, μL)
5:1	150	60	18.3
2:1	200	200	34.8
1:1	100	200	26
1:2	50	200	21.7
1:5	30	300	28.7

2.3 Rheological characterization

A rheometer (Discovery HR-2, TA Instruments, USA) was used to characterize the rheological properties of the hydrogel. The storage modulus (G') and loss modulus (G") of the hydrogels were tested in the oscillatory mode using a parallel plate configuration (25 mm in diameter) at 37 °C. G' and G" were quantified as a function of time at a constant angular frequency of 1Hz and a constant strain of 1% from the start to 10 minutes. Using a fixed strain level of 1%, the angular frequency was swept from 0.01 rad s⁻¹ to 100 rad s⁻¹. Using the same frequency (1 Hz), continuous step change of oscillatory strain between 1% and 1000% was used to assess the strain-induced damage and self-healing behavior of the hydrogel. The critical strain ($\gamma_{critical}$) was defined as the stain value at the cross point of G' and G".

2.4 Characterization

Attenuated total reflectance-Fourier Transform Infrared Spectroscopy (ATR-FTIR, Bruker Tensor II, Bruker, Germany) was used to assess the chemical composition of OSA. The microstructure of the hydrogels was assessed using scanning electron microscopy (SEM, Nova NanoSEM200, FEI, USA). The hydrogels were prepared using distilled water as solvent when fabricating the SEM samples. Then the hydrogels were lyophilized for 48 hours and sputter-coated with gold for 60 seconds before observation. The average pore size of the lyophilized hydrogels was quantified using Image-Pro Plus 6.0 software (Media Cybernetics, USA). Six pictures for each site, 5 samples for each group.

2.5 Equilibrium water content (EWC)

The swelling process was maintained by the weighing method. All the hydrogels reach the equilibrium point after 24 h immersing into PBS solution. The equilibrium water content of the hydrogels was calculated according to mass addition at the time point of 24 h. The dried hydrogels were weighed (m_o) and immersed into PBS (pH 7.4) for 24 h at 37 °C for fully swelling to equilibrium. Then, the excess PBS on the surface was removed and the hydrogel with equilibrium swelling state was weighed (m_e). The equilibrium water content of hydrogels was calculated as equation (1) [22]:

$$EWC = (m_e - m_o) / m_e \times 100\% \qquad (1)$$

Where m_e was the weight of the fully swelled hydrogel, m_o was the dried weight. Each sample was repeated three times.

2.6 *In-vitro* degradation kinetics

The degradation profile of hydrogels was followed *in vitro* by measuring the weight loss in PBS (pH 7.4) at 37 °C over time according to a previous study [23]. After wiping away excess water on the surfaces, the weight of the hydrogel samples was measured immediately at specified time points. The degradation rate was calculated using equation (2), where W_t is the weight of the hydrogel after degradation and W_o, the weight of hydrogel after incubating for 24 h, was chosen to be the initial weight of degradation because of its swelling behavior:

$$Remaining\ Weight\ (\%) = W_t/W_o \times 100\% \qquad (2)$$

2.7 SAB release study

To analyze the release property of the SS/OSA-SAB scaffolds, one 8-mm-diameter scaffold loaded with 10 ug SAB was packed into a dialysis bag with molecular weight cut-off of 3500 Da and then immersed into a 50-mL BD tube. 20 mL PBS (pH 7.4) was added into the tube as the release medium. The system was shaken on a table concentrator at 100 rpm at 37 °C. At the time point of 0.5 h, 1 h, 2 h, 4 h, 8 h, 1 d, 3 d, 5 d, 7 d, 11 d, 14 d, 23 d, 33 d, 3 mL release medium was obtained and equal volumetric pre-warmed fresh PBS was added. The release of SAB was assessed by Ultraviolet-visible near-infrared spectrometer (CARY5000, Agilent, USA) at a wavelength of 286 nm. The cumulative amount and percentage rate of SAB released from the SS/OSA-SAB scaffolds were computed according to a SAB standard concentration curve.

2.8 *In-vitro* biocompatibility

L929 mouse fibroblasts (ATCC, USA) were used to test the *in-vitro* cytocompatibility of the hydrogels. SS, OSA, and ADH were sterilized by ethylene oxide and dissolved in sterilized PBS. Before gel-forming, a 60 μL mixture of the precursor solution is absorbed and spread on the bottom of the 96-well plate. Then the plate was put into the incubator for 10 minutes at

37 °C for further crosslinking. L929 cells were cultured with the medium of 90% RPMI 1640 + 10% FBS + 1% penicillin-streptomycin and seeded onto the hydrogels at a density of 1000 cells per well. Cells that were cultured on TCP with the same medium were set as control. After 24 h culture, samples were washed with PBS and incubated with Cell Counting Kit 8 (CCK-8, Beyotime, China) for 3 h at 37 °C in dark. OD values were measured using an ELISA plate reader (Synergy NEO2, BioTek, USA), and cell viability (%) was calculated using the following equation:

$$\text{Cell viability (\%)} = OD_{test}/OD_{control} \times 100 \qquad (3)$$

In addition, a Live/Dead assay was carried out to evaluate the adherence and proliferation of cells on the hydrogels. In brief, L929 cells were seeded onto the hydrogels at a density of 1000 cells per well of 96-well TCPs. On Day 4 and Day 8, cells were stained with Live/Dead Viability and Cytotoxicity Kit for 30 min at 37 °C. Cells without hydrogels and treated with normal and treated with 75% ethanol for 10 min were set as negative and positive controls, respectively. After incubation for 30 min, cells were rinsed with prewarmed PBS for 3 times and observed under a fluorescence microscope (DMi8, Leica, Germany). Experiments were performed in triplicate.

2.9 *In-vitro* osteogenesis

To determine the capacity of different SS/OSA hydrogel (1:2, 1:5, 2:1) on promoting the *in-vitro* osteogenic differentiation, BMSCs were used for verification. Hydrogels were prepared in the 48-well plate sterilely according to paragraph of 2.8. BMSCs were cultured onto the hydrogels with a density of 4 × 10⁴ cells per well. The cells were cultured in Dulbecco's Modified Eagle's Medium (DMEM) containing 1000 mg/L of glucose, 10% fetal bovine serum (FBS), and 1% penicillin/streptomycin. After 24 hours of spreading, the cultured medium was changed by mineralized medium and changed every two days. After 17 days of culture, we evaluated osteogenic markers, such as the expression level of osteocalcin (OCN, a late osteogenic differentiation marker) and the activity of alkaline phosphatase (ALP).

For the ALP activity study of BMSCs embedded hydrogels, the detection was administrated according to the instructions for the ALP activity kit (TE0005, Leagene). Briefly, the mediums were removed and washed with 500 μL PBS. The culture system was lysed in radio-immunoprecipitation assay (RIPA) buffer (150 mM NaCl, 10 mM Tris, pH 7.4, 2 mM EDTA, 0.5% Igepal/NP40, 0.1% SDS, 1% Triton X-100, protease inhibitor mixture). The bicinchoninic acid assay (BCA Protein Assay Kit, Pierce) was used to determine protein concentration. The absorbance at 405 nm was measured using an ELISA plate reader (Synergy NEO2, BioTek, USA).

The supernatant was collected and assessed with an OCN ELISA kit (NJJCBIO Co., Ltd, Nanjing, China). The mineralization nodules were stained using an Alizarin red staining (ARS) kit (Cyagen, Guangzhou, China). In brief, after 17 days of incubation, the hydrogel constructs were rinsed three times with PBS, fixed with 95% ethanol for 15 minutes, washed with distilled water three times, and finally stained using Alizarin red staining solution for 1 hour at 37 °C. Stained samples were washed with water three times with each was lasting one minute. Pictures of the top surface were taken using an optical microscope (Nikon, Japan). For these experiments, an osteogenic induction medium (OM) without the presence of SAB or SS/OSA hydrogel was used as control. For quantification, the stained mineralization nodules were eluted with 10% (w/v) cetylpyridine chloride (CPC), and the absorbance of the supernatants was measured at 550 nm using a micro reader (Synergy NEO2, BioTek, USA).

2.10 Evaluation of mRNA expression using real-time PCR

Osteogenic differentiation markers were detected by RT-PCR. BMSCs were seeded at 4 × 10⁴ cells per well in 48-well plates. The mRNA expression levels for the alkaline phosphatase (ALP), osteogenic genes osteopontin (OPN), Runt-related transcription factor 2 (RunX2), and osteocalcin (OCN) were assessed by RT-PCR (Bio-Rad CFX96, Bio-Rad Laboratories, Inc., USA) according to our former study [24]. In brief, RNA was extracted from the samples and control groups using TRIzol reagent (Invitrogen, Thermo Fisher Scientific, Inc.). Complementary (c) DNAs were synthesized with 1 μg of total RNA and an oligo-dT primer using a Superscript II kit (Invitrogen, Molecular Probes, Eugene, OR). DNA was digested with gDNA Eraser (Takara, Otsu, Japan). RT-qPCR was performed with the SYBR Premix Ex Taq TM II kit (Takara Bio, Inc., Otsu, Japan). Briefly, the total reaction volume was 25 μL, and RT- qPCR was performed using 40 cycles with 10 minutes of denaturation at 95 °C, 15 seconds of annealing at 95 °C and 1 minute of extension at 60 °C. The relative expression level of each gene was normalized to GAPDH, and relative quantification of gene expression was performed using the $2^{-\Delta\Delta Cq}$ method. The primers used were as follows: ALP, 5'-GGGACTGGTACTCGGACAAT-3'(forward) and 5'-GGC-CTTCTCATCCAGTTCAT-3'(reverse); OCN, 5'-GGCGCTACCTCAACAATGGA-3' (forward) and 5'-TAGATGCGCTTGTAGGCGTC-3' (reverse); OPN, 5'-CTCACCTCCCGCATGAAGAG-3' (forward) and 5'-CTTCCCGTTGCTGT CCTGAT-3' (reverse); RunX2, 5'- GCACCCAGCCCATAATAGA-3' (forward) and 5'-TTGGAGCAAGGAGAACCC-3' (reverse); GAPDH, 5'-AGCCCAAGATGC CCTTCAGT-3' (forward) and 5'-CCGTGTTCCTAC CCCCAATG-3' (reverse).

2.11 Statistical analysis

The results are presented as the mean ± standard deviation (SD). Comparisons were made using analysis of variance (ANOVA) for multiple comparisons with Tukey's post hoc analysis for parametric data. Nonparametric tests were carried out using Kruskal –Wallis ANOVA with Dunn's post hoc analysis. Statistical significance was accepted for $P < 0.05$.

3. RESULTS

3.1 Preparation of hydrogels

Oxidized sodium alginate (OSA) was prepared using sodium periodate through transforming adjacent -OH groups into -CH = O groups. The oxidation degree of OSA was 80.16% (Figure 1A). The precursors, OSA, SS, and ADH were mixed with yellowish and cloudy state and turned into solid opaque hydrogel when warmed to 37 °C (Figure 1B-C). The gelation time ranged from several seconds to 5 minutes.

The sol-to-gel transition was further confirmed by rheological method as shown in Figure 2A. The storage modulus (G') and loss modulus (G") increased with time, G' increased faster than G" and finally went beyond G", which means the precursors gelled and formed an ideal gelation state of hydogel. The time at the cross point of G' and G" was the gelling time. All formulations ran the same tendency (data not shown) when applied to the rheological study at the condition of 1Hz and 1% strain.
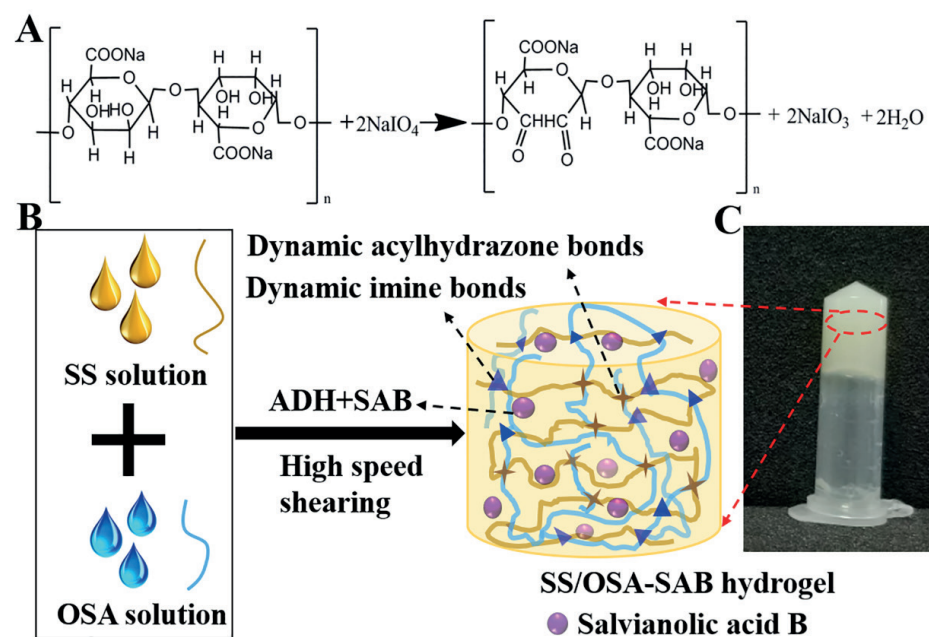

Figure 1. Synthesis of hydrogel: (A) synthesis scheme of oxidized sodium alginate; (B) schematic diagram of construction of SS/OSA hydrogels with high-speed shearing treatment based on imine bonds and acylhydrazone bonds; (C) tube inversion to confirm the hydrogel formation.

3.2 Rheology Behavior

As shown in Figure 2B, storage moduli (G') of 2:1, 1:1, 1:2, and 1:5 hydrogels were greater than loss moduli (G") and remained unchanged in the frequency range tests, indicating the gel-like character of the hydrogels. However, G' of the 5:1 hydrogel group decreased with the increase of angular frequency when the angular frequency was above 25 rad/s. When the ratio of OSA to SS was below 1:1, there was no significant difference of G' among the three groups with values of 6.81 ± 0.54 KPa, 5.93 ± 0.47 KPa, and 5.91 ± 0.46 KPa for 5:1, 2:1, and 1:1 hydrogel respectively (Figure 2C). Compared with these three groups, G' was significantly higher for 1:2 (15.03 ± 1.01 KPa) and 1:5 hydrogel group (22.0 ± 1.76 KPa). The G' of the 1:5 hydrogel group was significantly higher than that of the 1:2 hydrogel group.
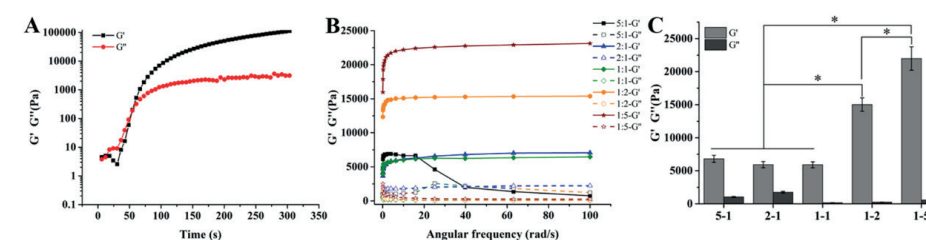

Figure 2. Rheological characterization of the hydrogels: (A) Hydrogel formation as monitored by dynamic time sweep measurement using an oscillatory rheometer; (B) Frequency-sweep measurements of SS/OSA hydrogels; (C) Storage modulus (G') and loss modulus (G") at 1Hz, 1% strain of the hydrogels.

3.3 Self-healing properties of the hydrogels

Figure 3A showed the visual evidence of self-healing property. A sphere form hydrogel was cut into two pieces and the two fragments immediately healed into one piece when brought together. And the self-healed hydrogel could be easily lifted vertically and horizontally without splitting apart. Furthermore, the quantitatively multi-step oscillatory rheological result (Figure 3B-F) showed the self-healing property of the prepared hydrogel. For all the 5:1, 2:1, 1:1, 1:2, and 1:5 hydrogels, G' was larger than G" under a 1% strain. G' and G" decreased quickly under a 1000% strain, and G' was lower than G". When the strain decreased to 1% again, G' and G" recovered. The same variation tendency occurred with the strain increased and decreased for five cycles. Notably, there was a cross point of G' and G", namely critical strain ($\gamma_{critical}$). G' remained larger than G" when the strain was smaller than the critical strain. When the strain was higher than the critical strain, G' became smaller than G". The $\gamma_{critical}$ of 5:1, 2:1, 1:1, 1:2, and 1:5 hydrogel was 402.78%, 173.26%, 483.66%, 205.08%, and 143.62% respectively. The self-healing efficiency was calculated by comparing the storage modulus of the healed hydrogels with the

original one [25]. The percent of mechanical self-healing efficiency was calculated by S_H / S_O X 100%. S_H represented the storage modulus of the healed hydrogel and S_O the original one. The mechanical self-healing efficiency was 72.9 ± 6.09%, 99.9 ± 12.9%, 90.8 ± 6.9%, 95.3 ± 18.8%, 74.0 ± 44.9% for 5:1, 2:1, 1:1, 1:2 and 1:5 hydrogel respectively.
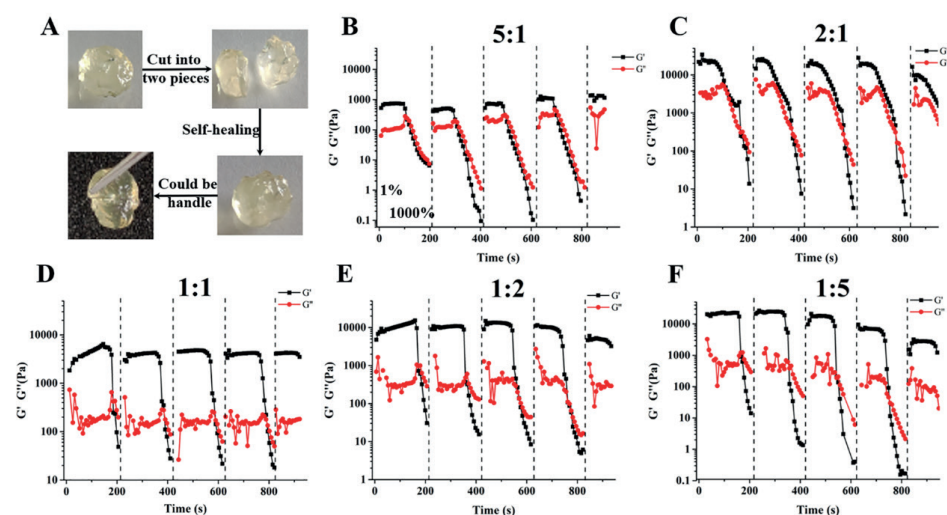

Figure 3. Self-healing property of the hydrogels: (A) Photographs of the self-healing process of the hydrogels; (B-F) Alternate step strain sweep test with strain from 1% to 1000% for every strain interval at an invariable angular frequency (1Hz) at 37 °C for 5:1, 2:1, 1:1, 1:2 and 1:5 hydrogels respectively.

3.4 Swelling behavior and *in-vitro* biodegradation

All the hydrogels swelled quickly in the first four hours and reached a balance at eight hours with the swelling ratio of 1000%-2600%. The equilibrium water content (Figure 4B) of the hydrogels was above 90%, with no significant difference among the five groups. As shown in Figure 4C, all the hydrogels, except the 1:1 hydrogel, degraded gradually with the remaining weight of 10% at 33 days. At first 2 days, the 5:1, 2:1, 1:2 and 1:5 hydrogels degraded slowly with the remaining weight of 67.7 ± 17.1%, 78.5 ± 1.5%, 84.9 ± 15.7% and 79.6 ± 10.1% respectively. However, the remaining weight was 7.8 ± 1.9% for 1:1 hydrogel at day 2. And then the 5:1, 2:1, 1:2, and 1:5 hydrogel groups degraded in a relatively rapid way in the following 3 days. At degradation time of day 11, the remaining weight was 34.7 ± 4.3%, 32.4 ± 2.9%, 70.6 ± 16.2%, 56.4 ± 10.8% for 5:1, 2:1, 1:2, and 1:5 hydrogels respectively. The remaining weight decreased to less than 10% in the following 22 days, and finally couldn't be handled to weigh.

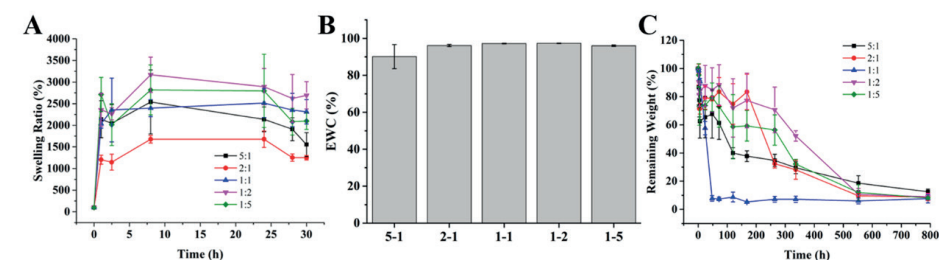**Figure 4.** (A) Swelling behavior of the hydrogels with time; (B) Equilibrium water content (EWC) at physiological pH and 37 °C; (C) Degradation kinetics of the hydrogels as a function of time at 37 °C in PBS.
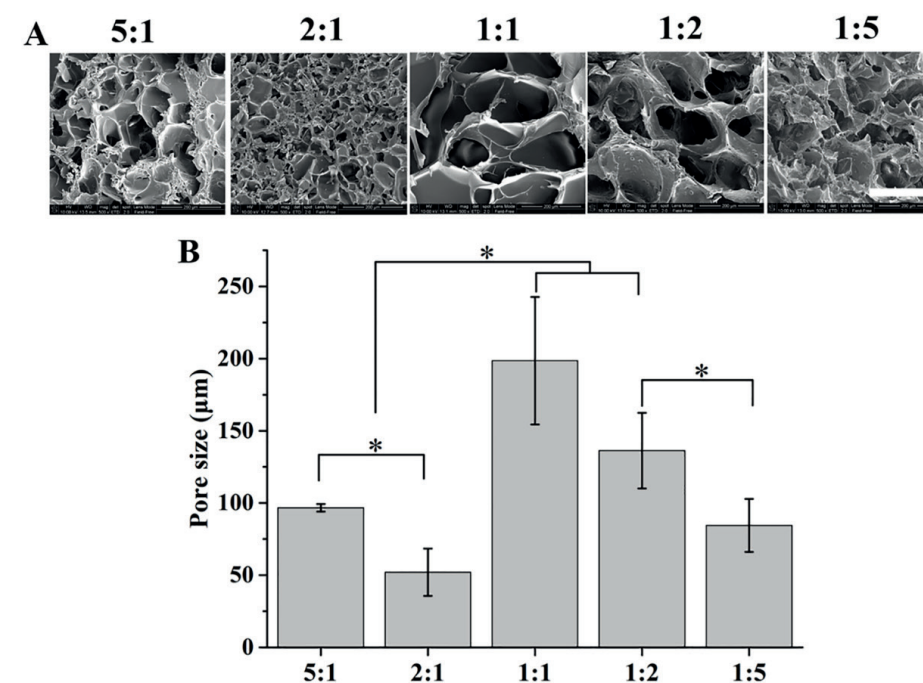

Figure 5. (A) Inner structure of the lyophilized hydrogel by SEM (bar = 200 μm); (B) The pore size of the prepared hydrogels calculated by Image J. Value represented as mean ± SD. Asterisk represents $P < 0.05$.

3.5 *In-vitro* drug release profile

The potential of the prepared hydrogels in tuning drug release was observed in PBS at 37 °C and the results were shown in Figure 6. SAB was slowly released from the scaffold in all groups. In the first 2 hours, the percentage of SAB in PBS was below 22.0% with no significant difference among all the hydrogels. The release slowed down in the next 48 hours with the cumulative release of 21.3 ± 0.8%, 24.8 ± 6.4%, 23.5 ± 10.5%, 35.4 ± 7.7%, and 28.6 ± 0.7% for the 5:1, 2:1, 1:1, 1:2, and 1:5 hydrogel groups respectively without significant difference among groups. The cumulative release of SAB from all groups of hydrogels reached a platform between 96 h and 120 h followed by slowly increase with different rates. After 11 days of incubating, the release rates of 2:1, 1:2, and 1:5 hydrogel were significantly higher than that of 5:1 and 1:1 hydrogel groups. At day 33, the cumulative release of SAB was 33.4 ± 0.8% (1:1 hydrogel) and 38.2 ± 14.1% (5:1 hydrogel), while 64.4 ± 5.9%, 72.9 ± 5.5%, and 67.9 ± 1.9% for 2:1, 1:2, and 1:5 hydrogel groups respectively. The values of the cumulative release of 2:1, 1:2, and 1:5 hydrogel groups were significantly higher than that of 5:1 and 1:1 hydrogel groups.
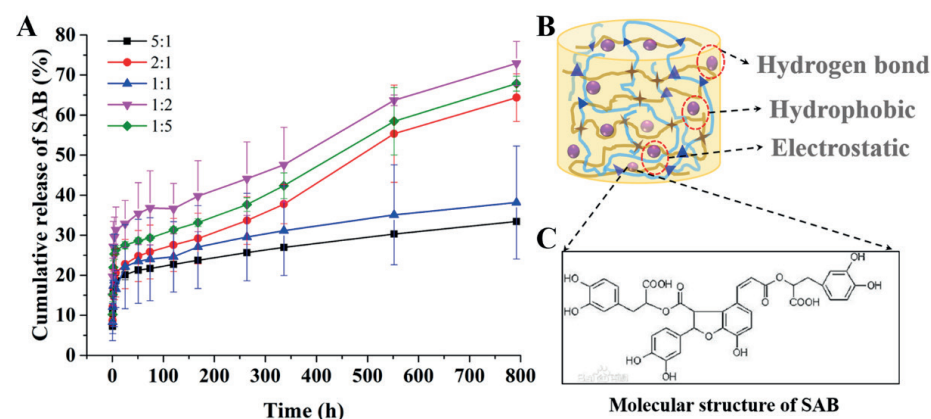

Figure 6. The release profile of the SS/OSA-SAB hydrogel.

3.6 *In-vitro* biocompatibility of the hydrogels

The cell viability of L929 cells was above 100% without significant difference among all hydrogel groups after 24 hours of incubation (Figure 7A). The Live/Dead staining (live cells were stained green and dead cells were stained red) showed that all the cells on/in the hydrogel were green, and no cells on the hydrogels showed red fluorescence (Figure 7B). The cells were uniformly attached to the hydrogel with an outstretched morphology and the density of the live cells increased with culture time.

BMSCs were also cultured onto the hydrogel to further confirm the viability and morphology of the cells (Figure 8). The cell viability of all the hydrogel was above 80% and increased with culture time. The Live/Dead staining results showed that all the BMSCs were spreading onto or into the hydrogel and no red fluoresce was detected. For optimization, we selected 1:2, 1:5 and 2:1 hydrogel for further study of extracellular matrix mineralization.
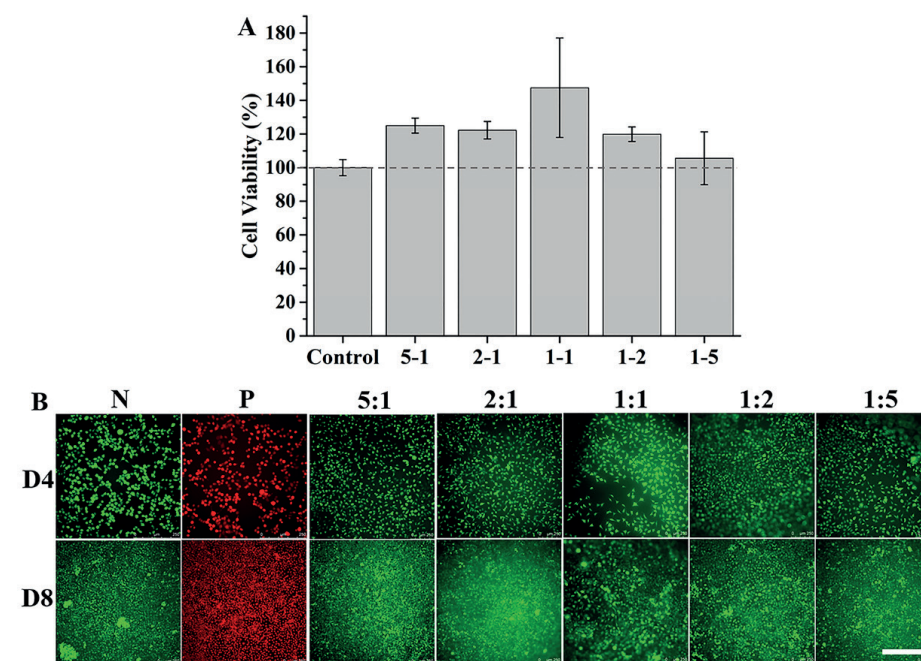

Figure 7. *In-vitro* biocompatibility of the hydrogels using L929 cells: (A) Cell viability of the hydrogels after cocultured for 24 hours; (B) Live/Dead staining of L929 cells in or on the hydrogels after 48 hours of culture, in which live cells were stained in green and dead cells were stained in red (bar = 250 μm).

3.7 Screening for the optimal combination of SS/OSA and SAB

To screen the optimal combination of SAB (0.1 μM, 0.5 μM, 1.0 μM and 5.0 μM) and SS/OSA (2:1, 1:2 and 1:5) to induce *in-vitro* osteogenesis, we separately assessed the extracellular matrix mineralization of BMSCs on various SS/OSA hydrogels (Figure 9A-B) and with different concentrations of SAB culture medium (Figure 9C-D) both qualitatively and quantitatively. Our results showed that the 1:2 SS/OSA hydrogel showed a significant improvement of extracellular matrix mineralization in comparison with OM, 2:1 and 5:1 hydrogels after 31 days. SAB could significantly improve the osteogenic differentiation of BMSCs after 21 days, but without significant difference among various concentrations.
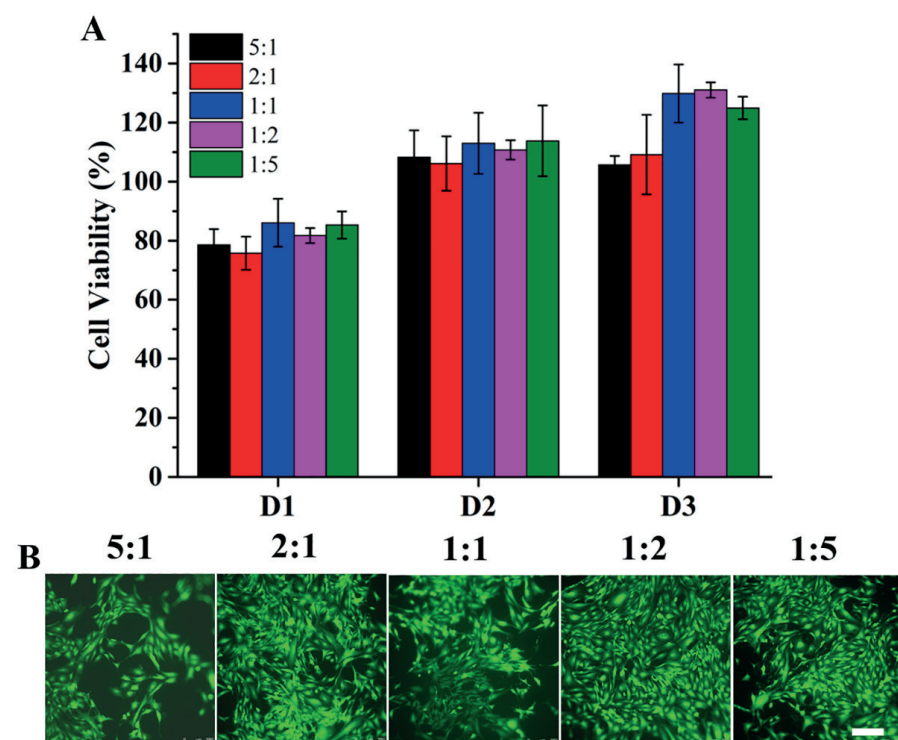
Figure 8. (A) Cell viability of BMSCs on the hydrogels tested on day 1, day 2 and day 3; (B) Representative images of BMSCs on the hydrogels after 3 days culture (Live/Dead staining, Scale bar = 250 μm).

Thereafter, we chose 0.1 μM as loading concentration of SAB to prepare the SS/OSA-SAB hydrogel and evaluated the *in-vitro* mineralization of the composite hydrogel. The mineralized nodules occurred in 17 days, which was shorter than of SS/OSA hydrogel group (31 days) and that of SAB alone group (21 days). Figure 10A showed that the 1:2 hydrogel exhibited a significant larger area of mineralized extracellular matrix nodules than that of OM, 1:5 and 2:1 hydrogel. The result was consistent with the quantitative results while the mineralized nodules were eluted with 10% (w/v) cetylpyridine chloride (CPC) as shown in Figure 10B. The ALP activity of 1:2 hydrogel group was significantly higher than that of OM, 2:1 and 1:5 hydrogel groups (Figure 10C). The OCN concentration of 1:2 hydrogel group was higher than that of OM, 2:1 and 1:5 hydrogel groups with significant difference (Figure 10D).

To confirm the mechanism of the optimized 1:2 SS/OSA-SAB hydrogel in inducing osteogenic differentiation, we detected ALP, OPN, OCN and RunX2 gene expression of BMSCs on the hydrogel scaffold after culturing for 2 days, 4 days and 7 days, and the result was shown in Figure 11. The ALP gene expression of SS/OSA-SAB hydrogel group was significantly higher than that of OM group at day 2 and day 7 (Figure 11A). The relative expression of mRNA of OPN in the hydrogel groups was higher than that of OM group at day 2, day 4 and day 7 (Figure 11B). However, there was a significant decrease of OPN expression with the increase of time in the hydrogel group. Figure 11C showed that the SS/OSA-SAB hydrogel significantly increased the OCN expression of BMSCs at day 2 and day 7 compared with OM group. There was no significant difference of RunX2 expression between SS/OSA-SAB hydrogel group and OM group at day 2 and day 4. Moreover, the relative RunX2 expression in SS/OSA-SAB hydrogel group was significantly increased at day 7 and higher than that of OM group.
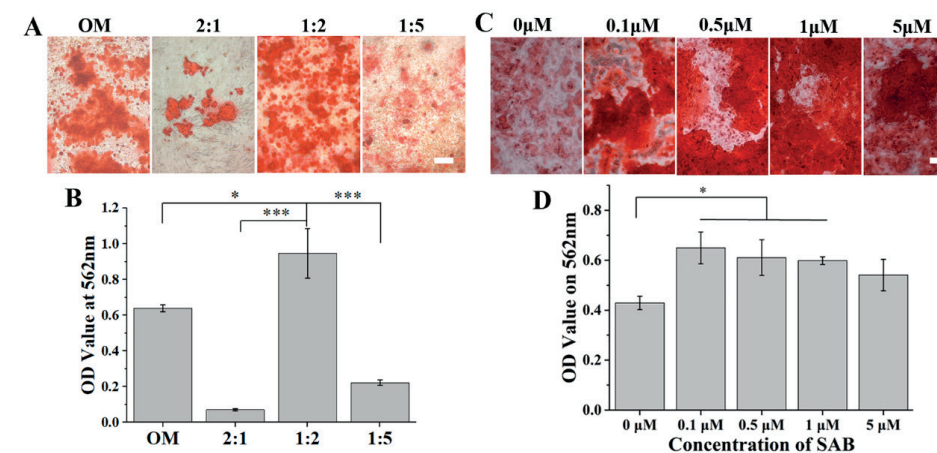

Figure 9. (A) *In-vitro* mineralization of BMSCs on hydrogels without SAB; (B) Quantitative analysis of the alizarin staining of A; (C) Alizarin red staining of BMSC cells after treating with SAB with various concentrations; (D) Quantitative analysis of the alizarin staining of C. (Scale bar = 200 μm)
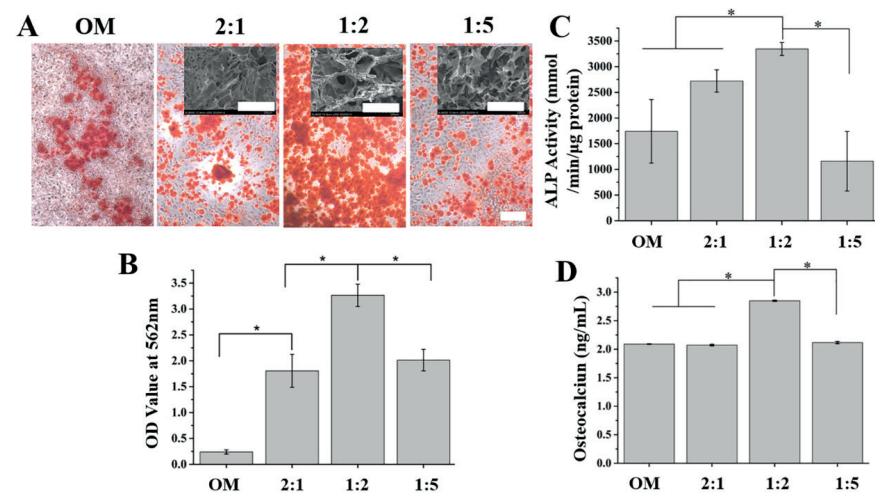
Figure 10. *In-vitro* mineralization of BMSCs. (A) Alizarin red staining of BMSC cells on 1:2, 1:5 and 2:1 hydrogel, inserts are representative images of the morphology of the scaffold after osteogenic differentiation, (B) Quantitative analysis of the alizarin staining of A, (C) ALP activity of BMSC after cultured on the hydrogel for 17 days, (D) OCN expression in the supernatant of BMSC cultured on the hydrogels (Scale bar = 200 μm).
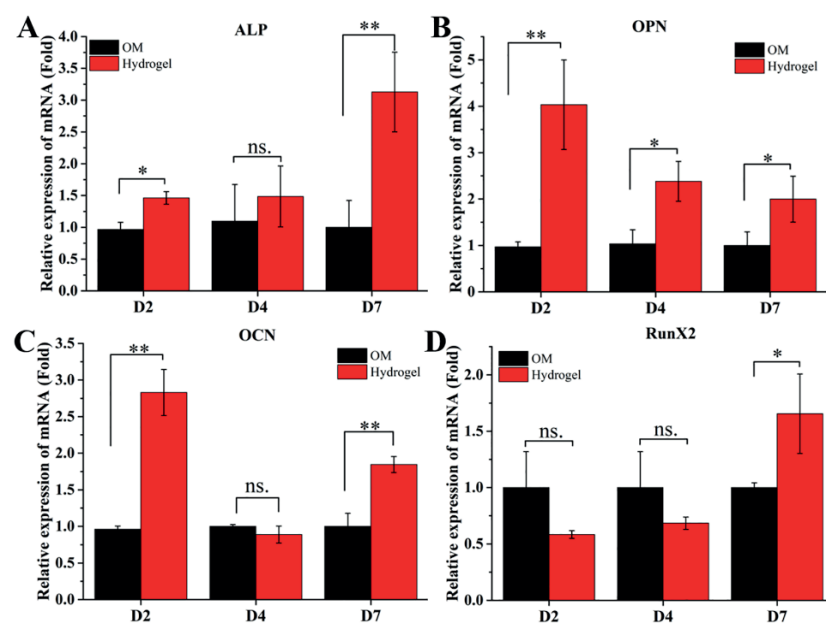

Figure 11. Effects of SS/OSA-SAB hydrogel scaffold on osteogenic gene expression. Real-time analysis of ALP (A), OPN (B), OCN (C), and RunX2 (D) expression of BMSCs after cultured with the scaffold for 2 days, 4 days and 7 days.

4. DISCUSSION

In comparison with conventional osteconductive CaP-based bone filling materials, an injectable, self-healing and pro-osteogenic hydrogel will be more suitable to fill large jumping distance and preserve buccal bone. In this study, we prepared an injectable self-healing pro-osteogenic SS/OSA-SAB hydrogel with an aim of developing an ideal jumping distance filling material to maintain the height of the buccal bone plate. Our results showed that the storage moduli of SS/OSA at the ratios of 1:2 and 1:5 were significantly higher than the other ratios (5:1, 2:1 and 1:1) and the 1:2 SS/OSA hydrogel showed the highest extracellular matrix mineralization nodules of BMSCs. The addition of 0.1 μM SAB to the 1:2 SS/OSA hydrogel showed the highest enhancement in extracellular matrix mineralization nodules. These findings suggested a promising application potential of SS/OSA-SAB hydrogel to preserve buccal bone in the jumping distance.

In clinic, a jumping distance forms between bone wall of fresh extraction socket and dental implant, with a typical geometry of a wide opening and sharp narrowing down to apex. Such a geometry may cause handling difficulties and incomplete filling when filling with granular CaP-based bone grafts for bone regeneration and implant osteointegration. In comparison with granular CaP-based bone grafts, hydrogel holds a better handling property since in its liquid state, hydrogel precursor can be easily injected and spread to reach the bottom of a jumping distance and thereafter gel into solid state. Furthermore, hydrogels bear a better biodegradation than granular CaP-based bone grafts, thereby facilitating an earlier and more robust host bone replacement and implant osteointegration. One of the most widely used hydrogels in bone tissue engineering is photo-crosslinkable naturally-derived gelatin mechacryloyl (Gel-MA) due to its remarkable biocompatibility, processability, tunability, and low immunogenicity [26]. However, insufficient and inhomogeneous gelation may occur since UV radiation may be largely hindered by the long and narrow geometry of, and the bleeding in jumping gap. Self-healing hydrogel can be forced through the syringe and maintain a stable state after injection [27]. Consequently, in this study, to provide a biocompatible and applicable filling material specifically for jumping gap, we developed a self-healing hydrogel by adopting two naturally-derived polymers.

The biological goal of a jumping gap-filling material is to provide a favorable microenvironment for rapid bone regeneration so as to preserve buccal bone and enhance osteointegration. Such a microenvironment may be potentially challenged by mechanical instability caused by both the micromovement of broken buccal bone and oral dynamic occlusion. Therefore, the mechanical stability and self-healing property are important parameters to evaluate a hydrogel-based jumping gap-filling material. Our in-vitro characterization data showed that we successfully prepared a SS/OSA hydrogel

(Figure 1 and 2). The 1:2 and 1:5 SS/OSA hydrogels showed significantly higher storage moduli (Figure 2C) than the hydrogels at the other ratios, which helped to provide a more mechanically stable microenvironment for cell migration and osteogenic differentiation [28]. Rheological characterization (Figure 3) showed that all of the hydrogel structures were destroyed under a high strain but rebuilt under a small strain, indicating that the hydrogels can restore their functions in the case of physical damage. The self-healing efficiency of 2:1 (100.0 ± 12.9%), 1:1 (90.8 ± 6,9%), and 1:2 (95.3 ± 18.8%) SS/OSA hydrogel was significantly higher than that of 1:5 (74.0 ± 44.9%) and 5:1 (72.9 ± 6.0 %) hydrogel. This result indicated the optimal crosslinking of sericin and oxidized alginate when the ratio of SS to OSA was 2:1, 1:1 and 1:2. Thereafter, we characterized the swelling/degradation behavior and morphology of the SS/OSA hydrogels. The EWCs of all the SS/OSA hydrogels were above 90%, which might be attributed to the hydrophilic carboxyl and hydroxyl groups in the structures of sericin and OSA. Among the five hydrogels, the 1:2 SS/OSA hydrogel showed the least degradation with 52% remained after 14 days, providing sufficient time for surrounding osteogenic cells in-growing [29] and form new osteogenic tissue [30, 31]. While the 1:1 SS/OSA hydrogel degraded the most with 92% depleted after 2 days, which may due to the most loosen porous network (consistent with the result of SEM (Figure 5A)). Besides, the slow biodegradation process of the hydrogel was responsible for the stepwise drug release behavior. An interconnected porous microstructure was observed for all SS/OSA hydrogels with pore size between 52.1 ± 16.4 μm to 198.6 ± 44.1 μm (Figure 5). The great water content and interconnected porous structure may enable maintaining a significant extent of fluid and nutrients in interconnected porous structures, which provides a favorable microenvironment [32, 33] for not only the penetration of blood vessels from periosteum and the bone tissue but also the adhesion, migration, proliferation and differentiation of osteogenic cells [34].

To further confer the hydrogels the capacity of rapidly induce bone regeneration, we adopted SAB to functionalize SS/OSA hydrogels. In this study, we observed a slow-release profile of SAB from the SS/OSA-SAB hydrogel (Figure 6A), which enabled the continuous and stable delivery of the SAB to tissue to stimulate the osteogenesis [35]. There were three types of interactions between SAB and SS/OSA scaffold [36]: hydrogen bonds, hydrophobic associations, electrostatic interactions (Figure 6B), which were contributory to the long retention of SAB. These three interactions were derived from the large number of hydroxyl groups in SAB and amino, carboxyl and hydroxyl groups in the scaffold polymers (Figure 6C). The mechanism for SAB release from the scaffold might be the following four probabilities [37]: 1) Fickian diffusion, 2) polymer swelling, 3) polymer swelling and dissolution of the polymer and drug composite scaffold, and 4) the erosion and degradation of the polymer, in the next 33 days. In the beginning 24 hours the release

behavior was controlled by drug diffusion and hydrogel swelling, while it could not be simply explained by diffusion, swelling, degradation or erosion after 48 hours release, according to the power Korsmeyer–Peppas model [38].

We further evaluated the cytotoxicity of the SS/OSA hydrogels (Figure 7A-B). In comparison with the control group, the viabilities of L929 cells on all the hydrogels were all above 100%, which showed the noncytotoxicity of all the hydrogels according to ISO 10993-5. This property was also confirmed by the facts that nearly no dead cells were found on the hydrogels in the Live/Dead staining. Furthermore, we investigated the adhesion and spreading of BMSCs on the SS/OSA hydrogels (Figure 8B). After culture for 3 days, the highest cell viability was detected on the 1:2 SS/OSA hydrogel. No visible dead BMSCs were detected for all the hydrogels.

Thereafter, we evaluated the influence of the 1:2, 1:5 and 2:1 hydrogel in the osteogenic differentiation activities of BMSCs using extracellular matrix mineralization (Figure 9A-B). Our results showed that, after a 31-day osteogenic differentiation, the 1:2 hydrogel was associated with significantly enhanced extracellular matrix mineralization than 1:5 and 2:1 hydrogels. We also tested the osteogenic differentiation of BMSCs in a serial concentration of SAB. Results (Figure 9C-D) showed that 0.1 μM SAB significantly improved extracellular mineralization of BMSCs. As for the SS/OSA-SAB hydrogel, our results (Figure 10A-B) showed that the 2:1, 1:2 and 1:5 SS/OSA-SAB hydrogel significantly promoted the extracellular matrix mineralization of BMSCs by 7.5, 13.6, and 8.4 folds respectively, in comparison with the cell on culture plate. Besides, the period of mineralization induction was shortened, suggesting the potency of the SS/OSA-SAB hydrogel in inducing a faster bone formation. In addition, the 1:2 SS/OSA-SAB hydrogel exhibited significant increase of ALP activity and OCN expression, compared with 1:5 and 2:1 SS/OSA-SAB hydrogels. One possible explanation might be that the porous structure (Figure 10A, insert images) of the 1:2 SS/OSA-SAB hydrogel was still stable after culturing. In contrast, the 1:5 and 2:1 SS/OSA-SAB hydrogel groups showed collapsed or contracted inner porous structures, which may hinder the BMSCs to adhere and differentiation [39, 40]. These data combined with the results of mechanical modulus and the self-healing efficiency, highlighted the 1:2 SS/OSA-SAB hydrogel can be a promising candidate for full fill the jumping gap with enhanced pro-osteogenic property.

To elucidate the potential mechanism of the hydrogel on inducing mineralization, we further tested the relative ALP, OPN, OCN and RunX2 genes of BMSCs on the 1:2 SS/OSA hydrogel (Figure 10). Our results showed that the relative ALP gene expression of the hydrogel group was significantly higher than that of OM group after 7 days culture, indicating that the SS/OSA-SAB hydrogel have a strong effect on promoting osteogenic differentiation in the early stage of bone formation [41]. The SS/OSA-SAB hydrogels

showed significantly higher expression level of OPN during culture time, indicating the promotion effect of the SS/OSA hydrogel on BMSCs attachment and mineralization [42, 43]. The relative gene expression of OCN of the SS/OSA-SAB hydrogel group was significantly higher at day 2 and day 7 compared with the OM group, which confirmed the promotion capacity of the SS/OSA-SAB hydrogel on osteogenic differentiation of BMSCs. Runt related transcription factor 2 (RunX2), a critical transcriptional regulator of osteoblast differentiation, was significantly increased at Day 7, indicating the capacity of the SS/OSA-SAB hydrogels to enhance osteoblast-related genes and finally promote the regenerative bone formation [44]. All the bone-related genes, ALP, OPN, OCN, and RunX2 were expressed significantly higher of hydrogel group than that of OM group, leading to increased osteogenesis of the SS/OSA-SAB hydrogel. Taken together, we believe that the 1:2 SS/OSA-SAB hydrogel might be a good candidate for facilitating osteogenic gene expression and subsequently drive osteogenic differentiation of BMSCs.

One limitation of this study is that, for its application as bone regeneration material, the self-healing SS/OSA-SAB hydrogels still need to be optimized with respect to its mechanical strength and osteogenic capacity, possibly by incorporating inorganic bioactive agents without hindering the injectable and self-healing properties. After such optimization, further studies should also be performed to evaluate the *in-vivo* effect of bone regeneration and ulterior comparison with clinical materials. In addition, the molecular mechanism of osteogenic differentiation of the SS/OSA-SAB hydrogels are to be further certificated.

5. CONCLUSION

In summary, a novel injectable self-healing SS/OSA hydrogel was developed via Schiff's base reaction with enhanced pro-osteogenic property by incorporating SAB. The mechanical property of the prepared hydrogel could be modulated via altering the ratio of sericin and oxidized alginate, showing storage modulus reaching kilo pascals when the ratio of OSA to SS was higher than 2. The 2:1, 1:1 and 1:2 SS/OSA hydrogel showed self-healing efficiency higher than 90%. The SS/OSA hydrogels exhibited an inter-connective porous structure with pore size distributed between 50 μm and 200 μm with sustained drug release performance. *In-vitro* cytocompatibility study demonstrated that the SS/OSA hydrogel are non-cytotoxic. Live/Dead staining certificated that the BMSCs adhere to the hydrogel with spreading morphology. The result of the *in-vitro* extracellular matrix mineralization of BMSCs demonstrated that the 1:2 SS/OSA hydrogel can accelerate the formation of mineralized nodules with improved ALP staining and alizarin red staining. The bone-related gene expression, ALP, OPN, OCN and RunX2, was significantly promoted by 1:2 SS/OSA-SAB hydrogels. In conclusion, the newly formed injectable self-healing hydrogel may serve as a promising jumping gap filling material to promote bone formation and preserve the buccal bone.

ACKNOWLEDGEMENTS

REFERENCES

[1] C.T. Lee, T.S. Chiu, S.K. Chuang, D. Tarnow, J. Stoupel, Alterations of the bone dimension following immediate implant placement into extraction socket: systematic review and meta-analysis, Journal of clinical periodontology 41(9) (2014) 914-926.

[2] V. Chappuis, O. Engel, M. Reyes, K. Shahim, L. Nolte, D. Buser, Ridge alterations post-extraction in the esthetic zone: a 3D analysis with CBCT, Journal of dental research 92 (2013) 195S-201S.

[3] J. Xu, Y. Liu, S. Hsu, Hydrogels Based on Schiff Base Linkages for Biomedical Applications, Molecules (Basel, Switzerland) 24(16) (2019).

[4] D.-q. Li, S.-y. Wang, Y.-j. Meng, Z.-w. Guo, M.-m. Cheng, J. Li, Fabrication of self-healing pectin/chitosan hybrid hydrogel via Diels-Alder reactions for drug delivery with high swelling property, pH-responsiveness, and cytocompatibility, Carbohydrate Polymers (2021) 118244.

[5] M.T.I. Mredha, J.Y. Na, J.-K. Seon, J. Cui, I. Jeon, Multifunctional poly (disulfide) hydrogels with extremely fast self-healing ability and degradability, Chemical Engineering Journal 394 (2020) 124941.

[6] M. Zhu, H. Jin, T. Shao, Y. Li, J. Liu, L. Gan, M. Long, Polysaccharide-based fast self-healing ion gel based on acylhydrazone and metal coordination bonds, Materials & Design 192 (2020) 108723.

[7] X. Pei, L. Fang, W. Chen, X. Wen, L. Bai, X. Ba, Facile Fabrication of Multiresponsive Self-Healing Hydrogels with Logic-Gate Responses, Macromolecular Chemistry and Physics 222(2) (2021) 2000339.

[8] J. Venkatesan, I. Bhatnagar, P. Manivasagan, K.-H. Kang, S.-K. Kim, Alginate composites for bone tissue engineering: a review, International journal of biological macromolecules 72 (2015) 269-281.

[9] K. Tsubouchi, Y. Igarashi, Y. Takasu, H. Yamada, Sericin enhances attachment of cultured human skin fibroblasts, Bioscience Biotechnology and Biochemistry 69(2) (2005) 403-405.

[10] H. Sanz-Fraile, S. Amoros, I. Mendizabal, C. Galvez-Monton, C. Prat-Vidal, A. Bayes-Genis, D. Navajas, R. Farre, J. Otero, Silk-Reinforced Collagen Hydrogels with Raised Multiscale Stiffness for Mesenchymal Cells 3D Culture, Tissue engineering. Part A 26 (2020) 358-370.

[11] J. Barros, M. Ferraz, J. Azeredo, M. Fernandes, P. Gomes, F. Monteiro, Alginate-nanohydroxyapatite hydrogel system: Optimizing the formulation for enhanced bone regeneration, Materials science & engineering. C, Materials for biological applications 105 (2019) 109985.

[12] M. Yang, G. Zhou, Y. Shuai, J. Wang, L. Zhu, C. Mao, Bombyx moriCa-induced self-assembly of silk sericin into a nanofibrous network-like protein matrix for directing controlled nucleation of hydroxylapatite nano-needles, Journal of materials chemistry. B 3(12) (2015) 2455-2462.

[13] Z. Jiayao, Z. Guanshan, Z. Jinchi, C. Yuyin, Z. Yongqiang, Antheraea pernyi silk sericin mediating biomimetic nucleation and growth of hydroxylapatite crystals promoting bone matrix formation, Microscopy research and technique 80(3) (2017) 305-311.

[14] S. Nayak, T. Dey, D. Naskar, S. Kundu, The promotion of osseointegration of titanium surfaces by coating with silk protein sericin, Biomaterials 34(12) (2013) 2855-64.

[15] R. Zhao, X. Liu, L. Zhang, H. Yang, Q. Zhang, Current Progress of Research on Neurodegenerative Diseases of Salvianolic Acid B, Oxidative medicine and cellular longevity 2019 (2019) 3281260.

[16] Y. Wu, S. Xu, X.Y. Tian, The effect of salvianolic acid on vascular protection and possible mechanisms, Oxidative Medicine and Cellular Longevity 2020 (2020).

[17] X. Zhang, L. Zou, J. Li, B. Xu, T. Wu, H. Fan, W. Xu, W. Yao, Y. Yang, Y. Liu, L. Cui, Salvianolic acid B and danshensu induce osteogenic differentiation of rat bone marrow stromal stem cells by upregulating the nitric oxide pathway, Experimental and therapeutic medicine 14(4) (2017) 2779-2788.

[18] Y. Bian, J. Xiang, Salvianolic acid B promotes the osteogenic differentiation of human periodontal ligament cells through Wnt/β-catenin signaling pathway, Archives of oral biology 113 (2020) 104693.

[19] D. Xu, L. Xu, C. Zhou, W. Lee, T. Wu, L. Cui, G. Li, Salvianolic acid B promotes osteogenesis of human mesenchymal stem cells through activating ERK signaling pathway, The international journal of biochemistry & cell biology 51 (2014) 1-9.

[20] L. Wang, F. Deng, W.W. Wang, A.F. Li, C.L. Lu, H. Chen, G. Wu, K.H. Nan, L.L. Li, Construction of Injectable Self-Healing Macroporous Hydrogels via a Template-Free Method for Tissue Engineering and Drug Delivery, Acs Applied Materials & Interfaces 10(43) (2018) 36721-36732.

[21] B. Balakrishnan, A. Jayakrishnan, Self-cross-linking biopolymers as injectable in situ forming biodegradable scaffolds, Biomaterials 26(18) (2005) 3941-3951.

[22] A. Ai, A. Behforouz, A. Ehterami, N. Sadeghvaziri, S. Jalali, S. Farzamfar, A. Yousefbeigi, A. Ai, A. Goodarzi, M. Salehi, Sciatic nerve regeneration with collagen type I hydrogel containing chitosan nanoparticle loaded by insulin, International Journal of Polymeric Materials and Polymeric Biomaterials 68(18) (2019) 1133-1141.

[23] C. Qi, J. Liu, Y. Jin, L. Xu, G. Wang, Z. Wang, L. Wang, Photo-crosslinkable, injectable sericin hydrogel as 3D biomimetic extracellular matrix for minimally invasive repairing cartilage, Biomaterials 163 (2018) 89-104.

[24] L. Wang, H. Fu, W.W. Wang, Y. Liu, X.M. Li, J.J. Yang, L.L. Li, G. Wu, Y.H. Pan, Notoginsenoside R1 functionalized gelatin hydrogels to promote reparative dentinogenesis, Acta Biomaterialia 122 (2021) 160-171.

[25] X. Chen, M. Fan, H. Tan, B. Ren, G. Yuan, Y. Jia, J. Li, D. Xiong, X. Xing, X. Niu, X. Hu, Magnetic and self-healing chitosan-alginate hydrogel encapsulated gelatin microspheres via covalent cross-linking for drug delivery, Materials science & engineering. C, Materials for biological applications 101 (2019) 619-629.

[26] X. Fang, J. Xie, L. Zhong, J. Li, D. Rong, X. Li, J. Ouyang, Biomimetic gelatin methacrylamide hydrogel scaffolds for bone tissue engineering, Journal of materials chemistry. B 4(6) (2016) 1070-1080.

[27] Y. Tu, N. Chen, C. Li, H. Liu, R. Zhu, S. Chen, Q. Xiao, J. Liu, S. Ramakrishna, L. He, Advances in injectable self-healing biomedical hydrogels, Acta biomaterialia 90 (2019) 1-20.

[28] S.H. Parekh, K. Chatterjee, S. Lin-Gibson, N.M. Moore, M.T. Cicerone, M.F. Young, C.G. Simon Jr, Modulus-driven differentiation of marrow stromal cells in 3D scaffolds that is independent of myosin-based cytoskeletal tension, Biomaterials 32(9) (2011) 2256-2264.

[29] F. Akter, J. Ibanez, Bone and cartilage tissue engineering, Tissue Engineering Made Easy, Elsevier (2016), pp. 77-97.

[30] S. Clarke, Kinesiology: the Skeletal System and Muscle Function, Journal of the Australian Traditional-Medicine Society 17(4) (2011) 245-246.

[31] J. Sanz-Herrera, J. García-Aznar, M. Doblaré, On scaffold designing for bone regeneration: a computational multiscale approach, Acta Biomaterialia 5(1) (2009) 219-229.

[32] T.H. Qazi, D.J. Mooney, G.N. Duda, S. Geissler, Biomaterials that promote cell-cell interactions enhance the paracrine function of MSCs, Biomaterials 140 (2017) 103-114.

[33] N. Abbasi, S. Hamlet, R.M. Love, N.-T. Nguyen, Porous scaffolds for bone regeneration, Journal of Science: Advanced Materials and Devices 5(1) (2020) 1-9.

[34] N. Abbasi, S. Hamlet, R.M. Love, N.T. Nguyen, Porous scaffolds for bone regeneration, Journal of Science-Advanced Materials and Devices 5(1) (2020) 1-9.

[35] A.K. Mahanta, S. Senapati, P. Paliwal, S. Krishnamurthy, S. Hemalatha, P. Maiti, Nanoparticle-induced controlled drug delivery using chitosan-based hydrogel and scaffold: application to bone regeneration, Molecular pharmaceutics 16(1) (2018) 327-338.

[36] J. Li, D.J. Mooney, Designing hydrogels for controlled drug delivery, Nature Reviews Materials 1(12) (2016) 1-17.

[37] C. Maderuelo, A. Zarzuelo, J.M. Lanao, Critical factors in the release of drugs from sustained release hydrophilic matrices, Journal of controlled release 154(1) (2011) 2-19.

[38] L. Wang, H. Fu, W. Wang, Y. Liu, X. Li, J. Yang, J. Li, G. Wu, Y. Pan, Notoginsenoside R1 functionalized gelatin hydrogels to promote reparative dentinogenesis, Acta Biomaterialia 122 (2021) 160-171.

[39] H.J. Kim, S.J. You, D.H. Yang, H.J. Chun, M.S. Kim, Preparation of novel RGD-conjugated thermosensitive mPEG-PCL composite hydrogels and in vitro investigation of their impacts on adhesion-dependent cellular behavior, Journal of Industrial and Engineering Chemistry 84 (2020) 226-235.

[40] M. Yao, J. Zhang, F. Gao, Y. Chen, S. Ma, K. Zhang, H. Liu, F. Guan, New BMSC-laden gelatin hydrogel formed in situ by dual-enzymatic cross-linking accelerates dermal wound healing, ACS omega 4(5) (2019) 8334-8340.

[41] S. Vimalraj, Alkaline phosphatase: structure, expression and its function in bone mineralization, Gene 754 (2020) 144855.

[42] A. Altıntaş, G. Saruhan-Direskeneli, G. Benbir, M. Demir, S. Purisa, The role of osteopontin: a shared pathway in the pathogenesis of multiple sclerosis and osteoporosis?, Journal of the neurological sciences 276(1-2) (2009) 41-44.

[43] P.H. Scalize, K.F. Bombonato-Prado, L.G. de Sousa, A.L. Rosa, M.M. Beloti, M. Semprini, R. Gimenes, A.L. de Almeida, F.S. de Oliveira, S.C.H. Regalo, Poly (Vinylidene Fluoride-Trifluorethylene)/barium titanate membrane promotes de novo bone formation and may modulate gene expression in osteoporotic rat model, Journal of Materials Science: Materials in Medicine 27(12) (2016) 1-10.

[44] J.C. Lee, C.T. Pereira, X. Ren, W. Huang, D. Bischoff, D.W. Weisgerber, D.T. Yamaguchi, B.A. Harley, T.A. Miller, Optimizing collagen scaffolds for bone engineering: effects of cross-linking and mineral content on structural contraction and osteogenesis, The Journal of craniofacial surgery 26(6) (2015) 1992.

Chapter 6

A novel *in-situ* hybrid-crosslinked oxidized hyaluronic acid/Gel-MA hydrogel membrane with significantly enhanced mechanical and osteogenic properties for guided bone regeneration

Lei Wang, Wenwen Wang, Lingli Li, Tymour Forouzanfar*, Gang Wu*

*: corresponding authors

ABSTRACT

The aim of the study is to develop an *in-situ* formed barrier membrane with enhanced mechanical and osteogenic property using naturally-derived polymers. Methacrylated gelatin (Gel-MA), hydrolyzed form of collagen without immunogenicity, can be crosslinked in the presence of photo-initiator. Hyaluronic acid (HA) is an abundant component of extracellular matrix (ECM), showing a potential capacity as a pro-osteogenic agent. With the aim to enhance the mechanical and pro-osteogenic properties of Gel-MA, HA was first oxidized to confer aldehyde groups to construct hybrid-crosslinking with Gel-MA (OHA/Gel-MA) through UV crosslinking and Schiff's base reaction. The morphology, physicochemical properties, swelling and degradation behavior of the hydrogels were investigated. The mechanical modulus of the hydrogel was enhanced by 6.8 times. *In-vitro* biocompatibility assays revealed that MC3T3-E1 pre-osteoblasts adhered well to the hydrogel membrane and proliferated with significant osteogenic differentiation and extracellular matrix mineralization. The results indicated that the enhanced OHA/Gel-MA membrane can promote the attachment of pre-osteoblasts, facilitate the osteogenic differentiation of MC3T3-E1. It could be potentially used as alternative candidate barrier membrane for guiding bone regeneration.

Keywords: Gel-MA, Hyaluronic Acid, Simultaneously crosslinked double-network, Guided bone regeneration membrane

1. INTRODUCTION

In the field of implant dentistry, guided bone regeneration (GBR) technique is widely used reconstructive procedure that adopts barrier membranes and particulate bone-defect-filling materials to direct the growth of new bone to restore bone volume and dimensions, such as socket preservation, alveolar ridge augmentation, maxillary sinus elevation [1]. In the classic GBR technique, the barrier membrane mainly functions to prevent the invasion of surrounding connective tissues that bears proliferation advantage over osteoblasts so as to facilitate bone tissue regeneration [2]. Clinically available barrier membranes can be classified into non-resorbable and resorbable membrane. Although clinical trials, a systematic review and meta-analysis have shown no statistically significant difference in most clinical indications between both types of membranes, non-resorbable membranes such as titanium mesh and polytetrafluoroethylene membranes are associated with a series of concerns, such as premature exposure, gingival irritation, infection and the need of second surgery for their removal [3]. Therefore, resorbable membranes with both naturally-derived (such as collagen and chitosan) and synthetic (such as polylactic acid) materials are widely used in clinic. However, these membranes have too mild stickiness to enable surrounding bone tissues to immobilize bone-defect-filling materials, the displacement or deformation of the graft is often found in clinical practice, which may lead to poor clinical outcomes such as delayed osteogenesis, even infection [4]. Consequently, continuous efforts have been attempted to develop more suitable membrane materials.

Apart from being biocompatible and biodegradable, an ideal GBR membrane should also bear 1) good handling property, 2) a strong stickiness to bone tissue and bone-defect-filling materials so as to maintain mechanically stable microenvironment and prevent displacement and 3) an excellent capacity to promote bone regeneration. Among several candidate materials, hydrogel appears to meet most of the abovementioned requirements. First of all, hydrogels, particularly the naturally-derived ones, bear excellent biocompatibility, tunable biodegradability, and abundant recognition sites to facilitate cell adhesion, migration and proliferation. Furthermore, hydrogels can form GBR membrane *in-situ*, which is highly convenient for clinical handling and can adaptively fit to the bone defects with highly diverse shapes. In our recent study, we adopted a clinically-available fibrin glue hydrogel that have strong stickiness to surrounding tissues, which can effectively stabilize particulate bone-defect-filling materials [5]. However, this glue may greatly compromise osteogenic activities, which drive us to develop more pro-osteogenic hydrogel materials. Methacrylated gelatin (Gel-MA) is one of the most widely used hydrogels in bone tissue engineering [6]. Gel-MA is a hydrolyzed form of collagen, a major organic component of bone tissue. It can be crosslinked in the presence of photo-initiator [7]. It bears a good capacity to bond to mineralized tissue through non-covalent

bonding mechanisms [8], which may greatly help to both form a stable osteogenic microenvironment in GBR and prevent the displacement of particulate bone-filling materials. However, for the application as GBR membrane, Gel-MA should still be greatly improved in mechanical stiffness and pro-osteogenic properties.

One promising approach to modify the physicochemical and biofunctional properties of a hydrogel is to introduce a hybrid crosslinking mechanism, for example, thermal-photo-crosslinking [9] and ionically–covalently crosslinking [10]. With the inspiration of hybrid crosslinking, we wished to further enhance the mechanical property of Gel-MA by introducing an additional dynamic bond. For this purpose, we added a modified hyaluronic acid (HA). HA is an important component of the extracellular matrix (ECM) consisting of D-N-acetylglucosamine and D-glucuronic acid repeating units. It is widely used in the field of biomedical research due to its excellent biocompatible, biodegradable, and nonimmunogenic property [11]. Particularly in the field of bone tissue engineering, HA also shows promising application both as a scaffold component and a pro-osteogenic agent [12]. HA-based biomaterial has been attempted in clinic to promote bone regeneration in post-extractive defects [13]. To realize the dynamic bond, we first oxidized HA with sodium periodate to confer aldehyde groups to HA. Thereafter, the mixture of OHA and Gel-MA in different ratios was subjected to reaction condition with UV light and 37 °C for 2 min so as to achieve a hybrid-crosslinked (dynamic bond and photo-crosslinking) OHA/Gel-MA hydrogel membrane.

In this study, we optimized OHA/Gel-MA ratio with an aim to develop a novel GBR membrane with significantly enhanced osteogenic and mechanical properties than Gel-MA. We characterized the rheological properties, the surface morphology, the swelling and degradation performances of the hydrogel membrane. The cytocompatibility of the membrane was evaluated by culturing L929 cells onto the OHA/Gel-MA hydrogel membrane. The cell adhesion onto the hydrogel was assessed by Live/Dead staining using osteoblast MC3T3-E1 cells. The *in-vitro* osteogenic differentiation was further estimated using ALP and OCN as biomarkers.

2. MATERIALS AND METHODS

2.1 Materials

Gelatin, methacrylic anhydride (MA), Irgacure 2959, and sodium periodate were purchased from Sigma-Aldrich (St. Louis, MO). Hyaluronic acid (HA) was purchased from Bloomage BioTechnology Co. LTD (Shandong, China). MC3T3-E1 cell was obtained from the institute of Biochemistry and Cell Biology (Chinese Academy of Sciences, China). Dulbecco's modified Eagle Medium (DMEM), fetal bovine serum (FBS), penicillin-streptomycin solution, Live/Dead Viability and Cytotoxicity Kit, and Cell Counting Kit-8 (CCK-8) were purchased from Life Technology (Carlsbad, CA). All aqueous solutions were prepared from analytical grade reagents (Sigma-Aldrich, St. Louis, MO).

2.2 Preparation of methacrylated gelatin (Gel-MA)

A uniform 10% (w/v) gelatin solution was obtained by dissolving type-A porcine skin gelatin (Type A, Bloom 300) into phosphate buffered saline (PBS) at 50 °C. MA was added to the gelatin solution at a rate of 0.5 mL min^{-1} under rigorous stirring (800 rpm). The final concentration of MA was 1% (v/v). After addition of MA, 5 M NaOH was used to adjust the pH value of the reacting mixture to a value of 7.4-8 and the mixture was allowed to react for 3 h at 50 °C. The samples were dialyzed against deionized water for 5 d at 50 °C using 3500 Da cut-off dialysis tubes to remove unreacted MA and additional by-products. The dialyzed samples were frozen at -80 °C for 48 h and stored at room temperature in the dark. The degree of methacrylation was quantified by ^{1}H NMR method (Advanced III, 600MHz, Bruker, Germany) as we previously described [14] using D_2O as solvent.

2.3 Oxidized sodium hyaluronate (OHA) Synthesis

Oxidized sodium hyaluronate (OHA) was synthesized using sodium periodate ($NaIO_4$) as oxidizing agent. Briefly, 1 g sodium hyaluronate was dispersed in 25 mL ethanol. $NaIO_4$ (~0.551 g) was dissolved in 50 mL distilled water to prepare $NaIO_4$ solution, which was added dropwise to sodium hyaluronate dispersion and stirred at room temperature for 72 h. The reaction was quenched by adding equimolar ethylene glycol (0.2 mL) under continuous stirring for 30 minutes. The resultant suspension was dialyzed against ultrapure water (UPT-11-20T, ULUPURE, China) using a dialysis membrane (MWCO: 3500 Da, Spectrum Lab, USA) for 7 days, changing water several times until the dialysate was periodate free. The absence of periodate was ensured by adding a 0.5 mL aliquot of the dialysate to 0.5 mL of a 1% solution of silver nitrate. OHA was obtained by lyophilizing the dialysate. The oxidation degree of HA was determined by quantifying the concentration of unconsumed periodates by iodometry as described previously [15]. In brief, 1 mL of the reaction mixture was mixed with a sufficient quantity of potassium iodide solution and allowed to react for 10 min to consume all unreacted periodate ions. Next, liberated iodine was titrated with a standardized sodium thiosulfate solution using starch as the

indicator. The titration volume of used sodium thiosulfate was monitored and indicated by disappearance of the color. Oxidation degree values were calculated as the average of three independent oxidation experiments.

2.4 Preparation of the hydrogels

Desired amounts of precursors (Gel-MA, OHA) were firstly pre-dissolved in phosphate buffered saline (PBS) to form 20%, and 5% (w/v) solutions, respectively. Irgacure 2959 (50 mg/mL, in 75% ethyl alcohol solution) was used as UV initiator with addition of 0.5wt%. Certain volumes of these solutions (Table 1) were pipetted into plastic tubes and mixed by vortex to obtain uniform solutions and immediately transferred into a tailor-made plastic mold for UV curing for 120 s at 37 °C. To investigate the influence of formulation on the structure and morphology of hydrogels, different formulations were adopted to prepare hydrogel (OHA/Gel-MA) and single Gel-MA was chosen as control. For each sample, every measurement was performed in triplicate.

Table 1. Hydrogels Preparation

Samples	Gel-MA (20%, μL)	OHA (5%, μL)	I2959 (5%, μL)	I2959 Concentration (%)	Gelled
OHA/Gel-MA 0:1	200	0	20	0.5wt%	+
OHA/Gel-MA 0.0625:1	200	50	25	0.5wt%	+
OHA/Gel-MA 0.25:1	200	200	40	0.5wt%	+
OHA/Gel-MA 1:1	200	800	100	0.5wt%	+
OHA/Gel-MA 0:1	0	200	20	0.5wt%	-

2.5 The Fourier Transform Infrared Spectroscopy (FTIR)

The Fourier Transform Infrared Spectroscopy (FTIR) of various hydrogel samples and precursors was performed using a Tensor II ATR-FTIR spectrophotometer (Bruker, Germany) via ATR-FTIR mode and KBr tableting respectively.

2.6 Scanning Electron Microscopy (SEM)

The morphology of the OHA/Gel-MA hydrogels was observed using a scanning electron microscopy (SU8010, Hitachi, Japan). Lyophilized hydrogel samples (ϕ = 8mm) were sputter-coated with gold for 60 s before the observation.

2.7 Rheological Characterizations

Rheological characterization of the OHA/Gel-MA hydrogels was performed using a rheometer (DHR-2, TA Instruments, USA). The storage modulus (G') and loss modulus (G") of the hydrogels were tested in the oscillatory mode as a function of angular frequency (0.01 rad s^{-1} to 100 rad s^{-1}) at a constant strain of 1% using a parallel plate configuration (8 mm in diameter) at 37 °C. Using the same frequency (1 Hz), continuous step change of oscillatory strain between 1% and 1000% was used to assess the strain-induced damage of the hydrogel, which reflects the toughness of the hydrogels. To prevent water evaporation, a thin layer of silicon oil was used to seal the samples.

2.8 Swelling and degradation properties

The swelling ratio of each sample was determined by immersing them in PBS at 37 °C. The swelling ratio of the hydrogels was calculated using the following equation:

$$SR\ (\%) = (W_t - W_d) / W_d \times 100\% \qquad (1)$$

Where W_t and W_d are the weights of the swollen hydrogels at pre-determined time points and dry hydrogels, respectively. SR was presented as the mean ± standard deviation of three separate measurements. The degradation profile of hydrogels was followed *in vitro* by measuring the weight loss in PBS at 37 °C over time. After wiping away excess water on the surfaces, the weight of the hydrogel samples was measured immediately at specified time points. The degradation rate was calculated using equation (2), where W_t is the weight of the hydrogel after degradation and W_o (the weight of hydrogel after incubating for 24 h) was chosen to be the initial weight of degradation because of its swelling behavior:

$$Remaining\ Weight\ (\%) = W_t/W_o \times 100\% \qquad (2)$$

2.9 *In-vitro* biocompatibility

L929 cells were used to test the *in-vitro* cytocompatibility of the OHA/Gel-MA hydrogels, and were directly seeded onto the hydrogel surfaces. OHA and Gel-MA were sterilized by ethylene oxide and dissolved in sterilized PBS. L929 cells were cultured in 90% RPMI 1640 + 10% FBS + 1% penicillin–streptomycin and seeded onto preformed hydrogels at a density of 1000 cells per well of a 96-well polystyrene cell culture plate. Cells that were cultured under the similar cell culture medium conditions but without hydrogels were used as

control. At indicated time points (1 day, 4 days, and 7 days), hydrogels were washed with PBS and incubated with Cell Counting Kit-8, CCK-8 for 3 h at 37 °C in the dark. OD values were measured using an ELISA plate reader (Varioskan LUX, Thermo- Fisher, USA) and cell viability (%) was calculated using the following equation:

$$Cell\ viability\ (\%) = OD_{test} / OD_{control} \times 100\%. \qquad (3)$$

2.10 *In-vitro* mineralization study

The *in-vitro* osteogenic differentiation was studied using MC3T3-E1 cells. Before mineralization study, cell adhesion and spreading were investigated. MC3T3-E1 cells were cultured onto the OHA/Gel-MA hydrogels (0:1, 0.0625:1, 0.25:1, 1:1) with cell density of 1000/well in 96-well plate. After 2 days culture, the cells on the hydrogels were visualized by Live/Dead staining (containing 2 mM calcein AM and 4 mM ethD-1) in PBS for 30 min at 37 °C. After 30 minutes of incubation, cells were rinsed 3 times with pre-warmed PBS and observed under a DMi8 microscope (LEICA, Germany). All experiments were performed in triplicates. The cells were cultured in Dulbecco's Modified Eagle's Medium (DMEM) containing 1000 mg/L of glucose, 10% fetal bovine serum (FBS) and 1% penicillin/streptomycin. As for mineralization, MC3T3-E1 cells were cultured onto the hydrogels with the density of 3×10^4 cells per well in a 48-well plate. 24 hours after spreading, the culture medium was changed by mineralized medium (medium supplemented with 50 μg/mL ascorbic acid (Sigma), 10 mM sodium β-glycerophosphate (Sigma) and 10 nM dexamethasone) to initiate cell differentiation and matrix mineralization. After 17 days culture, the mineralization nodules were stained using an Alizarin red staining (ARS) kit (Cyagen, Guangzhou, China). Briefly, the hydrogels with cells were rinsed three times with PBS, fixed with 95% ethanol for 15 minutes, washed with distilled water three times and finally stained using Alizarin red staining solution for 1 hour at 37 °C. Stained samples were washed with water three times with each was lasting one minute. Pictures of the top surface were taken using an optical microscope (Nikon, Japan). For quantification, the stained mineralized nodules were eluted with 10% (w/v) cetylpyridine chloride (CPC), and the absorbance of the supernatants was measured at 550 nm using a micro reader (Synergy NEO2, BioTek, USA). As for ALP staining, the cells were fixed in 4% paraformaldehyde followed by a reaction with ALP staining solution (Yeasen, Shanghai, China) for 20 minutes. The ALP-positive cells were stained blue and visualized by microscopy.

3. RESULTS

3.1 Preparation of the OHA/Gel-MA hydrogels

In comparison with the ^{1}H NMR spectrum of gelatin, two peaks occurred at 5.34 and 5.60 ppm in the spectrum of Gel-MA, which corresponded to the vinyl protons (Figure 1A-B). The degree of methacrylation calculated from ^{1}H NMR was 25.10%. The FTIR analysis (Figure 1C) showed no different absorption peaks between Gel and Gel-MA. In comparison with ^{1}H NMR spectrum of HA, the two new peaks (9.12 ppm and 6.54 ppm) were detected in the spectrum of OHA (Figure 1E), which represented protons in the aldehyde groups. When compared with the FTIR spectrum of HA, there were two new absorption peaks at 1735 cm^{-1} and 1650 cm^{-1} detected in the spectrum of OHA (Figure 1F), which represented the stretching vibration of C = O of the aldehyde group. The successful modification to introduce aldehyde groups to HA (Figure 1D) was confirmed by ^{1}H NMR [16, 17] (Figure 1E). The oxidation degree of OHA was 86.87%, which was determined by quantifying the concentration of unconsumed periodates by iodometry. In 0.0625:1 OHA/Gel-MA hydrogel, the molar ratio of amino group to aldehyde group was 4:1 (the oxidation degree of OHA was 86.87%, according to the iodometry method, indicating 3.341 mmol aldehyde groups in one-gram OHA; 74.9% of amino left in Gel-MA, indicating 0.809 mmol amino in one gram Gel-MA).

Figure 2A showed the gelatinization process. Right after mixing, OHA/Gel-MA mixtures at different ratios retained their flowability to be poured into round modes. After UV irradiation (365 nm) for 2 minutes, the mixtures gelled and formed round membranes (Figure 2B). Figure 2C showed the FTIR result of the hydrogels. The absorption peak at 1639 cm^{-1} in the spectrum of Gel-MA hydrogel corresponded to amido bond. In the spectra of 0.25:1 and 1:1 OHA/Gel-MA hydrogels, this absorption peak shifted to 1645 cm^{-1} and 1655 cm^{-1}, respectively, indicating the successful hybrid crosslinking between Gel-MA and OHA. After gelation (Figure 1F), the characteristic absorption peak at 1735 cm^{-1} for the aldehyde group of OHA disappeared in the spectrum of OHA/Gel-MA hydrogels, representing that the aldehyde groups favorably bridged with amino groups (dynamic imine bonds). A single set of OHA couldn't gel (Table 1), due to no coordinate bonds.
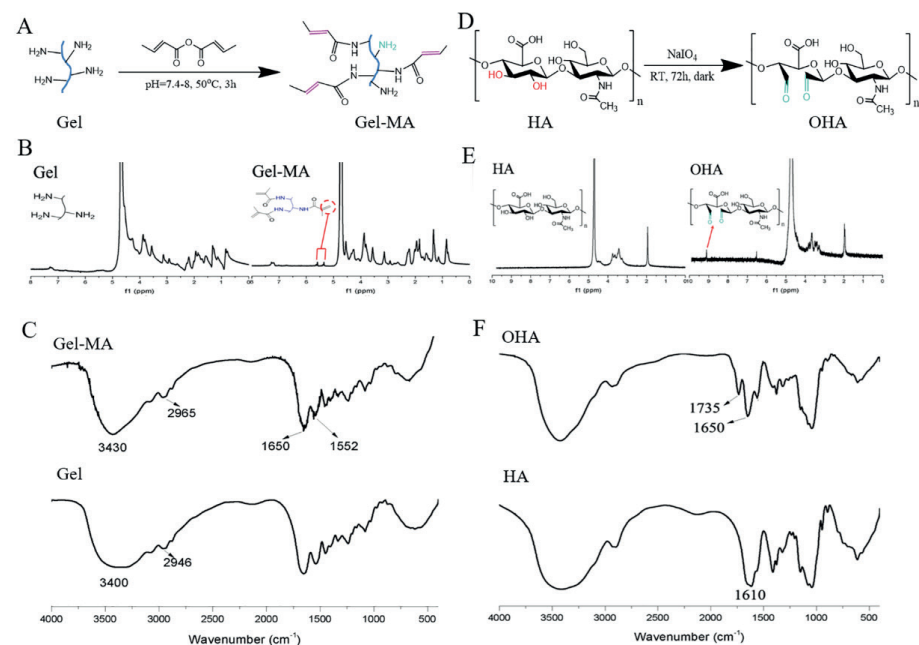
Figure 1. A) Schematic diagram of modification of Gelatin; B) ¹H NMR spectra of Gel and Gel-MA; C) FTIR spectra of Gel and Gel-MA; D) Schematic diagram of modification of HA; E) ¹H NMR spectra of HA and OHA; F) FTIR spectra of HA and OHA.
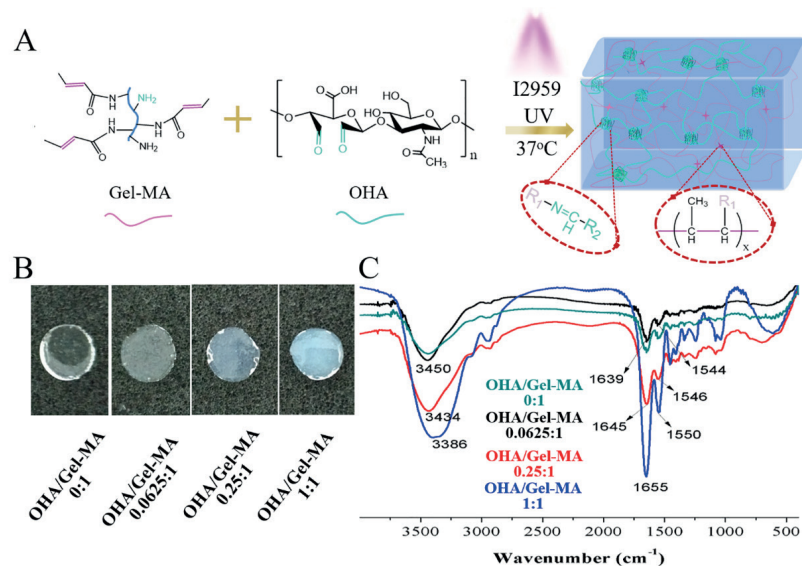

Figure 2. A) Schematic diagram of the hydrogel formation; B) Representative photograph of the hydrogels; C) FTIR spectra of the various component hydrogels.

3.2 Rheological study

Figure 3 showed the evolution of G' and G" for the hydrogels. All samples showed a gel-like behavior, i.e., G' > G", and the viscoelastic parameters were independent on the oscillation frequency. The storage modulus of 0.0625:1 hydrogel (176.4 ± 35.3 KPa) was significantly higher (6.8 times) than that of Gel-MA (25.9 ± 9.8KPa). In contrast, the storage modulus of 0.25:1 hydrogel (7.9 ± 1.9 KPa) and 1:1 hydrogel (3.4 ± 0.8 KPa) was significantly lower than that of Gel-MA hydrogel.
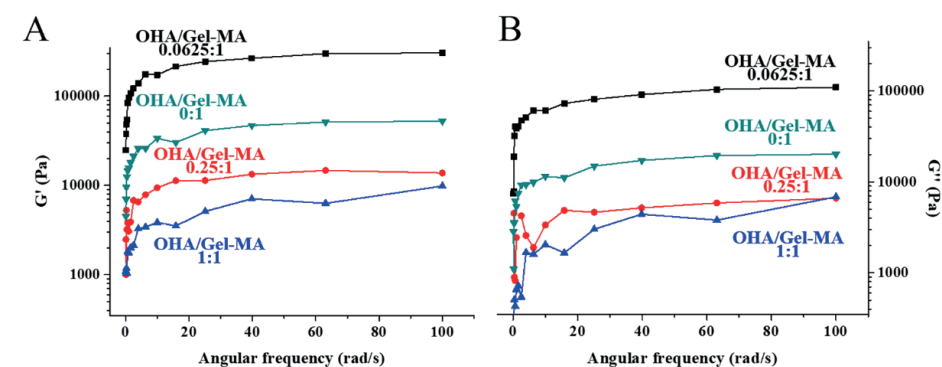

Figure 3. Rheological characterizations of the hydrogels: frequency-sweep measurements of the hybrid crosslinking hydrogels with different ratios of OHA/Gel-MA.

3.3 Swelling behavior and *in-vitro* degradation property

4 hours after immersion into PBS, the swelling ratios of OHA/Gel-MA hydrogels at the three mixture ratios and Gel-MA hydrogel were all above 500% (Figure 4A). All the hydrogels reached an equilibrium water content after 6 hours. Figure 4B showed the *in-vitro* biodegradation of hydrogels. At the first 48 hours, 10.4% 11.3%, 22.4% and 18.0% were degraded for Gel-MA, 0.0625:1, 0.25:1 and 1:1 hydrogel, among which no significant difference was detected. 72 hours after incubation, the remaining weight ratios were 75.0 ± 13.4%, 72.7 ± 10.5% and 76.3 ± 10.0% for 0.0625:1, 0.25:1 and 1:1 OHA/Gel-MA hydrogels, which was significantly lower than that (90.0 ± 3.1%) of Gel-MA. 8 days later, the 0.0625:1 hydrogel exhibited a reduction in mass loss after 8 days with remaining weight of 78.7 ± 10.1% and degraded at a slower rate than that of 0.25:1 and 1:1 hydrogel.
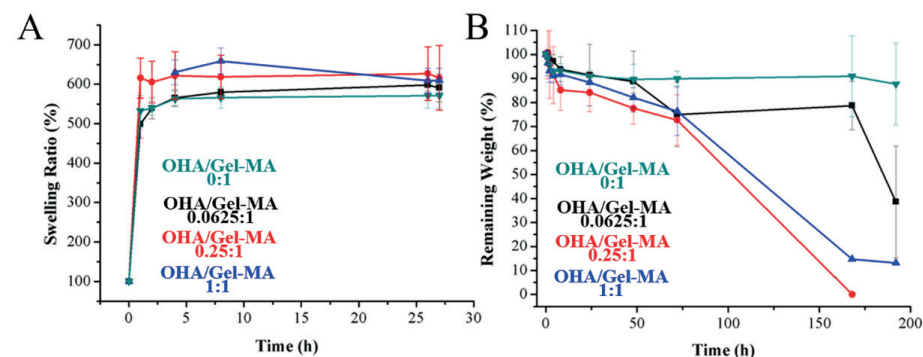
Figure 4. The swelling and degradation profiles of the hydrogels.

3.4 Morphology study

The microstructures of the hydrogels were observed using SEM and the images were shown in Figure 5A. The prepared hydrogels had a porous structure with inter-connective pores. The pore size of 0.0625:1 OHA/Gel-MA hydrogel (37.7 ± 7.23 µm) was significantly lower than that of Gel-MA hydrogel (95.6 ± 22.6 µm) (Figure 5B). The pore sizes of 0.25:1 and 1:1 hydrogels were 40.6 ± 8.9 µm and 71.6 ± 8.5 µm, respectively.
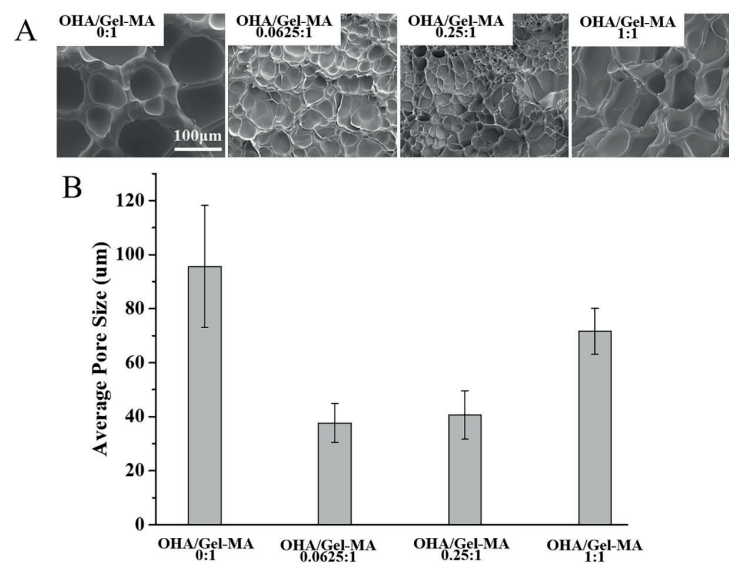

Figure 5. A) Representative SEM images (Bar:100 µm); B) The average pore size of the OHA/Gel-MA hydrogels.

3.5 *In-vitro* cell viability

The viability of L929 cells was above 75% for 0:1, 0.0625:1 and 0.25:1 hydrogel groups on day 1, day 4 and day 7 (Figure 6A), which can be defined as noncytotoxic according to ISO 10993-5, showing sufficient cell viability to support the proliferation of cells. However, the viability of 1:1 hydrogel group differed significantly over time, the viability was 92.2 ± 5.4% on day 1, and decreased further to 57.2 ± 3.9% on day 4 and 17.3 ± 1.3% on day 7, showing cytotoxicity, which may due to superfluous aldehyde released from the hydrogel [18]. The Live/Dead assay showed that the MC3T3-E1 cells attached well onto or into the hydrogels, presenting a spreading morphology (Figure 6B). The cell density of the 1:1 hydrogel was lower than that of 0:1, 0.0625:1 and 0.25:1 hydrogel. The result verified the existing of excessive aldehyde groups in 1:1 hydrogel (the ratio of $-NH_2/-CHO$ was 1:4). This result is consistent with that of degradation profile, both indicated the inadequate crosslinking of Gel-MA with OHA in 1:1 hydrogel.
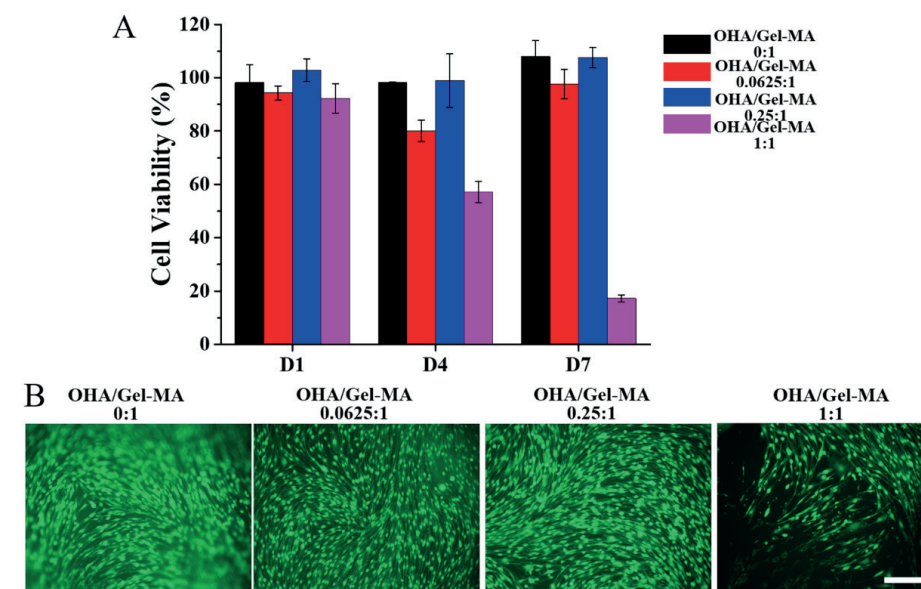

Figure 6. A) Cell viability of L929 on the hydrogels detected by CCK-8; B) The adhesion and spreading of MC3T3-E1 cells on the hydrogels on Day 3. (Scale bar = 250 µm)

3.6 *In-vitro* mineralization

Figure 7 showed the ALP staining and its quantitative analysis. The blue ALP staining in 0.0625:1 and 0.25:1 hydrogel groups was darker than that in the groups of Gel-MA and 1:1 hydrogel. The mean optical densities of 0.0625:1 hydrogel group (0.48 ± 0.04) and 0.25:1 hydrogel group (0.46 ± 0.07) were significantly higher than that of Gel-MA hydrogel group (0.31 ± 0.01). The mean optical density value was 0.34 ± 0.04 for 1:1 hydrogel group. The alizarin red staining result was shown in Figure 8. Compared with Gel-MA and 1:1 hydrogel groups, the MC3T3-E1 cells on 0.0625:1 and 0.25:1 hydrogel groups produced a denser and a more homogeneous spread staining. The OD values of the eluted extracellular matrix mineralization nodules of 0.0625:1 hydrogel group (2.81 ± 0.10) and 0.25:1 hydrogel group (2.67 ± 0.27) were significantly higher than that of 1:1 hydrogel group (1.37 ± 0.11) and Gel-MA hydrogel group (1.57 ± 0.10).
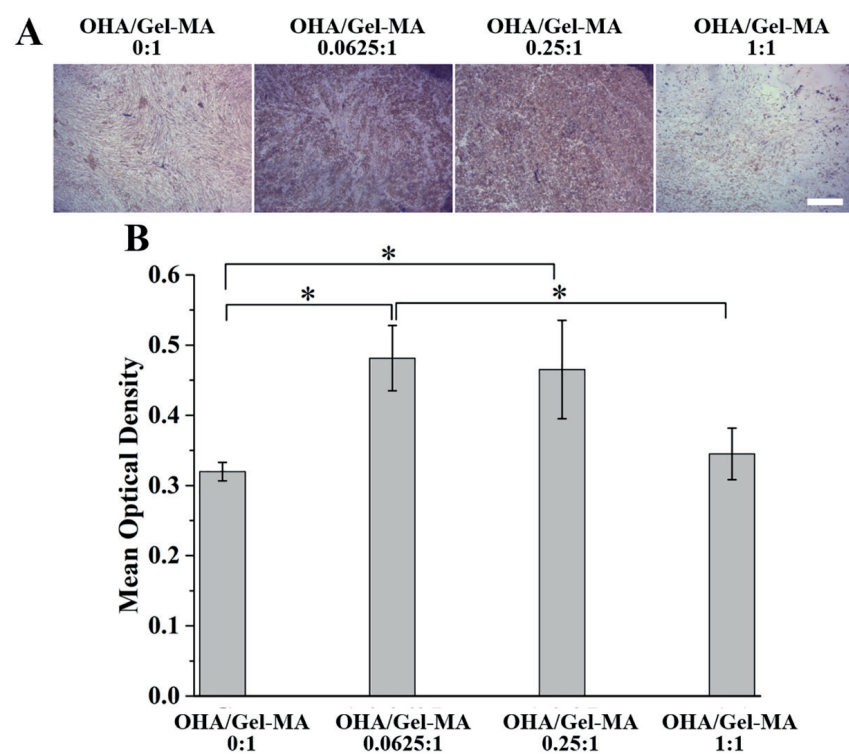
Figure 7. A) ALP staining of MC3T3-E1 cells on the hydrogels after 17 days differentiation culture; B) Quantitative analysis of the ALP staining.(Scale bar = 250 μm)
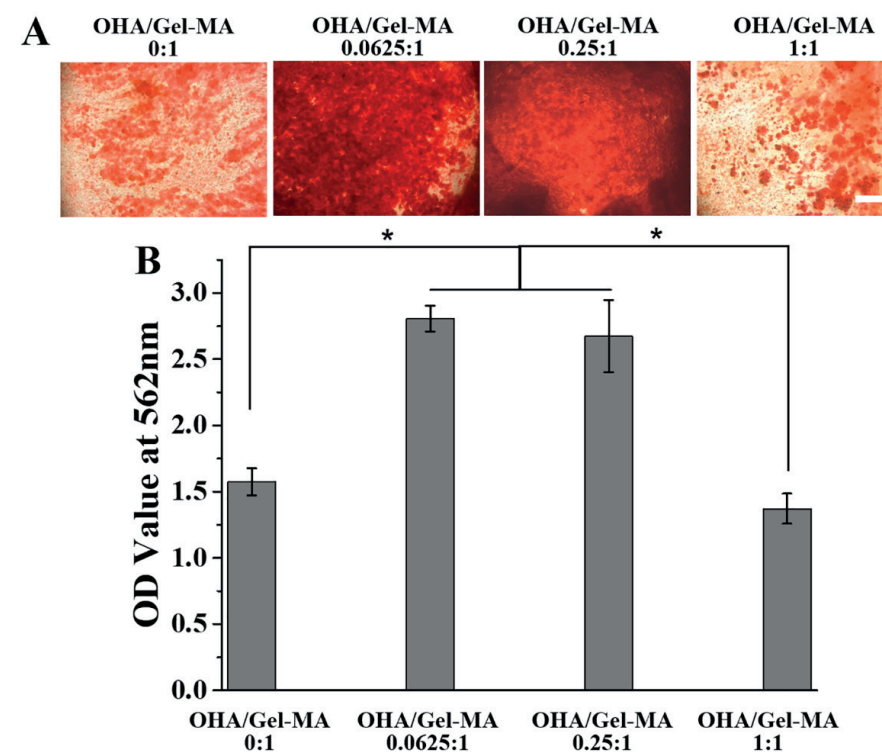
Figure 8. A) Alizarin red staining of MC3T3-E1 cells on the hydrogels after 17 days differentiation culture; B) Quantitative analysis of the alizarin staining. (Scale bar = 250 μm)

4. DISCUSSION

In-situ formed Gel-MA hydrogel GBR membrane is advantageous in clinical handling and stabilizing bone graft materials over the current clinically-available GBR membranes. However, its pro-osteogenic and mechanical properties are still suboptimal. In this study, we significantly enhanced the storage modulus of Gel-MA by 6.8 times by introducing OHA in a ratio 0.0625:1 and thus an additional dynamic chemical bond to Gel-MA. To the best of our knowledge, this is, for the first time, to *in-situ* hybrid-crosslink Gel-MA with OHA via UV initiated free-radical polymerization and Schiff's base reaction. Furthermore, such hybrid-crosslinked OHA/Gel-MA could also significantly promote

the *in-vitro* osteogenic differentiation of MC3T3-E1 cells. These findings suggested a promising application potential of the novel OHA/Gel-MA hydrogel membrane in GBR technique.

The essence of GBR technique is to provide a mechanically-stable and biologically-favorable microenvironment to facilitate bone tissue regeneration in intended area [19]. GBR membrane is critical for the success of this technique because 1) it covers and stabilizes bone-defect-filling materials to ensure mechanical stability and 2) it serves as a barrier to both prevent invasion of surrounding profibrotic connective tissues and allows the infiltration of nutrients and blood supplies so as to support bone tissue regeneration. Naturally-derived resorbable collagen is one of the most widely adopted GBR membranes in clinic [20] and it provides ECM-like surface to guide the adhesion and migration of osteogenic cells as well as good barrier function [21]. However, collagen membrane does not bear sufficient stickiness to bone tissues or CaP-based bone-defect-filling materials so that it still needs additional sutures, double membranes or even non-resorbable metallic minipins to achieve sufficient fixation. Furthermore, the preformed collagen membrane always needs an on-the-spot trimming to fit the shapes of bone defects [22]. All these properties greatly increase the time and complexity of GBR technique. Consequently, continuous efforts have been attempted to develop alternative GBR membrane materials. Among attempted materials, photo-crosslinkable Gel-MA-based hydrogels, show a series of promising properties [23, 24], such as 1) non-immunogenicity, 2) good degradability and biocompatibility, 3) the good fluidity of Gel-MA enables an easy spreading and thus complete coverage of bone-defect-filling materials and surrounding healthy bone tissues so as to form an excellent seal, functioning to both allow the penetration of nutrients/blood vessels and stabilize the filling materials without the needs of additional fixation or trimming. In this study, to further enhance the application potential of Gel-MA, we aimed to further enhance both the mechanical strength and pro-osteogenic property of Gel-MA.

One possible method to enhance the mechanical property of Gel-MA is to increase the degree of methacrylation of Gel-MA, which may increase the crosslinking density. However, it seems that the storage modulus of Gel-MA is not significantly influenced when the degree of methacrylation is increased from 23.1% to 76.0% [25]. In our previous study, we also show that the incorporation of a bioactive small-molecule compound — notoginsenside R1 may dramatically enhance the storage modulus of Gel-MA by about 1.8 times [26]. In other studies, doxorubicin [27] and tannic acid [28] are also shown to significantly increase the storage modulus of hydrogels. Such enhancements may be attributed to the formation of intermolecular hydrogen bonding or host-guest interactions between drugs and hydrogels, leading to a more compact structure [28]. However, the introduction of additional drugs will inevitably increase the complexity for

such a medical device to receive regulatory approval. To provide a more viable approach, we put forward a hybrid-crosslinking by adding OHA to form dynamic chemical bonds with Gel-MA in additional to its intrinsic photo-crosslinking. For this purpose, we first controlled the methacrylation degree of Gel-MA (calculated according to the result of ¹H NMR (Figure 1B)) as low as 25.10% (with about 0.809 mmol amino retained in one gram Gel-MA), which was designed to enable the Schiff's base reaction between the unsubstituted amino groups of Gel-MA with the aldehyde groups of OHA. We chose OHA since HA is also widely used in many approved medical devices [29]. We adopted the iodometry method, which showed that one-gram OHA contained about 3.341 mmol aldehyde groups and the oxidation degree of OHA was 86.87%. After the mixture, FTIR analysis showed that a significant peak shift from 1639 cm^{-1} for Gel-MA to 1645 cm^{-1} and 1655 cm^{-1} for 0.25:1 and 1:1 OHA/Gel-MA, respectively. Furthermore, the characteristic peak for aldehyde group from OHA disappeared (Figure 2). These results indicated the aldehyde groups favorably bridged with amino groups and the successful hybrid crosslinking between Gel-MA and OHA.

We further characterized the swelling/degradation behavior and morphology of OHA/Gel-MA hydrogel membrane. The equilibrium water content of this study was between 90-95% for all the OHA/Gel-MA hydrogels (Figure 4A), which might be attributed to the hydrophilic carboxyl and hydroxyl groups in the structures of Gel-MA and OHA. Mass loss of the 0.0625:1 OHA/Gel-MA hydrogel was 60% after 8 days degradation, which was still comparable with Gel-MA. In contrast, the 0.25:1 and 1:1 OHA/Gel-MA hydrogels degraded much faster, which might compromise their application potential. An interconnected porous microstructure was observed for all OHA/Gel-MA hydrogels with pore size between 40.6 ± 8.9 μm to 95.6 ± 22.6 μm (Figure 5). The great water content and interconnected porous structure may enable maintaining a significant extent of fluid and nutrients in interconnected porous structures, which provides a favorable microenvironment [30] for not only the penetration of blood vessels through the membrane but also the adhesion, migration, proliferation and differentiation of osteogenic cells [31].

When the mixing ratio of OHA to Gel-MA was 0.0625:1 with the molar ratio of -NH$_2$/-CHO at about 4:1, the storage modulus of OHA/Gel-MA reached 176.4 ± 35.3 KPa, which was significantly higher (about 6.8 times) than that of Gel-MA (25.9 ± 9.8 KPa). However, as OHA content was increased to 0.25:1 or 1:1 (with the molar ratio of -NH$_2$/-CHO at 1:1 or 1:4), the storage moduli (7.9 ± 1.9 KPa for 0.25:1 and 3.4 ± 0.8 KPa for 1:1) of OHA/Gel-MA hydrogels were significantly lower than that of Gel-MA. These phenomena might be explained by two independent mechanisms. On one hand, it has been shown that dynamic Schiff base linkage-based hydrogel with the molar ratio of -NH$_2$/-CHO at 4:1 or 8:1 bore much higher storage modulus than that at 2:1 or 1:1 [32], which contributed to the significant promoting effect of OHA when being mixed at the ratio of 0.0625:1. On

the other hand, the overdosage of OHA might, whereas, caused a steric hindrance to the photocrosslinking efficiency of Gel-MA, thereby resulting in a compromised mechanical property for the hydrogels with mixing ratio at 0.25:1 and 1:1. These data highlighted the importance of an appropriate ratio for producing hybrid-crosslinked hydrogels with enhanced mechanical property. Furthermore, the higher mixing ratios were associated with significantly enhanced degradation rate, which made those hydrogels less suitable for the intended application.

Thereafter, we evaluated the cytotoxicity of the hybrid-crosslinked hydrogels (Figure 6A). The 0.0625:1, 0.25:1 hydrogels showed sufficient cell viability to support the proliferation of cells, all above 75%, which can be defined as noncytotoxic according to ISO 10993-5. However, the cell viability of 1:1 hydrogel decreased after 4 days (60%) and 7 days culture (20%), which may due to the cell-toxicity effect of superfluous aldehyde [18]. And, on the other hand, the result verified the existing of excessive aldehyde in 1:1 hydrogel. This result is consistent with that of degradation, both indicated the inadequate crosslinking of Gel-MA with OHA in 1:1 hydrogel. Furthermore, we investigated the adhesion and spreading of MC3T3-E1 cells on the OHA/Gel-MA hydrogels (Figure 6B). The result showed that the OHA/Gel-MA hydrogels did not cause cytotoxicity to MC3T3-E1 cells except the 1:1 hydrogel group, which was consistent with the result of CCK-8.

We further evaluated the influence of OHA/Gel-MA hydrogels in the osteogenic activities of MC3T3-E1 cells by assessing the ALP staining and using extracellular matrix mineralization (Figure 7). Our results showed that 0.0625:1 and 0.25:1 OHA/Gel-MA hydrogels were associated with significantly enhanced ALP staining and extracellular matrix mineralization than 1:1 OHA/Gel-MA and pure Gel-MA hydrogels. However, the underlying mechanisms remained largely unknow. It has been reported that mechanical stiffness may greatly modulate osteogenic activities through regulating integrin-binding (integrin-mediated signal transduction pathway) as well as the reorganization of adhesion ligands [33]. For example, $\alpha 5$ integrins bond formation was higher in soft matrix than that in stiff matrix, which in return promote the osteogenesis [34]. However, this possibility was excluded by our finding that the storage moduli of the 0.0625:1 and 0.25:1 OHA/Gel-MA hydrogels differed greatly although they were both associated with significantly enhanced osteogenic activities. Similarly, neither cytotoxicity seemed to be responsible since 0.0625:1 and 0.25:1 OHA/Gel-MA hydrogels bore similar levels of cytotoxicity. All the results indicated that the 0.0625:1 and 0.25:1 OHA/Gel-MA hydrogels can be a potential candidate for guided bone regeneration. One potential plausible mechanism is that OHA may bind and promote the availability and activity of paracrine bone morphogenetic protein, which promotes the osteogenic differentiation [35]. Another potential mechanism is that certain ratio of OHA may trigger the expression of a

low level of pro-inflammatory cytokine, such as tumor necrosis factor-α (TNF-α), which promotes the osteogenic differentiation of mesenchymal stem cells. TNF-α signaling has shown to play an important role in biomaterials-triggered osteogenic differentiation [36].

Bone regeneration is an inflammation-involved complex process, where different levels of proinflammatory cytokine expression is included. In our study, HA was designed to have a function to induce the production of TNF-α [37], which further promote bone formation through accelerating cells migration [38] and osteogenic differentiation [39] in a short time when the concentration of TNF-α was lower than 10 ng/mL [40]. Furthermore, the initial inflammatory response is not only responsible for recruiting leucocytes, but also for stimulation of mesenchymal stem cell migration, differentiation, and new bone formation, what is specific for the repair and remodeling phases. Thus, in our future work, the TNF-α mediated mechanism of OHA/Gel-MA will be studied, such as ERK or p38 MAPK signaling pathway [41].

5. CONCLUSION

In summary, a novel *in-situ* hybrid-crosslinked OHA/Gel-MA hydrogel membrane was developed via Schiff's base reaction and UV initiated polymerization with enhanced mechanical property and improved osteogenic property for guided bone regeneration. The mechanical modulus was improved by 6.8 times. *In-vitro* cytocompatibility study demonstrated that the OHA/Gel-MA hydrogels are non-cytotoxic. The result of the *in-vitro* extracellular matrix mineralization of MC3T3-E1 demonstrated that the OHA/Gel-MA hydrogel can accelerate the formation of mineralized nodules with improved ALP staining and alizarin red staining. In conclusion, the newly formed hybrid-crosslinked OHA/Gel-MA hydrogel may provide a good choice as a barrier membrane for guiding bone regeneration.

ACKNOWLEDGEMENTS

REFERENCES

[1] M.A. Saghiri, A. Asatourian, F. Garcia-Godoy, N. Sheibani, The role of angiogenesis in implant dentistry part II: The effect of bone-grafting and barrier membrane materials on angiogenesis, Medicina Oral Patologia Oral Y Cirugia Bucal 21(4) (2016) E526-E537.

[2] T. Spinell, J. Saliter, B. Hackl, K. Unger, R. Hickel, M. Folwaczny, In-vitro cytocompatibility and growth factor content of GBR/GTR membranes, Dental Materials 35(7) (2019) 963-969.

[3] M. Trobos, A. Juhlin, F.A. Shah, M. Hoffman, H. Sahlin, C. Dahlin, In vitro evaluation of barrier function against oral bacteria of dense and expanded polytetrafluoroethylene (PTFE) membranes for guided bone regeneration, Clinical Implant Dentistry and Related Research 20(5) (2018) 738-748.

[4] J. Mir-Mari, H. Wui, R. Jung, C. Hämmerle, G. Benic, Influence of blinded wound closure on the volume stability of different GBR materials: an in vitro cone-beam computed tomographic examination, Clinical oral implants research 27(2) (2016) 258-65.

[5] C. Tu, A. Bajwa, A. Shi, G. Wu, J. Wang, Effect of fibrin glue on the healing efficacy of deproteinized bovine bone and autologous bone in critical-sized calvarial defects in rats, Clinical Oral Investigations (2022).

[6] B. Klotz, D. Gawlitta, A. Rosenberg, J. Malda, F. Melchels, Gelatin-Methacryloyl Hydrogels: Towards Biofabrication-Based Tissue Repair, Trends in biotechnology 34(5) (2016) 394-407.

[7] M.X. Zhu, Y.Y. Wang, G. Ferracci, J. Zheng, N.J. Cho, B.H. Lee, Gelatin methacryloyl and its hydrogels with an exceptional degree of controllability and batch-to-batch consistency, Scientific Reports 9 (2019).

[8] X.J. Cai, J. Cai, K.N. Ma, P. Huang, L.L. Gong, D. Huang, T. Jiang, Y.N. Wang, Fabrication and characterization of Mg-doped chitosan-gelatin nanocompound coatings for titanium surface functionalization, Journal of Biomaterials Science-Polymer Edition 27(10) (2016) 954-971.

[9] J.W. Seo, S.R. Shin, M.-Y. Lee, J.M. Cha, K.H. Min, S.C. Lee, S.Y. Shin, H. Bae, Injectable hydrogel derived from chitosan with tunable mechanical properties via hybrid-crosslinking system, Carbohydrate Polymers 251 (2021) 117036.

[10] Y. Yang, X. Wang, F. Yang, L. Wang, D. Wu, Highly elastic and ultratough hybrid ionic–covalent hydrogels with tunable structures and mechanics, Advanced Materials 30(18) (2018) 1707071.

[11] J.B. Leach, K.A. Bivens, C.N. Collins, C.E. Schmidt, Development of photocrosslinkable hyaluronic acid-polyethylene glycol-peptide composite hydrogels for soft tissue engineering, Journal of Biomedical Materials Research Part A 70A(1) (2004) 74-82.

[12] P. Zhai, X. Peng, B. Li, Y. Liu, H. Sun, X. Li, The application of hyaluronic acid in bone regeneration, International journal of biological macromolecules 151 (2020) 1224-1239.

[13] A. Baldini, D. Zaffe, G. Nicolini, Bone-defects healing by high-molecular hyaluronic acid: preliminary results, Annali di stomatologia 1(1) (2010) 2.

[14] L. Wang, C.L. Lu, H.H. Liu, S. Lin, K.H. Nan, H. Chen, L.L. Li, A double network strategy to improve epithelization of a poly(2-hydroxyethyl methacrylate) hydrogel for corneal repair application, Rsc Advances 6(2) (2016) 1194-1202.

[15] B. Balakrishnan, A. Jayakrishnan, Self-cross-linking biopolymers as injectable in situ forming biodegradable scaffolds, Biomaterials 26(18) (2005) 3941-3951.

[16] L. Koivusalo, J. Karvinen, E. Sorsa, I. Jonkkari, J. Valiaho, P. Kallio, T. Ilmarinen, S. Miettinen, H. Skottman, M. Kellomaki, Hydrazone crosslinked hyaluronan-based hydrogels for therapeutic delivery of adipose stem cells to treat corneal defects, Materials Science & Engineering C-Materials for Biological Applications 85 (2018) 68-78.

[17] D.A. Ossipov, S. Piskounova, O.P. Varghese, J. Hilborn, Functionalization of Hyaluronic Acid with Chemoselective Groups via a Disulfide-Based Protection Strategy for In Situ Formation of Mechanically Stable Hydrogels, Biomacromolecules 11(9) (2010) 2247-2254.

[18] W.Y. Su, Y.C. Chen, F.H. Lin, Injectable oxidized hyaluronic acid/adipic acid dihydrazide hydrogel for nucleus pulposus regeneration, Acta Biomaterialia 6(8) (2010) 3044-3055.

[19] M. Toledano-Osorio, F.J. Manzano-Moreno, C. Ruiz, M. Toledano, R. Osorio, Testing active membranes for bone regeneration: A review, Journal of Dentistry 105 (2021).

[20] R.E. Jung, N. Fenner, C.H.F. Hammerle, N.U. Zitzmann, Long-term outcome of implants placed with guided bone regeneration (GBR) using resorbable and non-resorbable membranes after 12-14years, Clinical Oral Implants Research 24(10) (2013) 1065-1073.

[21] A. Turri, I. Elgali, F. Vazirisani, A. Johansson, L. Emanuelsson, C. Dahlin, P. Thomsen, O. Omar, Guided bone regeneration is promoted by the molecular events in the membrane compartment, Biomaterials 84 (2016) 167-183.

[22] J.P. Berridge, T.M. Johnson, A.W. Cheng, D.T. Swenson, P.D. Miller, Focus on Epithelialized Palatal Grafts. Part 3: Methods to Enhance Patient Comfort at Palatal Donor Sites, Clinical Advances in Periodontics 9(4) (2019) 177-184.

[23] K. Yue, G. Trujillo-de Santiago, M.M. Alvarez, A. Tamayol, N. Annabi, A. Khademhosseini, Synthesis, properties, and biomedical applications of gelatin methacryloyl (GelMA) hydrogels, Biomaterials 73 (2015) 254-271.

[24] B.J. Klotz, D. Gawlitta, A. Rosenberg, J. Malda, F.P.W. Melchels, Gelatin-Methacryloyl Hydrogels: Towards Biofabrication-Based Tissue Repair, Trends in Biotechnology 34(5) (2016) 394-407.

[25] G. Irmak, T. Demirtaş, M. Gümüşderelioğlu, Highly Methacrylated Gelatin Bioink for Bone Tissue Engineering, ACS biomaterials science & engineering 5(2) (2019) 831-845.

[26] L. Wang, H. Fu, W.W. Wang, Y. Liu, X.M. Li, J.J. Yang, L.L. Li, G. Wu, Y.H. Pan, Notoginsenoside R1 functionalized gelatin hydrogels to promote reparative dentinogenesis, Acta Biomaterialia 122 (2021) 160-171.

[27] L. Xiong, Q. Luo, Y. Wang, X. Li, Z. Shen, W. Zhu, An injectable drug-loaded hydrogel based on a supramolecular polymeric prodrug, Chemical communications (Cambridge, England) 51(78) (2015) 14644-7.

[28] B. Liu, Y. Wang, Y. Miao, X. Zhang, Z. Fan, G. Singh, X. Zhang, K. Xu, B. Li, Z. Hu, M. Xing, Hydrogen bonds autonomously powered gelatin methacrylate hydrogels with super-elasticity, self-heal and underwater self-adhesion for sutureless skin and stomach surgery and E-skin, Biomaterials 171 (2018) 83-96.

[29] J. Suchanek, R.K. Ivancakova, R. Mottl, K.Z. Browne, K.C. Pilneyova, N. Pilbauerova, J. Schmidt, T.S. Kleplova, Hyaluronic Acid-Based Medical Device for Treatment of Alveolar Osteitis-Clinical Study, International Journal of Environmental Research and Public Health 16(19) (2019).

[30] T.H. Qazi, D.J. Mooney, G.N. Duda, S. Geissler, Biomaterials that promote cell-cell interactions enhance the paracrine function of MSCs, Biomaterials 140 (2017) 103-114.

[31] N. Abbasi, S. Hamlet, R.M. Love, N.T. Nguyen, Porous scaffolds for bone regeneration, Journal of Science-Advanced Materials and Devices 5(1) (2020) 1-9.

[32] S. Li, M. Pei, T. Wan, H. Yang, S. Gu, Y. Tao, X. Liu, Y. Zhou, W. Xu, P. Xiao, Self-healing hyaluronic acid hydrogels based on dynamic Schiff base linkages as biomaterials, Carbohydrate polymers 250 (2020) 116922.

[33] J. Zhang, E. Wehrle, P. Adamek, G.R. Paul, X.-H. Qin, M. Rubert, R. Müller, Optimization of mechanical stiffness and cell density of 3D bioprinted cell-laden scaffolds improves extracellular matrix mineralization and cellular organization for bone tissue engineering, Acta Biomaterialia 114 (2020) 307-322.

[34] N. Huebsch, P. Arany, A. Mao, D. Shvartsman, O. Ali, S. Bencherif, J. Rivera-Feliciano, D. Mooney, Harnessing traction-mediated manipulation of the cell/matrix interface to control stem-cell fate, Nature materials 9(6) (2010) 518-26.

[35] H.R. Huang, J.Y. Feng, D. Wismeijer, G. Wu, E.B. Hunziker, Hyaluronic Acid Promotes the Osteogenesis of BMP-2 in an Absorbable Collagen Sponge, Polymers 9(8) (2017).

[36] A. Przekora, G. Ginalska, Chitosan/β-1,3-glucan/hydroxyapatite bone scaffold enhances osteogenic differentiation through TNF-α-mediated mechanism, Materials science & engineering. C, Materials for biological applications 73 (2017) 225-233.

[37] D. Boyce, A. Thomas, J. Hart, K. Moore, K. Harding, Hyaluronic acid induces tumour necrosis factor-alpha production by human macrophages in vitro, British journal of plastic surgery 50(5) (1997) 362-8.

[38] X. Fu, B. Han, S. Cai, Y. Lei, T. Sun, Z. Sheng, Migration of bone marrow-derived mesenchymal stem cells induced by tumor necrosis factor-alpha and its possible role in wound healing, Wound repair and regeneration : official publication of the Wound Healing Society [and] the European Tissue Repair Society 17(2) (2009) 185-91.

[39] Y. Cui, X. Han, Y. Lin, W. Lv, Y. Wang, TNF-α was involved in calcium hydroxide-promoted osteogenic differentiation of human DPSCs through NF-κB/p38MAPK/Wnt pathway, Die Pharmazie 72(6) (2017) 329-333.

[40] R. Aquino-Martínez, A. Angelo, F. Pujol, Calcium-containing scaffolds induce bone regeneration by regulating mesenchymal stem cell differentiation and migration, Stem cell research & therapy 8(1) (2017) 265.

[41] Z. Lu, G. Wang, C. Dunstan, Y. Chen, W. Lu, B. Davies, H. Zreiqat, Activation and promotion of adipose stem cells by tumour necrosis factor-α preconditioning for bone regeneration, Journal of cellular physiology 228(8) (2013) 1737-44.

Chapter 7

General Discussion

GENERAL DISCUSSION

Hydrogel is a three-dimensional network, providing channels for the transportation of oxygen, nutrients and other water-soluble metabolites. Hydrogels, particularly the naturally-derived ones, bear excellent biocompatibility, tunable biodegradability, and abundant recognition sites to facilitate cell adhesion, migration and proliferation. Importantly, hydrogels may act as a controlled drug delivery system for various bioactive agents, thereby conferring hydrogels with various potent functions [1]. Based on the different mechanism of crosslinking, hydrogels can be classified into physically crosslinked and chemically crosslinked ones [2]. Chemical crosslinking hydrogels are formed by covalent bonds, such as photopolymerization, Schiff base reactions [3], Diels–Alder reactions [4], disulfide bonds [5], acylhydrazone bonds [6], and phenylboronate esters [7]. Photopolymerization and Schiff base reaction are two most commonly used strategies to construct a covalent crosslinking hydrogel, which can be carried out under mild conditions and formed homogeneous and stable gel state *in situ*. The high fluidity of hydrogel precursors can easily enable its adaptive fit into the oral hard tissue defects with irregular shapes, such as dentinal defects in deep caries, jumping distance in alveolar bone, and osteochondral defects in temporomandibular joint (TMJ), and thus showing promising application potentials in oral hard tissue regeneration. Albeit so, hydrogels still lack intrinsic capacities of inducing reparative dentinogenesis or osteogenesis. Besides, the mechanical property of the hydrogels is still suboptimal to shield the interference of external mechanical forces, such as occlusal force on osteogenesis or dentinogenesis. In this thesis, we developed functionalized hydrogels with enhanced physicochemical and dentinogenic/pro-osteogenic properties for the regeneration of reparative dentin, bone and osteochondral tissues.

Photo-crosslinkable Gel-MA-based hydrogels, show a series of promising properties [8, 9], such as 1) non-immmunogenicity, 2) good degradability and biocompatibility, 3) the good fluidity of Gel-MA enables an easy spreading and thus complete coverage of bone-defect-filling materials and surrounding healthy bone tissues so as to form an excellent seal, functioning to both allow the penetration of nutrients/blood vessels and stabilize the filling materials without the needs of additional fixation or trimming. In this thesis, to enhance the application potential of Gel-MA, we aimed to further enhance the mechanical strength of Gel-MA. One possible method to enhance the mechanical property of Gel-MA is to increase the degree of methacrylation of Gel-MA, which may increase the crosslinking density. However, it seems that the storage modulus of Gel-MA is not significantly influenced when the degree of methacrylation is increased from 23.1% to 76.0% [10]. One promising way to improve the mechanical property of the hydrogel is incorporating small molecules. For example, doxorubicin [11] and tannic acid [12] are shown to significantly increase the storage modulus of hydrogels. Such enhancements may be attributed to the formation of intermolecular hydrogen bonding or host-guest interactions between drugs

and hydrogels, leading to a more compact structure [12]. In **chapter 2**, the notoginsenoside R1 (NGR1) incorporated Gel-MA hydrogel was associated with significantly enhanced mechanical properties compared with Gel-MA alone. Such a phenomenon might be attributed to the non-covalent interactions between NGR1 and Gel-MA network [13, 14], leading to a more compact structure, as shown by the SEM results. Such a change in mechanical properties is highly meaningful for a pulp capping material to provide sufficient resistant force to protect the underlying dental pulp and support further restoration. Another potential method to enhance the mechanical property of Gel-MA is to introduce hybrid-crosslinking. In **chapter 6**, we put forward a hybrid-crosslinking by adding oxidized hyaluronic acid (OHA) to form dynamic chemical bonds with Gel-MA in additional to its intrinsic photo-crosslinking to provide a more viable approach for guided bone regeneration (GBR). For this purpose, we first controlled the methacrylation degree of Gel-MA (calculated according to the result of ^{1}H NMR) as low as 25.10% (with about 0.809 mmol amino retained in one gram Gel-MA), which was designed to enable the Schiff's base reaction between the unsubstituted amino groups of Gel-MA with the aldehyde groups of OHA. When the mixing ratio of OHA to Gel-MA was 0.0625:1 with the molar ratio of $-NH_2$/-CHO at about 4:1, the storage modulus of OHA/Gel-MA reached 176.4 ± 35.3 KPa, which was significantly higher (about 6.8 times) than that of Gel-MA. However, as OHA content was increased to 0.25:1 or 1:1 (with the molar ratio of $-NH_2$/-CHO at 1:1 or 1:4), the storage moduli of OHA/Gel-MA hydrogels were significantly lower than that of Gel-MA. These phenomena might be explained by two independent mechanisms. On one hand, it has been shown that dynamic Schiff base linkage-based hydrogel with the molar ratio of $-NH_2$/-CHO at 4:1 or 8:1 bore much higher storage modulus than that at 2:1 or 1:1 [15], which contributed to the significant promoting effect of OHA when mixed at the ratio of 0.0625:1. On the other hand, the overdosage of OHA might, whereas, caused a steric hindrance to the photocrosslinking efficiency of Gel-MA, thereby resulting in a compromised mechanical property for the hydrogels with mixing ratio at 0.25:1 and 1:1. These data highlighted the importance of an appropriate ratio for producing hybrid-crosslinked hydrogels with enhanced mechanical property. Furthermore, the higher mixing ratios were associated with significantly enhanced degradation rate, which made those hydrogels less suitable for the intended application. For a better application as a pulp-capping material or bone-defect-filling material, hydrogels may be further optimized with respect to its mechanical strength [16], possibly by adding calcium-containing micro/nanoparticles.

Apart from mechanical strength, hydrogel materials for oral hard tissue regeneration should also bear the capacity of promoting cell differentiation into intended lineages, such as odontoblast and osteoblast. One viable way to confer pro-osteogenic/dentinogenic properties of hydrogels is to adopt bioactive agents, such as proteinous growth factors, peptides and small molecules. One of the most used proteinous growth factors for oral hard tissue regeneration is bone morphogenetic protein 2 (BMP2), a well-established osteoinductive growth factor under the TGF-β superfamily [17]. However, the use of BMP2 in oral hard tissue regeneration is associated with a series of concerns, such as rather costly

for its wide spreading [18], the induction of postoperative inflammation [19], and hardly improvement of physicochemical properties [20]. In contrast, most peptides and small-molecules are much cheaper and also exhibit various biofunctions, representing promising alternatives to functionalize hydrogels for oral hard tissue regeneration. In the thesis, NGR1 and SAB (small molecules), histatin 1 (peptide), and hyaluronic acid (macromolecule) were adopted to functionalize hydrogels.

An ideal pulp-capping material should be bioactive so as to pacify the inflammation of dental pulp and stimulate the formation of reparative dentin. The Gel-MA hydrogel can be potentially used as a pulp-capping material due to a series of beneficial properties, such as easy spreading and realistic handling, short and controllable setting time [21], tooth substrate adhesion [22], and non-carcinogenicity. However, Gel-MA still lacks the intrinsic capacity to pacify inflammation and induce dentinogenesis. This problem may be tackled by functionalizing Gel-MA with Notoginsenoside R1 (NGR1), a bioactive monomer isolated from *Panax notoginseng* [23]. NGR1 is a well-established pharmaceutical drug with potent anti-inflammatory and anti-apoptotic properties. Furthermore, our recent study for the first time shows that NGR1 dramatically promotes osteogenic differentiation of pre-osteoblasts [24]. In **chapter 2**, we, for the first time, showed that NGR1 could induce extracellular matrix mineralization of odontoblast-like cells — an important biological marker for dentinogenesis [25, 26]. We first found that dentinogenesis was not significantly influenced by the different physicochemical properties of Gel-MA with different solid contents (100, 150 and 200 mg/mL). In contrast, interestingly, the presence of NGR1 was associated with significantly enhanced *in-vitro* dentinogenesis on Gel-MA with a solid content of 100 mg/mL, while on Gel-MA with solid contents of 150 or 200 mg/mL, the addition of NGR1 resulted in compromised dentinogenesis. To investigate whether the Gel-MA/NGR1 hydrogel could induce reparative dentin formation *in vivo*, we adopted a modified direct pulp capping model. Our results showed that the Gel-MA/NGR1 was associated with a significantly larger amount of newly formed mineralized tissue than the Dycal control and Gel-MA groups. These data suggested a promising application potential of Gel-MA/NGR1 in pulp-capping therapy.

With the same strategy, in **chapter 5**, we adopted salvianolic acid B (SAB), a traditional Chinese herbal medicine-derived water-soluble small molecule, to functionalize sericin/oxidized alginate (SS/OSA) hydrogel with a pro-osteogenic property. For screening the optimal dosage for the functionalization of SS/OSA hydrogel with SAB, we first adopted *in-vitro* cell culture on well plates to screen the optimal concentration for inducing osteogenic differentiation. With thereby-obtained optimal dosage of the SAB, we further evaluated the effects of hydrogel compositions on the osteogenic differentiation of bone marrow mesenchymal stem cells (BMSCs) that were seeded on the hydrogels. Hydrogels with the ratios of SS:OSA at 5:1, 2:1, 1:1, 1:2 and 1:5 were adopted. Our results showed that the SS/

OSA-SAB hydrogel at the SS/OSA ratios of 2:1, 1:2 and 1:5 significantly promoted the extracellular matrix mineralization of BMSCs by 7.5, 13.6, and 8.4 folds, respectively in comparison with the SAB-treated cell on culture plate. Besides, the period of mineralization induction was shortened, suggesting that the SS/OSA-SAB hydrogel might also accelerate bone formation. In addition, the 1:2 SS/OSA-SAB hydrogel exhibited significant increases of ALP activity and OCN expression, compared with 1:5 and 2:1 SS/OSA-SAB hydrogel. One possible explanation might be that the structural stability of 1:2 SS/OSA-SAB hydrogel was much better than those of 1:5 and 2:1 SS/OSA-SAB since SEM analyses showed that the inner porous structure of the 1:2 SS/OSA-SAB hydrogel still stayed intact, while the inner porous structures of 1:5 and 2:1 SS/OSA-SAB hydrogel groups already collapsed after a 21-day culture. These data suggested that the 1:2 SS/OSA-SAB hydrogel could be a promising candidate for filling jumping gaps and enhancing bone regeneration.

Hst1 belongs to a cationic and histidine-rich peptide family that is originally found in the saliva of higher primates [27]. Hst1 shows cell types-independent cell-activating effects, such as stimulates the adhesion and migration of epithelial cells [28-31], fibroblasts [32] and osteoblasts [33, 34], promotes cell metabolic activity [31], maintains cell viability in various conditions [33, 34] and shows a very strong angiogenetic property [35]. These properties are of paramount importance particularly for the application in repairing osteochondral defects, which needs both recruitment of regenerative cells and the promotion of osteoblastic and chondrogenic activities [36, 37]. In **chapter 3**, to provide a viable treatment option for the repair of osteochondral defects in TMJ, we adopted Hst1 to functionalize Gel-MA hydrogel. Our results showed that the functionalized hydrogel (Hst1/Gel-MA) could significantly improve the osteochondrogenesis. Compared with the complicatedly designed material scaffolds that contain three parts with different physicochemical and biological properties in order to facilitate the regeneration of bone, cartilage, and the osteochondral interface, separately [38], the Hst1/Gel-MA showed more promising potential for clinical application. Interestingly, we found that 50 µg Hst1/Gel-MA was associated with insufficient new bone and cartilage formation, while 1000 µg Hst1/Gel-MA resulted in overstimulation of bone regeneration with compromised cartilage formation. It seemed that over-dosed Hst1 would be more beneficial for bone regeneration, but detrimental for cartilage formation. This might be due to an overstimulation of angiogenesis by Hst1. Consequently, elaborate modulation of Hst1 dosage is critical for balanced bone and cartilage formation. In this chapter, we showed that 500 µg Hst1/Gel-MA hydrogels significantly promoted the deposition of ECM compositions (collagen II and aggrecan) and the formation of zonally-structured cartilage in the defects in comparison with Gel-MA hydrogels and the control (the defects receiving no filling material) (p<0.05). The score of International Cartilage Repair Society (ICRS) and Modified O'Driscoll Score (MODS) in Hst1/Gel-MA group were also significantly higher than Gel-MA group. In addition, numerous chondroblasts in the newly formed cartilage layer, osteoblasts and osteoclasts in

the subchondral bone could be observed in our study, indicating a high level of metabolism and remodeling. Consequently, 500 μg Hst1/Gel-MA hydrogel was proved to be the most efficacious in repairing osteochondral defects in TMJ.

Apart from the abovementioned bioactive agents, some ECM components may also be used to improve pro-osteogenic properties. In **chapter 6**, we introduced oxidized hyaluronic acid (OHA) to Gel-MA and prepared a hybrid-crosslinking OHA/Gel-MA hydrogel with the aim to develop a novel GBR membrane with significantly enhanced osteogenic and mechanical properties than Gel-MA. We evaluated the effect of the hydrogels on the osteogenic activities of MC3T3-E1 cells by assessing the ALP staining and extracellular matrix mineralization. Our results showed that the OHA/Gel-MA hydrogels at the ratios of 0.0625:1 and 0.25:1 were associated with significantly enhanced ALP staining and extracellular matrix mineralization than the 1:1 OHA/Gel-MA and pure Gel-MA hydrogels. One plausible mechanism is that OHA may bind and promote the availability and activity of paracrine bone morphogenetic protein, which promotes the osteogenic differentiation [39]. Another potential mechanism is that certain ratio of OHA may trigger the expression of a low level of pro-inflammatory cytokine, such as tumor necrosis factor-α (TNF-α), which promotes the osteogenic differentiation of mesenchymal stem cells. TNF-α signaling has shown to play an important role in biomaterials-triggered osteogenic differentiation [40]. In conclusion, the newly formed hybrid-crosslinked OHA/Gel-MA hydrogel might provide a promising GBR membrane material to promote bone regeneration.

FUTURE PERSPECTIVE

Based on the present thesis, the developed functionalized hydrogels exhibited promising capacities of inducing pro-osteogenic/dentinogenic differentiation, showing a promising potential application in oral hard tissue regeneration. Several questions should be further considered in the future:

1. For the application of the functionalized hydrogels as oral hard tissue regeneration, they still need to be optimized in their mechanical strength, possibly by incorporating inorganic bioactive agents without hindering the injectable property.

2. For SS/OSA-SAB and OHA/Gel-MA, *in-vivo* studies should be performed to further corroborate their efficacies.

3. The molecular mechanisms accounting for the dentinogenic/pro-osteogenic effects of the functionalized hydrogels still need to be further revealed.

REFERENCES

[1] T. Komabayashi, A. Wadajkar, S. Santimano, C. Ahn, Q. Zhu, L.A. Opperman, L.L. Bellinger, J. Yang, K.T. Nguyen, Preliminary study of light-cured hydrogel for endodontic drug delivery vehicle, Journal of Investigative and Clinical Dentistry 7(1) (2016) 87-92.

[2] H.J. Haugen, P. Basu, M. Sukul, J.F. Mano, J.E. Reseland, Injectable biomaterials for dental tissue regeneration, International journal of molecular sciences 21(10) (2020) 3442.

[3] J. Xu, Y. Liu, S. Hsu, Hydrogels Based on Schiff Base Linkages for Biomedical Applications, Molecules (Basel, Switzerland) 24(16) (2019).

[4] D.-q. Li, S.-y. Wang, Y.-j. Meng, Z.-w. Guo, M.-m. Cheng, J. Li, Fabrication of self-healing pectin/chitosan hybrid hydrogel via Diels-Alder reactions for drug delivery with high swelling property, pH-responsiveness, and cytocompatibility, Carbohydrate Polymers (2021) 118244.

[5] M.T.I. Mredha, J.Y. Na, J.-K. Seon, J. Cui, I. Jeon, Multifunctional poly (disulfide) hydrogels with extremely fast self-healing ability and degradability, Chemical Engineering Journal 394 (2020) 124941.

[6] M. Zhu, H. Jin, T. Shao, Y. Li, J. Liu, L. Gan, M. Long, Polysaccharide-based fast self-healing ion gel based on acylhydrazone and metal coordination bonds, Materials & Design 192 (2020) 108723.

[7] X. Pei, L. Fang, W. Chen, X. Wen, L. Bai, X. Ba, Facile Fabrication of Multiresponsive Self-Healing Hydrogels with Logic-Gate Responses, Macromolecular Chemistry and Physics 222(2) (2021) 2000339.

[8] K. Yue, G. Trujillo-de Santiago, M.M. Alvarez, A. Tamayol, N. Annabi, A. Khademhosseini, Synthesis, properties, and biomedical applications of gelatin methacryloyl (GelMA) hydrogels, Biomaterials 73 (2015) 254-271.

[9] B.J. Klotz, D. Gawlitta, A. Rosenberg, J. Malda, F.P.W. Melchels, Gelatin-Methacryloyl Hydrogels: Towards Biofabrication-Based Tissue Repair, Trends in Biotechnology 34(5) (2016) 394-407.

[10] G. Irmak, T. Demirtaş, M. Gümüşderelioğlu, Highly Methacrylated Gelatin Bioink for Bone Tissue Engineering, ACS biomaterials science & engineering 5(2) (2019) 831-845.

[11] L. Xiong, Q. Luo, Y. Wang, X. Li, Z. Shen, W. Zhu, An injectable drug-loaded hydrogel based on a supramolecular polymeric prodrug, Chemical communications (Cambridge, England) 51(78) (2015) 14644-7.

[12] B. Liu, Y. Wang, Y. Miao, X. Zhang, Z. Fan, G. Singh, X. Zhang, K. Xu, B. Li, Z. Hu, M. Xing, Hydrogen bonds autonomously powered gelatin methacrylate hydrogels with super-elasticity, self-heal and underwater self-adhesion for sutureless skin and stomach surgery and E-skin, Biomaterials 171 (2018) 83-96.

[13] A.A. Nada, E.A. Ali, A.A.F. Soliman, Biocompatible chitosan-based hydrogel with tunable mechanical and physical properties formed at body temperature, International journal of biological macromolecules 131 (2019) 624-632.

[14] S. Khorshidi, A. Karkhaneh, A self-crosslinking tri-component hydrogel based on functionalized polysaccharides and gelatin for tissue engineering applications, Materials Letters 164 (2016) 468-471.

[15] S. Li, M. Pei, T. Wan, H. Yang, S. Gu, Y. Tao, X. Liu, Y. Zhou, W. Xu, P. Xiao, Self-healing hyaluronic acid hydrogels based on dynamic Schiff base linkages as biomaterials, Carbohydrate polymers 250 (2020) 116922.

[16] T.W. Xin, Y. Gu, R.Y. Cheng, J.C. Tang, Z.Y. Sun, W. Cui, L. Chen, Inorganic Strengthened Hydrogel Membrane as Regenerative Periosteum, Acs Applied Materials & Interfaces 9(47) (2017) 41168-41180.

[17] M. Lykissas, I. Gkiatas, Use of recombinant human bone morphogenetic protein-2 in spine surgery, World journal of orthopedics 8(7) (2017) 531.

[18] E.A. Olmsted-Davis, Z. Gugala, F.H. Gannon, P. Yotnda, R.E. McAlhany, R.W. Lindsey, A.R. Davis, Use of a chimeric adenovirus vector enhances BMP2 production and bone formation, Human gene therapy 13(11) (2002) 1337-1347.

[19] J. Shen, A.W. James, J.N. Zara, G. Asatrian, K. Khadarian, J.B. Zhang, S. Ho, H.J. Kim, K. Ting, C. Soo, BMP2-induced inflammation can be suppressed by the osteoinductive growth factor NELL-1, Tissue engineering. Part A 19(21-22) (2013) 2390-2401.

[20] S. Trujillo, C. Gonzalez-Garcia, P. Rico, A. Reid, J. Windmill, M.J. Dalby, M. Salmeron-Sanchez, Engineered 3D hydrogels with full-length fibronectin that sequester and present growth factors, Biomaterials 252 (2020) 120104.

[21] W.L.O. da Rosa, A.R. Cocco, T.M.D. Silva, L.C. Mesquita, A.D. Galarca, A.F.D. Silva, E. Piva, Current trends and future perspectives of dental pulp capping materials: A systematic review, J Biomed Mater Res B Appl Biomater 106(3) (2018) 1358-1368.

[22] J. Ribeiro, E. Bordini, J. Ferreira, L. Mei, N. Dubey, J. Fenno, E. Piva, R. Lund, A. Schwendeman, M.J.A.a.m. Bottino, interfaces, Injectable MMP-Responsive Nanotube-Modified Gelatin Hydrogel for Dental Infection Ablation, 12(14) (2020) 16006-16017.

[23] H.H. Fang, S.L. Yang, Y.Y. Luo, C. Zhang, Y. Rao, R.J. Liu, Y.L. Feng, J. Yu, Notoginsenoside R1 inhibits vascular smooth muscle cell proliferation, migration and neointimal hyperplasia through PI3K/Akt signaling, Scientific Reports 8 (2018).

[24] Y. Liu, Z. Lin, J. Guo, G. Xu, Y. Li, T. Xu, H. Lv, J. Chen, G. Wu, Notoginsenoside R1 significantly promotes in vitro osteoblastogenesis, Int J Mol Med 38(2) (2016) 537-44.

[25] C. Beguekirn, A.J. Smith, J.V. Ruch, J.M. Wozney, A. Purchio, D. Hartmann, H. Lesot, Effects of dentin proteins, transforming growth-factor beta-1 (TGF-beta-1) and bone morphologetic protein-2 (BMP2) on the differentiation of odontoblast in vitro, International Journal of Developmental Biology 36(4) (1992) 491-503.

[26] D. Tziafas, K. Kodonas, Differentiation Potential of Dental Papilla, Dental Pulp, and Apical Papilla Progenitor Cells, Journal of Endodontics 36(5) (2010) 781-789.

[27] P. Torres, M. Castro, M. Reyes, V.A. Torres, Histatins, wound healing, and cell migration, Oral Diseases 24(7) (2018) 1150-1160.

[28] M.J. Oudhoff, J.G. Bolscher, K. Nazmi, H. Kalay, W. van 't Hof, A.V. Amerongen, E.C. Veerman, Histatins are the major wound-closure stimulating factors in human saliva as identified in a cell culture assay, FASEB J 22(11) (2008) 3805-12.

[29] I.A. van Dijk, K. Nazmi, J.G. Bolscher, E.C. Veerman, J. Stap, Histatin-1, a histidine-rich peptide in human saliva, promotes cell-substrate and cell-cell adhesion, FASEB J 29(8) (2015) 3124-32.

[30] I.A. van Dijk, A.F. Beker, W. Jellema, K. Nazmi, G. Wu, D. Wismeijer, P.M. Krawczyk, J.G. Bolscher, E.C. Veerman, J. Stap, Histatin 1 Enhances Cell Adhesion to Titanium in an Implant Integration Model, J Dent Res 96(4) (2017) 430-436.

[31] D. Shah, M. Ali, D. Shukla, S. Jain, V.K. Aakalu, Effects of histatin-1 peptide on human corneal epithelial cells, PLoS One 12(5) (2017) e0178030.

[32] M.J. Oudhoff, P.A. van den Keijbus, K.L. Kroeze, K. Nazmi, S. Gibbs, J.G. Bolscher, E.C. Veerman, Histatins enhance wound closure with oral and non-oral cells, J Dent Res 88(9) (2009) 846-50.

[33] M. Castro, P. Torres, L. Solano, L.A. Cordova, V.A. Torres, Histatin-1 counteracts the cytotoxic and antimigratory effects of zoledronic acid in endothelial and osteoblast-like cells, J Periodontol 90(7) (2019) 766-774.

[34] G.Q. Huang, G.G. Yi, L.W. Wu, S.F. Feng, W. Wu, L. Peng, R.W. Yi, W. Ma, X. Lu, Protective effect of histatin 1 against ultraviolet-induced damage to human corneal epithelial cells, Exp Ther Med 15(1) (2018) 679-684.

[35] P. Torres, J. Diaz, M. Arce, P. Silva, P. Mendoza, P. Lois, A. Molina-Berrios, G.I. Owen, V. Palma, V.A. Torres, The salivary peptide histatin-1 promotes endothelial cell adhesion, migration, and angiogenesis, FASEB J 31(11) (2017) 4946-4958.

[36] P.C. Bessa, M. Casal, R.L. Reis, Bone morphogenetic proteins in tissue engineering: the road from laboratory to clinic, part II (BMP delivery), J Tissue Eng Regen Med 2(2-3) (2008) 81-96.

[37] P.M. van der Kraan, E.N. Blaney Davidson, W.B. van den Berg, Bone morphogenetic proteins and articular cartilage: To serve and protect or a wolf in sheep clothing's?, Osteoarthritis Cartilage 18(6) (2010) 735-41.

[38] M.T. Frassica, M.A. Grunlan, Perspectives on Synthetic Materials to Guide Tissue Regeneration for Osteochondral Defect Repair, ACS Biomater Sci Eng 6(8) (2020) 4324-4336.

[39] H.R. Huang, J.Y. Feng, D. Wismeijer, G. Wu, E.B. Hunziker, Hyaluronic Acid Promotes the Osteogenesis of BMP-2 in an Absorbable Collagen Sponge, Polymers 9(8) (2017).

[40] A. Przekora, G. Ginalska, Chitosan/β-1,3-glucan/hydroxyapatite bone scaffold enhances osteogenic differentiation through TNF-α-mediated mechanism, Materials science & engineering. C, Materials for biological applications 73 (2017) 225-233.

Chapter 8

General Summary

GENERAL SUMMARY

Oral hard tissue refers to the hard and mineralized tissues, such as enamel, dentin, and bone, which form an integral complex, playing a vital role in aesthetics and oral functions. The osteochondral complex of temporomandibular joint (TMJ) also functions to dissipate or transfer the masticatory force. In this thesis, we mainly focused on the regeneration of dentin, bone and osteochondral complex by using functionalized hydrogels.

Pulp-capping materials are commonly adopted in the clinic to stimulate the formation of reparative dentin and thus protect dental pulp tissues from pathological stimuli. Some traditional pulp capping materials used in the clinic include calcium hydroxide and mineral trioxide aggregates. However, there are limitations to thin restorative dentin, and a long period of time is needed to cause degenerative changes in dental pulp. In **chapter 2**, we developed injectable colloidal gels through a simple UV method from methacrylic acid functionalized gelatin (Gel-MA) loaded with notoginsenoside R1 (Gel-MA/NGR1). We investigated the physicochemical properties of Gel-MA/NGR1 and its efficacy to induce *in-vitro* dentinogenesis and *in-vivo* reparative dentin formation. Our results showed that the hydrogel retained porous inner structure and hydrophilicity with a sustained drug release. Gel-MA/NGR1 hydrogel could significantly promote *in-vitro* dentinogenic markers, extracellular matrix mineralization, and *in-vivo* reparative dentin formation in comparison with Gel-MA. These findings suggested a promising application potential of Gel-MA/NGR1 in pulp-capping techniques.

The avascular structure and lack of regenerative cells make the repair of osteochondral defects in the TMJ highly challenging in clinic. To provide a viable treatment option, in **chapter 3,** we developed a histatin-1 (Hst1)-functionalized Gel-MA hydrogel to combine the chondroconductive property of Gel-MA and the cell-activating capacity of Hst1. We surgically created critical-size osteochondral defects (3 mm in diameter and 3 mm in depth) of TMJ in New Zealand White rabbits to evaluate the healing efficacy of Hst1/Gel-MA. Our data showed that Hst1/Gel-MA hydrogel group possessed a significant higher International Cartilage Repair Society (ICRS) score and Modified O'Driscoll Score (MODS) in comparison with the Gel-MA group and control group. Furthermore, histomorphometric analysis showed significantly higher expression of collagen II, aggrecan, collagen fiber, GAG, and more newly formed subchondral bone and cartilage in Hst1/Gel-MA hydrogel group than the Gel-MA group and control group. Our data suggested a promising application potential of Hst1/Gel-MA hydrogels in promoting the repair of critical-size osteochondral defects in TMJ.

The usage of Gel-MA may not be very suitable for the partially exposed defects, such as, jumping gap in immediate implantation since the long and narrow geometry of, and the bleeding in jumping gap may largely hinder the photocrosslinking-based gelation process and lead to insufficient gelation. To approach this situation, we resorted to another type of hydrogel — injectable self-healing hydrogels with dynamic crosslinking, which could be gelled without the needs of additional chemical/physical initiations. In **chapter 4**, we adopted gelatin and oxidized alginate (OSA) to construct an injectable self-healing hydrogel. The rheological results confirmed the successful dynamic crosslinking and self-healing property of the hydrogel. The physicochemical and *in-vitro* and *in-vivo* biological characterization showed that the self-healing hydrogels could support cell survival, proliferation, and migration, and had a good injectability, *in-situ* gelation, and biocompatibility, suggesting a promising candidate for tissue engineering scaffold and drug delivery vehicle.

In comparison with conventional osteoconductive CaP-based bone filling materials, an injectable, self-healing and pro-osteogenic hydrogel will be more suitable to fill large jumping gap and preserve buccal bone. In **chapter 5**, we developed an injectable self-healing sericin/oxidized alginate hydrogel (SS/OSA), and functionalized the hydrogel with a pro-osteogenic agent — salvianolic acid B (SAB). The *in-vitro* physicochemical characterization showed that the pore size and the mechanical properties of prepared hydrogels could be regulated by adjusting the mixing ratios of SS/OSA. The storage moduli of SS/OSA at the ratios of 1:2 and 1:5 were significantly higher than the other ratios (5:1, 2:1 and 1:1) and the 1:2 SS/OSA hydrogel showed the highest extracellular matrix mineralization nodules of BMSCs. The addition of 0.1 μM SAB to the 1:2 SS/OSA hydrogel showed the highest enhancement in extracellular matrix mineralization nodules. Our results suggested that the SS/OSA-SAB hydrogel might be a promising scaffold candidate for promoting bone regeneration in jumping gaps.

Barrier membrane is an indispensable element in GBR technique to prevent the invasion of surrounding connective tissues that bears proliferation advantage over osteoblasts so as to facilitate bone tissue regeneration. Gel-MA bears certain stickiness to mineralized tissue and UV crosslinking is also very suitable for this application. However, the mechanical property of Gel-MA should still be improved to be used as a GBR membrane. In **chapter 6**, we adopted a hybrid-crosslinking method (Schiff's base reaction and UV initiated polymerization) to develop an *in-situ* formed barrier membrane with enhanced mechanical property and osteogenesis. Our results showed that the storage modulus of Gel-MA by 6.8 times by introducing OHA in a ratio 0.0625:1 and thus an additional dynamic chemical bond to Gel-MA. Furthermore, such hybrid-crosslinked OHA/Gel-MA could also significantly promote the *in-vitro* osteogenic differentiation of MC3T3-E1 cells in comparison with Gel-MA. These findings suggested that the hybrid-crosslinked hydrogel might provide a good choice as a barrier membrane for guiding bone regeneration.

In this thesis, we adopted different bioactive agents or ECM components to functionalize hydrogels with enhanced mechanical and pro-osteogenic/dentinogenic properties. These data suggested a promising potential of the functionalized hydrogels in the regeneration of oral hard tissues.

Appendices

LIST OF AUTHOR CONTRIBUTIONS

ACKNOWLEDGEMENTS

CURRICULUM VITAE

LIST OF CONTRIBUTING AUTHORS OF THE MANUSCRIPTS IN THIS THESIS

T. Forouzanfar

Department of Oral and Maxillofacial Surgery/Pathology, Amsterdam UMC and Academic Center for Dentistry Amsterdam (ACTA), Vrije Universiteit Amsterdam (VU), Amsterdam Movement Science (AMS), Amsterdam, The Netherlands

Department of Oral Cell Biology, Amsterdam UMC and Academic Center for Dentistry Amsterdam (ACTA), Vrije Universiteit Amsterdam (VU), Amsterdam Movement Science, Amsterdam, The Netherlands

G. Wu

Department of Oral and Maxillofacial Surgery/Pathology, Amsterdam UMC and Academic Center for Dentistry Amsterdam (ACTA), Vrije Universiteit Amsterdam (VU), Amsterdam Movement Science (AMS), Amsterdam, The Netherlands

Department of Oral Cell Biology, Amsterdam UMC and Academic Center for Dentistry Amsterdam (ACTA), Vrije Universiteit Amsterdam (VU), Amsterdam Movement Science, Amsterdam, The Netherlands

L. Li

State Key Laboratory of Ophthalmology, Optometry and Visual Science, Wenzhou Medical University, Wenzhou, Zhejiang 325027, China

Y. Pan

Institute of Stomatology, School & Hospital of Stomatology, Wenzhou Medical University, Wenzhou, Zhejiang 325027, China

K. Nan

Wenzhou Eye Hospital, Wenzhou Medical University, Wenzhou, Zhejiang 325000 China

H. Chen

Wenzhou Eye Hospital, Wenzhou Medical University, Zhejiang Province, 325000 China

H. Fu

Institute of Stomatology, School & Hospital of Stomatology, Wenzhou Medical University, Wenzhou, Zhejiang 325027, China

W. Wang

Nanjing Drum Tower Hospital Clinical College of Traditional Chinese and Western Medicine, Nanjing University of Chinese Medicine, Nanjing 210008, China

Y. Liu

Key Laboratory of Oral Medicine, Guangzhou Institute of Oral Disease, Stomatology Hospital of Guangzhou Medical University, Guangzhou Medical University, Guangzhou 510140, China

X. Li

Institute of Stomatology, School & Hospital of Stomatology, Wenzhou Medical University, Wenzhou, Zhejiang 325027, China

J. Yang

Institute of Stomatology, School & Hospital of Stomatology, Wenzhou Medical University, Wenzhou, Zhejiang 325027, China

C. Shi

School of Stomatology, Zhejiang Chinese Medical University, Hangzhou, Zhejiang 310053, China;

Y. Yao

School of Stomatology, Zhejiang Chinese Medical University, Hangzhou, Zhejiang 310053, China;

P. Sun

The Affiliated Hospital of Stomatology, School of Stomatology, Zhejiang University School of Medicine, and Key Laboratory of Oral Biomedical Research of Zhejiang Province, Hangzhou, Zhejiang 310006, China.

J. Feng

School of Stomatology, Zhejiang Chinese Medical University, Hangzhou, Zhejiang 310053, China;

F. Deng

Wenzhou Eye Hospital, Wenzhou Medical University, Wenzhou, Zhejiang 325027, China

A. Li

Wenzhou Eye Hospital, Wenzhou Medical University, Wenzhou, Zhejiang 325027, China

C. Lu

Wenzhou Eye Hospital, Wenzhou Medical University, Wenzhou, Zhejiang 325017, China

C. Tu

Department of Oral and Maxillofacial Surgery/Pathology, Amsterdam UMC and Academic Center for Dentistry Amsterdam (ACTA), Vrije Universiteit Amsterdam (VU), Amsterdam Movement Science (AMS), Amsterdam, The Netherlands

D. Wu

Institute of Stomatology, School & Hospital of Stomatology, Wenzhou Medical University, Wenzhou, Zhejiang 325027, China

L. Wang

Department of Oral Implantology and Prosthetic Dentistry, Academic Centre for Dentistry Amsterdam (ACTA), University of Amsterdam (UvA) and Vrije Universiteit Amsterdam (VU), 1081 LA Amsterdam, Netherlands

Department of Oral and Maxillofacial Surgery/Pathology, Amsterdam UMC and Academic Center for Dentistry Amsterdam (ACTA), Vrije Universiteit Amsterdam (VU), Amsterdam Movement Science (AMS), 1081 LA Amsterdam, The Netherlands

Wenzhou Institute of Biomaterials & Engineering, University of Chinese Academy of Science, Wenzhou, Zhejiang 325027, China

LIST OF CONTRIBUTING AUTHORS OF THE MANUSCRIPTS IN THIS THESIS

Authors	Initials
T. Forouzanfar	TF
G.Wu	GW
L. Li	LL
Y. Pan	YP
H. Chen	HC
K. Nan	KN
H. Fu	HF
W. Wang	WW
Y. Liu	YL
X. Li	XL
J. Yang	JY
C. Shi	CS
Y. Yao	YY
P. Sun	PS
J. Feng	JF
F. Deng	FD
A. Li	AL
C. Li	CL
C. Tu	CT
D. Wu	DW
L. Wang	LW

CHAPTER 2

Published as:

Notoginsenoside R1 functionalized gelatin hydrogels to promote reparative dentinogenesis

Authors:

Lei Wang, Hui Fu, Wenwen Wang, Yi Liu, Xumin Li, Jijing Yang, Lingli Li , Gang Wu, Yihuai Pan

Author contributions:

Investigation, conceptualization: LW, GW, YP, LL; Data curation, original draft writing: LW, WW; Validation, experimental animal study: HF, LW; Resources: LL, YL; Performed the study: LW, HF, WW, YL; Data analysis: LW, HF, XL, JY, GW; Manuscript review & editing: LW, GW, YP, LL. Supervision, project administration: GW, YP.

Conflict of interest statement:

The authors declare that the research was conducted in the absence of any commercial or financial relationships that could be construed as a potential conflict of interest.

CHAPTER 3

Published as:

Human salivary histatin-1-functionalized Gelatin Methacrylate Hydrogels promotes the regeneration of cartilage and subchondral bone in temporomandibular joint

Authors:

Changjing Shi[#], Yu Yao[#], Lei Wang[#], Ping Sun, Jianying Feng and Gang Wu
([#]: shared first author)

Author contributions:

Conceptualization, CS, YY, LW, JF and GW; methodology, CS, YY, LW, JF and GW; software, CS, and YY; formal analysis, CS, and YY; investigation, LW, GW and JF; resources, CS, and YY; writing—original draft preparation, CS, and YY; writing—review and editing, JF and GW; funding acquisition, PS, GW; All authors have read and agreed to the published version of the manuscript.

Conflict of interest statement:

The authors declare that the research was conducted in the absence of any commercial or financial relationships that could be construed as a potential conflict of interest.

CHAPTER 4

Published as:

Construction of injectable self-healing macroporous hydrogels via a template-free method for tissue engineering and drug delivery

Authors:
Lei Wang, Fen Deng, Wenwen Wang, Afeng Li, Conglie Lu, Hao Chen, Gang Wu, Kaihui Nan, Lingli Li

Author contributions:
Conceived and designed the study: LL, GW, KN; Performed the study: LW (material preparation, cell study, *in-vivo* exploration), FD (part of the material characterization), AL (part of the cell experiments); Analyzed the data: LW, WW, CL; Critical revised the manuscript: LW, HC, GW, LL.

Conflict of interest statement:
The authors declare that the research was conducted in the absence of any commercial or financial relationships that could be construed as a potential conflict of interest.

CHAPTER 5

A novel injectable self-healing sericin-alginate/salvianolic acid B hydrogel as jumping distance fillings

Authors:
Lei Wang, Wenwen Wang, Chengwei Tu, Danni Wu, Yihuai Pan, Kaihui Nan, Tymour Forouzanfar, Lingli Li, Gang Wu

Author contributions:
Conceived and designed the study: LW, CT, TF, GW
Performed the study: LW, WW, DW, LL
Analyzed the data: LW, DW, YP, KN, GW
Critical revised the manuscript: LW, TF, LL, GW

Conflict of interest statement:
The authors declare that the research was conducted in the absence of any commercial or financial relationships that could be construed as a potential conflict of interest.

CHAPTER 6

A novel *in-situ* hybrid-crosslinked oxidized hyaluronic acid/Gel-MA hydrogel membrane with significantly enhanced mechanical and osteogenic properties for guided bone regeneration

Authors:
Lei Wang, Wenwen Wang, Lingli Li, Tymour Forouzanfar, Gang Wu

Author contributions:
Conceived and designed the study: LW, TF, GW; Performed the study: LW (material preparation and characterization), WW (*in-vitro* cell study), LL (part of the hydrogel characterization); Analyzed the data: LW, WW, LL; Wrote the original draft: LW, WW; Critical revised the manuscript: LW, TF, GW. Supervision, project administration: GW, TF.

Funding sources:
The National Natural Science Foundation of China (31971278, 81870757), Key Research and Development Plan of Zhejiang Province (2021C04013), Engineering Research Center of Clinical Functional Materials and Diagnosis & Treatment Devices of Zhejiang Province (WIUCASK20004), Wenzhou Scientific Research Project (Y20210266 and 2019Y0411) and support of Academic Centre for Dentistry Amsterdam (ACTA).

Conflict of interest statement:
The authors declare that the research was conducted in the absence of any commercial or financial relationships that could be construed as a potential conflict of interest.

ACKNOWLEDGEMENTS

It would not have been possible to finish this doctoral thesis, at the Academic Centre for Dentistry Amsterdam (ACTA), without the help and support of the kind people around me, and to whom I am greatly indebted.

To prof. dr. **Tymour Forouzanfar**: Dear **Tim**, I am so grateful for having you as my supervisor. Thank you for offering the opportunity to perform my PhD in your group. Your unwavering enthusiasm for exploring the truth of the matter kept me constantly engaged with my research, and your generosity helped me have a great time at ACTA. Thank you for supporting me to participate in academic conferences and encouraging me to communicate with outstanding professors. You are a professional doctor, a precise researcher, and an excellent mentor. You always gave me warm smile. You always encouraged me when I got frustrated and that made me more determined to do my PhD.

To dr. **Gang Wu**: Dear **Gang**, I am so lucky to have you as co-promotor of my thesis. You have vast knowledge and always have distinctive ideas during my research procedure. These ideas have helped me greatly improve my researches and manuscripts. I still remember the first day we talked about my research work, your affirmation and encouragement kept me going. You also generously and effectively supervised me in scientific writing, critical thinking, oral presentation, language polishing, and image processing, and gave me a lot of detailed and specific help. I learned a lot of excellent qualities from you, precision, perseverance, patience, and no complaints. You are the most reliable friend for me in Amsterdam and the most contributive partner in my PhD project.

To prof. dr. **Lingli Li**: Dear **Lingli**, thank you very much for your support of my PhD study. I feel grateful to be one of your group members and love the great working environment you create for us. I really enjoyed the time working with you, during which time you always encouraged me and helped me. You are a hard-working researcher. I have learned a lot from you, not only about how to do scientific work meditatively, but also about how to raise a daughter wisely. And I am also happy to have been able to hang out with you outside of work.

To dr. **Astrid D Bakker** and prof. dr. **Jenneke Klein-Nulend**: Dear **Astrid**, thank you for your guidance and advice on my registration, lab work and life in OCB. You are a passionate leader and an enthusiastic colleague. The positive and efficient working atmosphere in the laboratory impressed me a lot. Also thank you for introducing us to the beautiful Amsterdam city in a league-building activity. That is the best-organized and most unforgettable activity I have ever joined in Amsterdam. Dear **Jenneke**, you are

always meticulous in academic research, even in details. This inspired me a lot. Thank you for your contribution in OCB data meeting, during which I always got new knowledge and became familiar with our colleagues even when I worked from home during Corona. Also thank you for providing me opportunity to share my research with our group members, their comments and advice were helpful and instructive.

To my colleagues: **Jianfeng, Jolanda, Cor, Behrouz, Menghong, Henk, Irena, Naichuan, Jan Harm, Hans, Andi, Yiwen, Shuyi, Yan, Jiayi, Gaoli.** Dear **Jianfeng**, thank you for your help. You are meticulous in your experiments. We have been working together on one project and I could always count on your help for anything. I am grateful that you have been there during my PhD. Dear **Jolanda**, thank you for your help in ordering experimental materials for me. We were one team to clean our lab and prepare experimental materials. I enjoyed working with you. I like your passionate laughter and will miss the coffee time with you and cakes. Dear **Cor**, thank you for all your help. Thank you for guiding me into the laboratory of OCB and training me about laboratory safety rules and experimental norms. You are a nice and patient person. You always helped me solve my problems in the lab. Dear **Behrouz**, you are intelligent, thank you for giving me the suggestions about EDS analyses. Dear **Menghong**, I am so happy to have had such a wonderful friend sharing PhD experiences. It was very nice to travel together to the Annual Meeting of the Dutch Society for Calcium and Bone metabolism in Zeist. You gave me lots of pertinent suggestions about my presentation, English writing, and speaking. I will always remember fondly our lunchtime at OCB and many other good times in the Nethelands. Dear **Henk**, Thank you for your great contribution in course registration and credits approval. You are always approachable and apprehensive when I encountered with some problems. Your helpful advice and fast response kept my project going well. Dear **Irena and Naichuan,** thank you for your guidance in Statistical Methods. Dear **Jan Harm**, thank you for organizing the course Oral Biology. Thank you for giving us wonderful lectures, and so that I have a more systematic understanding of oral biology. Dear **Hans**, thank you for giving me the offer of the course Dentistry for non-dentist. The lectures you gave us were so helpful for me. Dear **Andi**, thank you so much for helping me with the course Statistical Methods and Bioinformatics. You always answered my questions about these courses very prudentially and that helped me a lot to put them into practice during my PhD study. Dear **Yiwen**, we are both from Wenzhou, I am very grateful to you for your shelter when I first arrived in Amsterdam without accommodation. You are cheerful. We were working in the same office, and you always gave me a big warm hug when I felt down. Dear **Shuyi**, I learned from you the calm attitude and hardheaded ways of dealing with things. Thank you for giving me an unforgettable birthday dinner in Uilenstede together with Yiwen. Dear **Yan**, we met each other in the course oral cell biology, thank

you for giving me help during the course. Thank you for inviting me to your place to have a cup of drink, it is tasteful. Dear **Gaoli**, thank you for bringing experimental materials from China. You are a very friendly person. I like to talk with you.

To my neighbors in Uilenstede: **Yahua, Wenxuan, Chengguang, Xi, Sherry, Max, Yu, Linlin, Xumin, Jiayi.** Dear **Yahua**, you cook so well. I like your pancake and Youpo noodles. I am still grateful that you stayed with me for the weekend, we played badminton and did cycling. You are a professional photographer. I like the pictures you took. Maybe, someday, you will invite me to your exhibition. I wish you find the other half soon. Dear **Wenxuan**, we are the driving team. As a geological boy, you brought us new knowledge about the earth. Thank you for your chicken soup and steamed bun dipped with Lao Gan Ma, I will never forget the journey days with you. Dear **Chengguang**, newboy, the most handsome guy in Uilenstede, you are always passionate, thank you for the fun you brought us. Dear **Xi**, you are a "cruel" girl who seldom speaks. As a doctor of laws, you broadened my horizons about the law. Dear **Sherry**, you are a very good singer, especially the Cantonese songs. I like your singing. You are a sweet girl. Thank you for the bus pass. Dear **Max**, you are good at playing badminton and yoga. We have the same interests. Thank you for inviting me to your place to have Swiss-special dinner fondue, we talked a lot about the differences between China and Switzerland, such as daily life, working style, delicious food, and so on. I still remember we have a badminton competition agreement; hope one day we can make it. Dear **Yu**, thank you for offering your big room for us to have a hot pot together, we had a nice time there. Dear **Linlin**, I like playing badminton with you and thank you for taking me to the VU sports center. Dear **Xumin**, you are a lovely girl, thank you for picking me up from the Amsterdam Airport Schiphol. Dear **Jiayi**, thank you for helping me solve the internet problem in the dormitory.

To my colleagues in WIUCAS. Dear **Fangfu, Xiaoyun, Kaihui, Hao, Shi, Qing, Huaqiong, Changcan, Yi, Jinyan, Sen, Jingjie, Yangjun, Xiaoxu, Baoshan, Hongmei, Xiaodao, Xiaowei, Bo, Huawei, Lingnan, Huiqing, Gaofan, Si, Yu, Luqi, Yili, Shanshan, Xiao, Haiyan,** thank you so much all for your support and help. I really enjoy working with you and appreciate your assistance. I'm extremely fortunate to have you as colleagues.

To my family. Dear **dad, mom, husband (Wenwen Wang), daughter (Ruoyu Wang), mother-in-law, father-in-law, grandfathers, grandmothers, sisters (Yiman Wang and Shanhu Wang and Wenjuan Wang), uncle (Shihan Hu), aunt (Jianjing Jin), 2 cousins (Libang Hu and Yiduo Lin)**, thank you for your support and understanding. Without you, I would not have been able to achieve as much as I have so far. I wish my family all the best.

CURRICULUM VITAE

Personal Information
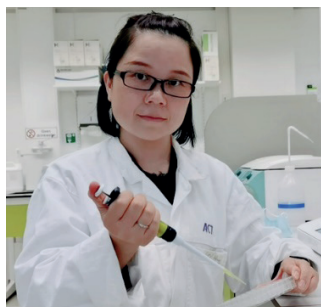
Name	Lei Wang
Date of birth	July. 07. 1987
Place of birth	Zhejiang Province, China
Institution	Department of Oral and Maxillofacial Surgery/Pathology, Department of Oral Cell Biology, Amsterdam UMC and Academic Centre for Dentistry Amsterdam (ACTA), Vrije Universiteit Amsterdam (VU), Amsterdam Movement Science (AMS), Amsterdam, The Netherlands
E-mail	wanglei20111213@gmail.com

Publications

1. Changjing Shi#, Yu Yao#, **Lei Wang#**, Ping Sun, Jianying Feng, Gang Wu. Human salivary histatin-1-functionalized gelatin methacrylate hydrogels promote the regeneration of cartilage and subchondral bone in temporomandibular joints. Pharmaceuticals 2021, 14, 484.

2. **Lei Wang#**, Hui Fu**#**, Wenwen Wang**#**, Yi Liu, Xumin Li, Jijing Yang, Lingli Li, Gang Wu, Yihuai Pan. Notoginsenoside R1 functionalized gelatin hydrogels to promote reparative dentinogenesis. Acta Biomaterialia 2021, 122, 160-171..

3. **Lei Wang**, Fen Deng, Wenwen Wang, Afeng Li, Conglie Lu, Hao Chen, Gang Wu, Kaihui Nan, Lingli Li. Construction of Injectable Self-Healing Macroporous Hydrogels via a Template-Free Method for Tissue Engineering and Drug Delivery. ACS Applied Materials & Interfaces, 2018,10(43), 36721-36732.

4. Lingli Li, Conglie Lu, **Lei Wang**, Mei Chen, Jacinta White, Xiaojuan Hao, Keith McLean, Hao Chen[1],*, Timothy C. Hughes*. Gelatin-Based Photocurable Hydrogels for Corneal Wound Repair. ACS Applied Materials & Interfaces, 2018,10(16), 13283-13292.

5. **Lei Wang**, Wenwen Wang, Ping Fan*, Menglong Zhou, Jintao Yang, Feng Chen, Mingqiang Zhong. Ionic liquid modified graphene/poly (vinyl alcohol) composite with enhanced properties. Journal of Applied Polymer Science 2017, 134(26), 45006.

6. Fan P, **Wang L**, Jia SX, Chen F, Yang JT and Zhong MQ. Encapsulated graphenes through ultrasonically initiated *in-situ* polymerization: A route to high dielectric permittivity, low loss materials with low percolation threshold. Journal of Applied Polymer Science. 2017, 134(12), 44628.

7. **Lei Wang**, Conglie Lu, Huihua Liu, Sen Lin, Kaihui Nan, Hao Chen, Lingli Li. A double network strategy to improve epithelization of a poly (2-hydroxyethyl methacrylate) hydrogel for corneal repair application. RSC Advances 2016, 6, 1194-1202.

Presentations

1. **Lei Wang**, Wenwen Wang, Lingli.Li, Tymour Forouzanfar, Gang Wu. Hyaluronic acid improves the performance of Gel-MA scaffold for bone tissue engineering application. 31th Annual Meeting of the Dutch Society for Calcium and Bone metabolism, Zeist, The Netherlands, October, 2021. (Oral presentation)

2. **Lei Wang**, Wenwen Wang, Lingli Li, Gang Wu. Preparation of Sericin-Alginate microporous hydrogel via Schiff base and its application for tissue engineering. National Symposium on Polymer Materials Science and Engineering, Haikou, China, October, 2020. (Poster)

3. **Lei Wang**, Hui Fu, Wenwen Wang, Yi Liu, Xumin Li, Lingli Li, Gang Wu, Yihuai Pan. NGR1 loaded gelatin hydrogels as substitutes for dentinogenesis. Chinese Biomaterials Congress & International Symposium on Advanced Biomaterials, Dalian, China, August, 2019. (Poster)

4. **Lei Wang**, Wenwen Wang, Afeng Li, Yan Jiang, Haijun Qiu, Conglie Lu, Hao Chen, Gang Wu, Kaihui Nan, Lingli Li, Injectable in-situ curable double network hydrogel, International Seminar on Advanced Materials Research, Shanghai, China, August, 2018. (Oral presentation)